Understanding Nucleosome Assembly Regulation in *Drosophila melanogaster*

Dissertation

A thesis submitted for the degree of

'Doctor of Philosophy'

Georg August University, Göttingen
Postgraduate program 'Genes and Development'
Göttingen Graduate Center for Neurosciences, Biophysics, and Molecular Biosciences (GGNB)

Dominik Sebastian Mühlen, from Münster
Max Planck Institute for Multidisciplinary Sciences
Göttingen 2022

Thesis Advisory Committee

Prof. Dr. Herbert Jäckle (First reviewer)
Director Emeritus Group Molecular Developmental Biology
Max Planck Institute for Multidisciplinary Sciences, Göttingen

Dr. Ufuk Günesdogan
Department of Developmental Biology
Johann-Friedrich-Blumenbach Institute, Georg August University, Göttingen

Prof. Dr. Patrick Cramer
Director Department of Molecular Biology
Max Planck Institute for Multidisciplinary Sciences, Göttingen

Further Members of the Examination Board

Prof. Dr. Ernst A. Wimmer (Second reviewer)
Head of Department of Developmental Biology
Johann-Friedrich-Blumenbach Institute, Georg August University, Göttingen

Prof. Dr. Argyris Papantonis
Group Leader of Translational Epigenetics
Institute of Pathology, University Medical Center Göttingen

Prof. Dr. Jörg Großhans
Department of Developmental Biochemistry
Institute of Biochemistry and Molecular Cell Biology, University Medical Center Göttingen

Declaration of Independence

Herewith I declare that the dissertation entitled 'Understanding Nucleosome Assembly Regulation in *Drosophila melanogaster*' was written on my own and independently without any other aids and sources than indicated.

Dominik Sebastian Mühlen

Göttingen April 30, 2022

This work was conducted in the emeritus group ‘Molecular Developmental Biology’ of Prof. Dr. Herbert Jäckle, Max Planck Institute for Multidisciplinary Sciences, Göttingen

and in the group ‘Vertebrate Germ Cell Development’ of Dr. Ufuk Günesdogan, Department of Developmental Biology, Johann Friedrich Blumenbach Institute for Zoology and Anthropology, Georg August University, Göttingen.

Summary

Nucleosomes consist of a complex of DNA and an octameric core of histone proteins, which represent the basic subunit of chromatin. The N-terminal tails of histones are target for chemical modifications, which play an important role in chromatin structure and the control of gene activity shaping the epigenome of a cell which was defined by Cold Spring Harbor Laboratories in 2008 as the "Stably heritable phenotype resulting from changes in a chromosome without alterations in the DNA sequence" (*1*). "Heritable" implies, that the epigenetic landscape needs to be maintained or re-established during or after cell division. During DNA replication, pre-existing or parental nucleosomes are disrupted and re-assembled behind the replication fork together with newly synthesized histones. However, it is not well understood how parental histones decorated with posttranslational modifications are recycled and positioned during the assembly of nucleosomes in the course of DNA replication. In this study I have addressed the question whether modified parental histones 'remember' their position after replication. For this purpose, I used a *Drosophila melanogaster* mutant that lacks all canonical histone genes (encoding histone H1, H2A, H2B, H3, and H4). This mutant, referred to as His^C mutant, is therefore not able to express new histones during replication. Owing to special characteristics of the early embryonic development, I analysed the first cell cycle when zygotic histone synthesis is required during embryonic development, and the histone deletion exerts its effect.

Chapter I represents the main findings of my study. I show that upon lack of histone synthesis in homozygous His^C mutant embryos, parental histones are faithfully recycled, but they are not sufficient to re-establish the characteristic chromatin landscape. This results in reduced nucleosome occupancy and increased inter dyad distances ultimately resulting in increased chromatin accessibility. Arrays of nucleosomes at transcription start sites (TSS) were irregular, with the +2 and +3 nucleosomes shifted downstream. This is accompanied by a drastic upregulation of genes, spurious transcription within gene bodies and intergenic regions, as well as a potential premature release of RNA polymerase II (RNAPII) towards productive elongation from the TSS. Consistently, active chromatin marks were strongly reduced in the mutant, whereas repressive marks maintained similar enrichment levels. Interestingly, however, in both cases, the enrichment patterns and peak calling suggests that decorated parental histones are incorporated in close vicinity of their original location. This observation suggests a positional memory of epigenetic marks during DNA replication.

In chapter II, I address the question how histone depletion affects cell cycle progression. His^C mutant embryos, which fail to zygotically express canonical histones, arrest in cell cycle 15 during the G2/M15 transition, which normally is driven by $String^{Cdc25}$. In His^C mutants, *string*

mRNA is downregulated, which is controlled by the RNA binding protein called Held-out-wings (How). How is expressed in two isoforms (long and short How, respectively). Long How, which was shown to destabilize target RNAs, is upregulated in *His*^{C} mutant embryos. Deletion of the How binding site in *string* mRNA results in an increased *string* mRNA abundance. Thus, my data suggests that in the absence of histone synthesis, the cell cycle arrests at the G2/M transition by destabilizing *string* mRNA based on a How-dependent regulatory mechanism.

Table of Contents

1 Introduction

1.1 Nucleosome assembly and epigenetic inheritance

In all eukaryotic species, two copies of each of the four canonical histones, two (H2A-H2B) dimers and one $(H3\text{-}H4)_2$ tetramer associate further by four-helix bundles to make up the tripartite octameric nucleosome core particle (*2*). The histone octamer and ~147 bp of DNA, that are wrapped roughly 1.65 times around the core particle, form a nucleosome (*3–5*). Together with the linker histone H1 forming the chromatosome (*6*), they not only represent the fundamental repeating unit of chromatin that protect and pack the DNA, play an integral part in chromatin structure, but they also support transcriptional regulation (*7, 8*). Further condensation is mediated by H1, resulting in a 30nm wide DNA filament with six nucleosomes per turn. This arrangement is sometimes also referred to as coiled-coil solenoid structure (*9*) in which histone H1 also plays an integral role in the establishment of higher order chromatin (*6, 10*). In contrast to the histones of the core particle, histone H1 does not contain a histone fold domain but attributes a winged-helix domain which binds the linker DNA (*11*). Prior to replication, removal of linker histone H1 relaxes the chromatin structure and thereby facilitates eviction of DNA bound proteins and nucleosomes. Analysis in plants and fungi (i.e., *Arabidopsis* and *Physarum,* respectively) showed that knocking down H1 activity by siRNA as well as phosphorylation of H1 increase the nuclear volume, indicating that phosphorylation might precede nucleosome disruption. In addition, chromatin condensation impairment also resulted in a loss of proper replication timing (*12–15*).

The canonical or replicative histones are exclusively transcribed during S-phase of the cell cycle, accounting to their high demand due to the increase of replicating DNA. Their mRNAs are translated in the cytoplasm and the histones are imported into the nucleus where they form new nucleosomes together with the pool of recycled parental histones (*16–18*). Although histones are transcribed and translated individually under tight cell-cycle control (*19*), it remains uncertain if they are imported into the nucleus as dimers or as separate proteins shown for HeLa cells (*12, 20–22*). Work done in *Physarum* revealed that only exogenous (H3-H4) dimers could be retrieved from a nuclear isolate, but monomers were absent when overexpressed during S-phase. This observation shows that histones form a complex before nuclear import at least in *Physarum* (*22*). In addition, it was suggested that modifications, such as lysine acetylation, are crucial for nuclear import as shown for the acetylated histones H4K5ac and H4K12ac (*23, 24*).

Although the canonical histones are highly conserved within the eukaryotic kingdom, their genomic organization differs between species. A mutual characteristic that all histone genes

share is the lack of introns (*2*). In metazoans, several copies of each histone genes are typically clustered in histone gene units in animals. However, the number and location of these gene units differs between species. Humans, for example, have a total of 65 histone genes arranged in three cluster (*25*). Of those, 14 H4 genes are mostly arranged in two clusters, interleaved by other canonical histone genes (*26*). Their mRNAs are stabilized by a conserved 26 bp-stem loop (*27, 28*) and they are regulated by a specific stem-loop-binding protein and their processing is tightly controlled by the U7 small nuclear ribonuclear protein complex (*19*). Plants, however, comprise fewer histone genes which are less dispersed in the genome (*29, 30*), and their mRNAs are polyadenylated (*31*).

1.1.1 Chromatin remodelers form nucleosome arrays

Nucleosomal DNA length (~147 bp) is mostly constant, but the length of linker DNA can vary among different cell types and species however usually ranges between ~18 to ~90 bp (*5*). Intriguingly, regular arrays are formed for example at active promotors characterized by a nucleosome depleted region (NDR) at the transcription start site (TSS) followed by the +1, +2, +3, etc. nucleosome (*32*). Nucleosomes form regular arrays with fixed distances between each other (spacing) which are spatially organized with regard to a barrier (phasing) (*33*). The formation of those arrays is controlled by four classes of ATP dependent chromatin remodelers of the CHD (Chromodomain-Helicase-DNA binding), INO80, SWI/SNF (SWItch/Sucrose Non-Fermentable) and ISWI (imitation SWI) families (*34, 35*). Early evidence for trans-acting remodelers originated from experiments expressing *Kluyveromyces lactis* Chd1 in *Saccharomyces cerevisiae*. This switch resulted in longer linker DNA regions corresponding to the *Kluyveromyces lactis* linker length, which is possibly due to the high inter species variety of Chd1 N-terminal domain (*36*). Remodellers can establish regular arrays. It was proposed that a passive mechanism balances distances between nucleosomes by nucleosome sliding velocities (*37*) depending on the linker DNA length to both sides, and the nucleosome composition as distinct acidic patch symmetries which alter the ISWI nucleosome sliding activity (*38*). However, recent studies describe that different remodelers set distinct linker lengths in a manner which is independent of the nucleosome density (*38*), but they are formed symmetrically around barriers with the help of elements which are referred to as “protein rulers” *in vitro* (*33*). This proposal opposes in part earlier findings suggesting that histone depletion in chromatin assembly factor 1 (CAF-1) mutants results in an increased inter-nucleosomal spacing (*39*). Additionally, H1 loss also results not only in disturbed higher order chromatin structure but also in a global shortening of linker DNA length (*40*). The importance of histone H1 on spacing of nucleosomes is further stressed by findings in early *Drosophila* embryos showing that nucleosome sliding equalizes H1 shifts relative to the dyad centre over multiple cell generations. In this case, H1 offers the initial que for

nucleosome repositioning in subsequent embryonic development (*41*). Furthermore, H1 occupation levels affect the length of linker DNA as observed in regions with drastically reduced H1 levels. These regions exhibited long linker length of up to 150 bp contrasting the average linker length of 28 bp (*41*).

1.1.2 Nucleosome disruption and segregation during replication

During cell division, semiconservative replication safeguards that genetic information of the DNA is equally inherited by the daughter cells. It results in two genetically identical daughter cells, each containing one parental strand and a complementary strand which is newly synthesized (*42, 43*). This proliferation event is crucial for multicellular organisms to generate different tissues which serve specific functions (*44*). The corresponding differentiation events involve the expression of different and specific genes, which at least in part are mediated by epigenetic information such as DNA and/or histone modifications. In case of the histones, epigenetic information is encoded within the chromatin *inter alia* in post translational modifications (PTMs) at the N-terminal residues of the histone tails (*45–47*). In contrast to the well understood transmission of genetic information, it remains elusive how epigenetic information which participates in defining cell identity is passed on during cell division (*48, 49*). Therefore, many scientists addressed the issue whether PTMs are recycled together with their cognate histones, or if each cell generation establishes the epigenetic landscape *de novo* based on sequence intrinsic effects. In this regard, read-write mechanisms are also often postulated. In the following I want to point out some key findings shaping the current understanding how nucleosome and epigenetic information is propagated to the next cell generation, preventing loss of cell identity, and conserving the epigenetic landscape.

Nucleosome propagation, positional memory of modified histones and epigenetic inheritance have been subject to extensive studies using *in vitro* techniques as well as yeast, murine and human stem cells/cell lines, *Xenopus leavis* and *Drosophila melanogaster* as experimental systems. Yet, there are several obstacles for studying these questions. First, discrimination of parental and new histones as well as replicated and original DNA is not trivial. In addition, it is crucial to synchronize cell divisions using *in vivo* or *in vitro* systems which in organisms is barely possible (*12*). There is also not a single origin of replication, rather does DNA replication occur at multiple replication forks at different genomic locations simultaneously. That means that even perfectly synchronized cells not necessarily need to be amplifying the same regions of DNA (*50*). Furthermore, mapping of single nucleosomes requires resolution of roughly 10 bp, a resolution which is only difficult to achieve with current techniques. Also, additionally sequencing often requires large amounts of input material (*51*). Moreover, putative artifacts that might have been introduced by overexpressing recombinant histones need to be taken into account, as it was shown that the amount of free histones changes the

nucleosomal behaviour during replication and might also alter the ratio of free to chromatinized histones (*52–54*).

Despite these shortcomings, much progress has been made at least with respect to the question of how it is assured that both daughter chromatids receive enough parental histones during replication to faithfully recover the chromatin structure. First studies addressing the question whether nucleosomes are recycled and incorporated into the chromatin during replication were conducted already in the 1970s (*55, 56*). Recent studies show that chromatin-bound proteins are removed from the DNA as the replication fork progresses during S-phase. During this process, nucleosomes ahead of the replications fork are destabilized and evicted from the DNA (*57, 58*). The DNA is then unwound by the replicative complex, promoting the disruption of nucleosomes into two dimeric (H2A-H2B) and a tetrameric $(H3\text{-}H4)_2$ subunit (*57, 59, 60*). Thereby, only one or two nucleosomes ahead of the replication fork are destabilized. (H2A-H2B) dimers are first released from the nucleosome (*12, 61, 62*) as shown by electron microscopic analysis of chromatin replication in the cellular blastoderm of the *Drosophila* embryo (*63*).

Behind the replication fork the chromatin organization needs to be re-established including the duplication of histone proteins including their cognate PTMs (*48, 64, 65*). The question whether parental histones are degraded or recycled has been subject of various studies, showing that newly formed chromatin consists of both, recycled and new largely unmodified histones (*17, 59, 60, 66–69*). In this case it is either possible that one strand receives the parental histones and the other only newly synthesized ones, or that the parental histones are randomly distributed between both. Extensive work over the last years however has established that both chromatids receive equal amounts of parental histones (*49, 65, 70–73*). In this process, $(H3.1\text{-}H4)_2$ or $(H3.2\text{-}H4)_2$ are propagated as undisrupted tetramers and not mixed with new (H3-H4) dimers after replication (*74, 75*) (Figure 1.1). The way parental histones are disrupted and redistributed to each daughter chromatid in order to form new nucleosomes together with newly synthesized histones is a conserved process in the realm of eukaryotes which is not completely understood (*76*).

A key role in this context is taken over by the histone chaperones, like CAF-1, which orchestrate the formation of integer chromatin during replication. Their importance was further underlined by the observation of increased DNA damage (*77, 78*), or inhibited replication fork movement when the amount of histones or CAF-1 was reduced.

In the process of replication, attention must also be drawn to the special characteristics of DNA polymerase III holoenzyme (Pol III) which requires elongation directions of 5’ to 3’. Hence, only the leading strand can replicate in a consecutive way. As a consequence, the

leading strand is rapidly reproduced by DNA polymerase ε (Pol ε), whereas the lagging strand is fragmentarily reproduced by DNA polymerase α and δ (Pol α and δ), resulting in single stranded DNA (ssDNA) loops behind the helicase, the minichromosome maintenance (MCM) complexes MCM2 and MCM7 (*48*).

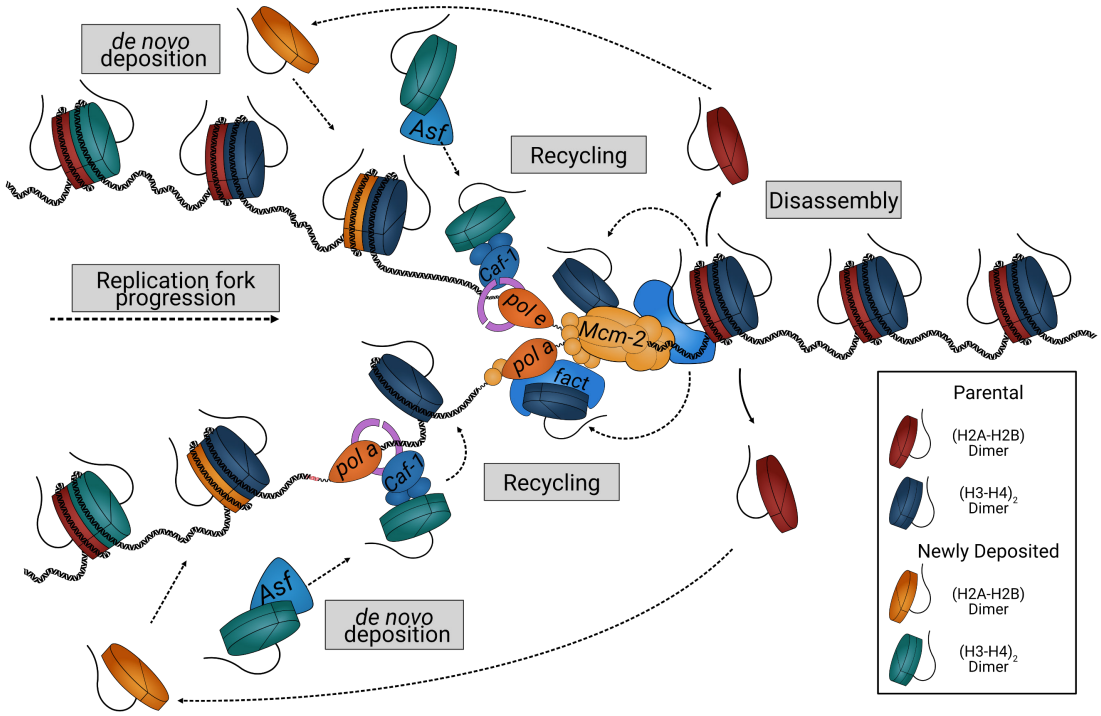

Figure 1.1 Nucleosome disruption in the vicinity of the replication fork. One to two nucleosomes ahead of the replication fork are destabilized and disrupted into two (H2A-H2B) dimers and one $(H3\text{-}H4)_2$ tetramer. Histone chaperones and subunits of the replicative complex deposit newly synthesized histone proteins to the replication fork and incorporate them together with recycled parental histones into new nucleosomes on the replicated DNA. How exactly the cell ensures equal distribution of parental histones, and if parental histones harbour a positional memory is still under debate. Modified from (*73*).

The replicating cell must therefore account for the different conditions in which chromatin is assembled on the leading versus the lagging strand and safeguard histone transfer to both. This is not a trivial issue as there are examples of asymmetric divisions in the animal kingdom. Some cells, like for example stem-cells, divide in an asymmetric manner, allocating cell fate determinants only to one of the two daughter cells (*79*). A well-studied example of asymmetric cell division in *Drosophila melanogaster* occurs during neural development, in which the protein Numb is asymmetrically inherited, making the receiving daughter cell immune to Notch signalling which in consequence results in a different cell fate (*80*). Likewise, parental histones are unevenly inherited in the male germline of *Drosophila melanogaster*. While the self-renewing stem cell receives the plethora of parental histones, the chromatin of the differentiating daughter cells is assembled by mainly newly synthesized histones (*81*). Here, the lagging strand loses most of its histone PTMs when the replication rate of the lagging strand is drastically reduced. Hence, evicted histones can only be incorporated into the leading strand. Therefore, the resulting daughter chromatid is void of parental histone PTMs

and is consequently prone for specific transcription factor binding to initiate the differentiation program (*82*). Histone segregation bias towards the leading strand in the absence of the lagging strand is consistent with passive histone capturing mechanism as described *in vitro* (*71, 83*).

Early studies on viral DNA showed that parental histones are equally distributed to the daughter chromatids and that newly synthesized histones are used to form new nucleosomes filling the resulting gaps (*84–86*). Still, it remained elusive whether the nucleosome core particle remembered its original position. Other *in vitro* studies using the *Simian Virus 40* (*SV40)* system as well as *Xenopus leavis* egg extracts implicated that although histones are inherited by daughter chromatids, histone positioning remained dynamic and independent prior to replication. In fact, this was suggested by studies on large T antigen, showing that it acts as a replicative helicase. However, this may not be the case in other systems like humans were helicase activity is promoted by MCM2 and MCM7 (*87*).

More recent studies suggest that histone segregation is intrinsically asymmetric which is overcome by a variety of specific histone chaperones as well as subunits of the MCM complex which devise the deposition of histones resulting from disrupted parental nucleosomes to the newly replicated DNA strands. Using a genome wide approach, it was shown that parental $(H3\text{-}H4)_2$ tetramers show a predilection for the lagging strand which is even increased by knock-out of the Dpb3 and Dpb4 subunits of Pol ε in budding yeast, indicating that subunits of Pol ε avert lagging strand bias (*49, 88*). This is of special importance as Dpb3/4 mutants showed impaired heterochromatin (*48*) and futile mating-type locus silencing (*49*).

Opposing the findings in budding yeast, parental histones of murine embryonic stem cells exhibit a strong bias towards the leading strand. In 2018, Petryk et al. (*65*) traced histone deposition of parental and newly synthesized histones in the vicinity of the replication fork by mapping Okazaki fragments. In a MCM mutant, where histone binding residues of MCM had been deleted, parental histones were mainly directed towards the leading strand and newly synthesized histones to the lagging strand (*48, 65, 88*). Similar results had previously been obtained using naked double stranded DNA (dsDNA) *in vitro* (*83*).

The tight control of histone segregation indicates the importance that the chromatin structure and nucleosome spacing is faithfully recapitulated, since the positioning of modified nucleosomes with regard to for example promotors has strong effects on gene transcription (*89*). Slowing down chromatin reassembly behind the MCM complex might also facilitate the recovery of evicted transcription factors especially on the leading strand (*51, 90*). Both models, however, show that specific histone chaperones are essential to overcome strand bias and achieve equal histone segregation to daughter chromatids (*48, 49, 65*). Additionally,

chaperones also overcome the negative charge of the basic histone molecules which prevents binding of histones to RNA molecules with an approximately 100-fold higher affinity (*55, 91*). Moreover, the importance of the correct deposition of the specific histone variant is demonstrated by the formation of paediatric diffuse midline gliomas due to deposition impairment (*92*), concluding that parental histone segregation ensues in a mostly symmetric way (*12, 49, 65, 71*).

Nucleosome disruption during replication is not the only process by which nucleosomes can be dispersed (*93*). Schlissel and Rine (*88*) tried to discriminate the effects on nucleosome positioning posed by transcription from those during replication in a recent study. Here, ~4 nucleosomes were covalently labelled with biotin *in vivo* in budding yeast using a BirA-TetR fusion protein. Because the tetracycline repressor (TetR) is exclusively tethered to its tetracycline operator (TetO*)* recognition site, a specific locus can be targeted by genetic engineering. The galactose inducible *Gal10* gene was targeted, hence the labelled nucleosomes can be tracked trough replication with and without previous transcriptional activity. Notably, the nucleosome core particle did not show any significant shift in the absence of transcription over several rounds of replication but only a dilution phenotype. *De novo* biotinylation was inhibited by the addition of doxycycline. In contrast, transcription leads to local dissociation from the original position but this shift is not propagated through the open reading frame (ORF) (*88*), concluding that passage of the replisome does not alter the epigenetic landscape. Consistent with findings by Yu et al. (*49*) and Petryk et al. (*65*) positional memory was lost in a Dbp3 or MCM2 mutant background (*71, 88*). Interestingly, real-time single molecule imaging in *Xenopus leavis* egg extract showed that parental histone recycling did not follow a single mechanism but rather displays three modes of nucleosomal behaviour in front of the replication fork. Among these are of course nucleosome eviction and transfer, but also sliding and replication fork stalling. The mode of nucleosomal behaviour seemed to depend on the amount of free H3/H4 histone, as depletion of those led to an increased nucleosomal transfer. Conversely, the supply of recombinant histones caused increased histone eviction (*54*).

In conclusion, nascent chromatin is composed of both parental and newly deposited histones with equal distribution although there are examples of asymmetric histone inheritance. During replication specific proteins of the replisome overcome strand specific bias by slowing down histone transfer to the leading strand (*49, 65*), which also depends on the amount of free histones available. Slowing down histone transfer is also believed to allow competing transcription factors to reassemble on new chromatin (*51, 84*) which all together indicates strong interdependencies between histone variants, transcription and replication which all contribute to the chromatin architecture.

1.1.3 Epigenetic information encoded in histone modifications

Histone PTMs are implicated in the orchestration of gene expression profiles. The finding that histones are subject to modifications leading to a fixed cell fate founded the 'histone code' theory (*94*). The core histone tails are subject to posttranslational modifications (*95*), among the most popular and best understood ones are mono-, di-, and tri-methylations as well as acetylation of histone H3. These modifications pose a direct effect on the chromatin dynamics, but a more recent understanding suggests that most modifications are not exclusive but rather require the combinatorial action of a set of modifications to divulge biological function (*12, 96, 97*).

These modifications are associated with transcriptional control. They not only establish chromatin states of active gene expression but also large transcriptionally repressed domains. Tri-methylations of H3, such as H3K4me3 for example, are enriched at promotor regions, di-methylated H3K4me2 additionally in enhancers. H3K36me3 and H3K79me3 are mainly found in gene bodies marking active chromatin states (*98*), whereas a trimethylation on lysine 27 (H3K27me3) are found in *polycomb*-dependent repressed genomic sites where H3K27me3 together with H3K9me3 marks transcriptionally repressed chromatin (*99*).

A hallmark for newly synthesized histone H4 are high levels of deacetylation (*100, 101*). Acetylated H3, such as H3K56ac, was not found to be enriched in nascent chromatin. This finding argued against general functions of acetylation/deacetylation during chromatin assembly in human cells (*100*). H3K16ac for example eases higher order open chromatin resulting in increased gene expression (*102*). Conversely, H4K16ac deacetylation mediated by the silent information regulator (Sir) complex causes repression of the mating type locus *HMRa* and *HMLα* in *S. cerevisiae* (*95, 103*).

These results essentially demonstrate two points. First, a specific PTM does not necessarily mean that the modified histone has a repressive or activating function, but secondly, that the appropriately modified histone acts in a site-specific manner. Furthermore, the studies show that to maintain cell-specific function, the appropriately modified histones must be positioned at the appropriate site in the replicated genome of the daughter cells.

1.1.4 Segregation of epigenetic information during replication

Early assumptions that nucleosomes inherit epigenetic information to daughter cells mediating developmental silencing originated from studies conducted in *Drosophila* where the Polycomb Repressive Complexes (PRCs) 1 and 2 were first identified. Of major interest is how epigenetic information is conserved through cell generations, and like mentioned above, if these mechanisms are dependent on sequence ques or nucleosome intrinsic signals. Additionally, distinct mechanisms are imaginable acting on repressed or active chromatin states. Early indications for sequence dependent effects where found during the formation of heterochromatin and epigenetic silencing, which widely depends on the recruitment of the proteins belonging to the Polycomb group (PcG) (*104*). Repressive activities of the PcG where first demonstrated by its effect on the *Bithorax* complex during early development in *Drosophila melanogaster* (*105*). PRC2 is known to establish H3K27me3 modifications which have been proven by many studies to conserve epigenetic information through replication. This however was challenged by a more recent report (*106, 107*) which proposed that in *Drosophila* embryos histone modifications are erased. In *Drosophila*, H3K27me3 marks are mostly found in the vicinity of Polycomb Response Elements (PREs) bound by sequence specific DNA-binding proteins. H3K27me3 acts in *cis*, which could account for re-establishing the epigenetic landscape. Therefore positional reminiscence of nucleosomes was thought not to be mandatory for epigenetic memory (*71, 108*). In contrast, recent studies showed that endogenous PREs play distinctive roles in gene silencing. Two PREs near the *vestigial* gene in *Drosophila* have been shown to act as repressors in transgenes. However, the deletion of one or both PREs did not result in a failure of gene silencing but gradual establishment of repressive chromatin marks *in vivo* (*109*), which argues against an exclusive dependency on PREs for epigenetic silencing.

Arguing for epigenetic inheritance uncoupled from sequence effects, it was shown that recycled histones maintain their PTMs, which can serve as a template recruiting their cognate modifying enzyme resultantly re-establishing modification patterns in a read-write manner. This was shown for repressive marks H3K9me3 and H3K27me3 and also allosteric regulation of PRC2 which promotes spreading of H3K27me3 (*89, 110, 111*). In fact, self-propagation and recycling of parental histones suggest an elegant epigenetic mechanism to assure that chromatin states are transmitted to replicated DNA. In addition, high histone turnover rates are also believed to maintain post translational modification levels within gene bodies and regulatory elements (*112*). In conclusion, there is evidence supporting both mechanisms, precise positional memory of nucleosomes but also nucleosome dispersal followed by reestablishment of epigenetic information *via* binding of modifying enzymes, might work

together and do not necessarily exclude each other. Unfortunately, in order to generalize, DNA features analogous to *Drosophila*'s PREs have yet to be identified in mammals (*71*).

First attempts to address the question whether different modifications propagate in distinct ways have been conducted in human cell cultures. Recently developed techniques, like Stable Isotope Labelling by Amino acids in Cell culture (SILAC) in combination with Nascent Chromatin Capture (NCC), serve to discriminate newly synthesized DNA and histones from parental ones, showing that distinct chromatin states exhibit distinct propagation patterns (*113*). Consistent with previously described findings in *Drosophila* (*112*) repressive marks like di- and trimethylation of H3K9 and H3K27 are acquired by both parental and new histones, arguing for an additional mechanism to restore pre-replication levels that acts independent from replication on all histones to establish repressive domains. In contrast, active marks were mostly acquired by new histones. Moreover, restoration speed of modification levels differs regarding the respective modification. Whereas most PTMs are gradually re-established on new histones to mimic parental ones and restore modification levels, repressive H3K9me3 and H3K27me3 were underrepresented on new histones after the first cell division. Moreover, modification levels also increased over several cell generations with histone age (*113*). Inhibiting lysine methyl transferase Enhancer of zeste homolog 2 (EZH2) reveals that H3K27me3 domains persisted through replication and do not erode over time arguing against impact of nucleosome turnover and for positional memory (*70*). Altogether, repressive marks like H3K27me3 and H3K9me3 are inherited by continuous modification of histones assuring their propagation over several cell generations consistent with previous findings in *Drosophila* (*109, 113*). Cells arrested in the G0 phase of the cell cycle showed an increase in H3K27me3 modification levels suggesting an ultimate determination of chromatin states while H3K9me3 was not increased (*113*). This finding suggests an S-phase arrest as a pre-requirement for further modification (*114*). Interestingly, no histone mark is underrepresented on parental histones in nascent chromatin which opposes findings in *Drosophila* (*107*). However, whether modified nucleosomes harbour a positional memory, as it had been shown with artificially modified nucleosomes, needs to be addressed *in vivo,* since small differences in nucleosomal positioning appear to have strong effects on transcriptional levels (*88, 89*).

This understanding is further supported by recent results applying Chromatin Occupancy after Replication (ChOR-seq). Nascent chromatin is marked by EdU pulse labelling, followed and analysed by Chromatin Immunoprecipitation (ChIP) (*70*). This method allows analysis of restoration kinetics of distinct histone modifications. Consistent with previous findings, the marks for active chromatin like H3K4me3 are in nascent chromatin not only accurately duplicated during DNA replication but undergo also quick and substantial accumulation

within the next 6 hours in cell culture. In fact, it reaches parental levels when the cell enters the G2 phase of the cell cycle, suggesting that reestablishment is mediated by a mechanism detached from replication during chromatin maturation (*68, 70*). Together, this demonstrates that precise parental histone propagation conserves positional information and allows PTM transmission to daughter cells. Modification of new histones sets basis for complex epigenome variations across the cell cycle that could account for cell identity and heterogeneity.

The kinetics of restoration on this occasion depend on DNA sequence. High levels of CpG at promotors, which is generally independent from transcription depleted of nucleosomes (*174*), increase the restoration speed as well as transcriptional activity (*70, 115, 116*).

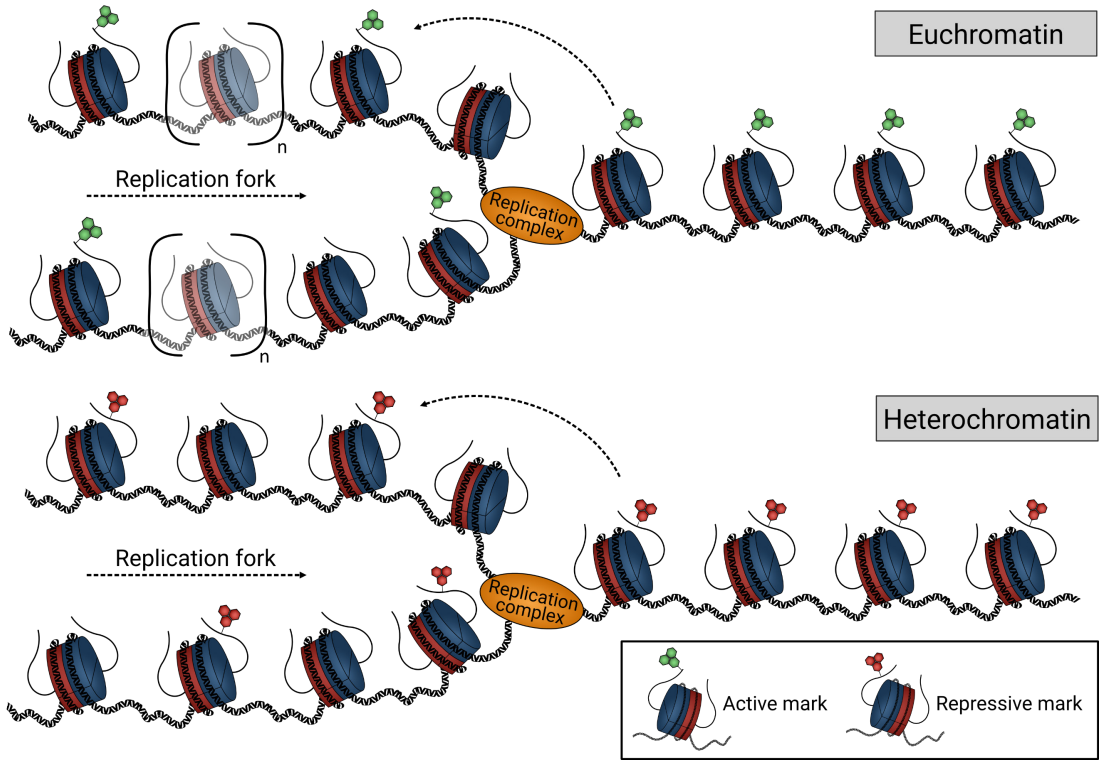

Figure 1.2 Two modes of epigenetic inheritance. Parental nucleosomes are disrupted and the histone subunits carrying post translational modifications are recycled. Two models are debated arguing that either nucleosomes in active and repressive regions are incorporated at the same sites (*70*) or only repressive regions exhibit a spatial memory whereas active marks do not segregate locally (*72*) Modified from (*72*).

In contrast, decoration levels of repressive marks like H3K27me3 did not recover prior to mitosis and the full chromatin landscape is established after cell division within 24 hours much longer than observed for active chromatin (*70*). This scenario is also consistent with previous findings using global quantitative mass spectrometry (*113*). Similar to H3K4me3, also H3K27me3 kinetics depend on DNA elements as a positive correlation between restoration speed and occupancy with domains of PRC2 or EZH2, which is the functional enzymatic part of the PRC2 domain (*70, 117*), was observed. Positional memory of nucleosome decorated with active marks was recently challenged by findings in mouse embryonic stem cells

(mESCs) (*72*). The results depictured in Figure 1.2 suggest that only repressive marks segregate locally, and that histone marks associated with active chromatin states are subsequently restored upon their reoccupation of transcription factors at their specific binding sites and transcription commencement (*72, 89, 118*).

This observation is consistent with findings highlighting how transcription factors compete with nucleosomes after replication (*51*). Additionally, it was suggested that transcriptional regulators mobilize cognate co-activators and RNA polymerase II (RNAPII) to promotor regions. Upon RNAPII binding independent methyltransferases drive modification of H3K4 and H3K36 which in turn facilitate transcription (*72, 119*). An explanation for the difference in local segregation dynamics of parental histones in this case might be that heterochromatin is replicated at slower speeds in late S-phase of the cell cycle, thereby maybe facilitating spatial memory nucleosomes (*120*). It was also shown that slowing down replication speed overcomes strand bias (*49, 65*) to allow for the binding for factors establishing repressive domains post replication (*71*). Also specific chaperons only active in late S-phase might facilitate the inheritance of repressive chromatin states (*72*).

In conclusion, propagation of epigenetic information needs to be well orchestrated. It was shown that histones decorated with active marks are faithfully inherited and that data for repressive marks are less consistent. Interestingly, there are striking differences regarding the timeframe in which chromatin marks are reestablished, with repressive marks like H3K27me3 taking longer to reach parental decoration levels. Moreover, there is evidence that for both chromatin states sequence-dependent features like polycomb responsive elements (PREs), or CpG islands and super enhancers pose stimulating effects on establishment kinetics, however are not exclusively responsible for propagation of epigenetic information. It is therefore implicated that additional mechanisms like transcriptional activity and decoration of PTMS by self propagation plays a crucial role in the establishment of the epignetic active chromatin landscape. In the following, I will focus on some of the aspects that transcriptional activity has on the establishment of active chromatin marks.

1.1.5 Transcription shapes active chromatin landscape

The haploid human genome consists of roughly 3.1 billion base pairs, yet only 1.5% of these belong to the 19,000 protein coding genes identified (*120*). Although the *Drosophila* genome is with ~135 million base pairs much smaller, it comprises roughly 16,000 protein coding genes, a number which is similar to the number of protein coding sequences of human (*121*). This implies that a large fraction of the genome contains *cis*-regulatory elements which interact by DNA looping. Enhancers interact with promotors to regulate transcription and can be distinguished as active and poised enhancers. While active enhancers are usually

decorated with H3K27ac and H3K4me2 and drive gene expression of steady state genes of a specific cell type, the poised enhancers are suggested to support transcription of developmental genes and situational genes necessary to react to environmental cues. They are characterized by high levels of H3K27me3 in combination with H3K4me1 and high chromatin accessibility (*122*). Both, enhancers, and promotors, are decorated with transcription factors and chromatin remodelers orchestrating gene expression of a cell. As mentioned in the former paragraph, these transcriptional regulators are disrupted by the replisome and compete with nucleosomes after replication (*51*). In this process, called chromatin maturation, accessibility and transcriptional profiles need to be restored, including the stereotypic nucleosomal landscape around TSSs (*32, 123*) in the otherwise inaccessible nascent chromatin. Generally it is believed that transcription factors bind regulatory elements and recruit chromatin remodelers setting the base for the preinitiation complex of transcription (*118*). After the preinitiation complex has formed, RNAPII binds and typically stalls at the +1 nucleosome before elongation (*93*). Transcription of non-coding RNAs from enhancers involves a similar mechanism (*124*). Nucleosomes act as barriers for transcriptional elongation, however, they are disrupted as the RNA polymerase passes through (*93*). Earlier studies claimed that nucleosomes shift upon RNA polymerase passage in 3' to 5' direction (*125*). This result was obtained from analysing countless genes and variations in turnover rates at the same time (*71*). However, more recent studies mentioned several hinderances hampering studies on nucleosome assembly in the context of replication, which result from the high speed of replication events of 2-4 kb/min (*126*). Hence, the limited temporal resolution of current techniques obscures transcription dependent maturation events of nascent chromatin in the vicinity of the replication fork. First indications that nascent chromatin undergoes maturation and regain accessibility were found in yeast where the NDRs at promotors gain rapid accessibility after replication and independent from the level of transcriptional activity (*84, 127, 128*). These initial observations were supported by studies in *Drosophila* S2 cells reporting that origin of replication (ORC) sites, which are highly accessible during the G1 phase of the cell cycle (*112, 129, 130*). ORCs become like other accessible regions drastically stronger occupied in nascent chromatin immediately after replication, however, they were opened in G1 within the course of one hour regardless of transcription (*51*).

Chromatin accessibility and nucleosome positioning in nascent chromatin was analysed by Mapping *In vivo* Nascent Chromatin with EdU and sequencing (MINCE-seq) in *Drosophila* S2 cells (*51*). Nascent DNA is labelled, and DNA fragments covered with nucleosomes and non-histone proteins can be sequenced. This method allows nascent chromatin analysis of high resolution (*131*), covering 10 - 20 kb of nascent chromatin at each replication fork (*51*). This study showed that nascent chromatin undergoes maturation directly after replication as

transcription is not limited to G1/0 phases of the cell cycle, but it also happens throughout the interphase.

The same observation was made in a global comparison for highly accessible promotors in G1 phase. These regions showed a rather uniform coverage in nascent chromatin with higher occupancy at former NDRs and reduced occupancy at +1 nucleosome positions. This suggests that nucleosomes fill in the NDR gaps during replication and replace transcription factors. Accordingly, abundance of transcriptional activators correlates with gain in nucleosomal signal in nascent chromatin demonstrating a direct link to transcription factor eviction. During the first hour after replication, the steady state pattern of G1 phase was largely re-established (Figure 1.3). Although individual nucleosomes are not discriminated like in other studies presented before, nucleosome positions at transcriptional inactive sites are conserved which further supports a positional memory of histones.

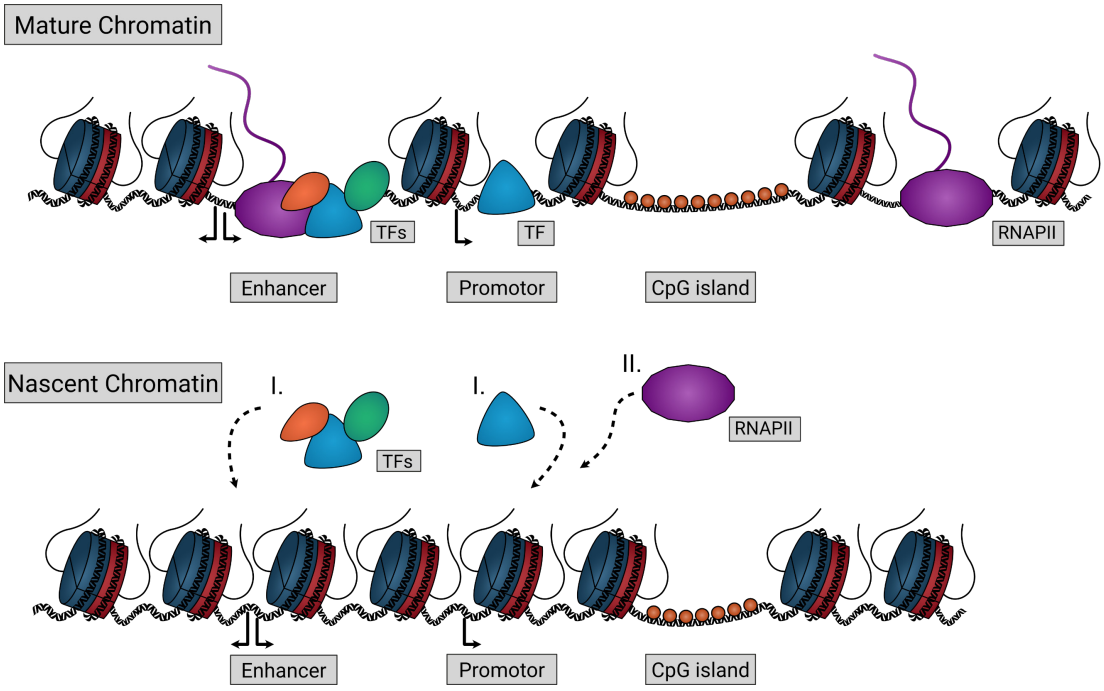

Figure 1.3 Chromatin maturation depends on transcription. Nascent chromatin is not accessible directly after replication as revealed by repliATAC. During maturation the chromatin becomes first accessible at CpG islands and super enhancers. Full accessibility patterns resembling the mature steady state relies however on active transcription (*118*). Modified from (*118*).

Evidence that the re-establishment of chromatin accessibility/nucleosomal landscape is mediated by the transcriptional program, which is maintained through replication, was achieved by comparing to distinct cell types of *Drosophila melanogaster*, namely S2 and BG3 cells, with different expression profiles, due to their different origin. S2 cells are of embryonic origin whereas BG3 cells are derived from the central nervous system (CNS) of 3rd instar larvae. The study showed that although the underlying DNA sequence is identical between both cell lines, only those genes which are actively transcribed in the respective cell line

regained accessibility during chromatin maturation. This finding argues against DNA sequence-dependent chromatin maturation and is consistent with previous findings showing that the chromatin landscape is only disrupted by passage of the replication at active sites and re-established in dosage depend manner by transcriptional activity (*51*).

Interplay of chromatin maturation and transcription was further supported by mapping global chromatin accessibility after replication by repliATAC-seq (Figure 1.3), where nascent chromatin is purified after EdU labelling and its accessibility analysed by ATAC-seq. Similar to results previously described for *Drosophila* S2 cells, nascent chromatin in mESCs showed no accessibility for transcription factors right after replication. Moreover, kinetics of restoration of accessibility patterns is dependent on DNA sequence (*118*), i.e. CpG-rich DNA elements are the first to be opened and thus resulting in accessible chromatin. In addition, super enhancers, previously described as highly active regions (*132*), are the first elements which are re-occupied with transcription factors (*51, 118*). Reduced chromatin accessibility for transcription factor binding in replicated chromatin is further supported by reduced occupation of RNAPII and transcriptional initiation marked by serine 5 phosphorylation (S5P) of its C-terminal domain (CTD) (*133*). Hence, it is not until transcription restarts that active chromatin states are re-established. Consistently, nascent chromatin does not regain G1 accessibility patterns in cells in which transcription had been blocked (*118*). Intriguingly, differences in chromatin maturation dynamics have been observed between distinct model systems. For example, transiently accessible chromatin regions were found in mESC as well as mouse embryonic fibroblasts (MEF) during reprogramming, which typically localize towards gene bodies, whereas in *Drosophila* S2 cells similar observations could not be made (*51, 84, 118*).

In conclusion, to re-establish the steady state transcription factor binding, remodeler recruitment, exposing of binding sites and promotors, and in turn re-establishment of methylation marks are important processes during chromatin maturation, relying at least in metazoans on transcription with distinct loci dependent kinetics (*70, 72, 118*). In this process, all transcription factors are disrupted and evicted from the replicating DNA, which prevents opportunistic transcription factor binding within gene bodies, hence potentially prevent spurious transcription.

.

1.1.6 Transcription coupled decoration of nucleosomes

To oppose the dilution of histone PTMs during DNA replication, histone modifying enzymes are required. Enzymes restoring PTM levels need to execute three main tasks which are reading existing modifications, writing new ones and/or erasing current ones (*134*). As indicated by the studies mentioned before, repressive chromatin domains extend over cell generations and repressive marks are acquired by parental and new nucleosomes equally (*113*). The common view is that two groups of proteins belonging to either the PcG, with its main actors PRC1 and PRC2 (see also above), and the antagonistic Trithorax group (TrxG) take over this responsibility in repressed and active chromatin states, respectively (*135*). Both protein groups were first described in *Drosophila melanogaster*, where TrxG proteins were shown to be involved in the activation of developmental *Hox* genes (*135, 136*). It remains unclear, whether in addition to this well characterized activity other global effects *Trx* might harbour (*137*). Additionally, many ATP dependent chromatin remodelers like Brahma (Brm) and female sterile homeotic (Fsh) which are related to mammalian SWI2 and Bromodomain-containing protein 4 (BRD4), respectively, belong to the TrxG group (*138, 139*). Albeit identification of Trx responsive elements (TRE), it was suggest that Trx histone methyltransferases (HMTs) rather interact with a specific subset of genes similar to PcG proteins which are recruited to PREs (*136*). More recent studies demonstrated that TrxG proteins are part of a bigger family of methyltransferases targeting nucleosomes, referred to as the COMPASS complex (complex of proteins associated with Set1) (*140*). The COMPASS complex distinguishes three COMPASS-like complexes in *Drosophila*, i.e., the trithorax-related (Trr)–like, Set1-like and finally the Trx-like complex. In Mammalia, six complexes have been identified which represent duplicates of the ones reported earlier in flies (*122, 141*). As described above, chromatin maturation depends on transcription and PTM decoration levels as well as restoration kinetics of active marks correlate with transcriptional activity and transcription factor abundance. The link between transcriptional activity and methylation of histones at TSSs and gene bodies is mediated by two methyltransferases, Set1 and Set2, which belong to Set1-like complex. Prominent modifications of the Set1-like complex in active chromatin are H3K4me3 and H3K36me3. Interestingly, both enzymes are recruited to their targets by interaction with the CTD of RNAPII. The CTD of RNAPII consists of several tandem repeats of YSPTSPS heptamers, the serines in this sequence undergo distinct phosphorylation states during the distinct phases of transcription. Set1 interacts with S5P of the CTD, predominantly found during transcriptional initiation, whereas Set2 binds predominantly to serine 2 phosphate (S2P) during transcriptional elongation. In turn, H3 histones are methylated in the vicinity of TSSs in gene bodies at lysine 4 and at lysine 36, respectively. In fact, the bulk di- or tri-methylations of H3K4 are mediated by Set1, as revealed by a drastic reduction of global H3K4me2/3 levels in dSet1 mutants (*141*). This

finding is consistent with the observation that in nascent chromatin , the absence of RNA polymerase II serine 5 phosphate (RNAPIIS5P) correlates with reduced levels of H3K4me3 (*70*). The analogues of Trx in mammals are mixed-lineage leukaemia 1 and 2 (MLL1 and MLL2), and MLL3 and MLL4 for Trr. Although they arose from duplication and exert similar functions in mammals as their *Drosophila* counterparts, all MLL lysine methyl transferases (KMTs) are mutually exclusive and not redundant. Several RNAi knockdowns revealed that in *Drosophila* dSet1 also acts through a multimeric protein complex like COMPASS in yeast and mammals by interaction with Ash2 (absent, small, or homeotic discs 2), Wds (will die slowly), dWdr82 (WD repeat domain 82) and dRbbp5 (Retinoblastoma binding protein 5) (*141*).

As described earlier, PcG members PRC1 and PRC2 were thought to execute antagonistic tasks and repress chromatin. With the identification of their roles in the decoration of poised enhancers, this image has shifted to a more context dependent manner of genome regulation. The catalytically active component of PRC2 is Enhancer of zeste (E(z)), which is mainly responsible for the establishment of H3K27me3 methylations (*142*), further supported by increased derepression in loss-of-function mutants and additional inappropriate *polycomb* silencing that leads to homeotic defect phenotypes in gain of function mutants (*143*). Other subunits of the PRC2 complex are responsible for nucleosome recognition and scaffolding (Su(z)12, Esc (extra sexcombs), Caf1-55/Nurf55) (*122*). In mammalian species, PRC1 is regarded to form two different complexes, a canonical and a non-canonical complex, respectively. Both variants contain mammalian RING1B/A which are E3 ubiquitin ligases acting on H2AK110 and correspond to *sex comb extra* (*Sce*) in *Drosophila melanogaster*. The canonical versions act by recruitment to H3K27me3 sites established by PRC2 which are recognized by Polycomb-like chromobox homolog (CBX) containing proteins that form subunits of PRC1. In contrast, the non-canonical PRC1 drives H2AK119 ubiquitination without previous action of PRC2. Intriguingly, non-canonical PRC1 can recruit PRC2 *via* ubiquitin marks which are recognized by PRC2 through its AEBP2 (AE Binding Protein 2) and JARID2 (Jumonji And AT-Rich Interaction Domain Containing 2) subunits, indicating an interplay of PRC1 and PRC2 to establish large H3K27me3 decorated domains (*122, 143, 144*). Still, PRC1 and PRC2 are indispensable for determining cellular identity, epigenetic memory, embryonic development not only in *Drosophila* but also in mammals as shown in murine models. The exerted direct function on gene expression has been suggested by occupation of differentiation genes by RING1B (Ring Finger Protein 1B) and OCT4 (Octamer binding transcription factor 4) in mice (*145*) and by corresponding knockouts which result in severe embryonic defects (*137*). Methylations in transcriptionally repressed chromatin domains as well as telomeric or pericentric heterochromatin involving H3K9me3 are established by Suppressor of variegation 3-9 (Su(var)3-9). Su(var)3-9 forms a positive

feedback loop with heterochromatin-associated protein 1 (HP1). Here, HP1 is recruited to H3K9me3 sites and interacts consecutively with DNA methyltransferase DNMT3A/B. Subsequently, MECP2 binds methylated DNA which recruits then Su(var)3-9 (*146, 147*).

1.2 Histone variants and chaperones

In contrast to the canonical histones, histone variants serve additional functions in genome organization, transcriptional control and DNA repair (*148–150*). As previously mentioned not only histone PTMs are associated with epigenetic inheritance but also histone variants (*26*) have been shown to localize with respect to transcriptional activities (*151*). Albeit canonical histones are exclusively expressed during S-phase, histone variants are constitutively expressed. They act in a replication independent manner in histone turnover and replacement, shaping the chromatin landscape in a cell type specific way and thereby they contribute to cell identity and the epigenetic profile (*26*).

The type and number of histone variants is different between eukaryotes. It is best described for plants (*Arabidopsis*), yeast and mammalian species, but the nomenclature concerning the variants is not consistent. Many of the described variants for H3, H2A and H2B are germline specific and expressed in oocytes, sperm or early embryonic development, like human H3.Y.1 and H3.Y.2 (*2, 152*).The replication independent variant H3.3, which makes up roughly 15%-25% of the bulk histone H3, is associated with transcriptionally active chromatin. Labelling of individual nucleosomes revealed that canonical histone H3.1 is rather associated with chromatin regions which replicate at a late stage during S-phase, whereas H3.3 preferentially locates to early replicating regions (*151*). Intriguingly H3.3 can compensate for the loss of replicative H3 as shown in human, where depletion of CAF-1 resulted in predominant positioning of H3.3 at the replication fork (*153*).

Although H3.3 differs in only four amino acids from the canonical H3 (H3.1 and H3.2 in humans), its sequence is highly conserved between animals species (*2, 154*). Interestingly, these few changes impede the deposition in a replication independent manner of H3. In fact, canonical H3 coprecipitates with the chaperone CAF-1, whereas H3.3 copurifies with major components of replication-independent assembly complexes such as Histone regulator A (HIRA) in active chromatin and Death-associated protein 6 (DAXX), which has a high affinity to H3K4me0 and H3K9me3, in pericentric or repressed chromatin (*91, 155*). Here, DAXX first deposits H3.3 which is then replaced by the ATP-dependent remodelling factor ATRX (*91, 156, 157*).

The most prominent difference in the amino acid sequence is serine 31 at the N-terminal end which is subject to phosphorylation (S31P) in the before mentioned chromatin domains.

Phosphorylation of S31 is enriched during mitosis and is speculated to act as signal for acetylation of H3.3K27, which in turn facilitates gene activation in developmental context (*98*) and causes p300 mediated acetylation of enhancers (*2, 158*).

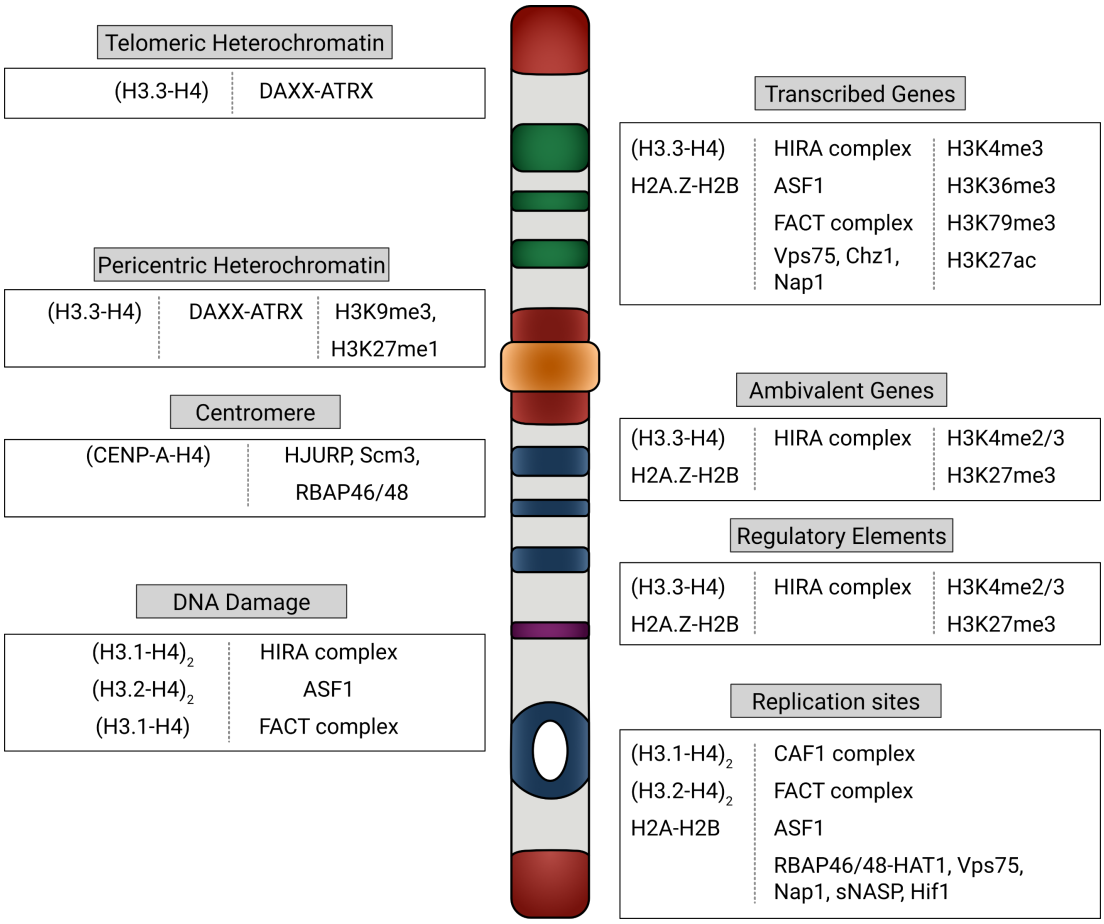

Figure 1.4 Histone variants and the cognate chaperons and chromatin remodelers. Histone variants are incorporated at specific sites by specific chaperones and chromatin remodelers to serve special functions by altering nucleosome lability or adding additional modification sites. Some variants like H3.3 are very similar to replication coupled H3 and might compensate for loss of H3 during transcription. Other variants like CENP-A, or cenH3, are specifically enriched at centromeric domains facilitating kinetochore formation. Modified from (*91, 159*).

Survivability of H3.3 knockouts differs between species. H3.3 knock-out mice are unable to form heterochromatin and show increased embryonic lethality (*160*) as well as histone to protamine transition defects (*161*), *Drosophila* males on the other hand exhibit meiosis impairment due to improper chromatin condensation. *Caenorhabditis elegans,* however, shows no scorable defect under such conditions (*162*).

Another histone H3 variant is CENP-A. This variant and similar isoforms (cenH3s) can be found in all eukaryotes at the centromeres (*163*) and, although it is a replication independent variant, its incorporation requires mitosis in metazoans (*164*). In contrast to the evolutionary conserved canonical H3, cenH3s have a rapidly evolving N-terminal domain (*165*). It was suggested that this reflects the need to adopt to the evolving underlying DNA sequence (*18, 166*). $(CENP\text{-}A\text{-}H4)_2$ nucleosome form alternating repeats, where the CENP-A containing

nucleosomes face the surface of the metaphase chromosome, whereas $(H3\text{-}H4)_2$ nucleosomes are located towards the inside of the condensed chromosome. This arrangement is thought to represent a scaffold for other kinetochore forming proteins which in turn facilitate the segregation of both chromatid (*26*).

For the canonical histone H2A several variants have been described in eukaryotes, which are H2A.X, H2A.Z, H2A.B and macroH2A. H2A variants are less conserved among recent species than H3.3, and the current believe is that H2A has evolved several times from an ancestral H2A.X, which is the only H2A isoform in yeast (*163, 166*). The variant H2A.B was found to accumulate over time at TSSs, gene bodies of transcribed genes as well as at DNA damage loci where it cause less compact chromatin with increased nucleosomal lability, which facilitates transcription and alternate splicing (*167*). The variant H2A.X functions as a demarcation of DNA double strand breaks by establishing large domains when phosphorylated in the vicinity of a double stand break (DSB) (*26*), but was also shown to be essential during chromatin condensation during spermatogenesis (*168*). H2A.Z has been linked with numerous, partly opposing functions, which seem also to differ among species (*169, 170*). It has been proposed to act in activation and repression of transcription, transcriptional elongation, DNA damage control and also in cell-cycle regulation and chromosome segregation (*163, 170–172*) as well as border formation of active and repressive chromatin domains (*173*). Most other H2A variants are predominantly expressed in the germline, where they are supposed to play an important role during histone to protamine transition and during female meiosis (*174, 175*).

While no H2B variant has been found in *Drosophila*, the *Arabidopsis* genome contains at least 11 H2B variants and additional ones were found in other angiosperm species (*176, 177*). In contrast, with H2B.1, subH2B and H2B.W, only 3 variants were initially described in mammalian species (*169*). All of these H2B variants are exclusively expressed in the germline and more recent findings suggest that they serve critical chromatin packaging functions in mammalian germ line cells, especially in oocytes (*178*). For humans, a single H4 variant is reported which localizes to rRNA transcription sites where it causes less compact chromatin due to an increased nucleosome lability (*179*).

It has been debated whether histone variants are recycled. However, recent studies showed that the histone variant H3.3 is indeed recycled with an efficiency similar to the canonical variants H3.1 and H3.2 (*100, 101*). Furthermore, H3.3 and H2A.X were shown to be represented in equal concentrations in nascent chromatin which argues for their accurate recycling. H2A.Z, on the other hand, was found to be completely depleted in replicated chromatin but its incorporation into chromatin increases within one cell cycle, although H2A.Z enriched domains do not necessarily need to localize at the same sites after the replication

(*113*). Interestingly, H3.3 containing nucleosomes are not disassembled into $(H3.3\text{-}H4)_2$ tetramers like the canonical H3 but are disrupted as two H3.3-H4 dimers as observed with the H2A-H2B complexes. This observation would in principle argue for a semiconservative segregation (*74, 180*).

1.3 *Df(2L)His^C* as model for parental histone segregation

Drosophila melanogaster is a prime model organism to address fundamental genetic and developmental questions. During embryogenesis and later larval and pupal development *Drosophila* undergoes complex morphological and genetic changes, yet these processes are well understood and characterized. Intriguingly, of all genomes known to date, the *Drosophila* genome is the only one that contains the canonical histone genes in two proximal histone clusters on one chromosome (*181*), which make them easily accessible for genetic manipulation. In these cluster, 23 histone gene units in total were annotated each containing one copy of every canonical histone gene. This, and an enormous number of assets for genetic manipulation make *Drosophila* a favourable model to study questions concerning nucleosome assembly and parental histone segregation.

In fact, the *DrosDel* deletion system (*182, 183*) was used to generate a chromosomal deletion of all histone gene units resulting in the defined histone null mutation called *Df(2L)His^C (184)* (subsequently referred to as "*His^C* mutants"). Although heterozygous flies are viable, homozygous *His^C* mutant embryos fail to express canonical histones during embryonic development. Before zygotic genome activation (ZGA) embryogenesis is supported by maternal contribution, however from mitotic cycle 15 onwards *de novo* histone supply would normally be maintained by synthesizing new histones from the zygotic histone clusters. It was shown that although *His^C* mutants cannot rely on newly deposited histones to the replication fork, the DNA is still faithfully replicated, yet mutant embryos arrest during the transition from G_2 to mitotic phase without activating DNA damage or replication checkpoints (*185*). This implies that chromatin assembly relying on parental histones only during S_{15} results in impaired chromatin architecture which leads to cell cycle arrest. Overexpression of histones during S_{15} in *His^C* mutants showed a rescue of the phenotype to different extents regarding the number of reintroduced histone gene units. (*184*). This implies that histone abundance and chromatin assembly during S phase have direct effects on cell cycle progression. The highly stereotypic phenotype and the invariant and well characterized embryonic development of *Drosophila* as well as the well-established tool kit for genetic manipulations, allows studies to address questions on parental histone segregation, positional memory, and epigenetic inheritance in the context of a developing organism.

1.4 Aims

Nucleosomes do not only serve to protect and package the DNA, but they also play an integral part in chromatin structure and gene regulation. Epigenetic information is encoded in post-translational modifications at the N-terminal residues of the different histone subunits. The combinatorial role of histone modifications, which beyond the DNA sequence itself represents an additional layer of control for transcriptional programs.

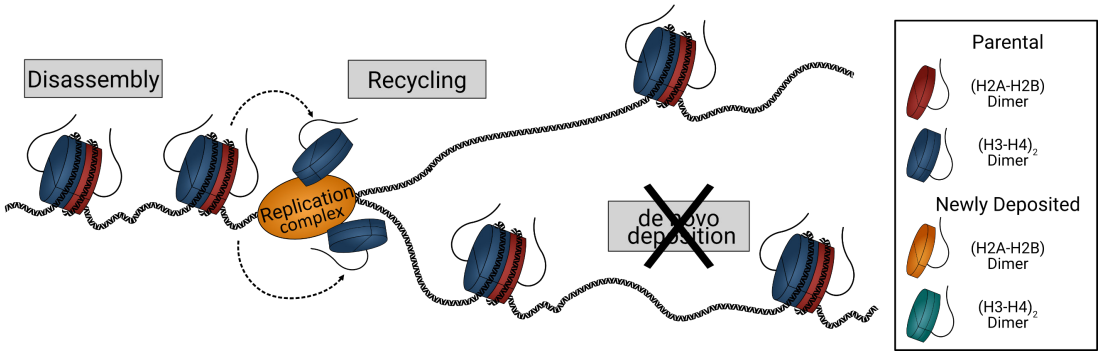

Figure 1.5 Histone *de novo* deposition in *His^C* mutants is not present. In *His^C* mutants the chromatin formation is supported by maternal contribution for the first 14 cell cycles. During mid blastula transition after mitosis 13 zygotic expression starts. Mutant embryos hence undergo one additional cell division without zygotic histone contribution but arrest subsequently in G2/M$_{15}$.

Chromatin and histone modifications need to be faithfully replicated during DNA synthesis. As the replication fork progresses during S-phase of the cell cycle, nucleosomes are disrupted, and the core particle is dismantled. Behind the replication fork new nucleosomes are formed by combining parental (pre-existing) and newly expressed histones. Accordingly, histones are exclusively transcribed during the S-phase of the cell cycle, which likely explains the presence of multiple copies of each histone gene to account for the high demand of histone protein during replication. The distribution of parental histones with newly synthesized DNA needs to be carefully coordinated to allow for re-establishment of the epigenetic landscape after DNA replication. Despite the rich body of results concerning specific aspects of these processes, which are in part still controversially discussed, the big picture of how regulatory chromatin is inherited from mother to daughter cells is not well understood.

Günesdogan et al. (*184*) reported that homozygous *Df(2L)His^C* deficiency mutants lack all canonical histone genes which are normally transcribed from the zygotic genome from S phase 14 (S$_{14}$) onwards. *His^C* mutant embryos undergo the first 15 nuclear divisions based on the maternally provided histones before they stop cell division prior to mitotic cycle 16, i.e., the cells arrest in the G2 phase of nuclear cycle 15 (G2$_{15}$). *His^C* mutant embryos still replicate DNA during S$_{15}$ at reduced speed but fail to upregulate the (*186*) String^{Cdc25} phosphatase, which drives the G2/M transition.

In the first chapter of my dissertation, I address the question of how parental histones are deposited onto newly synthesised DNA in the absence of *de novo* histone synthesis. Towards understanding this process, I studied parental nucleosome assembly in His^{C} mutants, which lack histone synthesis in S_{15} during embryonic development.

In the second chapter of my dissertation, I address the question which regulatory mechanisms are involved in the downregulation and control of String in cell cycle 15 of His^{C} mutants. To this end, I aimed to identify potential regulators of $String^{Cdc25}$ in the absence of histone synthesis.

2 Results

Chapter I: Positional memory of parental histones in the absence of *de novo* histone supply

Chapter II: The lack of histone synthesis results in a cell cycle arrest mediated by degradation of *string* RNA by How

2.1 Chapter I: Positional memory of parental histones in the absence of *de novo* histone supply

This manuscript contains the mayor part of data that was gathered in the project. It addresses with several genome wide approaches using next generation sequencing techniques, the effects that lack of histone *de novo* deposition poses on epigenetic inheritance and positional memory of nucleosomes during DNA replication. We analyse global chromatin accessibility, the effects on transcription and address the distribution of several histone modifications marking active and repressive states of chromatin. The model system we use is a *Drosophila melanogaster* mutant that lacks all genes to express canonical histones and that, due to its stereotypic embryonic development, allows us to analyse exactly the cell cycles in which histone supply is not present.

Authors

Dominik Mühlen*, Xiaojuan Li*, Oleksandr Dovgusha*, Herbert Jäckle, Ufuk Günesdogan

* These authors contributed equally

Status

in preparation for submission at 'Science, AAAS'

My contributions

- Contribution to the conceptualisation of the project[1]
- Husbandry of model system
- Preparation and conduction experiments
- Preparation or modification of figures[2]
- Data analysis[3]

[1] Together with Dr. Ufuk Günesdogan and Prof. Herbert Jäckle

[2] Together with Dr. Ufuk Günesdogan, Xiaojuan Li and Oleksandr Dovgusha

[3] Excluding data analysis of NGS data

Positional memory of parental histones in the absence of *de novo* histone supply

Dominik Mühlen[1,2,3], Xiaojuan Li[1,3], Oleksandr Dovgusha[1,3], Herbert Jäckle[2,*], Ufuk Günesdogan[1,2,*]

[1] University of Göttingen, Göttingen Center for Molecular Biosciences, Department of Developmental Biology, Justus-von-Liebig Weg 11, 37077 Göttingen, Germany

[2] Max Planck Institute for Biophysical Chemistry, Department for Molecular Developmental Biology, Am Fassberg 11, 37077 Göttingen, Germany

[3] These authors contributed equally

[*] Correspondence: hjaeckl@gwdg.de; ufuk.guenesdogan@uni-goettingen.de

2.1.1 Abstract

Epigenetic inheritance of histone modifications during cell division requires an orchestrated assembly of nucleosomes with parental and newly synthesized histones during DNA replication. We analysed *Drosophila* mutant embryos harbouring a deletion for all canonical histone genes, in which nucleosome assembly relies solely on parental histones from cell cycle 14 onwards. In the absence of histone synthesis, parental histones are recycled. However, they are not sufficient to re-establish the characteristic chromatin accessibility landscape. This results in upregulated as well as cryptic transcription, whereas the control of the developmental transcriptional program is partially maintained. During pre- and post-replication stages, histone modifications of H2A, H2B, and H3 are found in their original genomic position or close to it. The results suggest that parental histones harbour a 'positional memory' to propagate the epigenetic landscape after DNA replication *in vivo.*

2.1.2 Results

In eukaryotic cells, chromatin is composed of nucleosomes, which consist of DNA wrapped around a histone octamer with two copies of each of the proteins H2A, H2B, H3 and H4 as well as linker DNA and the linker histone H1. These histones are decorated with multiple posttranslational modifications (PTMs), which play an integral part in chromatin structure and transcriptional regulation. During replication of DNA in S phase, the replication fork disrupts parental nucleosomes into H3-H4 tetramers and H2A-H2B dimers (Fig. S1), which are recycled and reassembled together with newly synthesised histones to form the nucleosomes behind the replication fork (*1*). Recycled histones maintain their PTMs, which can serve as a 'template' for a read-write mechanism of old and new histones to re-establish the epigenetic landscape after cell division (*2, 3*). However, a pre-requisite for this process is that old histones harbour a genomic 'positional memory', i.e., they are reassembled in or close to their previous genomic position prior to replication fork passage. However, it is still unknown how parental nucleosomes are relocated during DNA replication *in vivo.*

*T*o study nucleosome distribution, the assembly as well as the positioning of histones carrying epigenetic marks during and after S phase in a developing embryo, we made use of a *Drosophila melanogaster* mutant, termed His^{C}, which harbours a deletion of all canonical histone genes (*His1, His2A, His2B, His3, His4) (4)*. Homozygous His^{C} mutant embryos (referred to as His^{C} mutants) fail to express histone genes after the maternal-to-zygotic transition from S phase 14 (S_{14}) onwards (Fig. S2A), causing a late embryonic lethal phenotype (*4*). The maternal histone pool is sufficient for the progression of the first 14 cell cycles (Fig. S2B, S3) (*4*). In the following S_{15}, the speed of DNA replication speed is reduced but completed, which results in a cell cycle arrest in $G2_{15}$ that is caused by the lack of $String^{Cdc25}$ phosphatase expression (Fig. 1A, S2B, S3) (*5*). Thus, nucleosome assembly during DNA replication in S_{15} relies solely on parental nucleosomes since no additional supply of newly synthesised histones in His^{C} mutant embryos is provided (Fig. 1A, S1).

Replication fork progression disrupts the binding of transcription factors and the nucleosomal landscape (*6*). Shortly after, nascent chromatin undergoes maturation by re-establishing the chromatin accessibility pattern (*6, 7*). To characterise this process in His^{C} mutant embryos, we performed ATAC-seq (Assay for Transposase-Accessible Chromatin using sequencing) with embryos at 3.5-4h, 4.5-5h, 5.5-6h, and 6.5-7h after egg laying (AEL) covering progression through S_{15}-S_{16} in wild type and S_{15}/$G2_{15}$ arrest in His^{C} mutants, respectively (Fig. 1A, S3, S4A) (*4*).

Principal component analysis (PCA) of ATAC-seq data shows global differences of the two genotypes along PC1 (68%), and separates samples based on developmental age by PC2

(12%) (Fig. S4B). This suggests that embryos lacking *de novo* histone synthesis partially proceed with the developmental programme albeit the prolonged S_{15} and subsequent cell cycle arrest as shown in an earlier study (*4*). Fragment size distribution showed that *His*^{C} mutants exhibit an enrichment for nucleosome-depleted regions (NDRs; ≤120bp) similar to wild type. However, the typical periodicity of nucleosome-spanning fragments (>120bp) is reduced with the most decreased median fragment size at 6.5-7h AEL (Fig. S5). To analyse the distribution of these fragments, we mapped the density of their midpoints and sizes relative to the nucleosome dyad centres (*8, 9*). Both wild types and *His*^{C} mutants show a characteristic V-shaped horizontal and vertical periodicity of nucleosome-spanning fragments at and around the dyad centres (Fig. 1B, Fig. S6), as described previously (*9*). However, the majority of these fragments is smaller in *His*^{C} mutants (~120-145bp) as opposed to wild types (~155bp-180bp), indicating the presence of subnucleosomes, which are wrapped by shorter stretches of DNA than complete nucleosomes (*10*). Overall, median nucleosome occupancy levels at transcription start sites (TSSs) +/-2kb and putative regulatory elements demarcated by ATAC-seq peaks were reduced, while the median distance between nucleosome dyad centres was increased (Fig. 1C, D, S7, S8). Thus, without the complementation with newly synthesised histones, parental histones are recycled but re-assembled at lower frequency and potentially as sub- and complete nucleosomes.

Next, we inspected ATAC-seq coverage tracks, which show relatively uniform distribution of reads with low but detectable enrichment at wild type peak locations throughout the genome (Fig. 1E, S9). This prompted us to analyse nucleosomal arrays around TSSs. ATAC-seq signals showed a characteristic positioning of nucleosomes in wild types. The NDR corresponded to TSSs and was surrounded by a -1-nucleosome upstream and a well-positioned +1 nucleosome downstream, followed by regular phased +2 and +3 nucleosomes (Fig. 1F, Fig. S10). In *His*^{C} mutants the -1/+1 nucleosomes were well-positioned comparable to wild type (Fig. 1F, Fig. S10). In contrast, the +2/+3 nucleosomes showed a positional shift and a gain in signal between the nucleosomes, which was particularly evident at TSSs of highly expressed genes, which we identified by RNA-seq (RNA sequencing, see below). This observation demonstrates that while parental nucleosomes are well-positioned around TSSs in *His*^{C} mutants, they are not regularly phased in nucleosomal arrays further downstream of TSSs. Thus, the characteristic nucleosomal landscape is only partially re-established and more accessible after S_{15}, resembling profiles of nascent chromatin shortly after DNA replication in *Drosophila* S2 cells or mouse embryonic stem cells (mESCs) (*6, 7*).

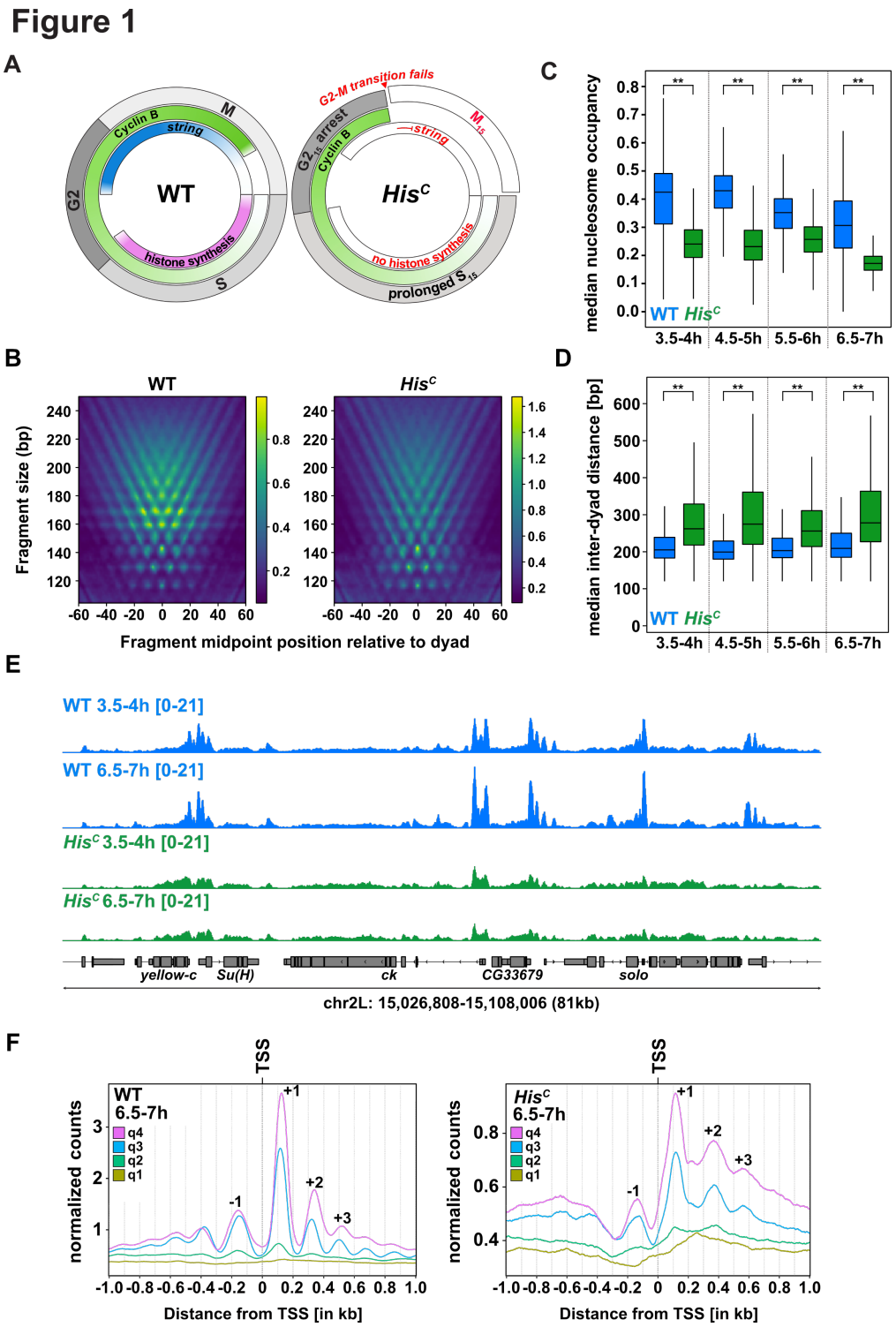

Figure 2.1 Fig. 1: Nascent chromatin in *His^C* mutants does not undergo maturation. (**A**) Schematic representation of cell cycle progression in wild type (WT) and *His^C* mutant embryos after the maternal-to-zygotic transition (based on (*4, 5*)). (**B**) V-plots show density of nucleosome-spanning fragments (>120bp) and sizes relative to nucleosome dyad centres. ATAC-seq data from embryos at 6.5-7h AEL (n = 3 biological independent replicates). (**C**) Median nucleosome occupancy +/- 2kb of TSSs. ATAC-seq data from embryos at 3.5-4h, 4.5-5h, 5.5-6h and 6.5-7h AEL (n = 3 biological independent replicates). Unpaired Wilcoxon test ***P<0.001.* (**D**) Median inter-dyad distances at ATAC-seq peaks demarcating putative regulatory elements in introns or intergenic region. Unpaired Wilcoxon test ***P<0.001.* (**E**) Representative snapshots of ATAC-seq coverage tracks. (**F**) Normalized ATAC-seq count distribution of mononucleosomal reads (180-240bp) at TSSs +/- 1kb of wild type (WT, left) and *His^C* mutant (right) embryos at 6.5-7h AEL. ATAC-seq reads were divided based on corresponding gene expression quartiles as determined by RNA-seq (q1 = lowest).

The formation of nucleosome arrays and chromatin compaction also depends on linker histone H1 *, 12*)(*11*. In HeLa cells, most histone H1 variants are incorporated into chromatin only after its maturation, suggesting a replication-independent deposition of linker histones (*13*). *Drosophila* harbours only a single somatic histone H1 variant (*14*). Thus, we asked whether the lack of zygotic histone H1 expression affects the chromatin structure in *His^{C}* mutant embryos. We performed CUT&Tag (Cleavage Under Targets and Tagmentation (*15*)) for H1 with embryos when most embryonic cells have completed or proceeded through late S_{15} at 5.5-6h AEL (*4*). Coverage tracks show a comparable H1 distribution in wild type and *His^{C}* mutants (Fig. 2A, S11A). H1 contacts the nucleosomal dyad as well as both linker DNAs of one nucleosome (*16*). Accordingly and consistent with a previous study (*12*), profiling of H1 occupancy around nucleosome dyad centres shows enrichment around nucleosome borders as well as a slight enrichment at the middle point of nucleosomes in wild type, which was also reminiscent in *His^{C}* mutants (Fig. 2B). Median H1 fragment length corresponds to mononucleosomal DNA as well as linker DNAs (~200bp) in wild type and is slightly increased in *His^{C}* mutants, which is consistent with increased inter-dyad distances of nucleosomes (Fig. S11B). These observations indicate that parental histone H1 is recycled and appropriately deposited during or after DNA replication despite the lack of zygotic histone H1 expression in *His^{C}* mutants.

Chromatin accessibility enables binding of transcription factors to regulatory elements and, in turn, the transcriptional machinery is directly or indirectly involved in maturation of nascent chromatin after DNA replication in mESCs (*7*). In *His^{C}* mutants, the chromatin landscape is apparently more accessible and reminiscent to nascent chromatin shortly after DNA replication (*6, 7*). Thus, we analysed transcriptional activity by RNA-seq with embryos at 3.5-4h, 4.5-5h, 5.5-6h, and 6.5-7h AEL. Consistent with the ATAC-seq data, PCA separates samples based on genotype (PC1, 68%) and developmental age (PC2, 18%) (Fig. S12A). Differential gene expression analysis identifies a large number of significantly upregulated genes in *His^{C}* mutants (2,944 at 6.5-7h AEL, absolute log2fold change>1, padj<0.01) (Fig. 2C, S12B). The upregulated genes include ectopic expression of genes associated with meiosis or post-meiotic stages such as *always early*, *wurstfest*, *protamine A*, and *protamine B*, which are normally not expressed during embryogenesis of wild type embryos (Fig. S12C). This finding prompted us to ask, whether the loss of *de novo* histone supply in S_{15} results in global loss of transcriptional control. To address this, we assigned significantly upregulated genes in *His^{C}* mutants to the corresponding expression levels in wild type (q0 = no reads, q1-4 = expression quartiles) (Fig. S12D). This shows that the majority of upregulated genes (>60%) belong to the lowly (q1) and moderately (q2) expressed genes in wild type embryos at the same stage. In addition, we clustered genes along the four developmental time points of wild type or *His^{C}* mutant embryos (Fig. 2D, Fig. S13). Subsequent gene ontology (GO)

analysis for the main cluster of upregulated genes reveals significantly enriched terms associated with developmental processes such as *cell migration*, *cell part morphogenesis* and *imaginal disc morphogenesis* (Fig. S14A). In contrast, the main cluster of downregulated genes is largely linked to 'general' cellular processes such as *RNA splicing* or *DNA metabolic process* in both genotypes (Fig. S14B). Taken together, these findings suggest that the recycling of parental histones in S_{15} is not sufficient to suppress inactive genes or maintain gene expression levels. However, *His^C* mutants are able to partially control the transcriptional program associated with embryonic development. Notably, despite the transcriptional activity the global nucleosomal landscape is not fully re-established, which is likely due to reduced nucleosome occupancy.

To gain mechanistic insight into how reduced nucleosome occupancy and altered nucleosome positioning results in the upregulation of transcription, we mapped transcriptional initiation and productive elongation by CUT&Tag for RNA Polymerase II (RNAPII), serine 2-phosphorylated RNAPII (RNAPIIS2P) and for the transcription-coupled histone mark H3K36me3 at 4.5-5h and/or 5.5-6h AEL, when most cells undergo and complete S_{15} in *His^C* mutants. In wild types, RNAPII is enriched at TSSs and throughout the gene body (Fig. S15A, B). RNAPIIS2P is associated with the transition from pausing to productive elongation and accordingly shows enrichment at TSSs and a decrease at transcription termination sites (Fig. 2E; Fig. S15B, C). H3K36me3 shows a promoter-proximal peak and an increasing enrichment from 5' to 3' of actively transcribed gene bodies (Fig. 2F; Fig. S15B, D, E). In contrast, RNAPII and RNAPIIS2P is enriched in gene bodies rather than TSSs in *His^C* mutant embryos (Fig. 2E; Fig. S15A-C). Similarly, promoter proximal H3K36me3 is depleted, but shows an enrichment towards the 3'end of gene bodies (Fig. 2F; Fig. S15B, D, E). These results suggest a premature release of RNAPII into transcriptional elongation and/or cryptic transcription initiation within gene bodies.

To address this conclusion, we analysed H3K4me2 enrichment at 4.5-5h and 5.5-6h AEL. H3K4me2 is enriched on nucleosomes flanking NDRs and associated with RNAPII stalling at TSSs and thus coupled to the onset of transcription (*15*). We performed CUTAC (Cleavage Under Targeted Accessible Chromatin (*17*)) for H3K4me2, which is an approach to re-direct tagmentation to NDRs to generate essentially chromatin accessibility maps that mirror NDR ATAC-seq reads (<120bp) at TSSs in wild type (Fig. 3A, Fig. S16**)**. However, in *His^C* mutants H3K4me2 CUTAC read coverage was broadly enriched downstream of TSSs (Fig. 3A, Fig. S16), suggesting a premature release of RNAPII into elongation.

Figure 2

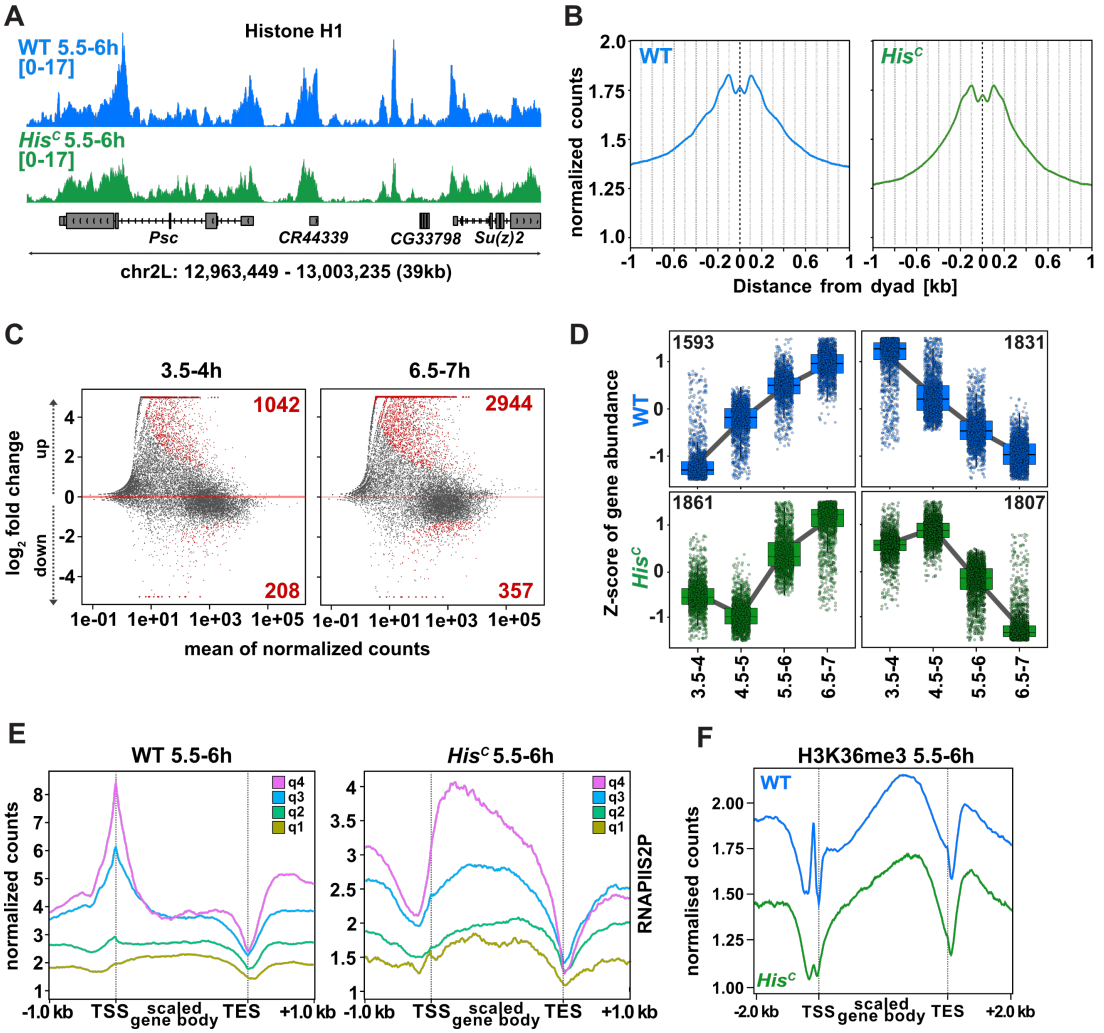

Figure 2.2 Fig. 2: Aberrant transcription in *His*^{C} mutants. (**A**) Representative snapshots of Histone H1 CUT&Tag coverage tracks of wild type (WT, blue) and *His*^{C} mutant (green) embryos at 5.5-6h AEL. (**B**) Profile plot of Histone H1 CUT&Tag normalized counts of wild type (WT, blue) and *His*^{C} mutant (green) embryos at 5.5-6h AEL at TSSs. (**C**) MA plots showing differential gene expression analysis of RNA-seq data with wild type (WT) and *His*^{C} mutant embryos at 3.5-4h and 6.5-7h AEL. Each transcript is represented by a dot (grey: not significant, red: significant (absolute log2fold change>1, padj<0.01)). (**D**) Clustering of genes based on their RNA-seq expression dynamics from 3.5-4h, 4.5-5h, 5.5-6h to 6.5-7h AEL for wild types (WT) and *His*^{C} mutants. Shown are the two major clusters of up- or down-regulated genes. (**E**) Profile plots of RNAPIIS2P CUT&Tag normalized counts across gene bodies of wild type (WT) and *His*^{C} mutant embryos at 5.5-6h AEL separated by associated gene expression quartiles (q1 = lowest). (**F**) Profile plots of H3K36me3 CUT&Tag normalized counts across gene bodies of wild type (WT) and *His*^{C} mutant embryos at 5.5-6h and 6.5-7h AEL separated by associated gene expression quartiles (q1 = lowest).

To examine, whether reduced nucleosome occupancy results in cryptic transcription, we performed STRIPE-seq (Survey of Transcription Initiation at Promoter Elements with high-throughput sequencing (*18*)) with embryos at 5.5-6h and 6.5-7h AEL to map transcription start regions (TSRs). STRIPE-seq counts at promoter regions were positively correlated with the level of gene expression (Fig. S17, S18A). The density of TSRs was centred around TSS positions but less pronounced in *His*^{C} mutants (Fig. S18B). Consistently, TSRs were largely annotated to promoter regions (≥75% in wild type; ≥55% in *His*^{C} mutant), but a considerable larger fraction was associated with other genomic regions including exons, introns, and

intergenic regions in *His^C* mutants (≤20% in wild type; ≤39% in *His^C* mutants) (Fig. 3B, Fig. S18C, S19). This difference became more evident, when we called differential TSRs in *His^C* mutants, many of which were associated with regions outside of promoters (≤57%) (Fig. 3C). Consistent with the TSR annotation, we found a significant increase of normalized STRIPE-seq read counts at exons and introns (Fig. 3D). To test, whether intergenic TSRs correlate with cryptic transcription, we analysed normalized RNA-seq counts 1kb upstream of these TSRs. This showed a significant increase in *His^C* mutants (Fig. 3E). Taken together, this suggests that reduced nucleosome occupancy and increased nucleosome spacing cause cryptic transcription initiation within gene bodies as well as intergenic regions.

PTMs are associated with chromatin accessibility and transcriptional control. Since *His^C* mutants are capable to partially control the developmental transcriptional programme, we asked whether the epigenetic landscape is re-established during and/or after S_{15} by performing CUT&Tag for H3K4me3 at 3.5-4h, 5.5-6h and 6.5-7h AEL. H3K4me3 deposition is transcription-coupled and represents a hallmark of active transcription (*15*). In wild types, it showed a bimodal enrichment at TSSs followed by a decline across gene bodies, while the level of enrichment positively correlated with gene expression quartiles (Fig. 4A, Fig. S20A). In *His^C* mutants, the enrichment profile at TSSs is comparable but followed by a broader profile across gene bodies (Fig. 4A, Fig. S20A). This finding is consistent with cryptic transcription initiation within gene bodies. However, coverage tracks show broadly a similar peak pattern between genotypes (Fig. 4B, S20B). To compare H3K4me3-enriched loci, we used narrow peak calling (MACS2). This comparison showed a subset of common peaks, which were robustly enriched for H3K4me3 (Fig. 4C, S20B, S21). Furthermore, we identified a subset of peaks with low but significant levels of H3K4me3 specific for *His^C* mutants, which however are predominantly found in close proximity to the common peaks (Fig. 4C, S20B, S21). Considering that H3K4me3 enrichment profiles did not significantly change across developmental time points, these results indicate that parental histones with H3K4me3 are deposited in close proximity or are located even at the genomic position they were holding prior to replication. Alternatively, unmodified parental histones could be sufficient to re-establish the H3K4me3 landscape as a result of transcriptional activity.

Figure 3

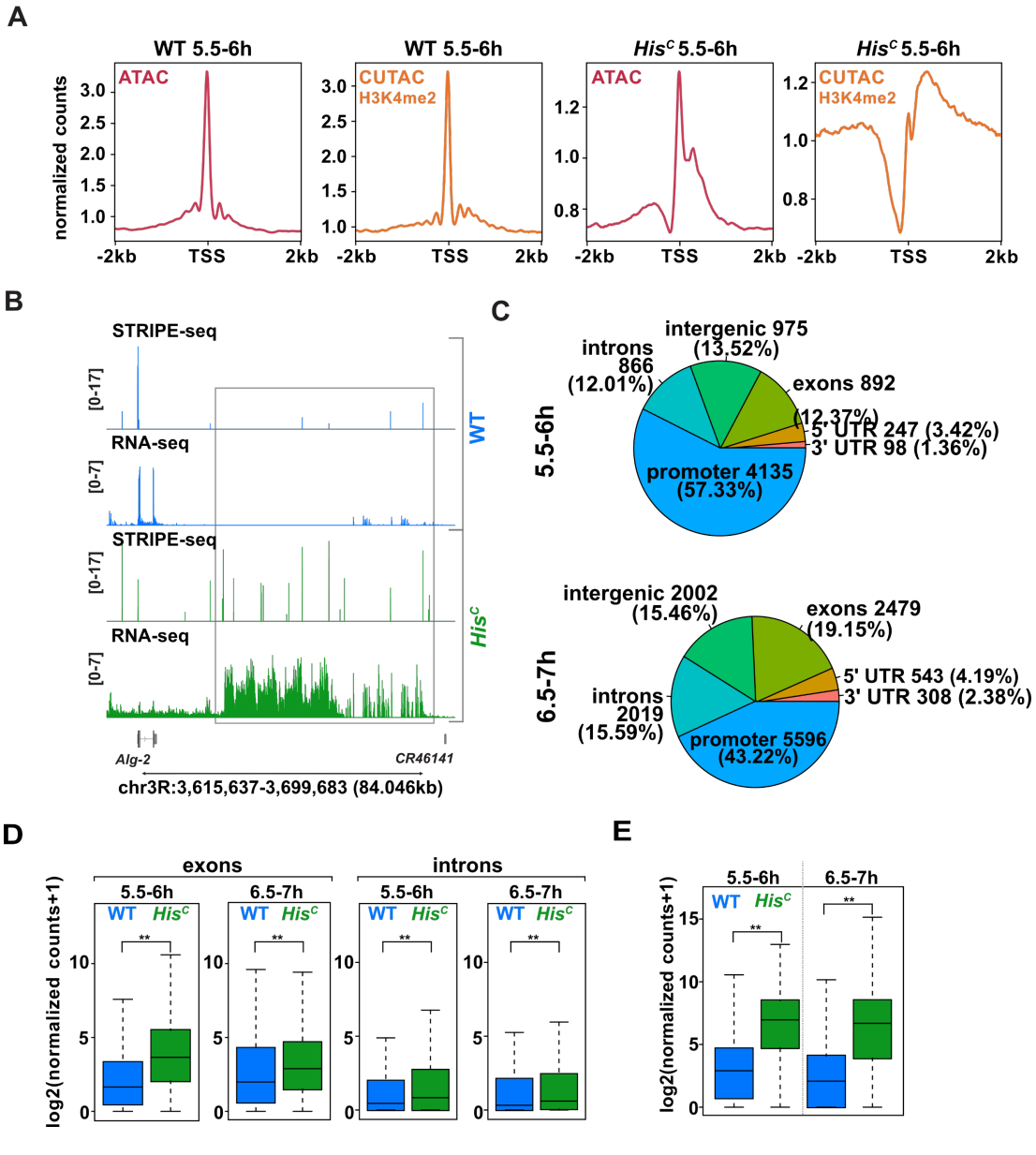

Figure 2.3 Fig. 3: Premature release of RNAPII into elongation and cryptic transcription initiation in *His^C* mutants (**A**) Comparison of ATAC-seq and H3K4me2 CUTAC profile plots (≤120bp reads) of wild type (WT) and *His^C* mutant embryos at 4.5-5h AEL at TSSs. (n = 2 biological independent replicates CUTAC). (**B**) Representative snapshot of STRIPE-seq and RNA-seq coverage tracks of wild type (WT, blue) and *His^C* mutant (green) embryos at 6.5-7h AEL on chromosome (chr) 3R. n = 5 biological independent replicates. (**C**) Genomic annotation of differential TSRs (*His^C* vs WT) at 5.5-6 and 6.5-7h AEL. (**D**) Box plots showing normalized STRIPE-seq counts (log2+1) within exons and introns of wild type (WT, blue) and *His^C* mutant (green) embryos at 5.5-6 and 6.5-7h AEL. Unpaired Wilcoxon t-test ***P*<0.0001. (**E**) Box plots showing normalized RNA-seq counts 1kb downstream of intergenic TSRs of wild type (WT, blue) and *His^C* mutant (green) embryos at 5.5-6 and 6.5-7h AEL. ***P*<0.0001.

To distinguish between these two possibilities, we performed CUT&Tag for the transcription-independent marks H3K27ac and H3K27me3 at 4.5-5h and/or 5.5-6h AEL. H3K27ac is associated with active promoters and enhancers (*19*). It shows a bimodal enrichment at TSSs and is depleted towards the 3'end of gene bodies in wild types (Fig. 4D, Fig. S22A). In *His^C* mutants, however, H3K27ac levels are generally low, reduced at TSSs but enriched

throughout the gene bodies (Fig. 4D, Fig. S22A). Narrow peak calling shows a robust subset of peaks common to both wild type and *His*^{C} mutants in addition to genotype-specific peaks (Fig. 4E, Fig. S22B). Inspection of coverage tracks reveal a similar enrichment of H3K27ac at many loci (Fig. 4B, Fig. S23A). However, the enrichment profiles were broader in *His*^{C} mutants, and some regions showed ectopic enrichment. The PRC2 (Polycomb Repressive Complex 2)-dependent mark H3K27me3 is associated with repression and shows enrichment in a common subset of broad peaks (Fig. 4F, Fig. S22B). However, in contrast to the active marks H3K4me3 and H3K27ac, H3K27me3 levels were comparable in both wild type and *His*^{C} mutants (Fig. 4G, Fig. S23B). Further, two subsets of peaks were called with high or low enrichment of H3K27me3 in *His*^{C} mutants or wild types (Fig. 4F, Fig. S22B). Taken together, the results show that H3K27ac and H3K27me3 enrichment is similar in both *His*^{C} mutants and wild type. This suggests that parental histones carrying active or repressive marks, which are deposited independent of transcription, largely maintain their genomic position during and after replication. While the deposition of parental histones with H3K27me3 correlates well between the two genotypes, H3K27ac enrichment is more broadly dispersed, which could be due to dis- and re-assembly of nucleosomes during transcription.

Finally, we asked whether H2A-H2B dimers decorated with PTMs are recycled in a similar manner as $(H3\text{-}H4)_2$. We performed CUT&Tag for H2AK9ac and H2BK16ac at 4.5-5h and 5.5-6h AEL. Both modifications are broadly enriched across gene bodies in both genotypes (Fig. S24A). Similar to the H3K27me3 data, peak calling shows a robust subset of common peaks, and two subsets of peaks with higher levels of the marks in either wild type or *His*^{C} mutants (Fig. 4H-I, Fig. S24B, S25). This result suggests that in the absence of newly synthesized histones, H2A-H2B dimers harbouring PTMs maintain their positional information.

Figure 4

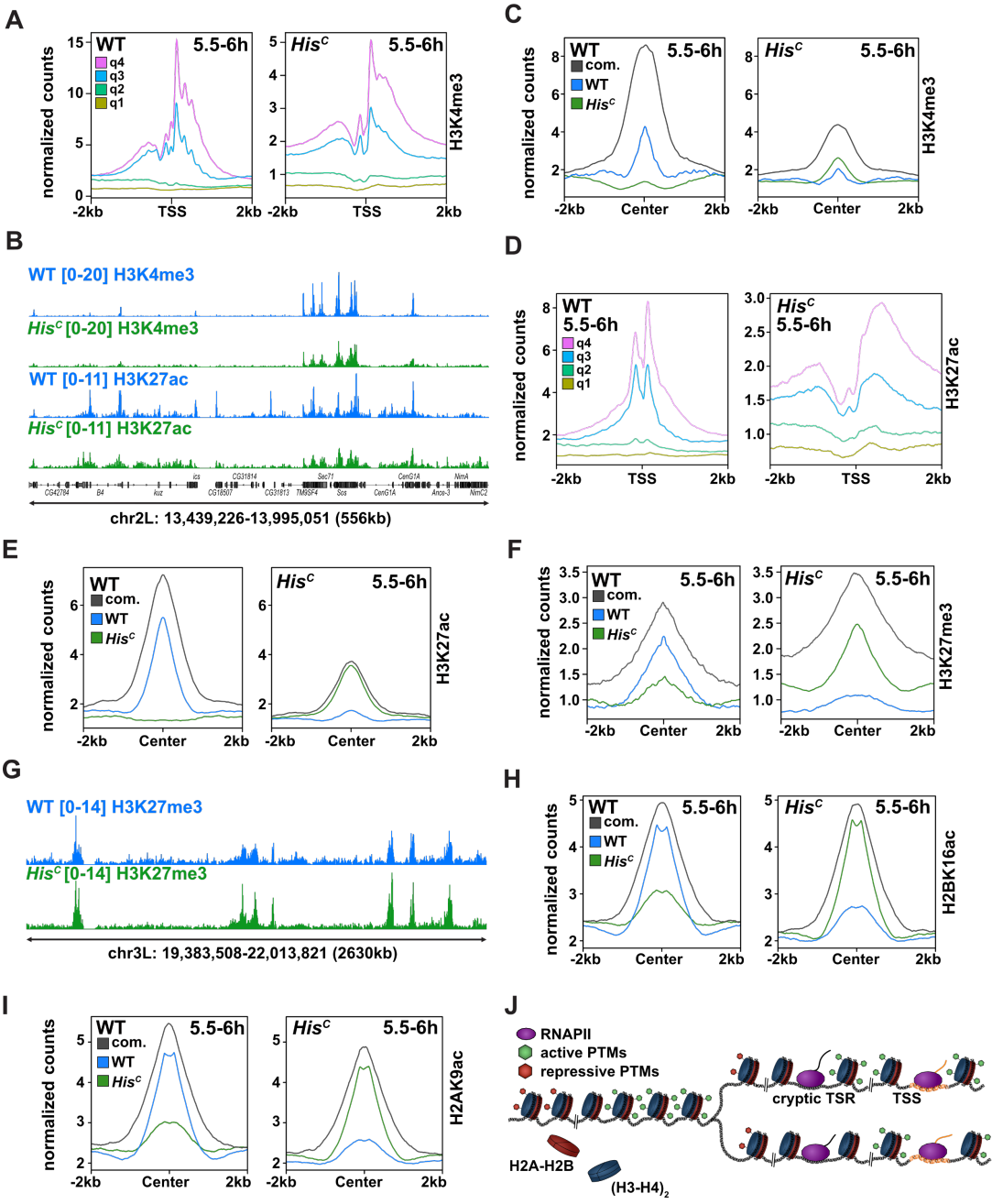

Figure 2.4 Fig. 4: The epigenetic landscape is re-established in *His*^{C} mutants. (A) Profile plots of H3K4me3 CUT&Tag normalized counts at TSSs of wild type (WT) and *His*^{C} mutant embryos at 5.5-6h AEL separated by associated gene expression quartiles (q1 = lowest). (B) Representative snapshot of H3K4me3 and H3K27ac CUT&Tag coverage tracks of wild type (WT, blue) and *His*^{C} mutant (green) embryos at 5.5-6h AEL on chromosome (chr) 2L. (C) Profile plots of H3K4me3 CUT&Tag normalized counts at called peaks (NarrowPeak) of wild type (WT) and *His*^{C} mutant embryos at 5.5-6h AEL. (D) Profile plots of H3K27ac CUT&Tag normalized counts at TSSs of wild type (WT) and *His*^{C} mutant embryos at 5.5-6h AEL separated by associated gene expression quartiles (q1 = lowest). (E) Profile plots of H3K27ac CUT&Tag normalized counts at called peaks (NarrowPeak) of wild type (WT) and *His*^{C} mutant embryos at 5.5-6h AEL. (F) Profile plots of H3K27me3 CUT&Tag normalized counts at called peaks (BroadPeak) of wild type (WT) and *His*^{C} mutant embryos at 5.5-6h AEL. (G) Representative snapshot of H3K27me3 CUT&Tag coverage tracks of wild type (WT, blue) and *His*^{C} mutant (green) embryos at 5.5-6h AEL on chromosome (chr) 3L. (H) Profile plots of H2BK16ac CUT&Tag normalized counts at called peaks (BroadPeak) of wild type (WT) and *His*^{C} mutant embryos at 5.5-6h AEL. (I) Profile plots of H2AK9ac CUT&Tag normalized counts at called peaks (BroadPeak) of wild type (WT) and *His*^{C} mutant embryos at 5.5-6h AEL. (J) Model showing nucleosome assembly in the absence of histone synthesis in *His*^{C} mutants.

Our study shows that parental nucleosomes are recycled and re-assembled during DNA replication in the absence of histone synthesis in a developing organism (Fig. 4J). This is consistent with results using *Xenopus* egg extracts, where depletion of free histones results in an increase of histone recycling rather than eviction (*20*). However, parental histones are insufficient to maintain normal regulation of transcription due to reduced nucleosome occupancy, associated with altered chromatin accessibility and irregular nucleosome positioning. This is associated with premature release of RNAPII into elongation as well as cryptic transcription. The latter result is consistent with previous studies showing that irregular nucleosome positioning results in cryptic transcription (*21*). Here we show that despite these notable effects on the chromatin landscape, the genomic positions of histone modifications are not substantially altered during or after DNA replication. One explanation for this observation is that histone variants could partially compensate for histone demand, as shown for H3.3, a variant functionally redundant with H3 (*22*). Alternatively, or in addition, nucleosomes of His^C mutants are only re-assembled as subnucleosomes including hexasomes or hemisomes. Such subnucleosomes are wrapped by shorter stretches of DNA and are more fragile than nucleosomes (*10*). Therefore, this might explain our results showing reduced ATAC-seq fragment length distribution and nucleosome occupancy while maintaining the epigenetic landscape.

Notably, it was shown that histones at the *GAL10* locus in yeast maintain a positional memory during DNA replication (*23*), which is also the case for parental histone H3 carrying active and repressive marks in HeLa cells (*24*). In mouse ESCs, however, only parental histone H3 with repressive marks maintain their genomic position during DNA replication (*25*). These differences could point towards a cell-type specific mode of epigenetic inheritance during cell division. Our study reveals that in a developing organism, active and repressive PTMs largely maintain their positional information, but show different degrees of variability, i.e., the active H3K27ac mark is locally enriched but more dispersed as opposed to the repressive mark H3K27me3, which exhibits a wild type-like profile. Moreover, our study establishes that parental histone H1 is recycled, and that not only histone H3 but also H2A and H2B marks maintain positional information during DNA replication

2.1.3 Material and Methods

2.1.3.1 Fly strains and embryo collection

w^{1118} flies were used as wild type controls. To generate homozygous *His*^{C} mutant embryos for genome-wide approaches, we crossed heterozygous *Df(2L)His*^{C}*, P{GAL4-twi.2xPE}/ CyO, P{ftz-lacB}E3* with *Df(2L)His*^{C}*, P{UAS:eYFP}AH2/ CyO, P{ftz-lacB}E3* flies. The resulting eYFP-expressing embryos with the genotype *Df(2L)His*^{C}*, P{GAL4-twi.2xPE}/ Df(2L)His*^{C}*, P{UAS:eYFP}AH2* were identified under a fluorescence stereomicroscope and collected with a P20 pipette. For time-staged embryo collections, flies were kept in cages covered by an apple agar plate at 25C. Egg deposition on apple agar plates was restricted to 30 min, which were subsequently aged at 25C for 3.5, 4.5, 5.5 or 6.5h. For fluorescent *in situ* hybridization and immunostaining, heterozygous *Df(2L)His*^{C}*/ CyO, P{ftz-lacB}E3* flies were crossed.

2.1.3.2 Total RNA isolation

Embryos were dechorionated in 50% bleach and washed three times with PBS with 0.1% Tween-20 (PBS-T). Embryos were preserved in RNAlater (Invitrogen) and macerated in 50µl RLT buffer (Qiagen RNeasy Plus Micro kit) using a pre-cooled 1ml Dounce homogenizer. The lysate was passed through a QIAshredder spin column (Qiagen). RNA was then isolated using the Qiagen RNeasy Plus Micro kit. RNA concentration and quality was determined using a NanoDrop 2000 Spectrometer (Thermo Scientific), Qubit 2.0 Fluorometer (Invitrogen) and/or a 2200 TapeStation with High Sensitivity RNA screen tapes (Agilent).

2.1.3.3 RT-qPCR

cDNA was amplified using QuantiTect Reverse Transcription kit (Qiagen) with 50ng of input RNA. qPCR was performed using KAPA SYBR FAST master mix (2x) (Kapa Biosystems). Relative gene expression was analysed using the comparative ΔΔCt method (*26*) using *act5C* for normalization.

2.1.3.4 Fluorescent *in situ* hybridization and immunostaining

RNA probes were designed to cover ~1000bp of the coding sequence of the *string* gene. A PCR fragment was amplified from genomic DNA using a reverse primer with a T7-promotor (GAA TTG TAA TAC GAC TCA CTA TAG G) overhang. *In vitro* transcription was performed using T7 Polymerase (Roche) and DIG (Digoxigenin)-RNA labelling mix (Roche): 1µl PCR product 150-250ng, 10x Buffer, 1µl DIG labelling mix, Protector RNAse Inhibitor (40U/µl; Roche), 0.5µl T7 Polymerase, DEPC- H_2O to 10µl). Reverse transcription was carried out for 2 hours at 37°C. The probe was precipitated and resuspended in 100µl resuspension buffer (50% formamide, 0.1% Tween-20, 5x SSC pH5, Heparin 20µg/µl). Fluorescent *in situ*

hybridization was performed as previously described (*27*) using sheep anti-Digoxigenin-POD antibody (Roche, 11207733910). Embryos were subsequently incubated with mouse anti-Cyclin B antibody (1:1000; Hybridoma Bank, #2245815) and chicken anti-beta galactosidase (1:1000; Rockland, 200-901-036) in PBS-T overnight at 4°C. The samples were washed 3 times for 15 min with PBS-T and incubated with secondary antibodies for 2h at room temperature in the dark on a rotator. Secondary antibodies were Alexa Flour 488 goat anti-chicken IgY (1:2000; Invitrogen, A11039) and Alexa Flour 647 goat anti-mouse IgG (1:2000; Invitrogen, A21235) in PBS-T. DNA was visualized by incubation for 15 min with DAPI (1:1000). Embryos were mounted using VectaShield antifade mounting medium (Vector Laboratories, VEC-H-1000). Fluorescence was detected using a LSM 980 and Axioplan2 microscopes (Carl Zeiss).

2.1.3.5 RNA-seq

80ng of total RNA was used as input for each library preparation using Nugen Ovation *Drosophila* RNA-seq Systems 1-16 (0350-32). cDNA fragmentation was performed using a Covaris S2 (duty factor 10%, cycle burst 200, intensity 5, 210s) sonicator. Libraries were amplified. Libraries were multiplexed and sequenced (single end read 50) using an Illumina Hi-Seq 4000 rapid run.

2.1.3.6 ATAC-seq

ATAC-seq was performed as previously described (*28, 29*) with minor changes. We isolated ~50,000 nuclei from 10 His^C mutant embryos for each experiment. To isolate a similar number of nuclei from wild type embryos, we collected 10 embryos at 3.5-4h AEL, 8 at 4.5-5h and 5.5-6h AEL, and 7 at 6.5-7h AEL. In brief, nuclei were isolated in 50µl lysis buffer (10mM Tris-HCl ph7.4, 10mM NaCl, 3 mM MgCl, 0.1% IGEPAL CA-630) and chromatin was tagmented in 45µl transposase mix (22.5µl TDE1 Buffer, 23.75µl dd H_2O, 1.25µl TDE1) for 75 minutes (Illumina TDE1 Tagment DNA Enzyme 15027865 , TD Buffer 15027866). Tagmented DNA was purified and subjected to PCR amplification using following parameters: Gap filling I 58°C for 5 min, Gap filling II 72°C for 5 min, Denaturation 98°C for 30s, 11x [Denaturation 98°C for 10s, Annealing 63°C for 30 sec, Extension 72°C for 1 min], final extension 72°C for 3 min. Library was purified using 1.3x volume AMPure XP Beads (Beckman Coulter, A63881) and resuspended in 22µl 0.1xTE buffer.

2.1.3.7 CUT&Tag

CUT&Tag was performed as described previously (*15*) with minor changes. Digitonin (Sigma-Aldrich, D141-100MG) was added to the final concentration of 0.05% to the respective buffers prior use. 15 His^C mutant and 12 wild type embryos were collected for each

experiment. Embryos were macerated using a 1ml Dounce homogenizer with 5-7 gentle strokes with a loose-fitting glass pestle in ice-cold PBS containing protease inhibitors (Roche, 4693132001). The cell lysate was centrifuged at 1200g for 5 min at 4°C. The supernatant was discarded, and the pellet resuspended in ice-cold nuclear extraction buffer. The volume of Concanavalin A (ConA) beads (Bangs Laboratories, BP531) per samples was adjusted to 5µl. The nuclei were treated as described (*15*) and bound to the ConA beads. The beads were incubated in 50µl antibody buffer containing 1x BSA and 0.5µg of primary antibody. Each sample was then incubated O/N at 4°C on an orbital shaker. The tubes were placed on a magnet and the supernatant was discarded. 50µl secondary antibody solution (1:100 in digitonin wash buffer 150), was added and then incubated for 1h at room temperature. The beads were bound to a magnet and washed twice with digitonin wash buffer 150. 1µl of Epicypher CUTANA pAG-TN5 (15-1017-EPC) mixed with 19µl digitonin wash buffer 300 was added to the beads and mixed by pipetting. After incubation at room temperature for 1h, the beads were separated on a magnet and washed twice with *stringent* digitonin wash buffer 300 without disturbing the beads. Tagmentation, stopping and nuclei release was performed as described (*5*). For library amplification 2x NEBnext HiFi PCR mix (M0541S) or 2x Epicypher HiFi PCR mix (15-1018-EPC) was used. The following PCR program was used for all libraries: Gap filling I 58°C for 5min, Gap filling II 72°C for 5min, Denaturation 98°C for 30s, 11x[Denaturation 98°C for 10s, Extension 60°C for 10s], final extension 72°C for 1min. Libraries were purified using 0.9x volume AMPure XP Beads (Beckman Coulter, A63881) and resuspended in 22µl 0.1xTE Buffer. Libraries were multiplexed and sequenced (paired-end read 100) using a NovaSeq 6000 (SP or S1 flow-cell).

2.1.3.8 CUTAC

CUTAC was performed as described previously (*17*) using a rabbit anti-H3K4me2 antibody (Active Motif, 39142). The same adjustments that were made for CUT&Tag were also applied for CUTAC. Tagmentation was performed by incubating the samples for 20 minutes at 37°C with CUTAC-hex tagmentation solution (5 mM MgCl2, 10 mM TAPS, 10% 1,6-hexanediol) in a thermocycler. Stopping, nuclei release and library amplification, as well as clean-up was performed as described for CUT&Tag. Libraries were multiplexed and sequenced (paired-end read 100) using a NovaSeq 6000 (SP flow-cell).

2.1.3.9 STRIPE-seq

STRIPE-seq was performed as described previously (*18*). 200ng of total RNA was used as input for each replicate. TEX master mix (MP Biomedicals, 0210309705) was prepared by mixing 0.2µl Terminator Exonuclease (Lucigen, 162370) and 0.2µl of Terminator Exonuclease Reaction Buffer A per sample. To digest uncapped or degraded mRNA, as well

as rRNA, 1.6µl or 200ng of total RNA was incubated with 0.4µl TEX master mix and incubated for 1 hour at 30°C in a thermocycler. After incubation, the reverse transcription oligonucleotide was annealed by adding 1.5µl sorbitol/trehalose solution (Dot Scientific, DSS23080-500, MP Biomedicals, 0210309705), 1µl RTO (10µM) and 0.5µl dNTPs (10mM each) to each sample. The reactions were mixed by vortexing, spun down, and incubated first at 65°C for 5 minutes and then kept at 4°C for 2 minutes. For the template switching reverse transcription reaction 2µl 5M betaine, 2µl 5x Superscript IV reaction buffer (Invitrogen, 18090050B), 0.5µl 0.1M DTT and 0.5µl SuperScript IV reverse transcriptase (Invitrogen, 18090010) were mixed by vortexing and added to each RTO annealing reaction. The samples were incubated in a thermocycler at 25°C for 10 minutes followed by 42°C for 5 minutes. Without removing the samples from the thermocycler 0.25µl of 400µM template switching oligonucleotide was added and the reactions were incubated subsequently for 25 minutes at 42°C followed by 10 minutes at 72°C. The samples were purified by adding 1.1x volume of AMPure XP beads (Beckman Coulter, A63881). After thorough mixing the samples were incubated at room temperature for 10 minutes followed by bead separation on a magnet. The beads were washed with 200µl 70% ethanol, air dried and eluted in 20µl nuclease free water after incubation at room temperature for 10 minutes. For library amplification 2.5µl of forward library oligo (FLO) and reverse library oligo (RLO) were added together with 25µl of 2x NEBnext ULTRAII Q5 HiFi PCR master mix. PCR was conducted with following parameters: Denaturation 98°C for 3min, 14x [Denaturation 98°C for 20s, Annealing 60°C for 15s, Extension 72°C for 45s], final extension 72°C for 2min. Libraries were purified with double sided size exclusion using first 0.5x volume AMPure XP beads than increasing to 0.9x volume. Libraries were resuspended in 22µl 0.1xTE Buffer. Libraries were multiplexed and sequenced (single-end read 100) using a NovaSeq 6000 (SP flow-cell).

2.1.3.10 RNA-seq data analysis

Quality check of the raw reads was done by FastQC v0.11.5 (https://www.bioinformatics.babraham.ac.uk/projects/fastqc/), and subsequently mapped to the *Drosophila melanogaster* reference genome assembly dm6 (FlyBase Dmel Release 6.23) using STAR v2.5.2b2 pass mode (*30*), with guidance from the gene models of FlyBase Dmel Release 6.23. Aligned reads were assigned to gene annotation using HTSeq-count version 0.10 (*31*). Differential gene expression was calculated using DESeq2 (*32*). Genes were considered differentially expressed between genotypes and timepoints if they had an absolute log2FoldChange exceeding 1 and an adjusted p-value of less than 0.01. PCA was performed by prcomp function and plotted by ggplot2 in R (*33*). Reads were normalized by scale factor using DESeq2 (*32*). Heatmaps were generated using the pheatmap R package (https://rdrr.io/cran/pheatmap/). Transcripts per kilobases million (TPM) were calculated by

RSEM v1.3.1 (*34*). Gene Ontology enrichment analysis was performed using clusterProfiler (*35*).

2.1.3.11 ATAC-seq data analysis

Quality check of paired end was done using FastQCv0.11.5 (https://www.bioinformatics.babraham.ac.uk/projects/fastqc/). Nextera Transposase adapter and low-quality bases were eliminated using TrimGalore v0.6.6 (https://www.bioinformatics.babraham.ac.uk/projects/trim_galore/) and Cutadapt v1.17 (*36*). PCR duplicates, mitochondrial reads were removed by sambamba v0.6.7 (*37*) as well as reads blacklisted by the ENCODE project (*38*). Remaining reads were mapped to the *Drosophila melanogaster* reference genome dm6 (FlyBase Dmel Release 6.23) assembly using bowtie2 v2.3.4.2 (*39*). Mapped pairs were further filtered to maintain mapping quality above 10, as well as FR orientation concordant alignments, using custom scripts and samtools v1.9 (*40*). Peaks of accessible chromatin were identified for each sample using MACS2 v2.1.2 (*41*)with the following settings: -f BED --nomodel --shift -100 --extsize 200 --keep-dup all after converting the bam to bed file. Coverage tracks requiring bigwig files and heatmaps were generated using Deeptools v3.3.1 (*42*). The nucleosome free region and nucleosome positions were analysed using NucleoATAC-0.3.4 (*9*). For Fig. 1C, D and fig. S8 paired-end reads were aligned to the Dmel R6.23 genome using Bowtie 2 (*39*) using --very-sensitive -X 2000 option. Low-quality (MAPQ < 30) and mitochondrial reads were discarded. PCR duplicates were marked and removed using Picard (MarkDuplicates). Peaks were called using MACS2 (*41*) with the –f BAMPE --keep-dup all options. For downstream analysis, we used peaks only present in at least two biological replicates. To identify inter-dyad distances around promoter regions a window of ± 2 kb around TSSs was used for nucleosome position extraction. Consistent peaks were annotated and the nucleosome positions within intronic and intergenic regions in wild types were extracted. These regions were used to define nucleosome positions within intronic and intergenic regions, respectively, for both wild type and His^{C} mutant samples. PCA analysis was performed using ATAC-seq BAM files and DESeq2 (*32*).

2.1.3.12 CUT&Tag

CUT&Tag and CUTAC datasets were processed as described for ATAC-seq. After read mapping using custom scripts and samtools v1.9 (*40*), peaks were called using MACS2 v2.1.2 (*41*) with following settings. NarrowPeak representation was used for histone marks H3K4me3, H2K27ac, H3K4me2 with following settings: -f BAMPE --keepdup all -p 5e-4 --call-summits. For histone marks enriched in broad domains including H3K36me3, H3K27me3, H2AK9ac, and H2BK16ac, the broadPeak representation was used applying

following settings: -f BAMPE --keepdup all -p 5e-4 -b 0.01. bigwig files required for coverage tracks as well as heatmaps were generated using Deeptools v3.3.1 (*42*).

2.1.3.13 STRIPE-seq

Quality of STRIPE-seq data sets was analysed using FastQC v0.11.5 (https://www.bioinformatics.babraham.ac.uk/projects/fastqc/). STRIPE-seq read files were processed and aligned to *Drosophila melanogaster* reference genome dm6 (FlyBase Dmel Release 6.23) following the GoSTRIPES workflow (https://github.com/BrendelGroup/GoSTRIPES) (*18*). Reads counts were further calculated and TSSs were called using TSRchitect (https://www.bioconductor.org/packages/release/bioc/html/TSRchitect.html). The threshold for a TSS to be called was set to at least 5 raw counts that had to cluster into a TSR consistently in at least three of the analysed replicates. Read counts were then normalized and differential TSR analysis was performed using DESeq2 (*32*) with default settings. TSR shape analysis was accomplished using TSRexplorer (*43*). Annotation of TSSs and TSRs was done with ChIPseeker (*44*) using a promoter window from -/+ 250bp of a TSS. Genome browser tracks in bigwig format were generated from merged replicates using deeptools bamCoverage (*42*).

2.1.4 References

1. K. R. Stewart-Morgan, N. Petryk, A. Groth, Chromatin replication and epigenetic cell memory. *Nature cell biology*. **22**, 361–371 (2020), doi:10.1038/s41556-020-0487-y.
2. K. Ragunathan, G. Jih, D. Moazed, Epigenetics. Epigenetic inheritance uncoupled from sequence-specific recruitment. *Science (New York, N.Y.)*. **348**, 1258699 (2015), doi:10.1126/science.1258699.
3. Audergon, Pauline N. C. B. *et al.,* Epigenetics. Restricted epigenetic inheritance of H3K9 methylation. *Science*. **348**, 132–135 (2015), doi:10.1126/science.1260638.
4. U. Günesdogan, H. Jäckle, A. Herzig, A genetic system to assess in vivo the functions of histones and histone modifications in higher eukaryotes. *EMBO reports*. **11**, 772–776 (2010), doi:10.1038/embor.2010.124.
5. U. Günesdogan, H. Jäckle, A. Herzig, Histone supply regulates S phase timing and cell cycle progression. *eLife*. **3**, e02443 (2014), doi:10.7554/eLife.02443.
6. S. Ramachandran, S. Henikoff, Transcriptional Regulators Compete with Nucleosomes Post-replication. *Cell*. **165**, 580–592 (2016), doi:10.1016/j.cell.2016.02.062.
7. K. R. Stewart-Morgan, N. Reverón-Gómez, A. Groth, Transcription Restart Establishes Chromatin Accessibility after DNA Replication. *Molecular cell*. **75**, 284-297.e6 (2019), doi:10.1016/j.molcel.2019.04.033.
8. J. G. Henikoff, J. A. Belsky, K. Krassovsky, D. M. MacAlpine, S. Henikoff, Epigenome characterization at single base-pair resolution. *Proceedings of the National Academy of Sciences*. **108**, 18318–18323 (2011), doi:10.1073/pnas.1110731108.
9. A. N. Schep *et al.,* Structured nucleosome fingerprints enable high-resolution mapping of chromatin architecture within regulatory regions. *Genome research*. **25**, 1757–1770 (2015), doi:10.1101/gr.192294.115.
10. S. Ramachandran, K. Ahmad, S. Henikoff, Transcription and Remodeling Produce Asymmetrically Unwrapped Nucleosomal Intermediates. *Molecular cell*. **68**, 1038-1053.e4 (2017), doi:10.1016/j.molcel.2017.11.015.
11. A. Bayona-Feliu, A. Casas-Lamesa, O. Reina, J. Bernués, F. Azorín, Linker histone H1 prevents R-loop accumulation and genome instability in heterochromatin. *Nat Commun*. **8**, 283 (2017), doi:10.1038/s41467-017-00338-5.
12. J. Hu *et al.,* Dynamic placement of the linker histone H1 associated with nucleosome arrangement and gene transcription in early Drosophila embryonic development. *Cell death & disease*. **9**, 765 (2018), doi:10.1038/s41419-018-0819-z.
13. C. Alabert *et al.,* Nascent chromatin capture proteomics determines chromatin dynamics during DNA replication and identifies unknown fork components. *Nature cell biology*. **16**, 281–293 (2014), doi:10.1038/ncb2918.
14. K. K. Li *et al.*, *Compensatory replacement of the BigH1 variant histone by canonical H1 supports normal embryonic development in Drosophila* (2019).
15. H. S. Kaya-Okur *et al.,* CUT&Tag for efficient epigenomic profiling of small samples and single cells. *Nature communications*. **10**, 1930 (2019), doi:10.1038/s41467-019-09982-5.
16. J. Bednar *et al.,* Structure and Dynamics of a 197 bp Nucleosome in Complex with Linker Histone H1. *Molecular cell*. **66**, 384-397.e8 (2017), doi:10.1016/j.molcel.2017.04.012.
17. S. Henikoff, J. G. Henikoff, H. S. Kaya-Okur, K. Ahmad, Efficient chromatin accessibility mapping in situ by nucleosome-tethered tagmentation. *eLife*. **9** (2020), doi:10.7554/eLife.63274.

18. R. A. Policastro, R. T. Raborn, V. P. Brendel, G. E. Zentner, Simple and efficient profiling of transcription initiation and transcript levels with STRIPE-seq. *Genome research*. **30**, 910–923 (2020), doi:10.1101/gr.261545.120.

19. M. P. Creyghton *et al.,* Histone H3K27ac separates active from poised enhancers and predicts developmental state. *Proceedings of the National Academy of Sciences*. **107**, 21931–21936 (2010), doi:10.1073/pnas.1016071107.

20. D. T. Gruszka, S. Xie, H. Kimura, H. Yardimci, Single-molecule imaging reveals control of parental histone recycling by free histones during DNA replication. *Science advances*. **6** (2020), doi:10.1126/sciadv.abc0330.

21. B. P. Hennig, K. Bendrin, Y. Zhou, T. Fischer, Chd1 chromatin remodelers maintain nucleosome organization and repress cryptic transcription. *EMBO reports*. **13**, 997–1003 (2012), doi:10.1038/embor.2012.146.

22. M. Hödl, K. Basler, Transcription in the absence of histone H3.2 and H3K4 methylation. *Current biology : CB*. **22**, 2253–2257 (2012), doi:10.1016/j.cub.2012.10.008.

23. G. Schlissel, J. Rine, The nucleosome core particle remembers its position through DNA replication and RNA transcription. *Proceedings of the National Academy of Sciences of the United States of America*. **116**, 20605–20611 (2019), doi:10.1073/pnas.1911943116.

24. N. Reverón-Gómez *et al.,* Accurate Recycling of Parental Histones Reproduces the Histone Modification Landscape during DNA Replication. *Molecular cell*. **72**, 239-249.e5 (2018), doi:10.1016/j.molcel.2018.08.010.

25. T. M. Escobar *et al.,* Active and Repressed Chromatin Domains Exhibit Distinct Nucleosome Segregation during DNA Replication. *Cell*. **179**, 953-963.e11 (2019), doi:10.1016/j.cell.2019.10.009.

26. T. D. Schmittgen, K. J. Livak, Analyzing real-time PCR data by the comparative C(T) method. *Nature protocols*. **3**, 1101–1108 (2008), doi:10.1038/nprot.2008.73.

27. M. Buescher, G. Oberhofer, N. C. Garcia-Perez, G. Bucher, in *Brain Development, Methods and Protocols*, S. G. Sprecher, Ed. (Humana, New York, NY, ed. 2, 2020), vol. **2047,** pp. 219–232.

28. J. D. Buenrostro, P. G. Giresi, L. C. Zaba, H. Y. Chang, W. J. Greenleaf, Transposition of native chromatin for fast and sensitive epigenomic profiling of open chromatin, DNA-binding proteins and nucleosome position. *Nature methods*. **10**, 1213–1218 (2013), doi:10.1038/NMETH.2688.

29. J. D. Buenrostro, B. Wu, H. Y. Chang, W. J. Greenleaf, ATAC-seq: A Method for Assaying Chromatin Accessibility Genome-Wide. *Current protocols in molecular biology*. **109**, 21.29.1-21.29.9 (2015), doi:10.1002/0471142727.mb2129s109.

30. A. Dobin *et al.,* STAR: ultrafast universal RNA-seq aligner. *Bioinformatics (Oxford, England)*. **29**, 15–21 (2013), doi:10.1093/bioinformatics/bts635.

31. S. Anders, P. T. Pyl, W. Huber, HTSeq--a Python framework to work with high-throughput sequencing data. *Bioinformatics (Oxford, England)*. **31**, 166–169 (2015), doi:10.1093/bioinformatics/btu638.

32. M. I. Love, W. Huber, S. Anders, Moderated estimation of fold change and dispersion for RNA-seq data with DESeq2. *Genome Biol*. **15**, 550 (2014), doi:10.1186/s13059-014-0550-8.

33. H. Wickham, *ggplot2: Elegant Graphics for Data Analysis*, *Create Elegant Data Visualisations Using the Grammar of Graphics*, A system for 'declaratively' creating graphics based on ``The Grammar of Graphics'' (Springer-Verlag New York, New York, NY, 2016).

34. B. Li, C. N. Dewey, RSEM: accurate transcript quantification from RNA-Seq data with or without a reference genome. *BMC Bioinformatics*. **12**, 323 (2011), doi:10.1186/1471-2105-12-323.

35. G. Yu, L.-G. Wang, Y. Han, Q.-Y. He, clusterProfiler: an R package for comparing biological themes among gene clusters. *Omics : a journal of integrative biology*. **16**, 284–287 (2012), doi:10.1089/omi.2011.0118.

36. M. Martin, Cutadapt removes adapter sequences from high-throughput sequencing reads. *EMBnet j.* **17**, 10 (2011), doi:10.14806/ej.17.1.200.

37. A. Tarasov, A. J. Vilella, E. Cuppen, I. J. Nijman, P. Prins, Sambamba: fast processing of NGS alignment formats. *Bioinformatics (Oxford, England)*. **31**, 2032–2034 (2015), doi:10.1093/bioinformatics/btv098.

38. H. M. Amemiya, A. Kundaje, A. P. Boyle, The ENCODE Blacklist: Identification of Problematic Regions of the Genome. *Scientific reports*. **9**, 9354 (2019), doi:10.1038/s41598-019-45839-z.

39. B. Langmead, S. L. Salzberg, Fast gapped-read alignment with Bowtie 2. *Nature methods*. **9**, 357–359 (2012), doi:10.1038/nmeth.1923.

40. H. Li *et al.,* The Sequence Alignment/Map format and SAMtools. *Bioinformatics*. **25**, 2078–2079 (2009), doi:10.1093/bioinformatics/btp352.

41. Y. Zhang *et al.,* Model-based analysis of ChIP-Seq (MACS). *Genome biology*. **9**, R137 (2008), doi:10.1186/gb-2008-9-9-r137.

42. F. Ramírez, F. Dündar, S. Diehl, B. A. Grüning, T. Manke, deepTools: a flexible platform for exploring deep-sequencing data. *Nucleic Acids Res*. **42**, W187-91 (2014), doi:10.1093/nar/gku365.

43. R. A. Policastro, D. J. McDonald, V. P. Brendel, G. E. Zentner, *Flexible analysis of TSS mapping data and detection of TSS shifts with TSRexploreR* (2021).

44. G. Yu, L.-G. Wang, Q.-Y. He, ChIPseeker: an R/Bioconductor package for ChIP peak annotation, comparison and visualization. *Bioinformatics (Oxford, England)*. **31**, 2382–2383 (2015), doi:10.1093/bioinformatics/btv145.

2.1.5 Appendix

2.1.5.1 Supplementary Information

Figure S1

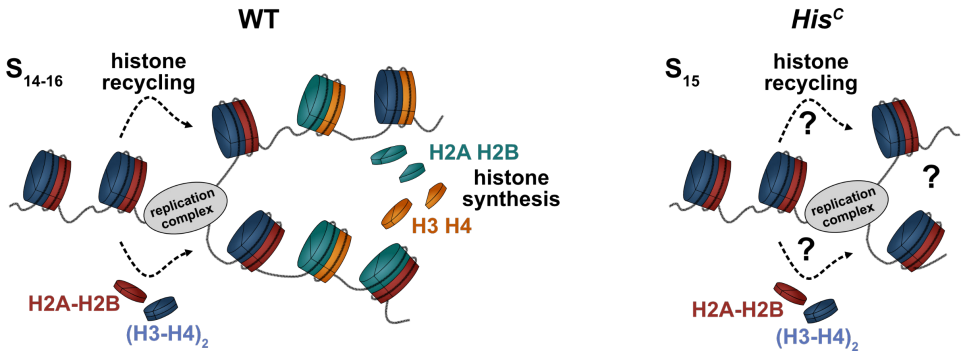

Figure 2.5 Fig. S1: Schematics of nucleosome assembly in wild type and *His*^{C} mutants. During DNA replication in S phase, new histones are synthesised and assembled into nucleosomes together with parental recycled histone tetramers $(H3\text{-}H4)_2$ and dimers H2A-H2B in wild type embryos (WT, left). In S_{15} of *His*^{C} mutant embryos, histone synthesis does not take place.

Figure S2

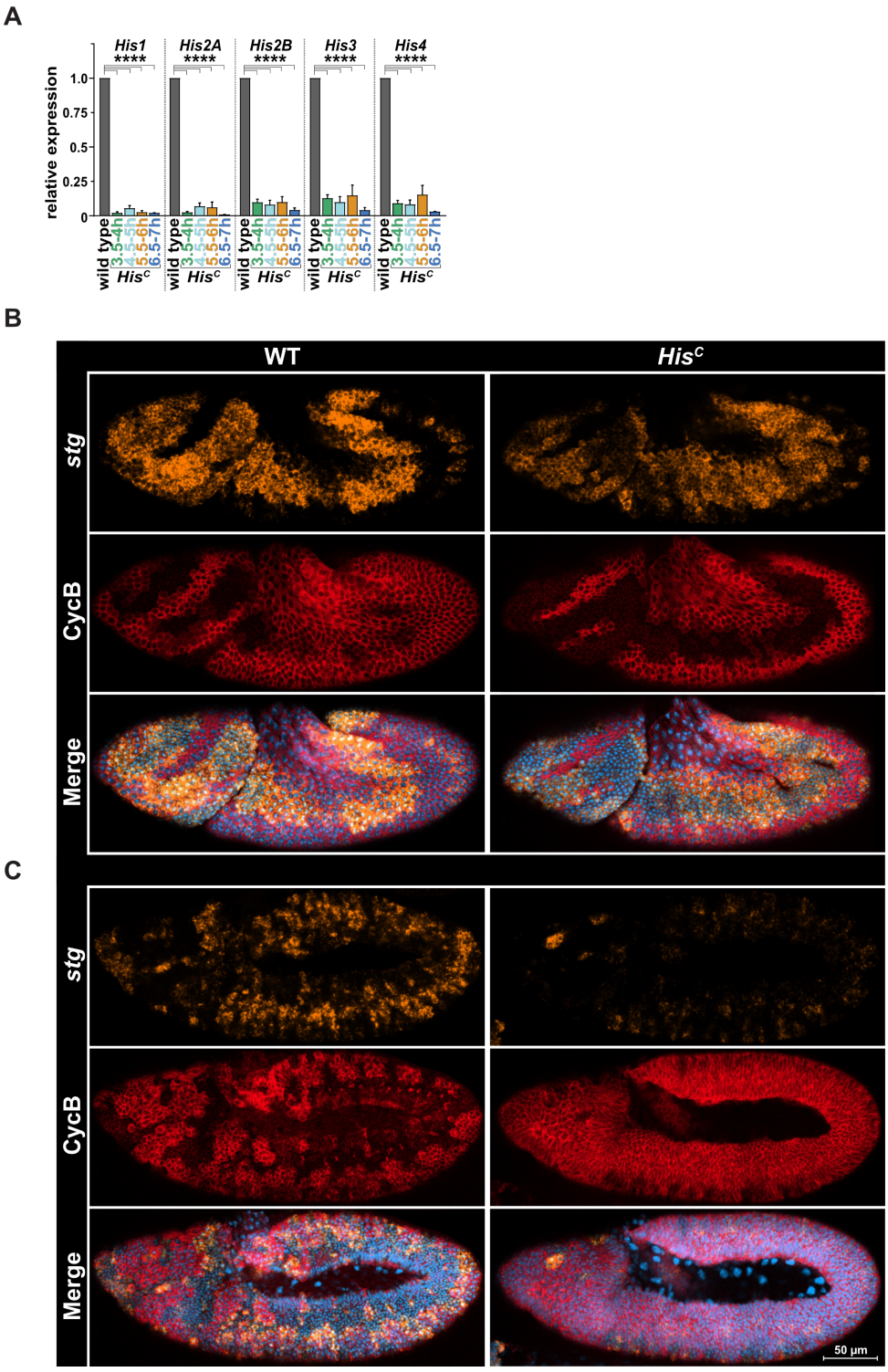

Figure 2.6 Fig. S2: *His*^{C} mutant embryos do not express histones zygotically and arrest in cell cycle 15. (A) qPCR for histone genes *His1, His2A, His2B, His3*, and *His4* with cDNA from wild type or *His*^{C} mutant embryos at indicated hours (h) after egg laying. ΔΔCt ± s.d.; normalisation using *act5c* (housekeeping gene) and matched wild type embryos as a reference (= 1); two-sided, unpaired Student's t-test **P<0.0001. (B), (C) Fluorescent *in situ* hybridisation using an exonic probe for string mRNA (*stg*, orange) combined with immunofluorescent protein staining using an antibody for Cyclin B (Cyclin B, red) of wild type (WT) and *His*^{C} mutant embryos (*His*^{C}). DAPI was used to stain DNA (blue). Wild type and *His*^{C} mutant embryos in cell cycle 14 degrade Cyclin B and express string (B). In cell cycle 15, *His*^{C} mutant embryos accumulate Cyclin B and do not upregulate string as opposed to wild types (C). Scale bar: 50µm.

Figure S3

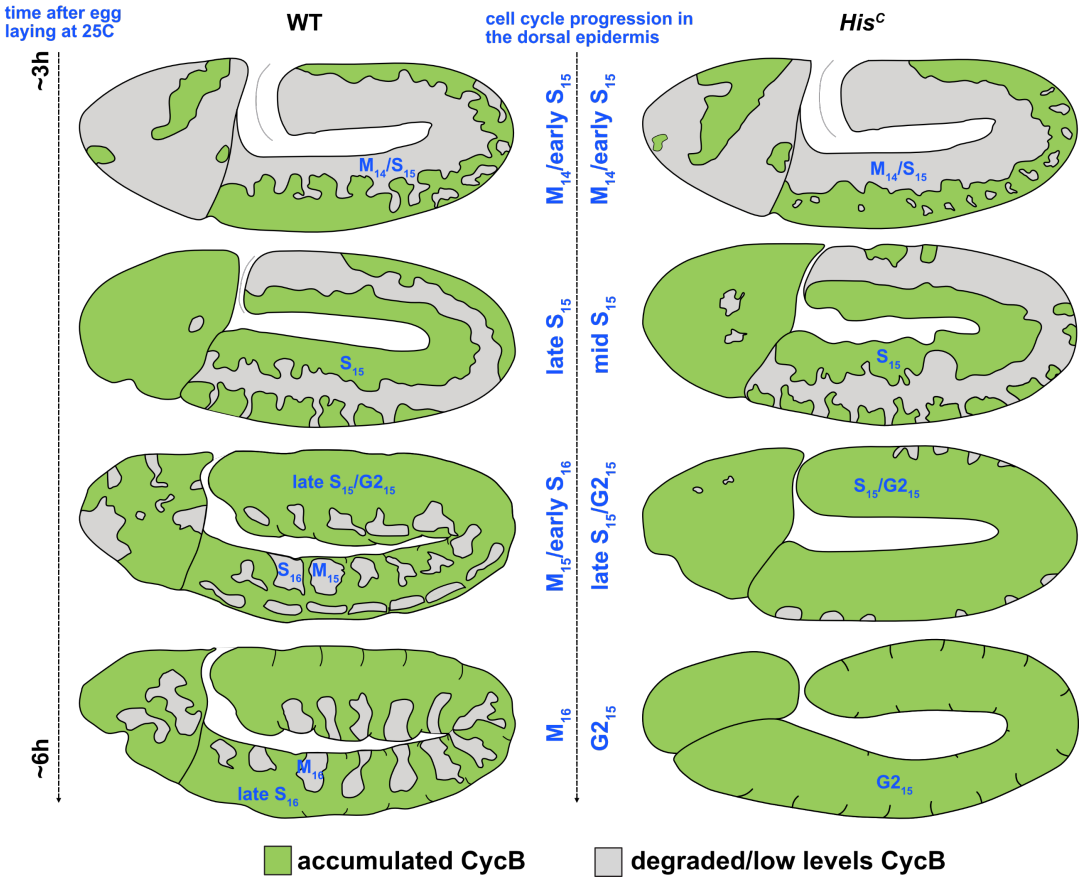

Figure 2.7 Fig. S3: Schematic representation of cell cycle progression and nucleosome assembly. Cyclin B accumulation/degradation pattern in the epidermis of wild type (WT) and *His*^{C} mutant embryos ~3 to ~6h after egg laying at 25C as previously described (*217*). Low Cyclin B levels (grey) indicate M/early S, whereas high levels (green) correspond to late S/G2 phases. In contrast to wild types (WT), *His*^{C} mutant embryos undergo M_{14}/S_{15} but arrest in the subsequent $G2_{15}$.

Figure S4

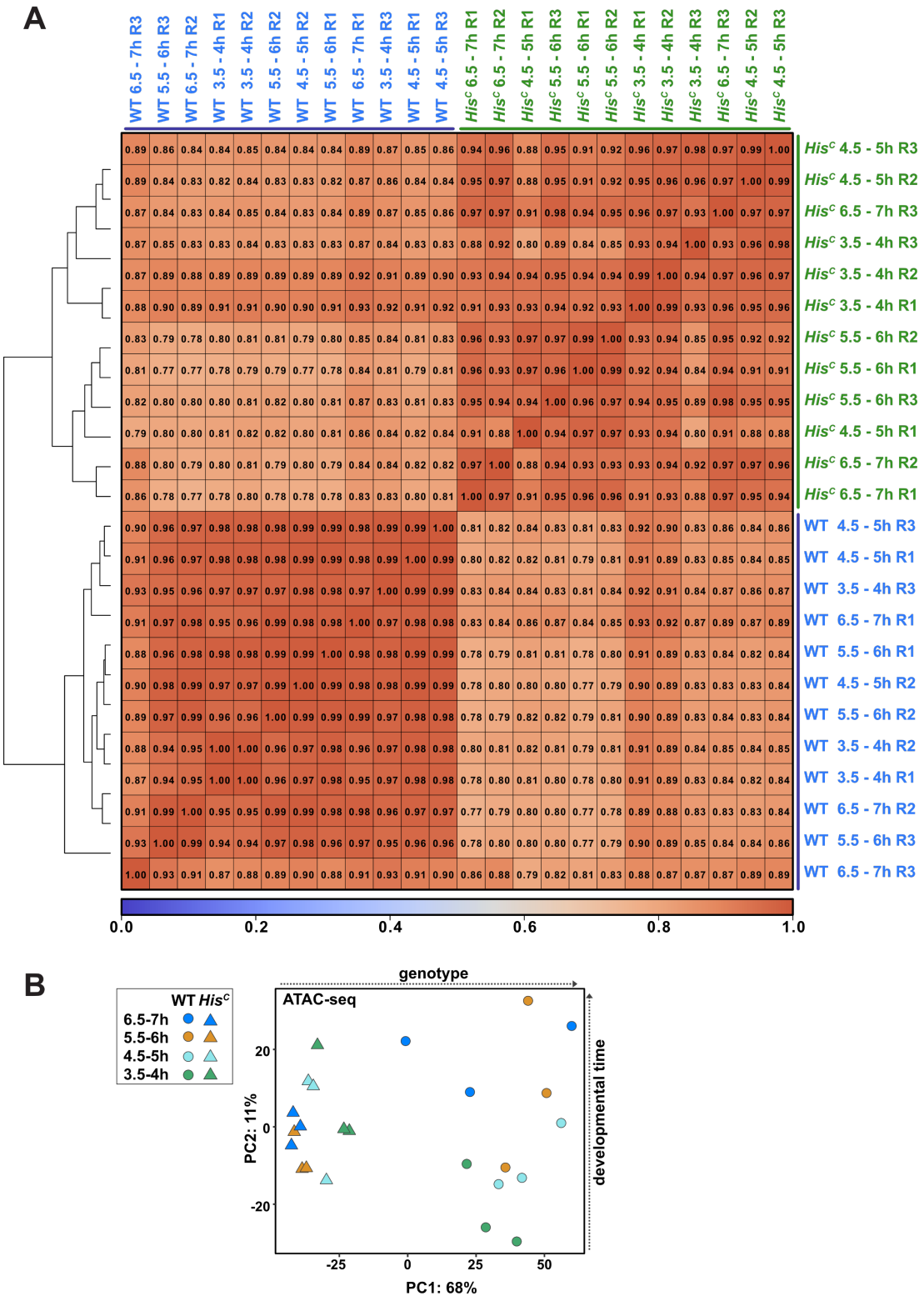

Figure 2.8 Fig. S4: Pearson coefficient correlations of ATAC-seq samples. (A) Pearson coefficient correlations of ATAC-seq samples from wild type (WT, blue) and *His*^{C} mutant embryos (green) at 3.5-4, 4.5-5, 5.5-6, and 6.5-7h AEL, R = replicate. (B) Two-dimensional principal component (PC) analysis of ATAC-seq data.

Figure S5

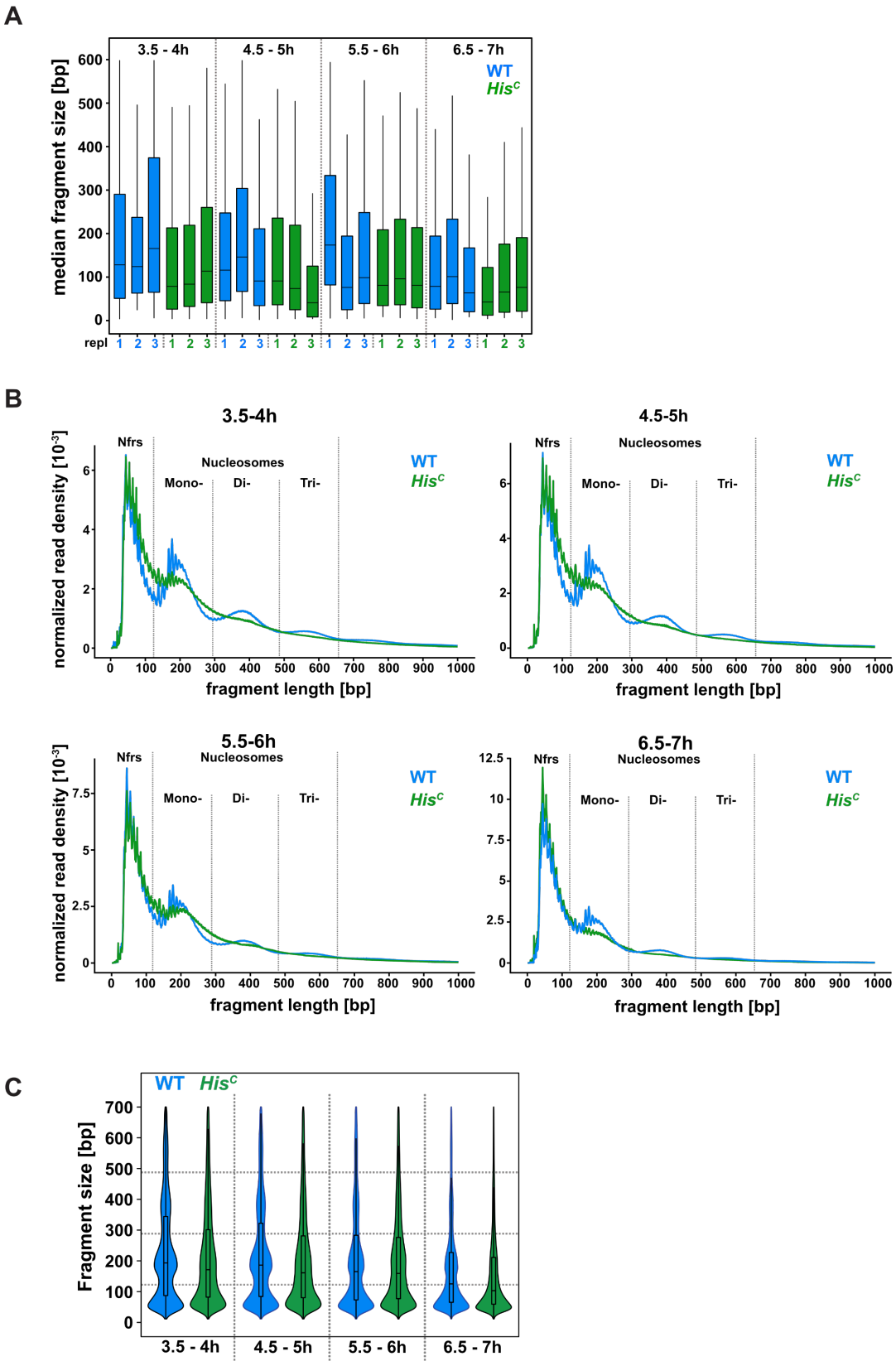

Figure 2.9 Fig. S5: ATAC-seq fragment size distribution. (A) Fragment size distribution of ATAC-seq data for each replicate at 3.5-4, 4.5-5, 5.5-6, and 6.5-7h AEL. (B), (C) Fragment size distribution of merged ATAC-seq data at 3.5-4, 4.5-5, 5.5-6, and 6.5-7h AEL.

Figure S6

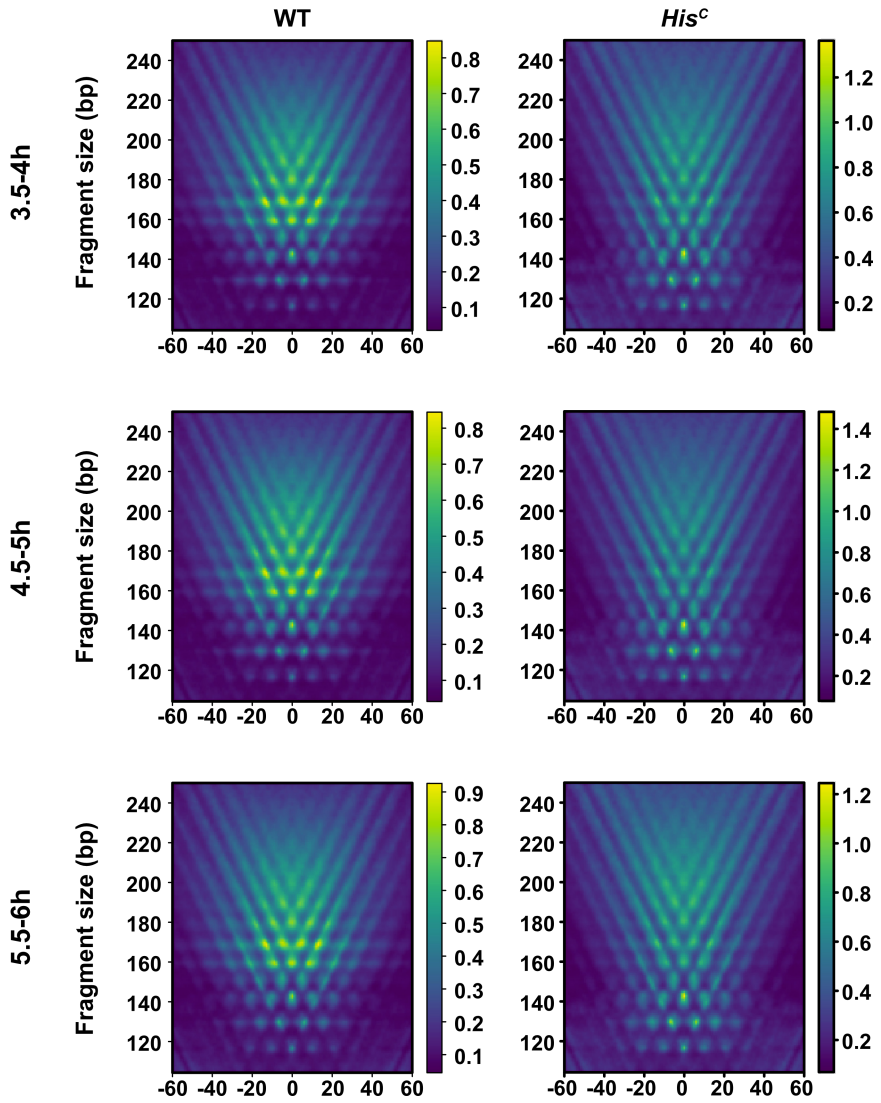

Figure 2.10 Fig. S6: Distribution of nucleosome-spanning fragments. V-plots show density of nucleosome-spanning fragment midpoints and sizes relative to nucleosome dyad centres, which exhibit a characteristic V-shaped horizontal and vertical periodicity in embryos at 3.5-4, 4.5-5, and 5.5-6h AEL. The majority of fragments is smaller in *His*^{C} mutants (~120-145bp) compared to wild type (WT, ~155-180bp).

Figure S7

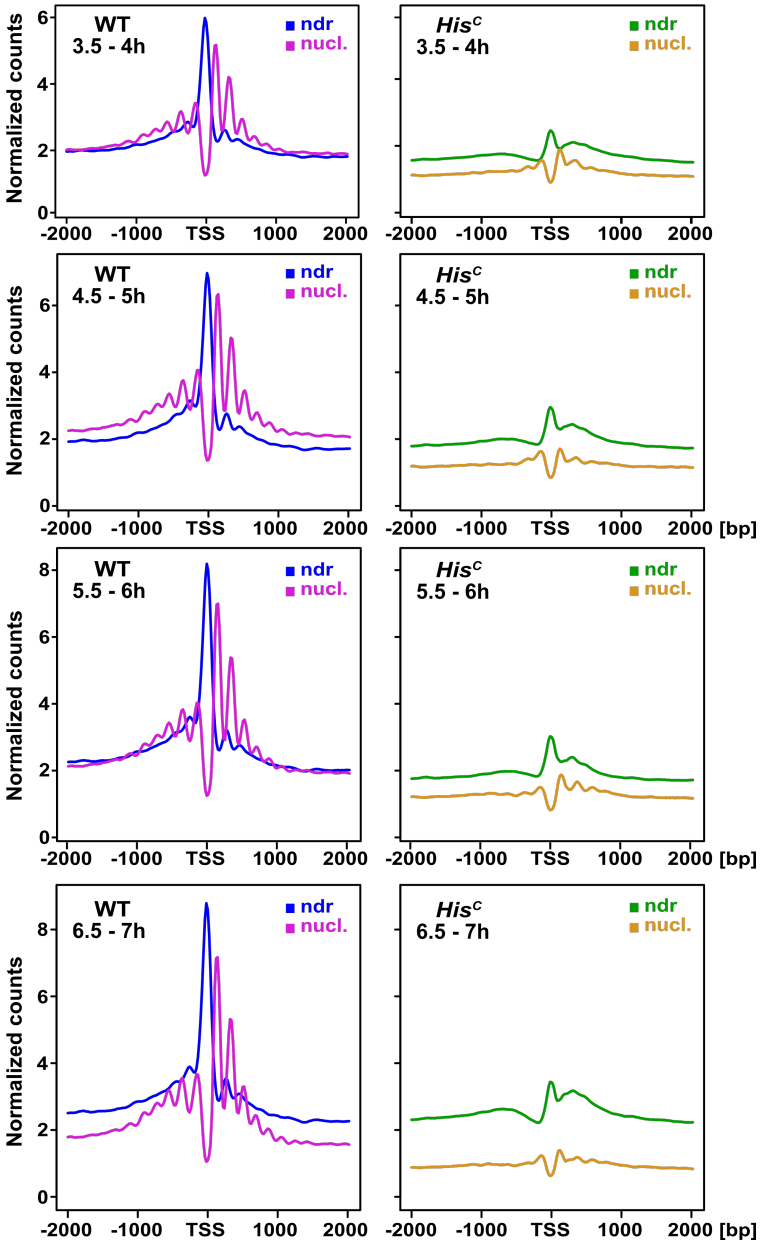

Figure 2.11 Fig. S7: Chromatin is more accessible in *His*^{C} mutants. Normalised counts of ATAC-seq reads ≤120bp (nucleosome-depleted fragments; ndr) and >120bp fragments (nucleosomal (nucl.) fragments) at transcription start sites (TSSs) +/- 2000bp with wild type (WT, left) and *His*^{C} mutant (right) embryos at 3.5-4, 4.5-5, 5.5-6, and 6.5-7h AEL.

Figure S8

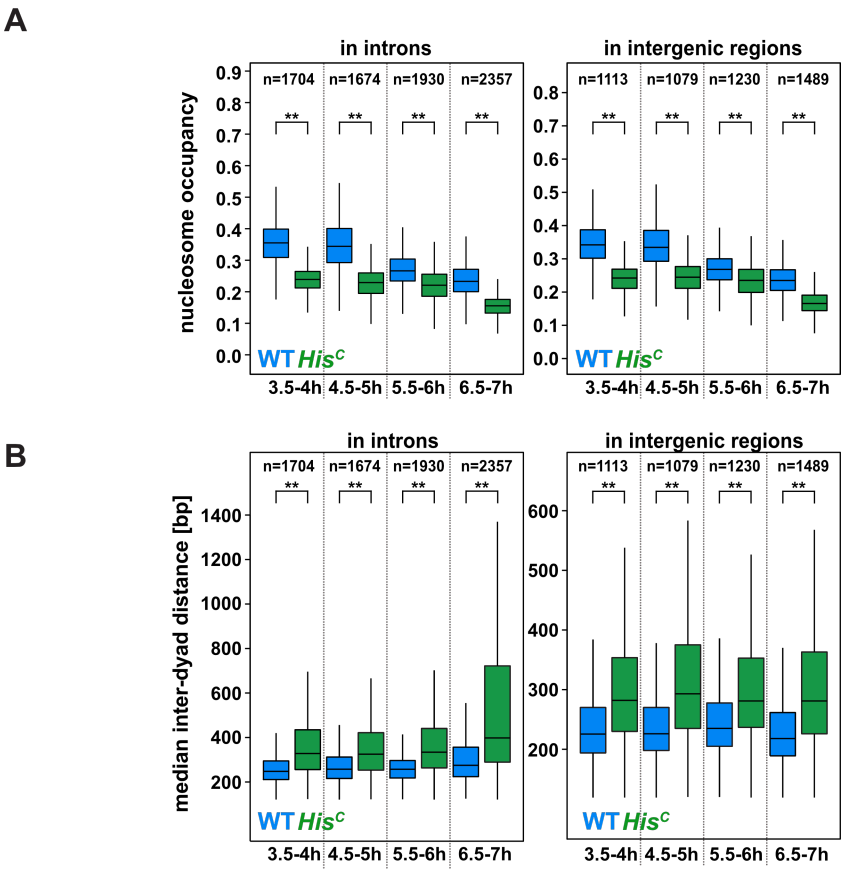

Figure 2.12 Fig. S8: Reduced nucleosome occupancy and increased inter-dyad distance at putative regulatory elements in *His*^{C} mutants. Median nucleosome occupancy (**A**) and inter-dyad distance (**B**) at ATAC-seq peaks demarcating putative regulatory elements in introns or intergenic region is reduced in *His*^{C} mutants (green) as compared to wild type (WT, blue); unpaired Wilcoxon t-test ***P*<0.0001.

Figure S9

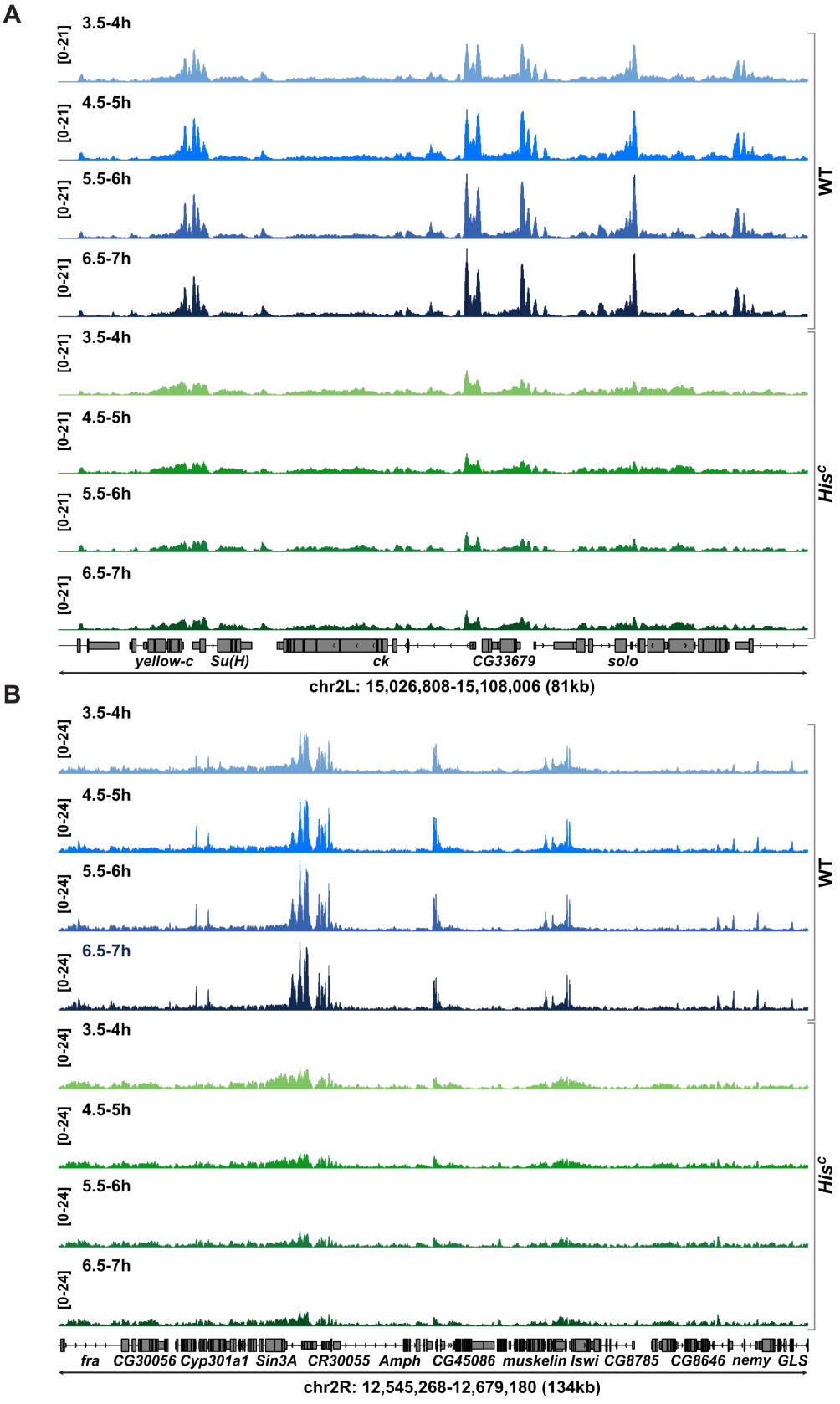

Figure 2.13 Fig. S9: Chromatin accessibility landscape is only partially re-established in *His*^{C} mutants. Representative snapshots of ATAC-seq coverage tracks on chromosome 2L (chr2L, (**A**)) and 2R (chr3R, (**B**)) at 3.5-4, 4.5-5, 5.5-6, and 6.5-7h AEL. (**A**) shows same genomic locus as Fig. 1E, but with additional time points.

Figure S10

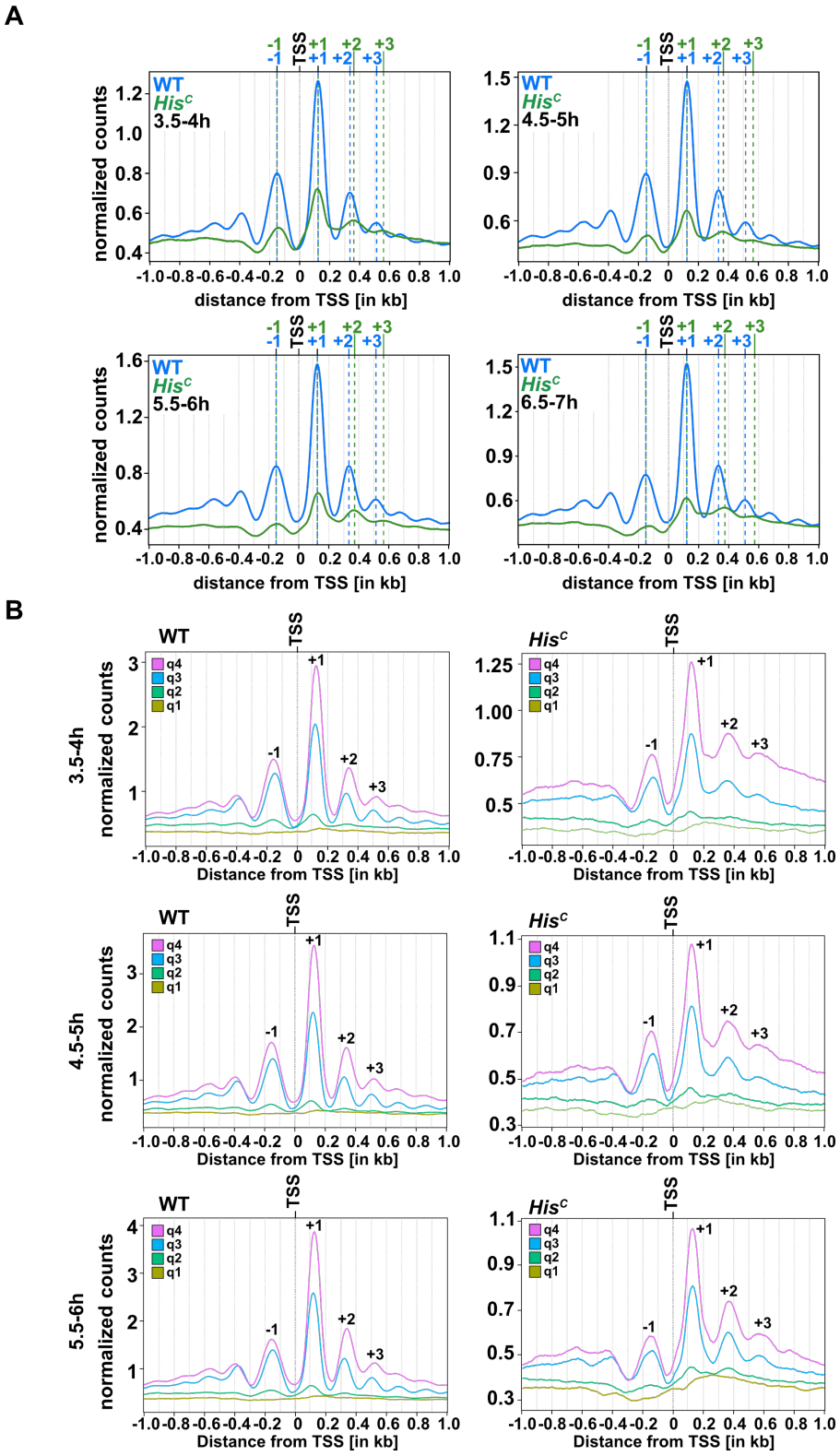

Figure 2.14 Fig. S10: Nucleosomal arrays downstream of TSSs are shifted in *His*^{C} mutants. (**A**) Normalised ATAC-seq count distribution of mononucleosomal reads (180-240bp) at TSSs +/- 1kb of wild type (WT, blue) and *His*^{C} mutant (green) embryos at 3.5-4h, 4.5-5h, 5.5-6h and 6.5-7h AEL show positioning of nucleosomes; -1 and +1 are TSS-flanking, +2/+3 are further downstream of TSSs. (**B**) Normalised ATAC-seq count distribution of mononucleosomal reads (180-240bp) at TSSs +/- 1kb of wild type (WT) and *His*^{C} mutant embryos at 3.5-4h, 4.5-5h, and 5.5-6h AEL. ATAC-seq reads were categorized based on corresponding gene expression levels subdivided in quartiles (q1 = lowest) as determined by RNA-seq.

Figure S11

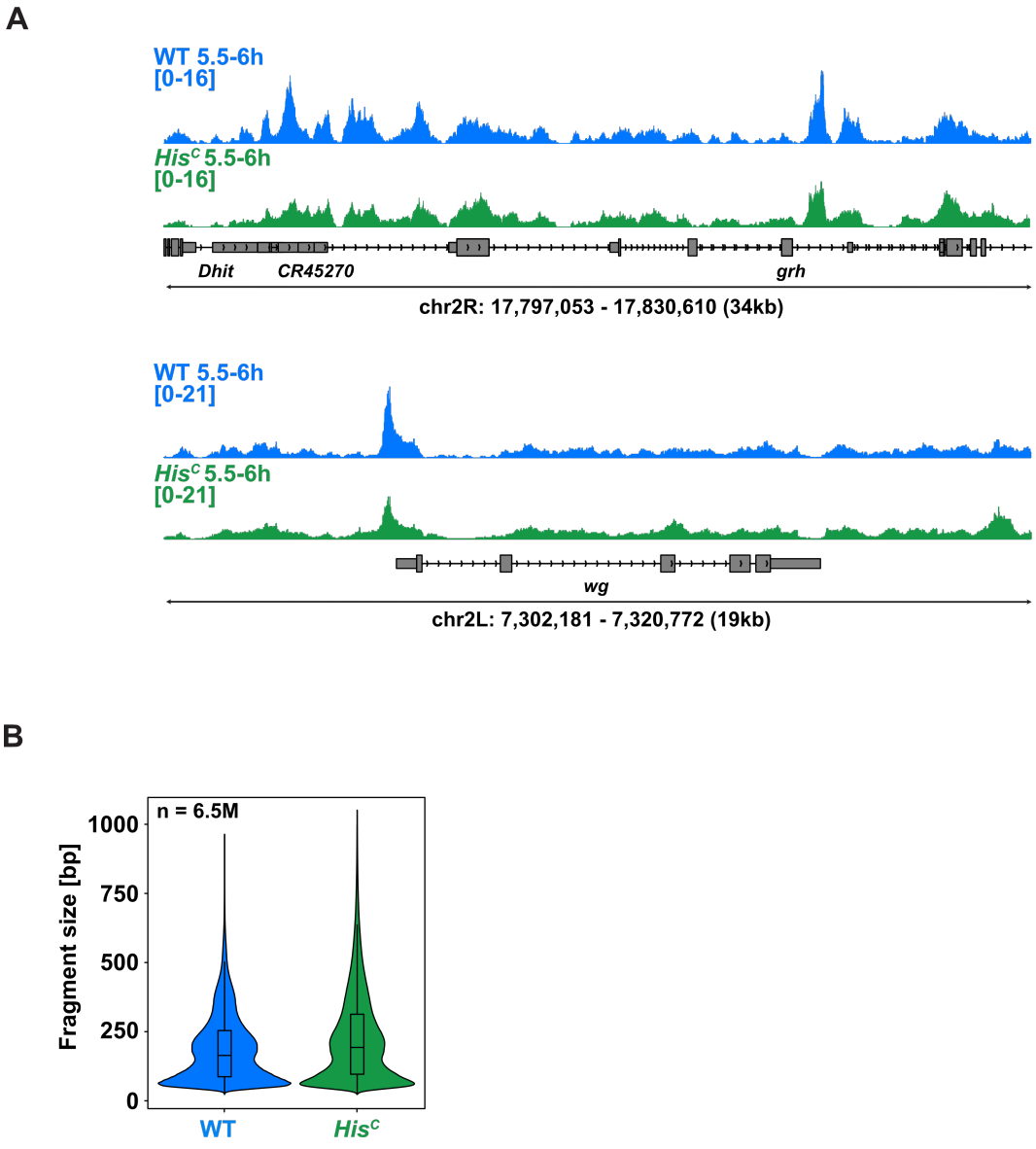

Figure 2.15 Fig. S11: Histone H1 distribution is comparable between wild types and *Hisᶜ* mutants. (**A**) Representative snapshots of Histone H1 CUT&Tag coverage tracks of wild type (WT, blue) and *Hisᶜ* mutant (green) embryos at 5.5-6h AEL on chromosomes (chr) 2R and 2L. (**B**) Fragment size distribution (n = 6.5M) of Histone H1 CUT&Tag data with wild type (WT, blue) and *Hisᶜ* mutant (green) embryos at 5.5-6h AEL.

Figure S12

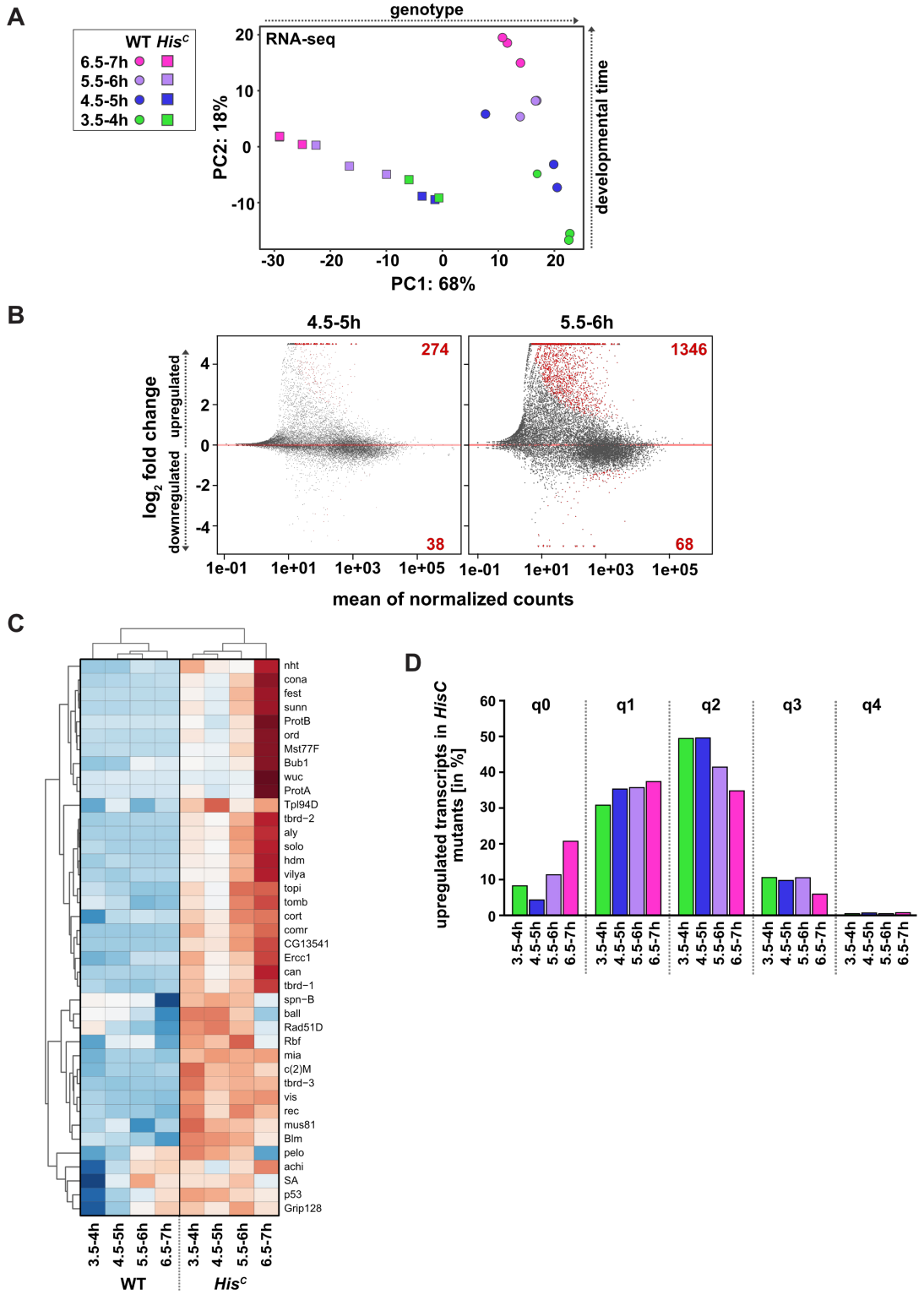

Figure 2.16 Fig. S12: *His*^{C} mutants upregulate a large number of transcripts. (**A**) Two-dimensional principal component (PC) analysis of RNA-seq data. (**B**) MA plots showing differential gene expression analysis of RNA-seq data with wild type (WT) and *His*^{C} mutant embryos at 4.5-5h and 5.5-6h AEL. Each transcript is represented by a dot (grey: not significant, red: significant (absolute log2fold change>1, padj<0.01)). (**C**) Heatmap of RNA-seq expression values (row z-score) of meiosis or post-meiotic-related genes, which are significantly upregulated in *His*^{C} mutants. (**D**) Bar plot shows the number (in %) of differentially upregulated genes in *His*^{C} mutants at 3.5-4h, 4.5-5h, 5.5-6h, and 6.5-7h AEL in corresponding wild type expression quartiles (q0 = no reads, q1 = lowest).

Figure S13

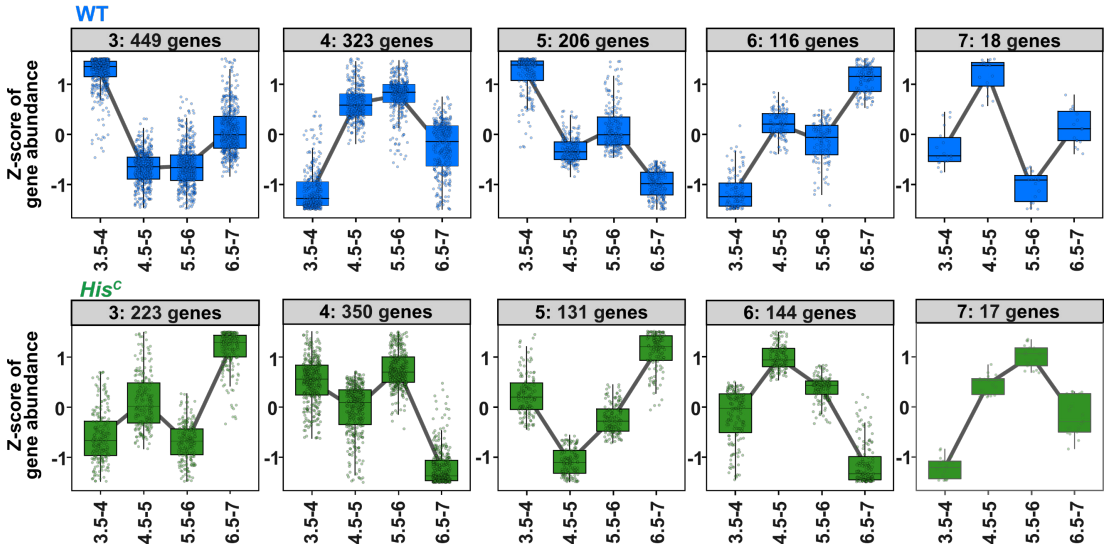

Figure 2.17: Fig. S13: Transcriptional dynamics in *His*^{C} mutants. Clustering of genes based on their RNA-seq expression dynamics from 3.5-4h, 4.5-5h, 5.5-6h to 6.5-7h AEL for wild types (WT) and *His*^{C} mutants. The two major clusters of up- or down-regulated genes are shown in Fig. 2D.

Figure S14

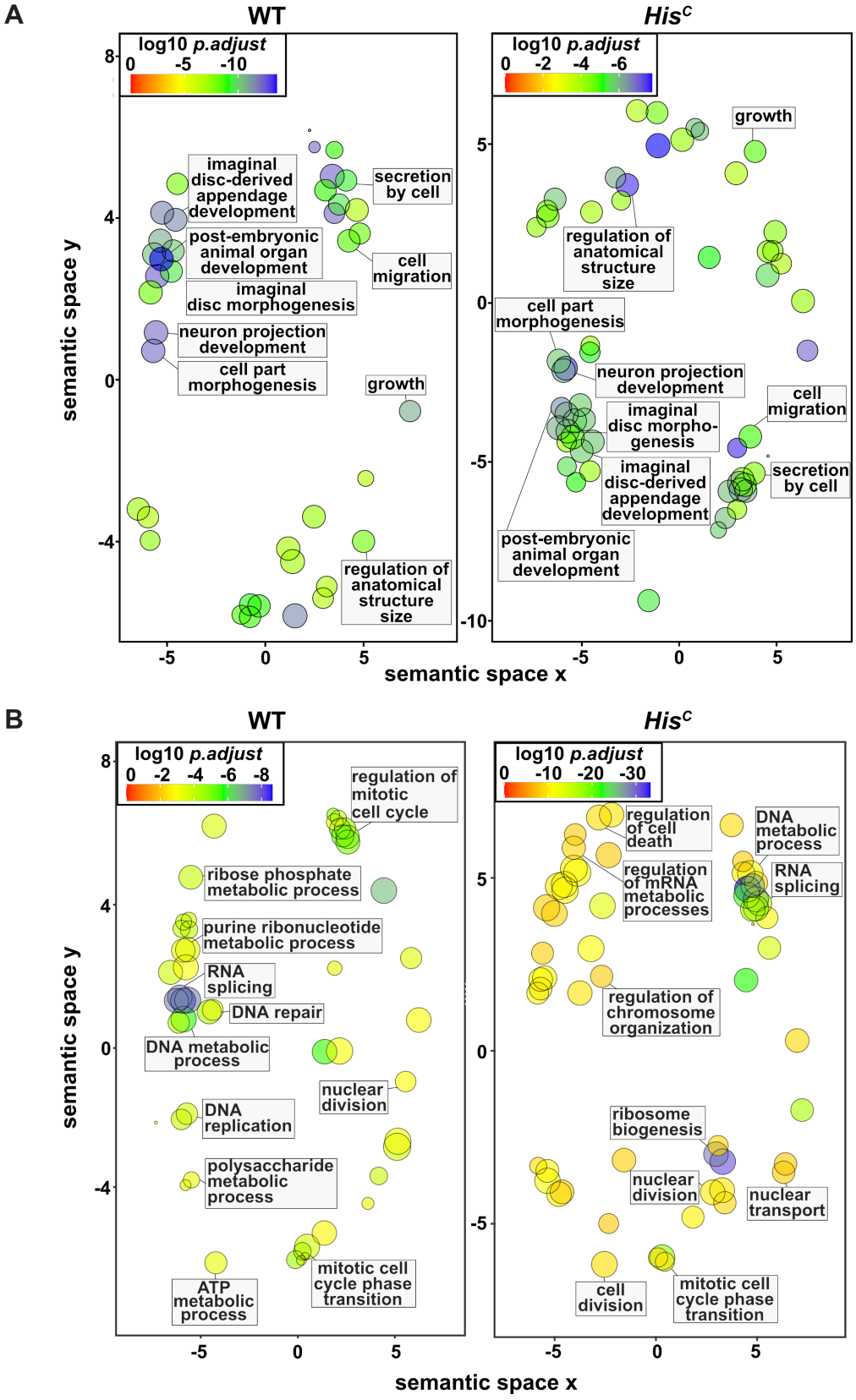

Figure 2.18 Fig. S14: *His*^{C} mutants maintain partial control of their developmental transcriptional program. Representation of the Top 75 significant Gene Ontology (GO) Terms associated with the clusters of up- (**A**) or downregulated (**B**) genes shown in Fig. 2D.

Figure S15

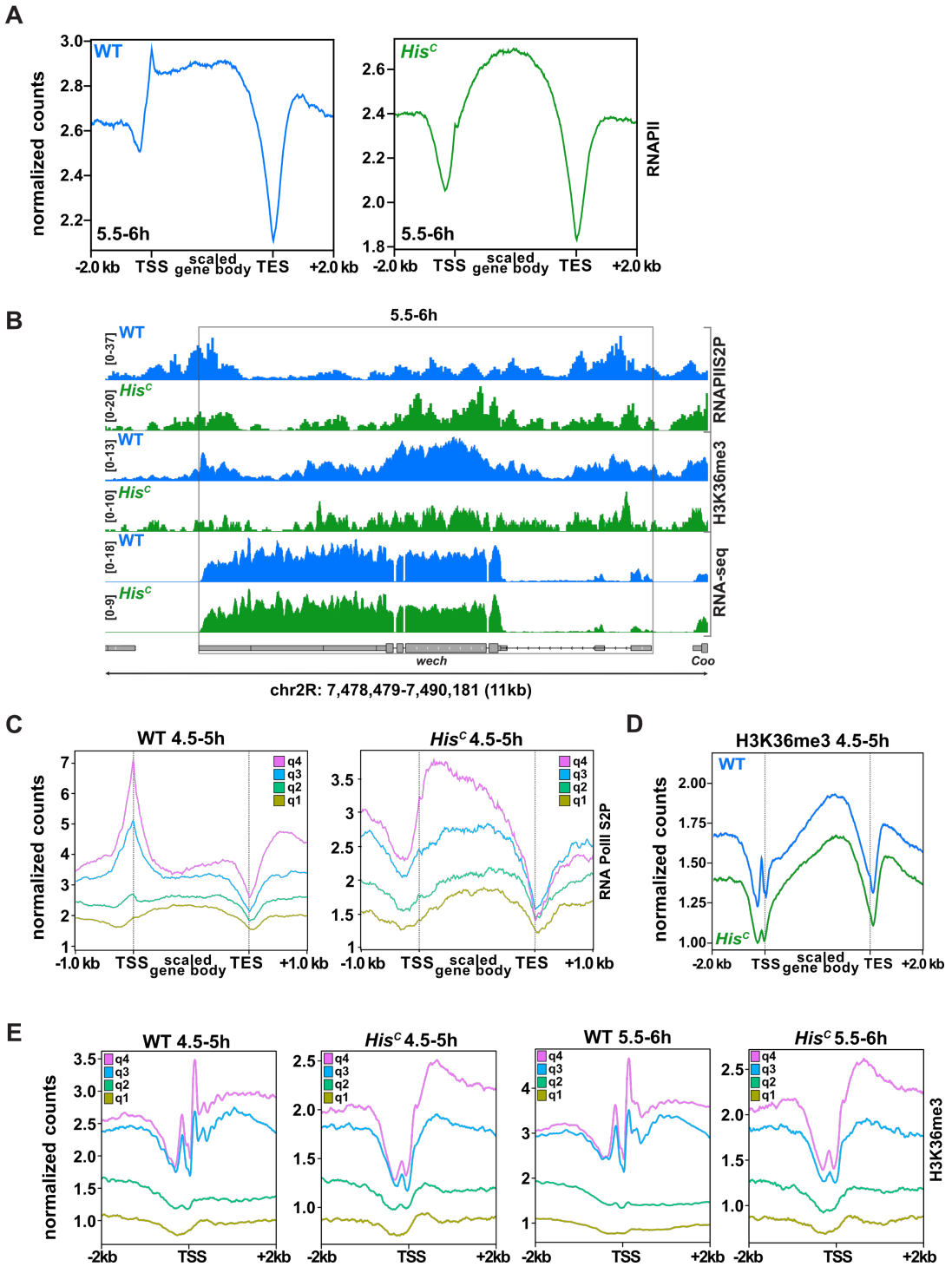

Figure 2.19: Fig. S15: RNAPII does not stall at TSSs in *His*^{C} mutants. (A) Profile plots of RNAPII CUT&Tag normalised counts at gene bodies with wild type (WT, blue) and *His*^{C} mutant (green) embryos at 5.5-6h AEL. (B) Representative snapshots of RNAPIIS2P CUT&Tag, H3K36me3 CUT&Tag and RNA-seq coverage tracks of wild type (WT, blue) and *His*^{C} mutant (green) embryos at 5.5-6h AEL on chromosome (chr) 2R. (C) Profile plots of RNAPIIS2P CUT&Tag normalised counts at gene bodies of wild type (WT) and *His*^{C} mutant embryos at 4.5-5h AEL separated by associated gene expression quartiles (q1 = lowest). (D) Profile plots of H3K36me3 CUT&Tag normalised counts at gene bodies of wild type (WT, blue) and *His*^{C} mutant (green) embryos at 4.5-5h AEL. (E) Profile plots of H3K36me3 CUT&Tag normalised counts at TSSs of wild type (WT) and *His*^{C} mutant embryos at 4.5-5h and 5.5-6h AEL separated by associated gene expression quartiles (q1 = lowest).

Figure S16

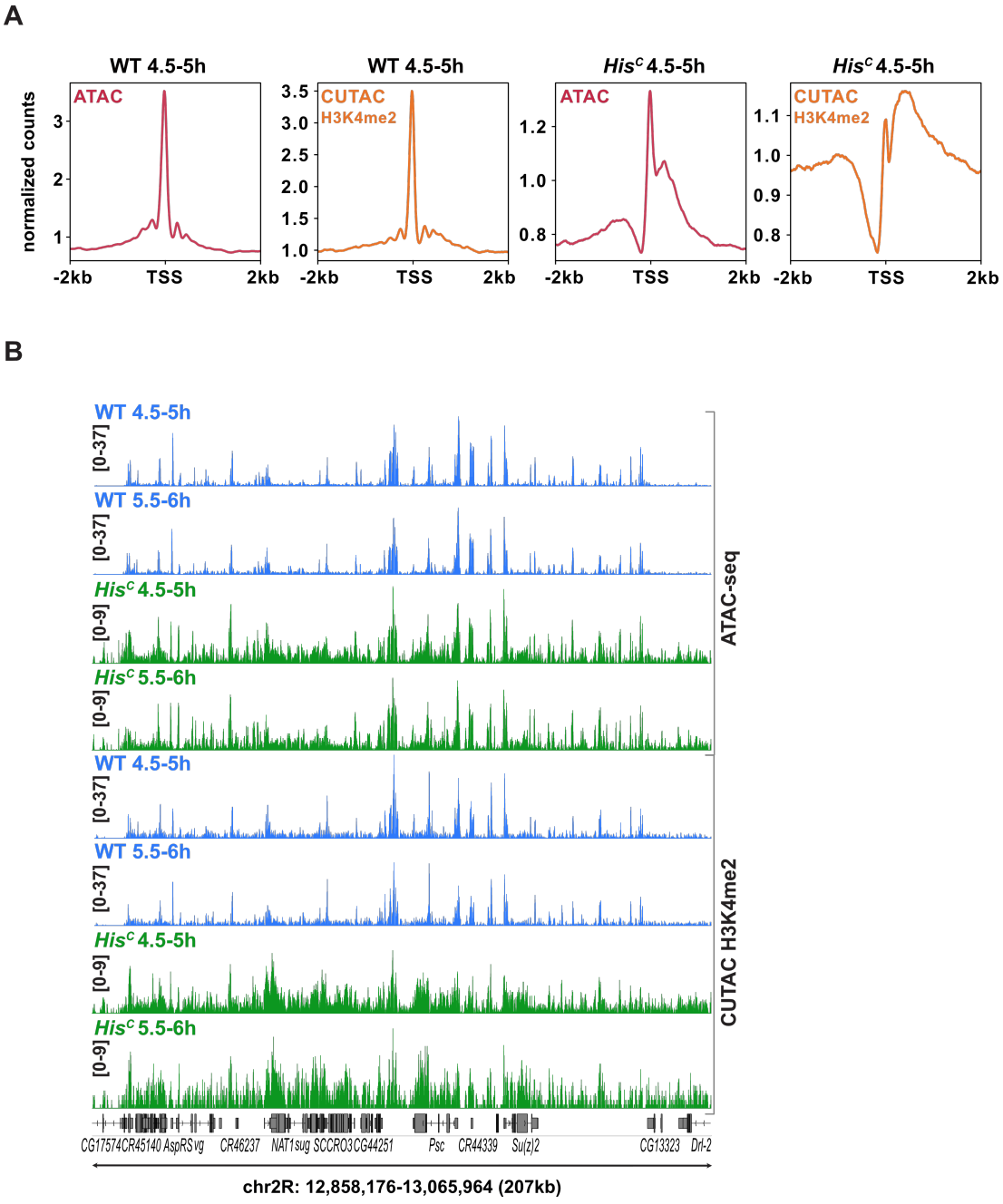

Figure 2.20 Fig. S16: Premature release of RNAPII into elongation in *His^C* mutants. (**A**) Comparison of ATAC-seq and H3K4me2 CUTAC profile plots (≤120bp reads) of wild type (WT) and *His^C* mutant embryos at 4.5-5h AEL. (**B**) Representative snapshot of ATAC-seq and H3K4me2 CUTAC coverage tracks (≤120bp reads) of wild type (WT, blue) and *His^C* mutant (green) embryos at 4.5-5 and 5.5-6h AEL.

Figure S17

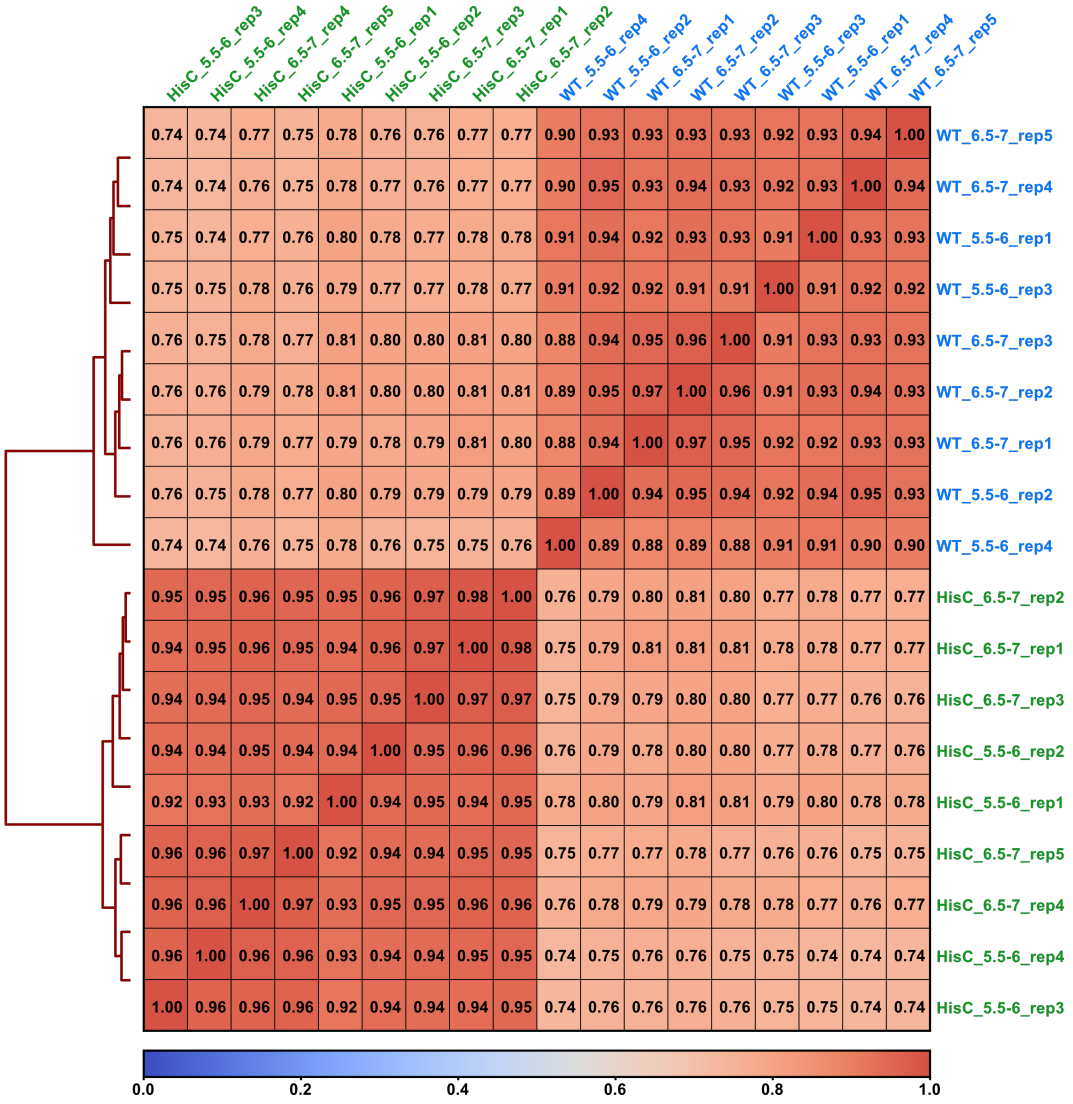

Figure 2.21 Fig. S17: STRIPE-seq quality control. Pearson coefficient correlations of STRIPE-seq samples from wild type (WT, blue) and *His*^{C} mutant embryos (green) at 5.5-6, and 6.5-7h AEL, rep = replicate.

Figure S18

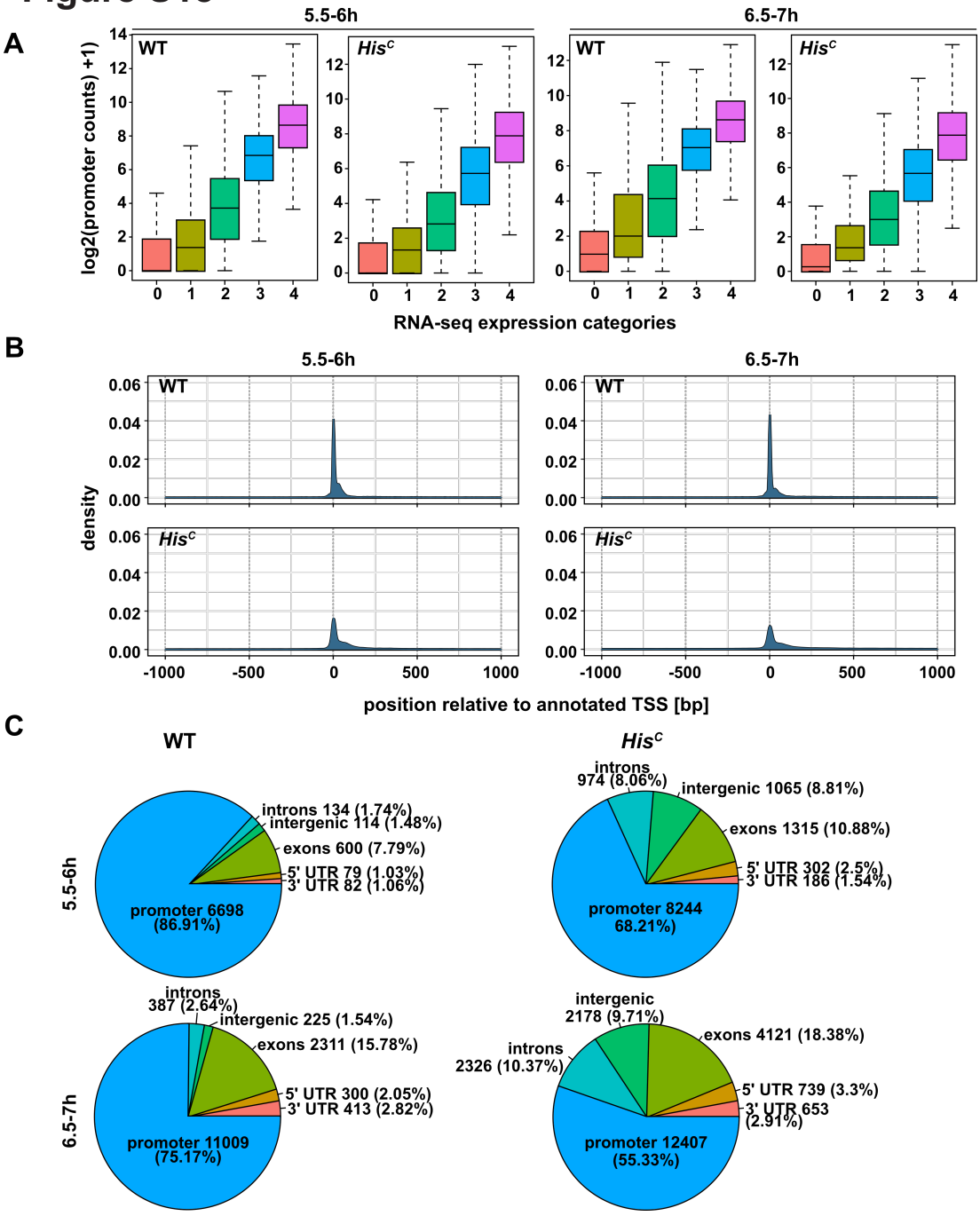

Figure 2.22 Fig. S18: Cryptic transcription initiation in *His*^{C} mutants. (**A**) Box plot showing correlation of STRIPE-seq promoter counts (log2+1), and gene expression levels (RNA-seq) separated in quartiles (q0 = no reads, q1 = lowest, q4 = highest) of wild type (WT) and *His*^{C} mutant embryos at 5.5-6 and 6.5-7h AEL. (**B**) Density plot showing STRIPE-seq read counts at TSSs of wild type (WT) and *His*^{C} mutant embryos at 5.5-6 and 6.5-7h AEL. (**C**) Genomic annotation of called TSRs of wild type (WT) and *His*^{C} mutant embryos at 5.5-6 and 6.5-7h AEL.

Figure S19

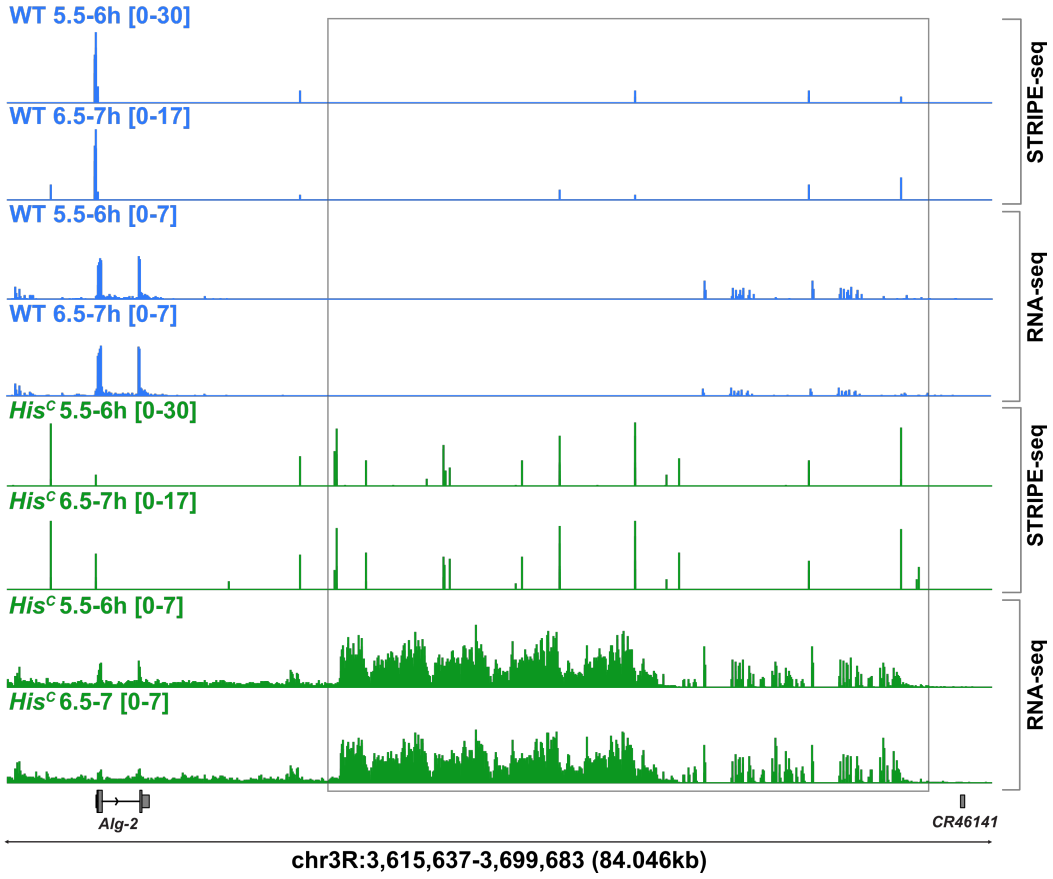

Figure 2.23 Fig. S19: Cryptic transcription initiation in intergenic regions in *His^{C}* mutants. Representative snapshot of STRIPE-seq and RNA-seq coverage tracks of wild type (WT, blue) and *His^{C}* mutant (green) embryos at 5.5-6h and 6.5-7h AEL on chromosome (chr) 3R.

Figure S20

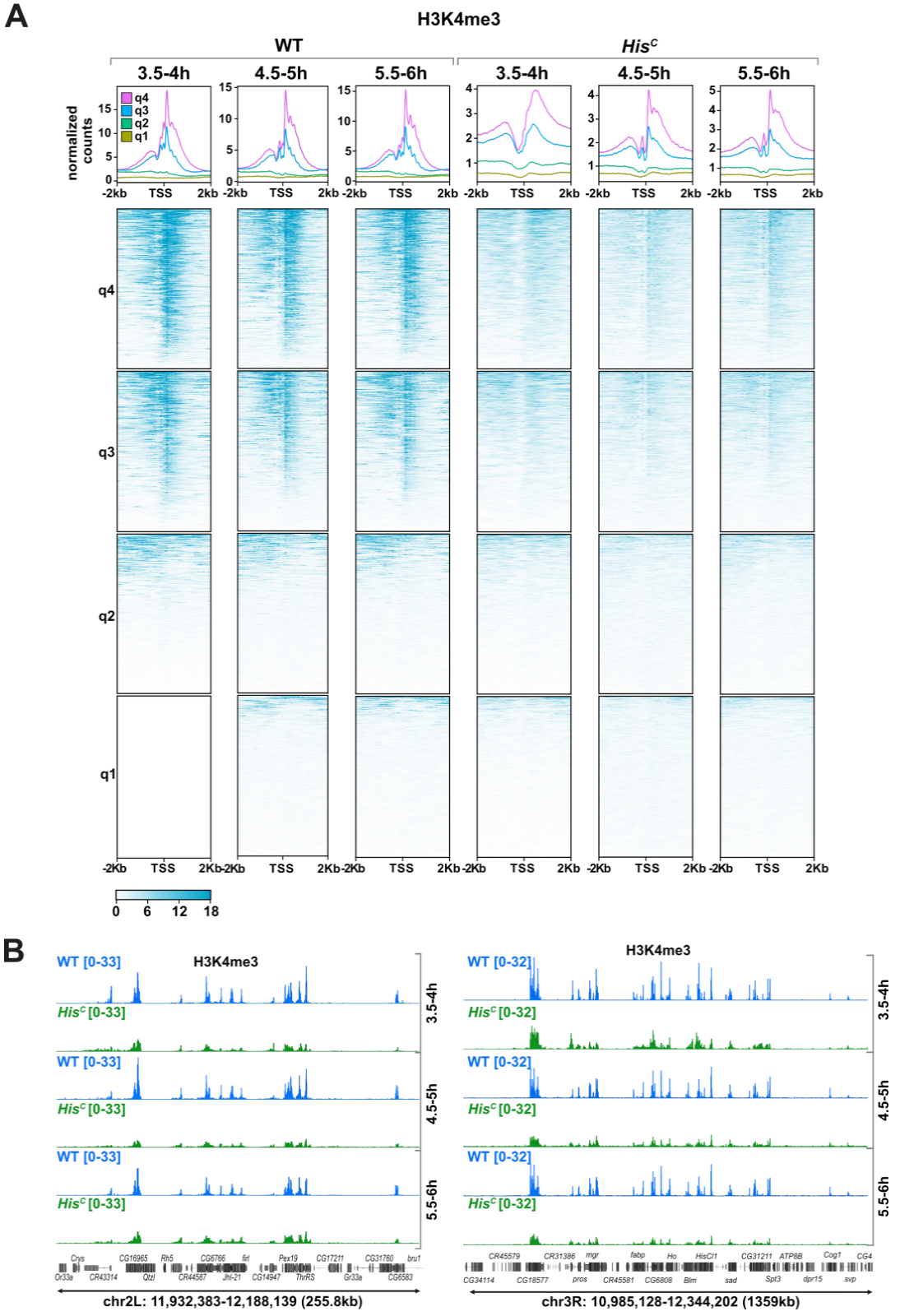

Figure 2.24 Fig. S20: H3K4me3 enrichment is largely re-established in *His^C* mutants. (**A**) Profile plots and heatmaps of H3K4me3 CUT&Tag normalised counts at TSSs of wild type (WT) and *His^C* mutant embryos at 3.5-4h, 4.5-5h and 5.5-6h AEL separated by associated gene expression quartiles (q1 = lowest). Profile plots for 5.5-6h are also shown in Fig. 4A. (**B**) Representative snapshot of H3K4me3 CUT&Tag coverage tracks of wild type (WT, blue) and *His^C* mutant (green) embryos at 3.5-4h, 4.5-5h and 5.5-6h AEL on chromosome (chr) 2L (left) and 2R (right).

Figure S21

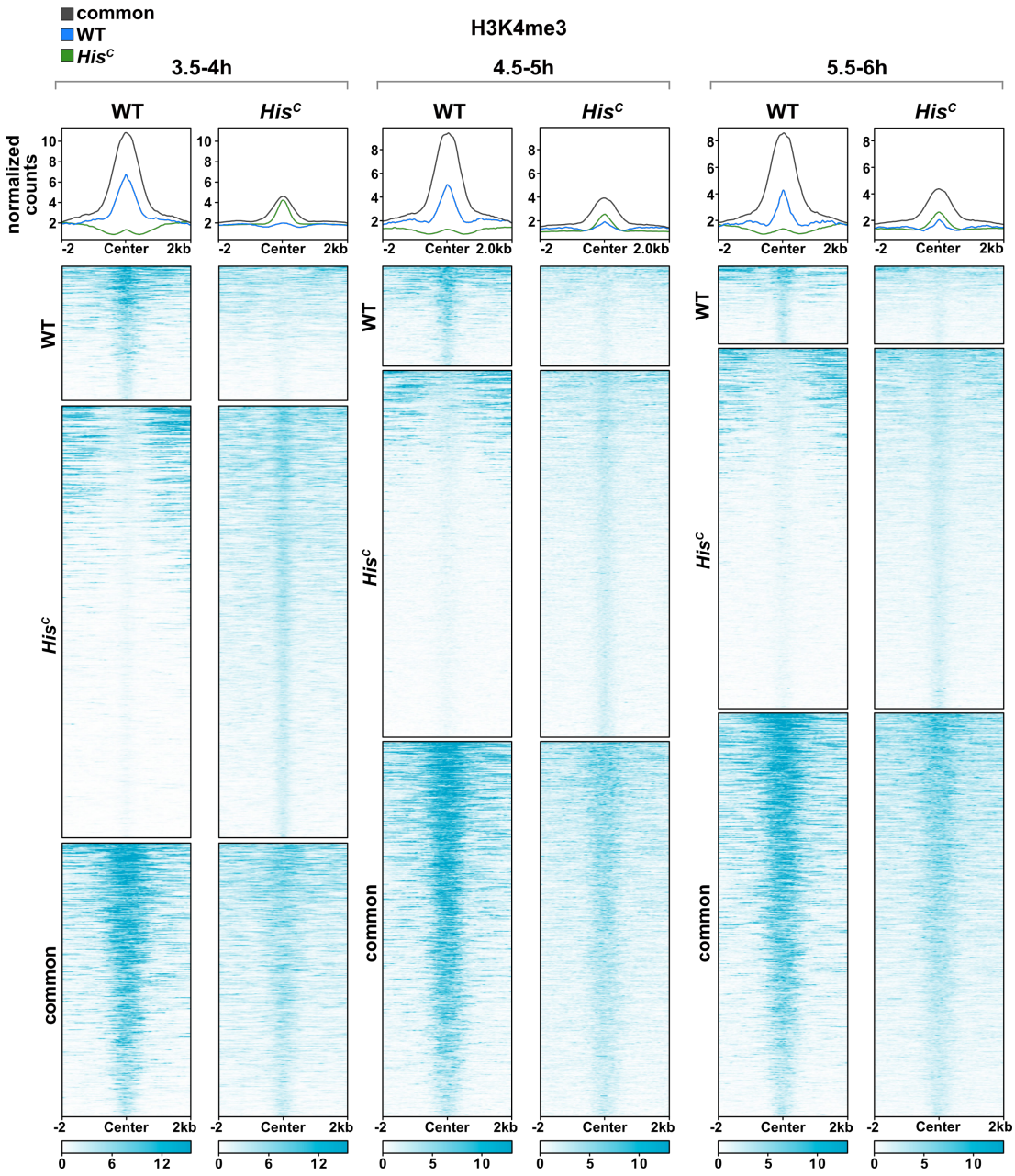

Figure 2.25 Fig. S21: Robust subset of H3K4me3 peaks in both wild type and *His*^{C} mutants. Profile plots and heatmaps of H3K4me3 CUT&Tag normalised counts at called peaks of wild type (WT) and *His*^{C} mutant embryos at 3.5-4h, 4.5-5h and 5.5-6h AEL. Profile plots for 5.5-6h are also shown in Fig. 4C.

Figure S22

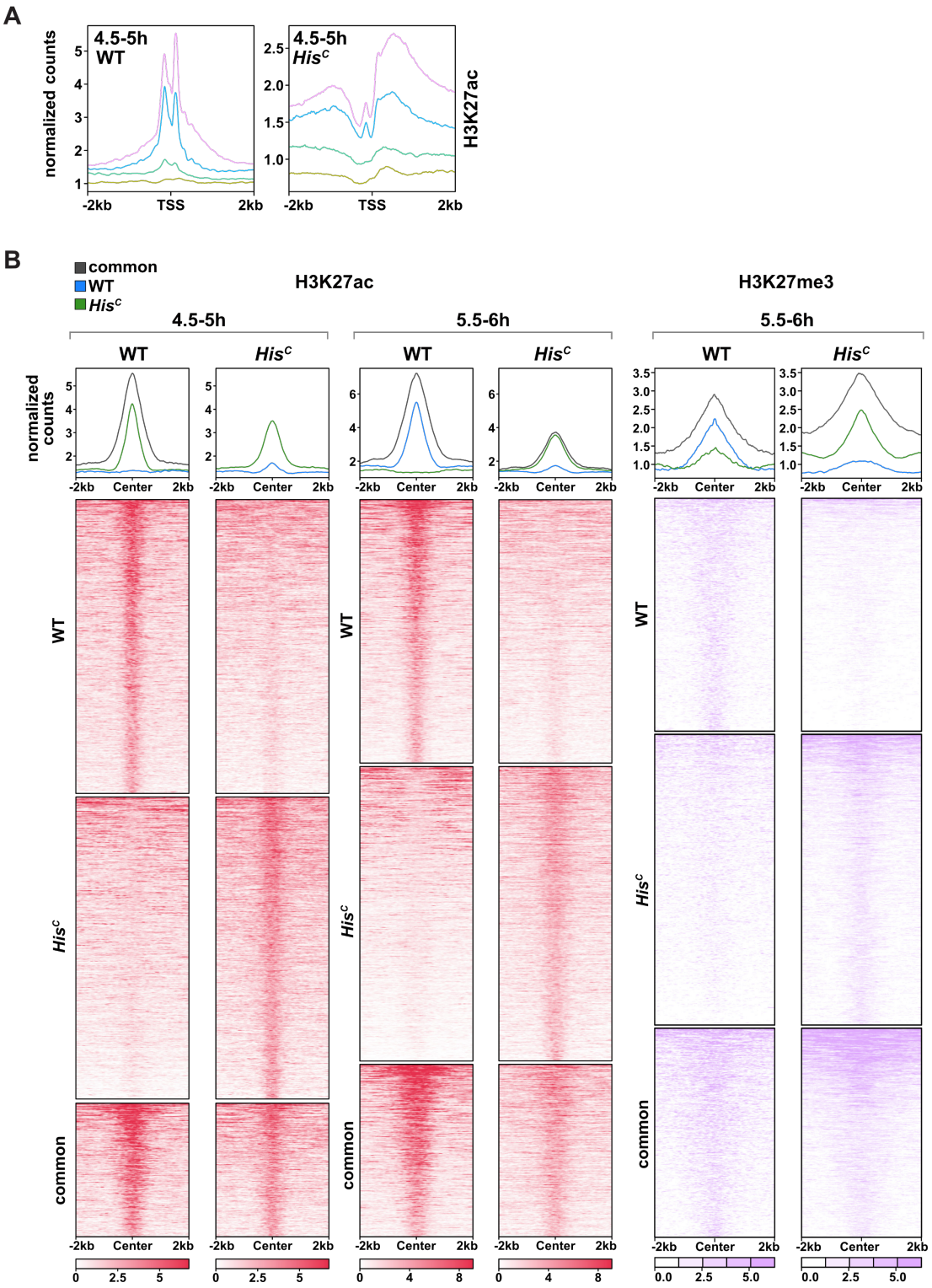

Figure 2.26 Fig. S22: Robust subset of H3K27ac and H3K27me3 peaks in both wild type and *His*^{C} mutants. (**A**) Profile plots of H3K27ac CUT&Tag normalised counts at TSSs of wild type (WT) and *His*^{C} mutant embryos at 4.5-5h AEL separated by associated gene expression quartiles (q1 = lowest). (**B**) Profile plots and heatmaps of H3K27ac and H3K27me3 CUT&Tag normalised counts at called peaks of wild type (WT) and *His*^{C} mutant embryos at 4.5-5h and/or 5.5-6h AEL. Profile plots for 5.5-6h are also shown in Fig. 4E, F.

Figure S23

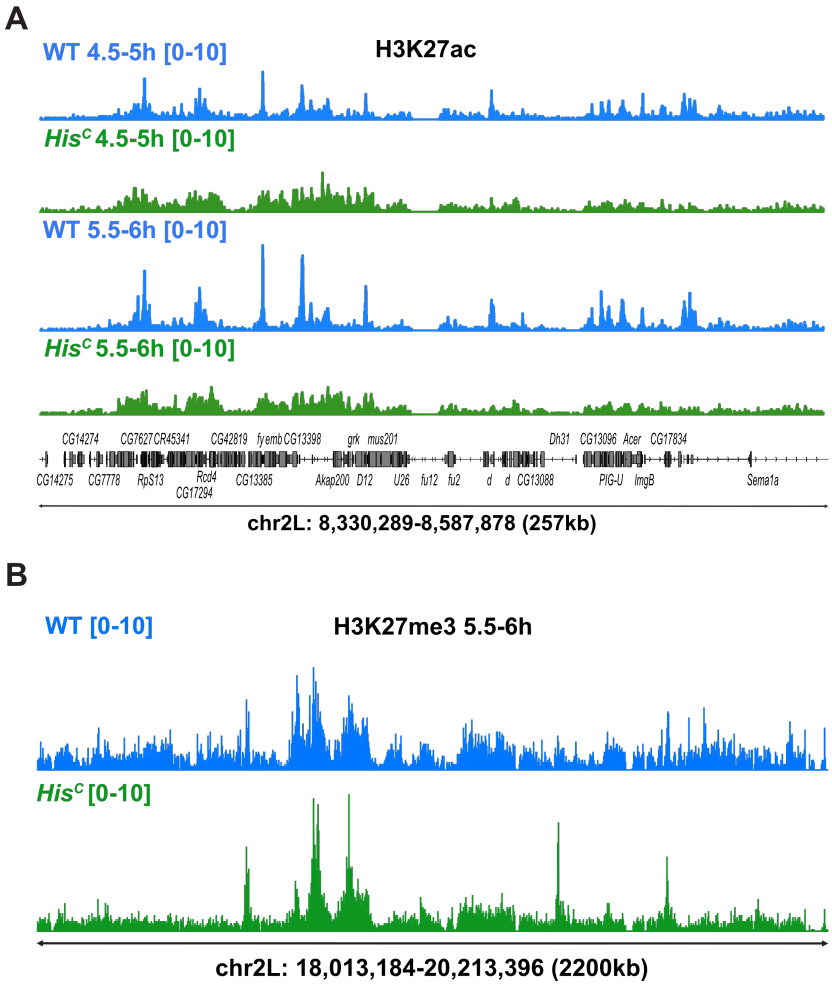

Figure 2.27 Fig. S23: H3K27ac and H3K27me3 coverage tracks. (**A**) Representative snapshot of H3K27ac CUT&Tag coverage tracks of wild type (WT, blue) and *His*^{C} mutant (green) embryos at 4.5-5h and 5.5-6h AEL on chromosome (chr) 2L. (**B**) Representative snapshot of H3K27me3 CUT&Tag coverage tracks of wild type (WT, blue) and *His*^{C} mutant (green) embryos at 5.5-6h AEL on chromosome (chr) 2L.

Figure S24

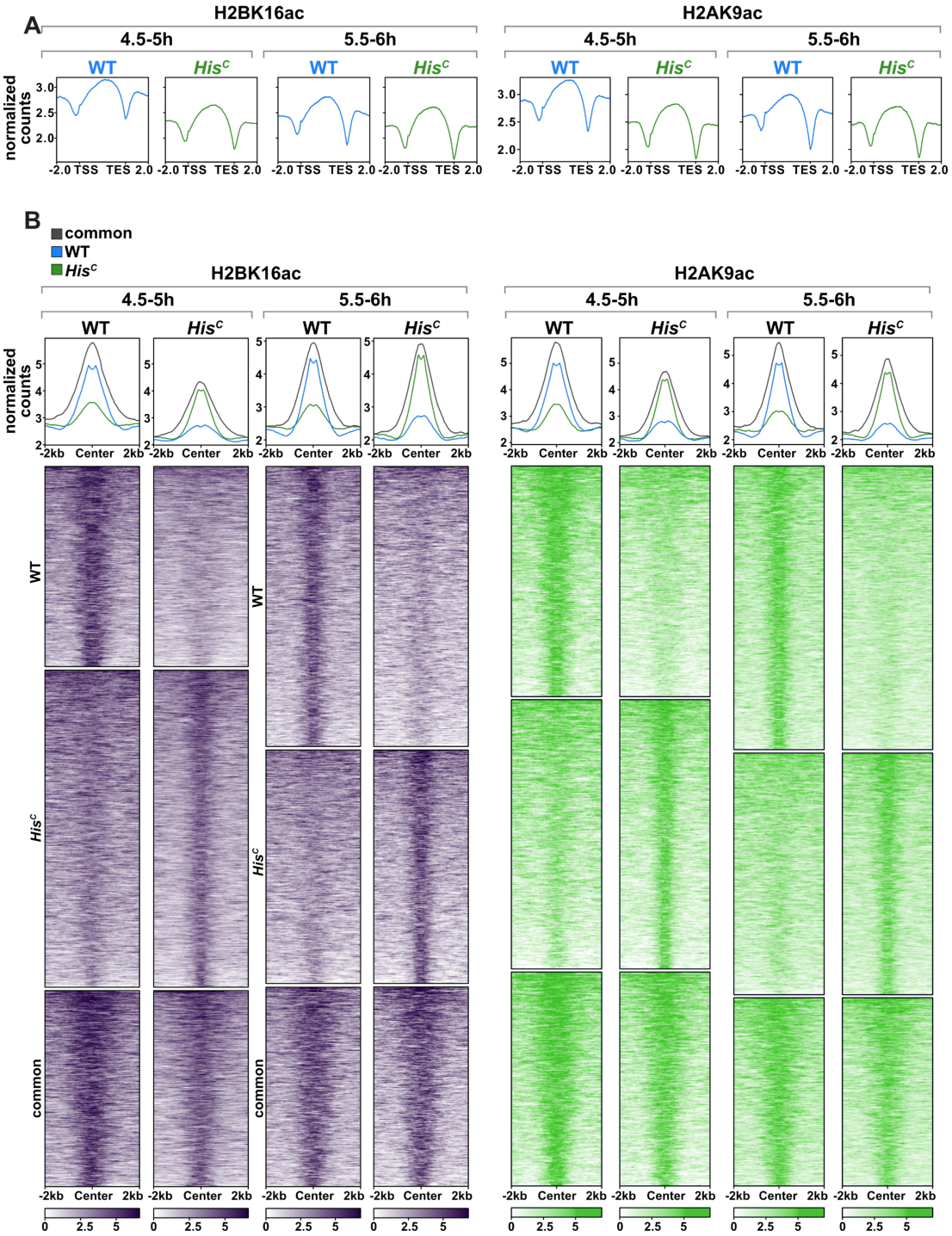

Figure 2.28 Fig. S24: Robust subset of H2BK16ac and H2AK9ac peaks in both wild type and *His*^{C} mutants. (**A**) Profile plots of H2BK16ac and H2AK9ac CUT&Tag normalised counts across gene bodies of wild type (WT, blue) and *His*^{C} mutant (green) embryos at 4.5-5h and 5.5-6h AEL. (**B**) Profile plots and heatmaps of H2BK16ac and H2AK9ac CUT&Tag normalised counts at called peaks (BroadPeak) of wild type (WT) and *His*^{C} mutant embryos at 4.5-5h and 5.5-6h AEL. Profile plots for 5.5-6h are also shown in Fig. 4H, I.

Figure S25

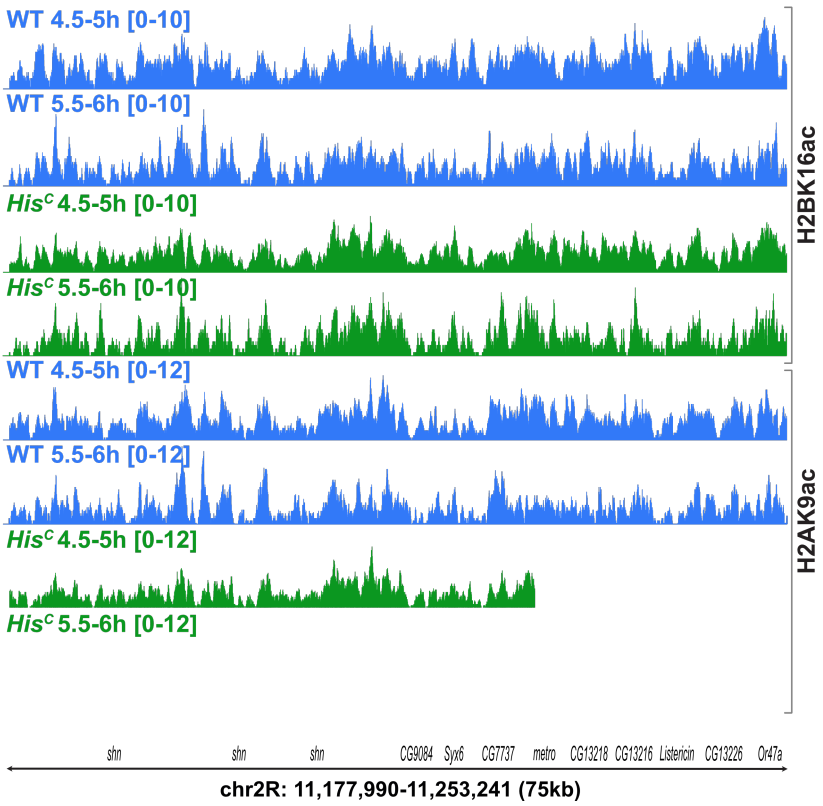

Figure 2.29 Fig. S25: H2BK16ac and H2AK9ac coverage tracks. Representative snapshot of H2BK16ac and H2AK9ac CUT&Tag coverage tracks of wild type (WT, blue) and *His*^{C} mutant (green) embryos at 4.5-5h and 5.5-6h AEL on chromosome (chr) 2R.

2.1.5.2 Resources

Table 1 Antibodies

Name	Cat. No.	Provider
α-H3K4me2	39142	Active Motif
α-H3K4me3	91264	Active Motif
α-H3K27me3	39157	Active Motif
α-H3K27ac	39134	Active Motif
α-H3K36me3	61102	Active Motif
α-H2AK9ac	39110	Active Motif
α-H2BK16ac	39122	Active Motif
α-RNAPII	61668	Active Motif
α-RNAPIIS2P	61084	Active Motif
α-H1	61786	Active Motif
α-Cyclin B	2245815	Hybridoma Bank
α-beta galactosidase	200-901-036	Rockland
α-Mn-647	A21235	Invitrogen/ThermoFisher
α-Chk-488	A11039	Invitrogen/ThermoFisher
α-Dig-POD	11207733910	Roche

Table 2 Primer ATAC-seq, CUTAC, CUT&Tag

Name	Sequence
DM122_Ad1_noMX:	AATGATACGGCGACCACCGAGATCTACACTCGTCG GCAGCGTCAGATGTG
DM123_Ad2.1_TAAGGCGA	CAAGCAGAAGACGGCATACGAGATTCGCCTTAGTC TCGTGGGCTCGGAGATGT
DM124_Ad2.2_CGTACTAG	CAAGCAGAAGACGGCATACGAGATCTAGTACGGTC TCGTGGGCTCGGAGATGT
DM125_Ad2.3_AGGCAGAA	CAAGCAGAAGACGGCATACGAGATTTCTGCCTGTC TCGTGGGCTCGGAGATGT
DM126_Ad2.4_TCCTGAGC	CAAGCAGAAGACGGCATACGAGATGCTCAGGAGTC TCGTGGGCTCGGAGATGT
DM127_Ad2.5_GGACTCCT	CAAGCAGAAGACGGCATACGAGATAGGAGTCCGTC TCGTGGGCTCGGAGATGT
DM128_Ad2.6_TAGGCATG	CAAGCAGAAGACGGCATACGAGATCATGCCTAGTC TCGTGGGCTCGGAGATGT
DM129_Ad2.7_CTCTCTAC	CAAGCAGAAGACGGCATACGAGATGTAGAGAGGTC TCGTGGGCTCGGAGATGT
DM130_Ad2.8_CAGAGAGG	CAAGCAGAAGACGGCATACGAGATCCTCTCTGGTC TCGTGGGCTCGGAGATGT

Name	Sequence
DM131_Ad2.9_GCTACGCT	CAAGCAGAAGACGGCATACGAGATAGCGTAGCGTC TCGTGGGCTCGGAGATGT
DM132_Ad2.10_CGAGGCTG	CAAGCAGAAGACGGCATACGAGATCAGCCTCGGTC TCGTGGGCTCGGAGATGT
DM133_Ad2.11_AAGAGGCA	CAAGCAGAAGACGGCATACGAGATTGCCTCTTGTC TCGTGGGCTCGGAGATGT
DM134_Ad2.12_GTAGAGGA	CAAGCAGAAGACGGCATACGAGATTCCTCTACGTC TCGTGGGCTCGGAGATGT
DM135_Ad2.13_GTCGTGAT	CAAGCAGAAGACGGCATACGAGATATCACGACGTC TCGTGGGCTCGGAGATGT
DM136_Ad2.14_ACCACTGT	CAAGCAKHGHGHJGGAAGACGGCATACGAGATACA GTGGTGTCTCGTGGGCTCGGAGATGT
DM137_Ad2.15_TGGATCTG	CAAGCAGAAGACGGCATACGAGATCAGATCCAGTC TCGTGGGCTCGGAGATGT
DM138_Ad2.16_CCGTTTGT	CAAGCAGAAGACGGCATACGAGATACAAACGGGTC TCGTGGGCTCGGAGATGT
DM139_Ad2.17_TGCTGGGT	CAAGCAGAAGACGGCATACGAGATACCCAGCAGTC TCGTGGGCTCGGAGATGT
DM140_Ad2.18_GAGGGGTT	CAAGCAGAAGACGGCATACGAGATAACCCCTCGTC TCGTGGGCTCGGAGATGT
DM141_Ad2.19_AGGTTGGG	CAAGCAGAAGACGGCATACGAGATCCCAACCTGTC TCGTGGGCTCGGAGATGT
DM142_Ad2.20_GTGTGGTG	CAAGCAGAAGACGGCATACGAGATCACCACACGTC TCGTGGGCTCGGAGATGT
DM143_Ad2.21_TGGGTTTC	CAAGCAGAAGACGGCATACGAGATGAAACCCAGTC TCGTGGGCTCGGAGATGT
DM144_Ad2.22_TGGTCACA	CAAGCAGAAGACGGCATACGAGATTGTGACCAGTC TCGTGGGCTCGGAGATGT
DM145_Ad2.23_TTGACCCT	CAAGCAGAAGACGGCATACGAGATAGGGTCAAGTC TCGTGGGCTCGGAGATGT
DM146_Ad2.24_CCACTCCT	CAAGCAGAAGACGGCATACGAGATAGGAGTGGGT CTCGTGGGCTCGGAGATGT
DM378_Ad1.1_GCGATCTA	AATGATACGGCGACCACCGAGATCTACACTAGATC GC TCGTCGGCAGCGTC AGATGTG
DM379_Ad1.2_ATAGAGAG	AATGATACGGCGACCACCGAGATCTACACCTCTCT AT TCGTCGGCAGCGTC AGATGTG
DM380_Ad1.3_AGAGGATA	AATGATACGGCGACCACCGAGATCTACACTATCCT CT TCGTCGGCAGCGTC AGATGTG
DM381_Ad1.4_TCTACTCT	AATGATACGGCGACCACCGAGATCTACACAGAGTA GA TCGTCGGCAGCGTC AGATGTG
DM382_Ad1.5_CTCCTTAC	AATGATACGGCGACCACCGAGATCTACACGTAAGG AG TCGTCGGCAGCGTC AGATGTG

Name	Sequence
DM383_Ad1.6_TATGCAGT	AATGATACGGCGACCACCGAGATCTACACACTGCA TA TCGTCGGCAGCGTC AGATGTG

Table 3 Primer STRIPE-seq

Name	Sequence
DM339_RTO_1	CAAGCAGAAGACGGCATACGAGATTAGTGCGTGACT GGAGTTCAGACGTGTGCTCTTCCGATCT NNNNN
DM340_RTO_2	CAAGCAGAAGACGGCATACGAGATACATCGGTGACT GGAGTTCAGACGTGTGCTCTTCCGATCTNNNNN
DM341_RTO_3	CAAGCAGAAGACGGCATACGAGATGCCTAAGTGACT GGAGTTCAGACGTGTGCTCTTCCGATCTNNNNN
DM342_RTO_4	CAAGCAGAAGACGGCATACGAGATTGGTCAGTGACT GGAGTTCAGACGTGTGCTCTTCCGATCTNNNNN
DM343_RTO_5	CAAGCAGAAGACGGCATACGAGATCACTGTGTGACT GGAGTTCAGACGTGTGCTCTTCCGATCTNNNNN
DM344_RTO_6	CAAGCAGAAGACGGCATACGAGATATTGGCGTGACT GGAGTTCAGACGTGTGCTCTTCCGATCTNNNNN
DM345_TSO	Biotin-CCTACACGACGCTCTTCCGATCTNNNNNNNNTATArG rGrG
DM346_RTO_7	CAAGCAGAAGACGGCATACGAGATGATCTGGTGACT GGAGTTCAGACGTGTGCTCTTCCGATCTNNNNN
DM347_RTO_8	CAAGCAGAAGACGGCATACGAGATTCAAGTGTGACT GGAGTTCAGACGTGTGCTCTTCCGATCTNNNNN
DM348_RTO_9	CAAGCAGAAGACGGCATACGAGATCTGATCGTGACT GGAGTTCAGACGTGTGCTCTTCCGATCTNNNNN
DM349_RTO_10	CAAGCAGAAGACGGCATACGAGATAAGCTAGTGACT GGAGTTCAGACGTGTGCTCTTCCGATCTNNNNN
DM350_RTO_11	CAAGCAGAAGACGGCATACGAGATGTAGCCGTGACT GGAGTTCAGACGTGTGCTCTTCCGATCTNNNNN
DM351_RTO_12	CAAGCAGAAGACGGCATACGAGATTACAAGGTGACT GGAGTTCAGACGTGTGCTCTTCCGATCTNNNNN
DM352_RTO_13	CAAGCAGAAGACGGCATACGAGATTTGACTGTGACT GGAGTTCAGACGTGTGCTCTTCCGATCTNNNNN
DM353_RTO_14	CAAGCAGAAGACGGCATACGAGATGGAACTGTGACT GGAGTTCAGACGTGTGCTCTTCCGATCTNNNNN
DM354_RTO_15	CAAGCAGAAGACGGCATACGAGATTGACATGTGACT GGAGTTCAGACGTGTGCTCTTCCGATCTNNNNN
DM355_RTO_16	CAAGCAGAAGACGGCATACGAGATGGACGGGTGAC TGGAGTTCAGACGTGTGCTCTTCCGATCTNNNNN

Name	Sequence
DM356_RTO_17	CAAGCAGAAGACGGCATACGAGATGCGGACGTGAC TGGAGTTCAGACGTGTGCTCTTCCGATCTNNNNN
DM357_RTO_18	CAAGCAGAAGACGGCATACGAGATTTTCACGTGACT GGAGTTCAGACGTGTGCTCTTCCGATCTNNNNN
DM358_FLO	AATGATACG
DM359_RLO	CAAGCAGAAGACGGCATACG
DM362_FLO i5_501	AATGATACGGCGACCACCGAGATCTACACTATAGCC TTCTTTCCCTACACGACGCTCTTCCG

Table 4 Primers used for qRT-PCR and *in vitro* transcription

Name	Sequence
DM9_*H1*_1f	AAGGCAAAAGCCAAGGATGC
DM10_*H1*_1R	CTTCGCTGCAGTCACTTTCG
DM13_*H2A*_1F	CGGAAGGGAAACTACGCAGA
DM14_*H2A*_1R	GAACCTCAGCGGCCAGATAT
DM17_*H2B*_1F	TCACTACAACAAGCGCTCGA
DM18_*H2B*_1R	ATGCTTGGCCAACTCTCCAG
DM21_*H3*_1F	TCTGCAGGAAGCTAGCGAAG
DM22_*H3*_1R	TATGGTGACACGCTTGGCAT
DM25_*H4*_1F	AATTCGTGATGCCGTGACCT
DM26_*H4*_1R	TTGCCTCTTCAGAGCGTACA
DM39_*Act5C*_fw	ATTTGCCGGAGACGATGCTC
DM40_*Act5C*_rv	TACGAGTCCTTCTGGCCCAT
DM5_*stg1*_fw	CCAGCAGTTCGAGTAGCATC
DM6_*stg1*_rv_T7	GAATTAATACGACTCACTATAGGGAGACTTTGCTGAAGTC GCCGATT

Table 5 Fly Stocks

Stock Number	Genotype
DM1	*Df(2L)His^{C} / CyO, P{ftz-lacB}E3*
DM3	*Df(2L)His^{C}, P{UAS:eYFP}AH2/ CyO, P{ftz-lacB}E3*
DM4	*Df(2L)His^{C}, P{GAL4-twi.2xPE}/ CyO, P{ftz-lacB}E3*

Table 6 Software, packages and scripts used for data analysis

Name	Reference
R version 3.6.0	(*218*)
DESeq2_1.22.2	(*204*)

Name	Reference
clusterProfiler_3.10.1	(*207*)
pheatmap_1.0.12	(*219*)
ggplot2_3.1.0	(*205*)
RSEM v1.3.1	(*206*)
FastQC v0.11.5	(*220*)
Deeptools v3.3.1	(*214*)
STAR v2.5.2b	(*202*)
HTSeq-count version 0.10	(*203*)
TrimGalore v0.6.6	(*221*)
Cutadapt v1.17	(*208*)
bowtie2 v2.3.4.2	(*211*)
samtools v1.9	(*212*)
sambamba v0.6.7	(*209*)
MACS2 v2.1.2	(*222*)
TSRchitect	(*223*)
TSRexplorer	(*215*)
ChIPseeker	(*216*)
GoSTRIPES	(*194*)
Encode Blacklist	(*210*)

Table 7 NGS libraries and replicates

Genotype	Time point (AEL)	Approach	Replicates
w^{1118}	3.5-4h	RNA-seq	3
w^{1118}	4.5-5h	RNA-seq	3
w^{1118}	5.5-6h	RNA-seq	3
w^{1118}	6.5-7h	RNA-seq	3
His^{C}	3.5-4h	RNA-seq	3
His^{C}	4.5-5h	RNA-seq	2
His^{C}	5.5-6h	RNA-seq	3
His^{C}	6.5-7h	RNA-seq	3
w^{1118}	3.5-4h	ATAC-seq	3
w^{1118}	4.5-5h	ATAC-seq	3
w^{1118}	5.5-6h	ATAC-seq	3
w^{1118}	6.5-7h	ATAC-seq	3
His^{C}	3.5-4h	ATAC-seq	3
His^{C}	4.5-5h	ATAC-seq	3
His^{C}	5.5-6h	ATAC-seq	3

Genotype	Time point (AEL)	Approach	Replicates
His^{C}	6.5-7h	ATAC-seq	3
w^{1118}	5.5-6h	Histone H1 CUT&Tag	2
His^{C}	5.5-6h	Histone H1 CUT&Tag	2
w^{1118}	5.5-6h	RNAPII CUT&Tag	2
His^{C}	5.5-6h	RNAPII CUT&Tag	2
w^{1118}	4.5-6h	RNAPIIS2P CUT&Tag	2
His^{C}	5.5-6h	RNAPIIS2P CUT&Tag	2
w^{1118}	4.5-6h	RNAPIIS2P CUT&Tag	2
His^{C}	5.5-6h	RNAPIIS2P CUT&Tag	2
w^{1118}	4.5-6h	H3K36me3 CUT&Tag	2
w^{1118}	5.5-6h	H3K36me3 CUT&Tag	2
His^{C}	4.5-6h	H3K36me3 CUT&Tag	2
His^{C}	5.5-6h	H3K36me3 CUT&Tag	2
w^{1118}	4.5-5h	H3K4me2 CUTAC	2
w^{1118}	5.5-6h	H3K4me2 CUTAC	2
His^{C}	4.5-5h	H3K4me2 CUTAC	2
His^{C}	5.5-6h	H3K4me2 CUTAC	2
w^{1118}	5.5-6h	STRIPE-seq	4
w^{1118}	6.5-7h	STRIPE-seq	5
His^{C}	5.5-6h	STRIPE-seq	4
His^{C}	6.5-7h	STRIPE-seq	5
w^{1118}	3.5-4h	H3K4me3 CUT&Tag	3
w^{1118}	4.5-5h	H3K4me3 CUT&Tag	3
w^{1118}	5.5-6h	H3K4me3 CUT&Tag	3
His^{C}	3.5-4h	H3K4me3 CUT&Tag	2
His^{C}	4.5-5h	H3K4me3 CUT&Tag	3
His^{C}	5.5-6h	H3K4me3 CUT&Tag	3
w^{1118}	4.5-5h	H3K27ac CUT&Tag	2
w^{1118}	5.5-6h	H3K27ac CUT&Tag	2
His^{C}	4.5-5h	H3K27ac CUT&Tag	2
His^{C}	5.5-6h	H3K27ac CUT&Tag	2
w^{1118}	5.5-6h	H3K27me3 CUT&Tag	3
His^{C}	5.5-6h	H3K27me3 CUT&Tag	2
w^{1118}	4.5-5h	H2BK16ac CUT&Tag	2
w^{1118}	5.5-6h	H2BK16ac CUT&Tag	2
His^{C}	4.5-5h	H2BK16ac CUT&Tag	2
His^{C}	5.5-6h	H2BK16ac CUT&Tag	2
w^{1118}	4.5-5h	H2AK9ac CUT&Tag	3

Genotype	Time point (AEL)	Approach	Replicates
w^{1118}	5.5-6h	H2AK9ac CUT&Tag	2
His^{C}	4.5-5h	H2AK9ac CUT&Tag	2
His^{C}	5.5-6h	H2AK9ac CUT&Tag	3

2.2 Chapter II: The lack of histone synthesis results in a cell cycle arrest mediated by degradation of *string* RNA by How

During the S-phase of the cell cycle, replication coupled histones are newly expressed and participate, together with parental histones, in the formation of nucleosomes during DNA replication to form the corresponding chromatin landscape in the daughter cells. In *Drosophila melanogaster* these canonical histone genes are clustered in a single histone complex, which has been deleted in the *Df(2L)His*^{C} mutant, referred to as "*His*^{C} mutant". As a consequence, the lack of new histone supply causes to a cell cycle arrest at the G2/M transition after nuclear division 15. Earlier results have shown that this cell cycle arrest correlates with the lack of *string* expression during the S phase of the nuclear cycle 15, and that transgene-dependent expression of *string* cancels this cell cycle arrest, indicating that the lack of *string* expression is the cause of the *Df(2L)His*^{C} mutant phenotype (*1*). I made an attempt to clarify whether the failure of *string* expression is due to specific lack of *string* transcription or a rapid degradation of *string* mRNA, and what factors are involved in suppressing *string* activity in the absence of newly synthesized histones.

Authors

Dominik Mühlen, Herbert Jäckle, Ufuk Günesdogan*

*corresponding author

Status

Preliminary results that require more controls, quantifications, and additional experiments

My contributions

- Contribution to the conceptualisation of the project[1]
- Husbandry of model system
- Preparation and conduction experiments
- Preparation or modification of figures
- Data analysis

[1] Together with Dr. Ufuk Günesdogan and Prof. Herbert Jäckle

The lack of histone synthesis results in a cell cycle arrest mediated by degradation of *string* RNA by How

Dominik Mühlen[1,2], Herbert Jäckle[2], Ufuk Günesdogan[1,2,*]

[1] University of Göttingen, Göttingen Center for Molecular Biosciences, Department of Developmental Biology, Justus-von-Liebig Weg 11, 37077 Göttingen, Germany

[2] Max Planck Institute for Biophysical Chemistry, Department for Molecular Developmental Biology, Am Fassberg 11, 37077 Göttingen, Germany

[*] Correspondence: ufuk.guenesdogan@uni-goettingen.de

2.2.1 Abstract

Canonical histones are expressed during DNA replication to re-assemble nucleosomes onto the newly synthesised DNA. The lack of histone synthesis in *Drosophila* embryos results in a cell cycle arrest at the G2/M transition in cycle 15, caused by a failure to upregulate the Cdc25-like tyrosine protein phosphatase String. However, the mechanism of *string* regulation in the absence of histone synthesis remains unclear. To address this issue, we made use of *Drosophila* mutant embryos which lack the canonical histone genes (His^C). We show that the long isoform of Held-out-wings (How(L)) is upregulated in His^C mutants but not in wild type embryos. Transgenes, where either the *5´UTR* or the 3´ end of *string* is replaced by corresponding sequences of the *heatshock protein A* gene (*HspA*) and *SV40*, respectively, suggest that the protein How(L) binds to the 3´untranslated region of *string* mRNA and mediates its degradation.

2.2.2 Introduction

In eukaryotes, DNA is packed into nucleosomes. They form the basic repeating subunit of chromatin. Each nucleosome contains an octameric core complex built from the 2 copies of each of the replicative or canonical histones H2A, H2B, H3, and H4. Recently, a histone null mutant, *Df(2L)His^{C}* of *Drosophila melanogaster*, hereafter referred to as *His^{C}* mutant, has been generated (*2*). This deficiency lacks all canonical histones which, in contrast to other known organisms, are located in two proximal gene clusters within the genome and thus, could be deleted by genetic means. Heterozygous *His^{C}* mutant flies are viable and fertile, whereas homozygous *His^{C}* mutants fail to continue with cell divisions during early embryogenesis in mitotic cycle 15, after zygotic transcription is activated, and new histones would normally be synthesized (*3, 4*). This cell cycle arrest occurs at the G2/M transition linked to the failure to upregulate the phosphatase String, an evolutionarily conserved Cdc25-like tyrosine protein phosphatase which is normally upregulated during G2 phase and functions as a dosage-dependent inducer of mitotic and meiotic progression (*5, 6*).

During the early phase of *Drosophila* development, when syncytial nuclei rapidly divide without a G2 phase of the cycle, Twine phosphatase activity is responsible for driving the induction of nuclear divisions prior to the mid blastula transition (MBT) stage. After MBT, when zygotic transcription has already started and G2 phases became part of the cell cycle, the activity of Twine becomes functionally replaced by String activity which from then onwards induces the G2/M transitions (see details in Figure 2.30).

Expression of *string* using the UAS/GAL4 (upstream activating sequence) system in *His^{C}* mutants rescues the cell cycle arrest phenotype, i.e. the G2/M phase transition occurs at the M-phase 15 (M_{15}) stage in those cells in which the *string* transgene is expressed (*1*). This observation not only confirms that *string* accumulation is essential for the G2/M transition but also shows that its activity is downregulated when the amount of histones is limited due to the absence of new histone synthesis.

Here, we have used the *His^{C}* mutant to address the question of how String activity is downregulated during the G2/M_{15} phase of embryonic cell cycle 15 in the absence of histone synthesis. We show that *string* mRNA is degraded in *His^{C}* mutants. Replacement of the *3´UTR* of *string* mRNA increases its stability. Further, we show that How(L) binds to the putative regulatory elements in the 3´region of *string* mRNA and promotes the degradation process.

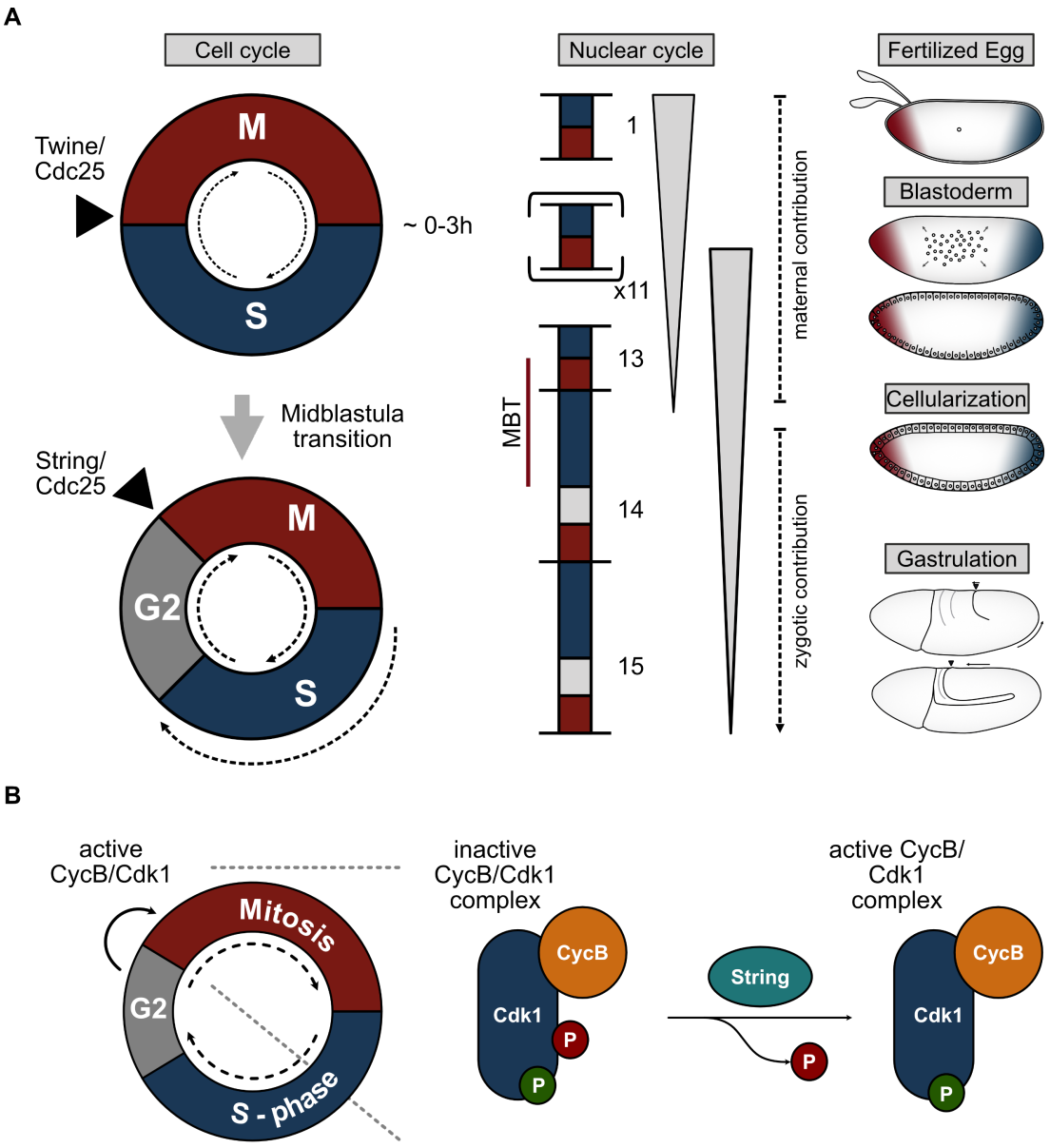

Figure 2.30 Maternal contribution organizes early nuclear divisions in *Drosophila* embryos. (A) Schematic representation of the first nuclear cycles (NC) during the embryonic development of *Drosophila melanogaster*. Maternally deposited mRNAs and proteins are sufficient to support the first fourteen nuclear cycles of the early embryo. These rapid nuclear divisions are characterized by rapid M and S phases that are not accompanied by drastic morphological changes. During NC10 the zygotic genome is activated in a process called zygotic genome activation (ZGA). During MBT in M_{13} and S_{14} the cell cycle slows which leads to a quick degradation of maternal mRNA in the now introduced $G2_{14}$ phase (2). The transition from S to M phase is regulated prior to MBT by the tyrosine phosphatase Cdc25 homologue Twine. After MBT G2/M transition is regulated by a second Cdc25 homologue called String. Mutant *His*^{C} embryos, which lack all replicative histone genes, however arrest in $G2/M_{15}$ because *string* is not upregulated upon lack of histone synthesis during S_{15}. (B) Cell cycle progression is mediated by the interplay of several cyclins and their cognate cyclin dependent kinases. The phosphatase String, Cdc25 in mammals, cleaves off the inhibitory phosphorylation of Y14 and Y15 on Cdk1 which leads to the activation of the Cyclin B/Cdk1 complex and the entry into mitosis. Modified from (*7, 8*).

2.2.3 Results

2.2.3.1 *string* expression in wild type and *His^C* mutants

In *His^C* mutants, *string* mRNA expression is not detected by fluorescent *in situ* hybridisation (FISH) in cell cycle 15 (*1*). Thus, we asked whether the expression of *string* is regulated on the level of transcription or mRNA stability. To test whether *string* is expressed, and mRNA is properly spliced and exported from the nucleus, we targeted mature *string* mRNA by FISH. Towards this, we generated a probe against the first exon and parts of the second exon of *string* mRNA. In addition, we stained for Cyclin B as a marker for mitosis, as Cyclin B accumulates during the cell cycle and is degraded during mitosis (*9*).

Wild type control embryos ~3h after egg laying (AEL) show a high level of *string* mRNA transcripts in the dorsal epidermis and lack of Cyclin B. This pattern indicates that these cells entered mitosis 14. Ventral cells still harbour high and low levels of Cyclin B and *string*, respectively, suggesting that they are still in S phase of cell cycle 14, and enter $G2_{14}$ when the *string* expression starts as described in Chapter I Figure 2.6 B. *His^C* mutant embryos show a similar expression pattern of *string* and Cyclin B at cell cycle 14, when the parental set of histones is still sufficient to drive mitosis.

Figure 2.6 B shows wild type embryos undergoing M_{15} in dorsal epidermal cells as indicated by the lack of Cyclin B and reduced *string* expression, weak Cyclin B signal suggests that some cells have already entered S_{16} as a mitotic wave moves from anterior to posterior. A parallel wave extends from dorsal to ventral epidermal cells, as shown by cells of the midline with strong *string* expression and lack of cells with Cyclin B accumulation indicating M_{15} stage.

Ventral cells in $S/G2_{15}$ have high levels of Cyclin B and start to upregulate *string.* In contrast, *His^C* embryos (Figure 2.6 B) lack signs for the upregulation of *string* in dorsal cells and accumulation of Cyclin B. Posterior ventral cells that haven't arrested in $G2/M_{15}$ yet still show a weak *string* signal.

Wild type embryos at a later stage (Figure 2.31 A (A)) show only patches of Cyclin B expressing cells in the dorsal epidermis which are about to enter M_{16}, whereas cells of the midline are still in the process of DNA replication in S_{16}.

Ventral cells expressing high levels of *string* already enter M_{15}. *His^C* mutant embryos (Figure 2.31 A (A)) however show strong accumulation of Cyclin B in all cells and only rudimentary *string* expression, indicating that they fail to enter M_{15} (Figure 2.31 A (A')).

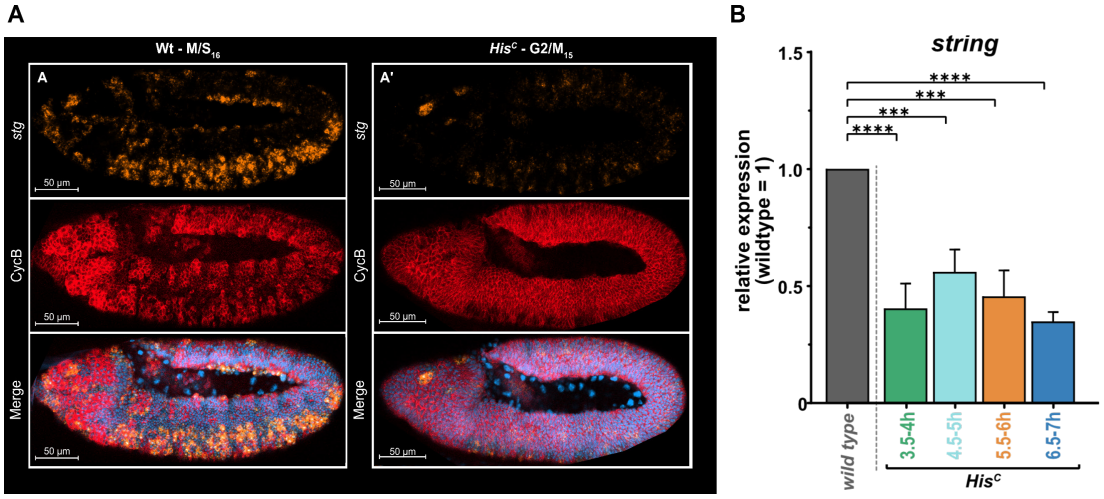

Figure 2.31 *string* expression pattern in wild type and *His^C* embryos (A) Expression pattern of *string* (orange) mRNA analysed by FISH targeting the first exon of the *string* transcript together with Cyclin B immunofluorescence (red) in wild type (A) and *His^C* mutant embryos (A'). Nuclei are stained by DAPI (blue). Depicted are embryos at cell cycle 16. (B) qRT-PCR for *string* based on 4 independent cDNA samples prepared from mutant and matched wild type embryos at four timepoints AEL as indicated. Each set was normalized by the corresponding expression of housekeeping gene *act5c* and analysed using ΔΔCt ± s.d. (8) and two-sided, unpaired Student's t-test. For simplicity only one wild type bar is displayed however each timepoint was normalized to the respective control. Four asterisks indicate p-values <0.0001, three asterisk p-values <0.0002 respectively.

Expression of *string* was further quantified by RT-qPCR using wild type and *His^C* mutant embryos at four different time points AEL (*10*). Consistent with the previous result, *string* transcripts were strongly reduced, but not completely absent (Figure 2.31 B). Taken together, these results suggest that mature *string* mRNA is not upregulated in *His^C* mutants.

2.2.3.2 *string* expression at the G2/M$_{15}$ arrest in *His^C* mutants by nascent mRNA FISH

Next, we asked whether *string* is transcribed during cell cycle 15 of *His^C* mutant embryos Figure 2.32. We performed nascent mRNA FISH using an RNA probe that was directed against intron sequences of *string*. This way *string* mRNA is captured during transcription and before the mRNA undergoes processing.

In wild type embryos, nascent *string* mRNA is present in cells together with intermediate levels of Cyclin B in cells of the dorsal epidermis which are at that stage in G2$_{15}$ phase. Cells of the posterior ventral epidermis express high levels of Cyclin B, showing that they are in late G2 phase where *string* transcription is reduced (Figure 2.32 A). Those cells, however, showed a strong signal for mature *string* mRNA (compare Figure 2.31 A). Dorsal cells undergoing M$_{15}$ are identified by the lack of Cyclin B and nascent *string* transcripts (Figure 2.32 B). Embryos at subsequent stages (Figure 2.32 C) also lack nascent *string* mRNA in cells of the dorsal epidermis which undergo M$_{16}$. Similarly, anterior cells of the ventral side exhibit high levels of Cyclin B, but no indication of nascent *string* transcripts (Figure 2.32 C), while *string* mRNA was observed with a probe directed against mature *string* mRNA (see

Figure 2.31 B). These observations indicate that nascent *string* mRNA can be observed prior to the detection of the mature mRNA in cells with high levels of Cyclin B. In contrast, *His*^{C} mutant embryos show minimal levels of nascent *string* expression (Figure 2.32 A' to C'). These findings indicate that the *string* gene is transcribed but mRNA fails to accumulate in the cells arrested at the M_{15} stage.

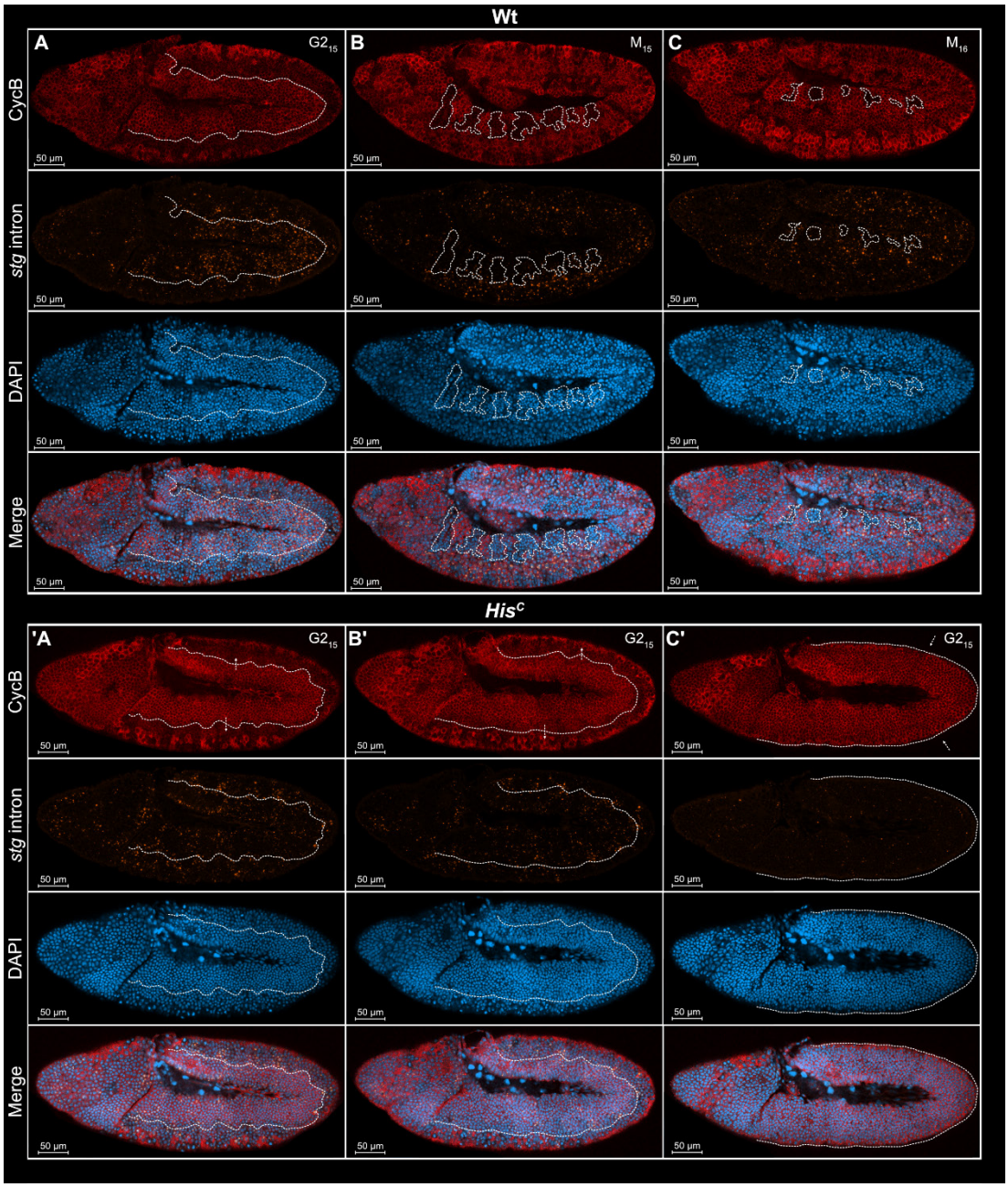

Figure 2.32 *His*^{C} mutant embryos still express *string* upon G2/M$_{15}$ arrest Expression pattern of nascent *string* (orange) mRNA analysed by whole mount FISH targeting the intronic sequence of the *string* transcript together with Cyclin B immunofluorescence (red) in wild type (A, B, C) and *His*^{C} mutant embryos (A', B', C'). Nuclei are stained by DAPI (blue). Embryos at different developmental stages undergoing cell cycle 15 (A, A'), 15 and 16 (B) and cell cycle 16 (C) as well as arrested *His*^{C} mutants (A' to C'). Encircled are mitotic cells lacking Cyclin B and nascent *string* signal (B and C). Dashed line separates G2/M$_{15}$ arrested cells from S$_{15}$ and G2$_{15}$ cells in mutants (A' to C').

2.2.3.3 Attempt to rescue the M_{15} arrest using *string*-based transgene constructs

Since *string* is actively transcribed in *His*^{C} mutant embryos, but transcripts fail to accumulate, it appears likely that the newly synthesized mRNA becomes rapidly degraded after transcription. Regulation of mRNA stability is generally under the control of RNA binding proteins which associate with the 5' and/or *3'UTR* of a specific mRNA. To test whether *string* mRNA stability is under control of such factors, we designed transgenes containing the *string* open reading frame and a replacement of the 5`untranslated region by the corresponding region of the heatshock protein A (*HspA* construct) and a replacement of the untranslated 3´region from *Simian Virus* 40 (*SV40* construct), respectively. The rational for this experimental design was that putative *string 5'UTR* binding regulators, which might negatively interfere with the stability of the mRNA, will not be able to bind mRNA encoded by the *HspA* construct and thus, its stability should increase. If such factors bind to *string 3´UTR*, the transcript accumulation should increase with mRNA encoded by the *SV40* construct.

The transgenes were expressed under the control of an UAS sequence in response to a driver line which expresses GAL4 under control of the *paired* (*prd*) promotor. Thus, the *string* mRNA transgenes will be expressed in a striped pattern along the anterior axis of the embryo in both dorsal and ventral cells. This design allows for a direct analysis of effects due to transgene expression in stripes, and for a direct comparison with neighbouring regions which lack expression in the same embryo. The transgenes were integrated into the genome using the PhiC31 system using chromosomal regions 86F6 and 51C1 on the 3rd and 2nd chromosome as insertion sites. To identify expression of the exogenous mRNA we designed mRNA probes against *HspA* 5' *UTR* and against *SV40* to discriminate the construct mRNA from endogenous *string* mRNA.

Figure 2.33 depicts wild type embryos of increasing developmental age (A to C) with integration of the *HspA* constructs in the 3rd chromosome (86F6). Wild type embryos show strong expression of the *HspA* transgene in the typical *paired* pattern of the otherwise wild type embryo. Notable, however is a temporal delay in signal detection by FISH in comparison to endogenous *paired* expression. This delay is caused by the binary UAS/Gal4 expression system. Within each domain, *HspA* expression is accompanied by the degradation of Cyclin B. Although it cannot be distinguished which part of Cyclin B degradation is caused by the *HspA* construct, comparison with the wild type Cyclin B pattern in Figure 2.6 B and Figure 2.31 A shows a clear disruption of the stereotypical Cyclin B domains when *HspA* is expressed in addition to the endogenous wild type *string* activity. This observation indicates that the *string* mRNA, which contains the 5´non-translated *HspA* sequences is translated into

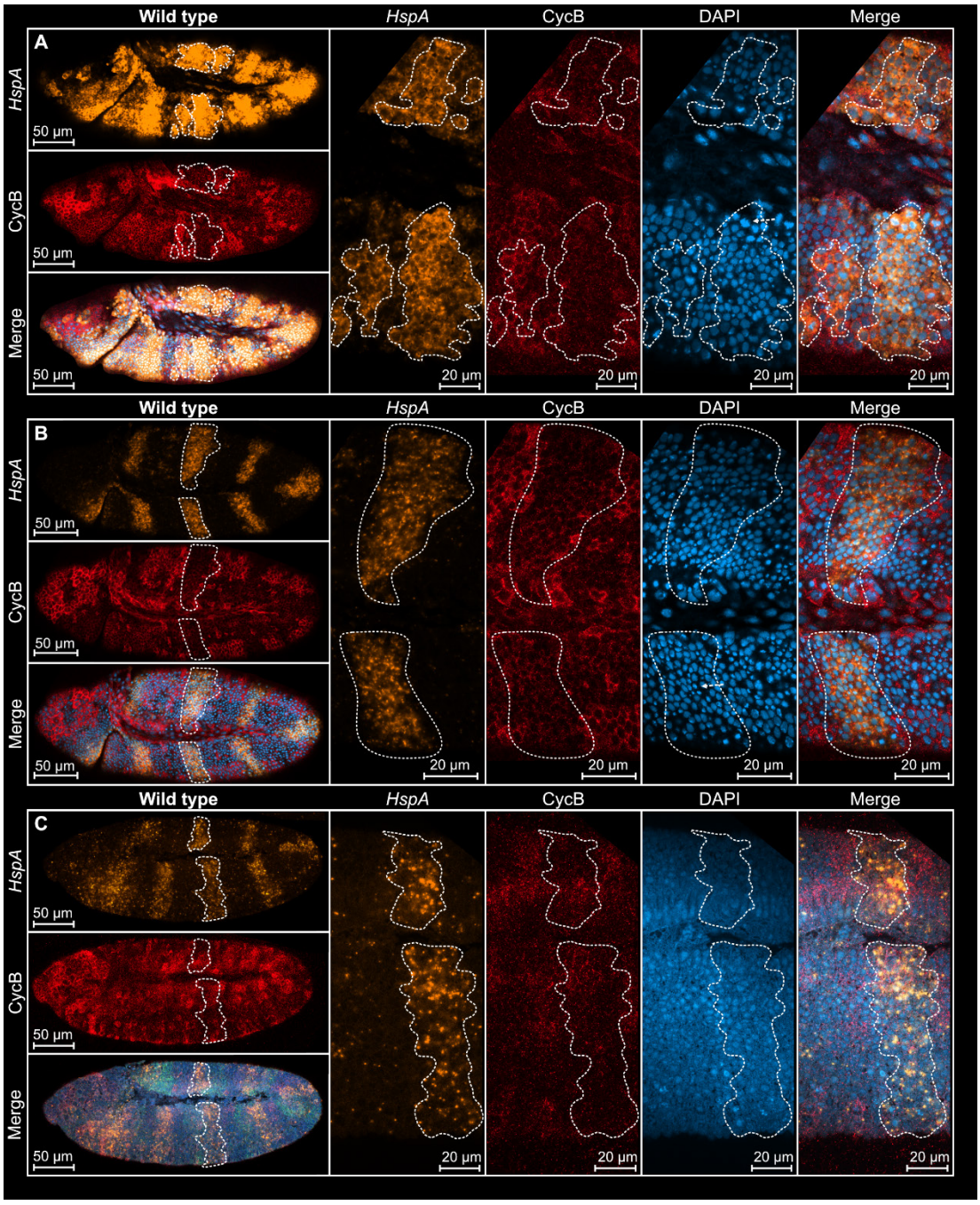

Figure 2.33 *paired* GAL4 driven expression of the *HspA-string* constructs Expression of the *HspA-string* transgene in the 3rd chromosome (86F6) (orange) analysed by FISH targeting the *HspA* sequence in the transgene together with Cyclin B immunofluorescence (red) in wild type embryos of increasing developmental age (A to C). Nuclei are stained by DAPI (blue). *paired* domains are encircled by dashed lines.

a functional String protein. However, it is not possible to directly infer that the *HspA* transgene drives the cells into mitosis (mitotic nuclei indicated by arrows), since there is still endogenous wild type *string* expression in these embryos.

His^{C} mutant embryos, however, show only weak signals of *HspA* expression at the corresponding stage (Figure 2.34 A). Intriguingly, *HspA-string* expression does not lead to a degradation of Cyclin B.

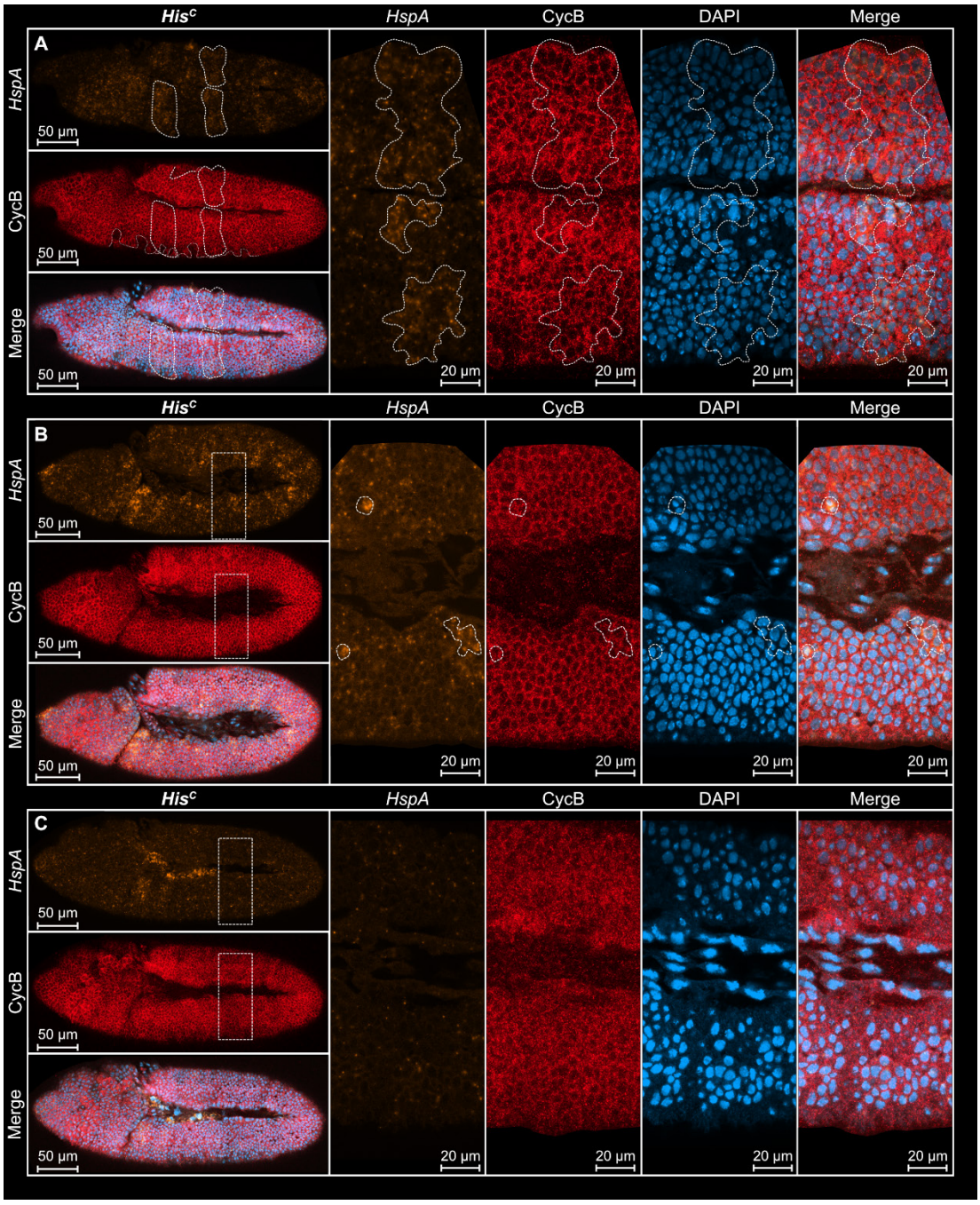

Figure 2.34 *paired* GAL4 driven expression of the *HspA-string* constructs Expression of the *HspA-string* transgene in the 3rd chromosome (86F6) (orange) analysed by FISH targeting the *HspA* sequence in the transgene together with Cyclin B immunofluorescence (red) in *His*^{C} mutant embryos of increasing developmental age (A to C). Nuclei are stained by DAPI (blue). *paired* domains are encircled by dashed lines (A), boxes indicate location of paired domains (B and C).

Moreover, *HspA* signal is reduced over time (Figure 2.34 B) and completely absent in late embryos (Figure 2.34 C). General expression levels are drastically reduced as compared to the wild types (Figure 2.33 A – C). Nuclei within *HspA* expressing domains do not show signs of mitotic chromosomes, suggesting that the transgene containing the *HspA 5'UTR* does not rescue the arrested cells.

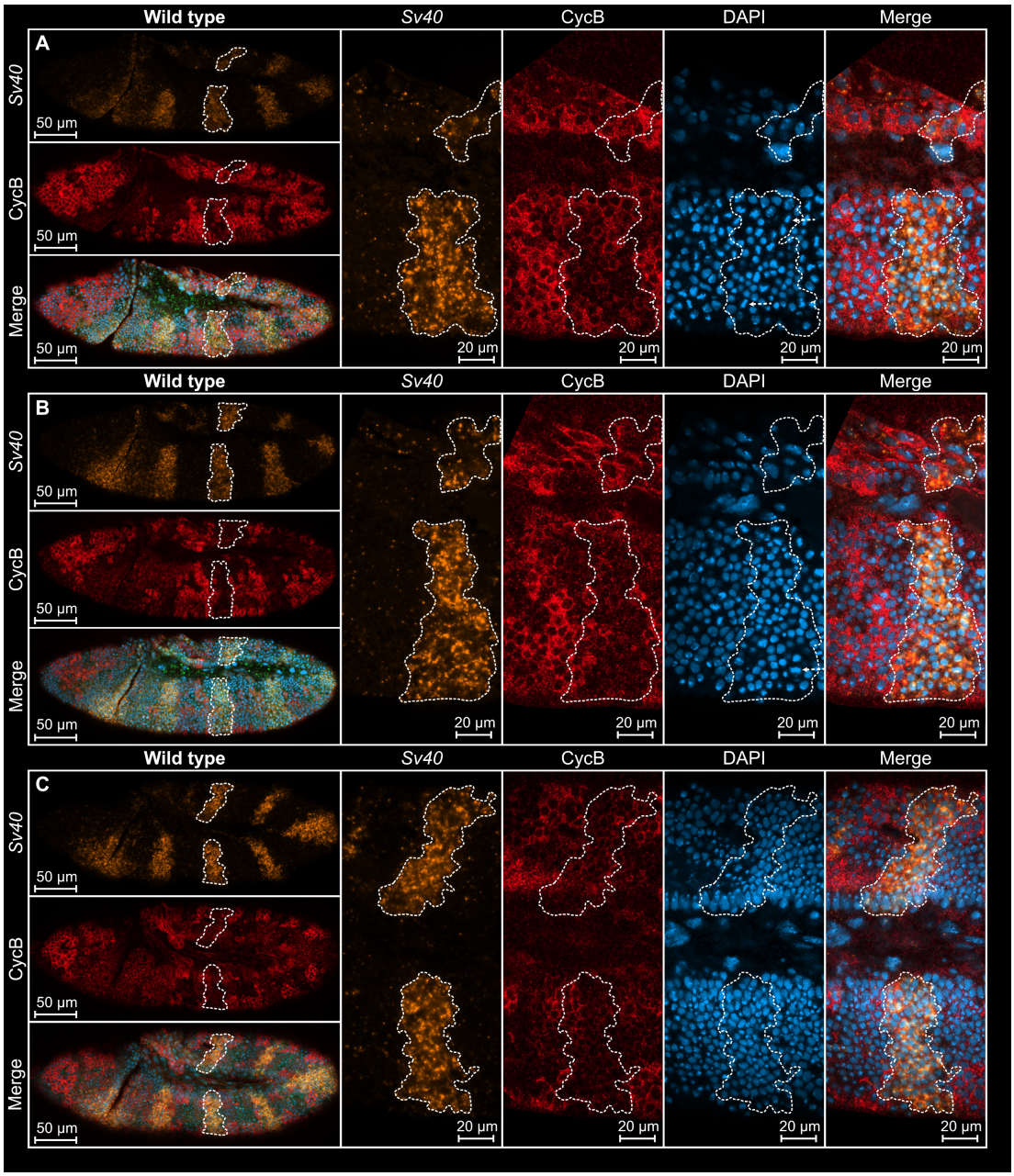

Figure 2.35 *paired* GAL4 driven expression of the *string-SV40* constructs Expression of the *string-SV40* transgene in the 3rd chromosome (86F6) (orange) analysed by FISH targeting the *SV40* sequence in the transgene together with Cyclin B immunofluorescence (red) in wild type embryos of increasing developmental age (A to C). Nuclei are stained by DAPI (blue). *paired* domains are encircled by dashed lines (A to C), arrows indicate mitotic chromosomes (A and B).

Wild type embryos expressing the *SV40* transgene, which contains the endogenous *string 5'UTR* and the *3'UTR* of the *Simian Virus 40*, from the 3rd chromosome in region 86F6, also show expression in the stereotypic *paired* domains (Figure 2.35 A – C). The Cyclin B protein is degraded in those domains and some of the nuclei within the domains undergo mitosis as indicated by the formation of mitotic chromosomes. Again, it is not possible in the wild type to safely discriminate between endogenous String contribution and the activity of the *SV40* transgene.

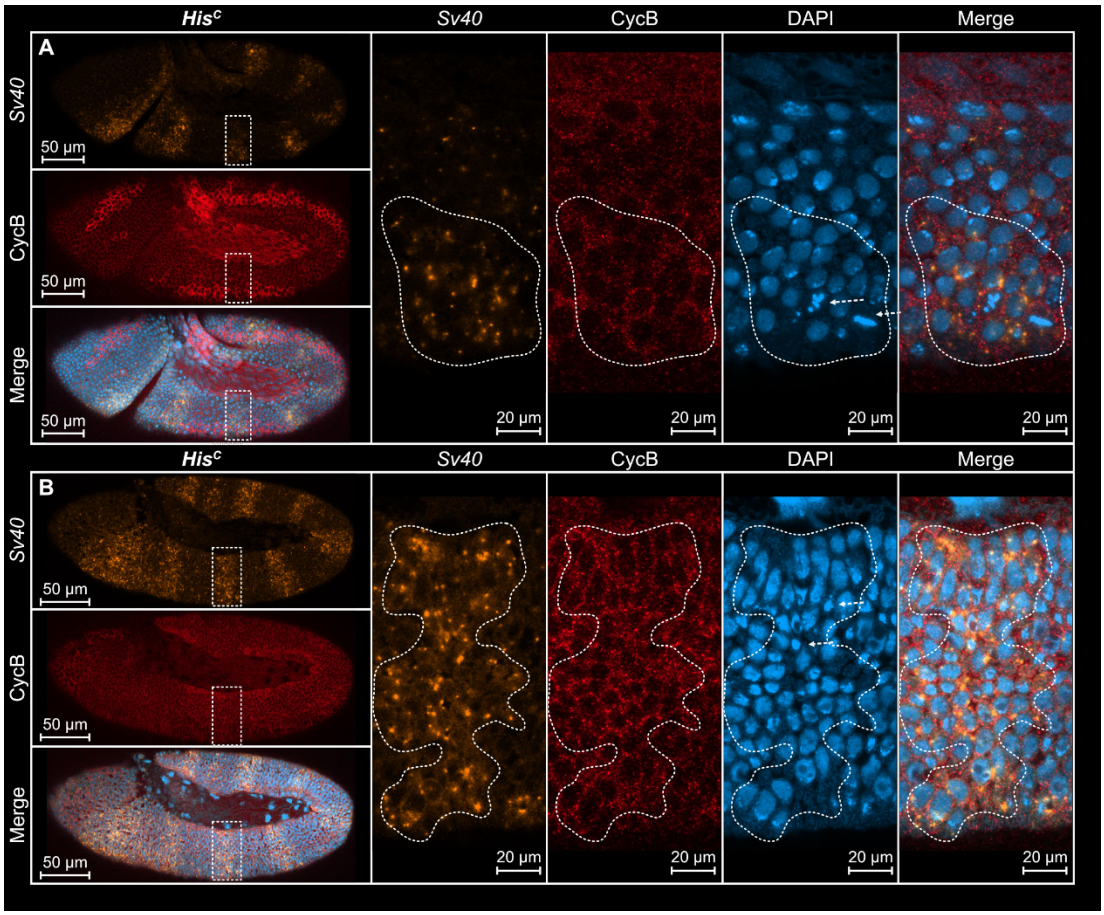

Figure 2.36 *paired* GAL4 driven expression of the *string-SV40* constructs Expression of the *string-SV40* transgene in the 3rd chromosome (86F6) (orange) analysed by FISH targeting the *SV40* sequence in the transgene together with Cyclin B immunofluorescence (red) in *His*^{C} mutant embryos of increasing developmental age (A to B). Nuclei are stained by DAPI (blue). *paired* domains are highlighted by dashed boxes (A, B), arrows indicate chromatin aggregates (A and B).

Intriguingly, *His*^{C} mutant embryos retain considerable levels *SV40* transcripts in early and late mutant embryos (Figure 2.36 A, B). In early embryos (Figure 2.36 A), overexpression of the *SV40* transgene coincides with degradation of Cyclin B in ventral cells and mitotic nuclei. However, these cells have not yet undergone G2/M$_{15}$ arrest because cell divisions are still supported by the parental histone supply. In late *His*^{C} mutants (Figure 2.36 B), Cyclin B is not degraded, and no mitotic cells can be unambiguously identified.

To exclude expression efficiencies of the transgenes which the genetic environment at the chromosomal insertion site might pose, the constructs were integrated into a different landing site on the second chromosome in region 51C1. In this location, the transgenes co-segregate with the *His*^{C} deletion, which is also located on the second chromosome. So far, we have only examined the effect of expression of the *SV40* transgene which is inserted in this location. The results resemble previous finding, i.e., when *SV40* was located on the 3rd chromosome.

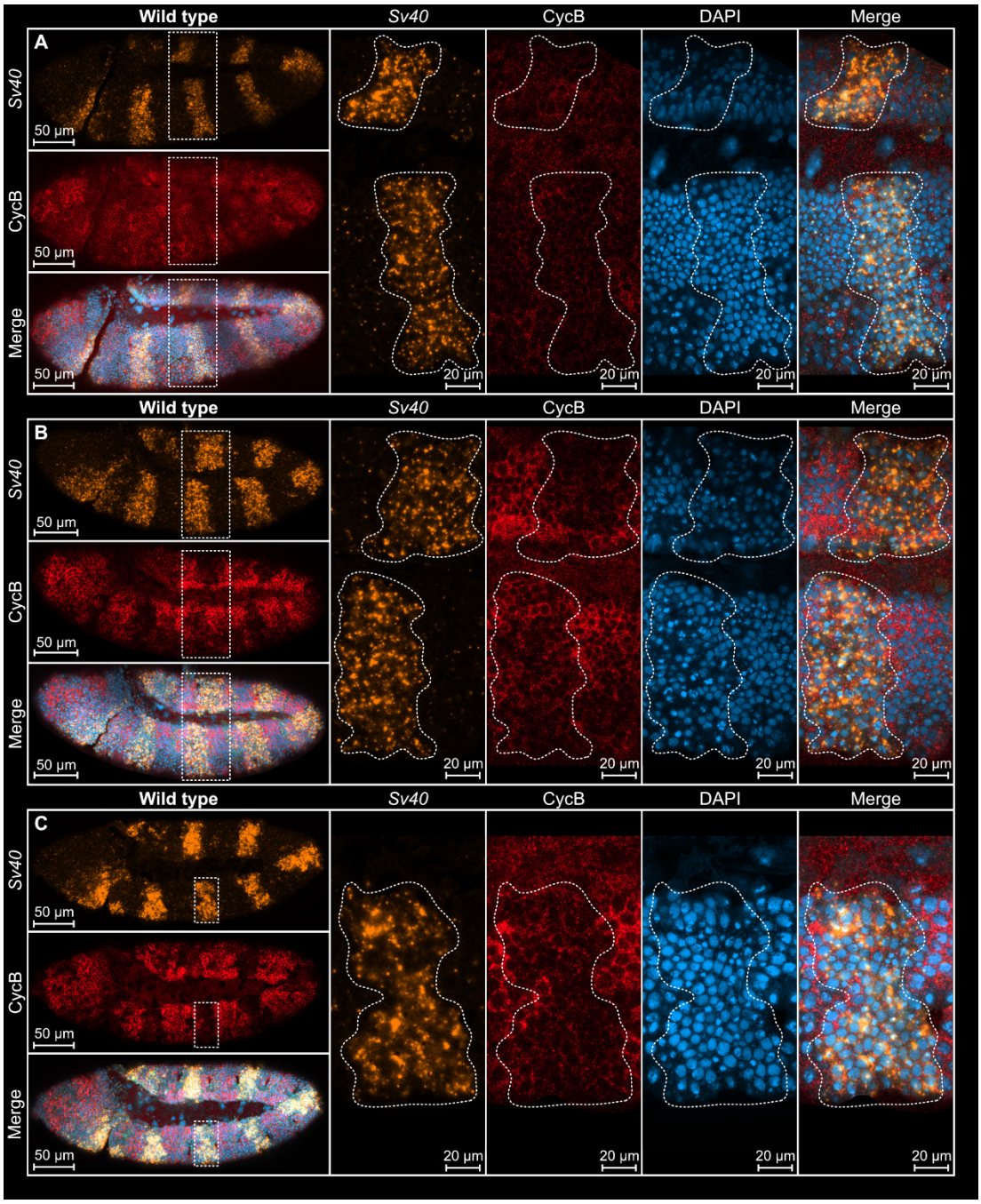

Figure 2.37 *paired* GAL4 driven expression of the *string-SV40* constructs Expression of the *string-SV40* transgene in the 2nd chromosome (51C1) (orange) analysed by FISH targeting the *SV40* sequence in the transgene together with Cyclin B immunofluorescence (red) in wild type embryos of increasing developmental age ((A) cell cycle 15, (B) cell cycle 16 and (C) embryos undergoing formation of tracheal pits). Nuclei are stained by DAPI (blue). *paired* domains are encircled by dashed lines/boxes (A to C).

Figure 2.37 shows *SV40* expression profiles in wild type embryos. In all developmental stages, cell cycle 15 (Figure 2.37 A), cell cycle 16 (Figure 2.37 B) and late embryos where tracheal pits already formed (Figure 2.37 C), strong *SV40* expression can be observed.

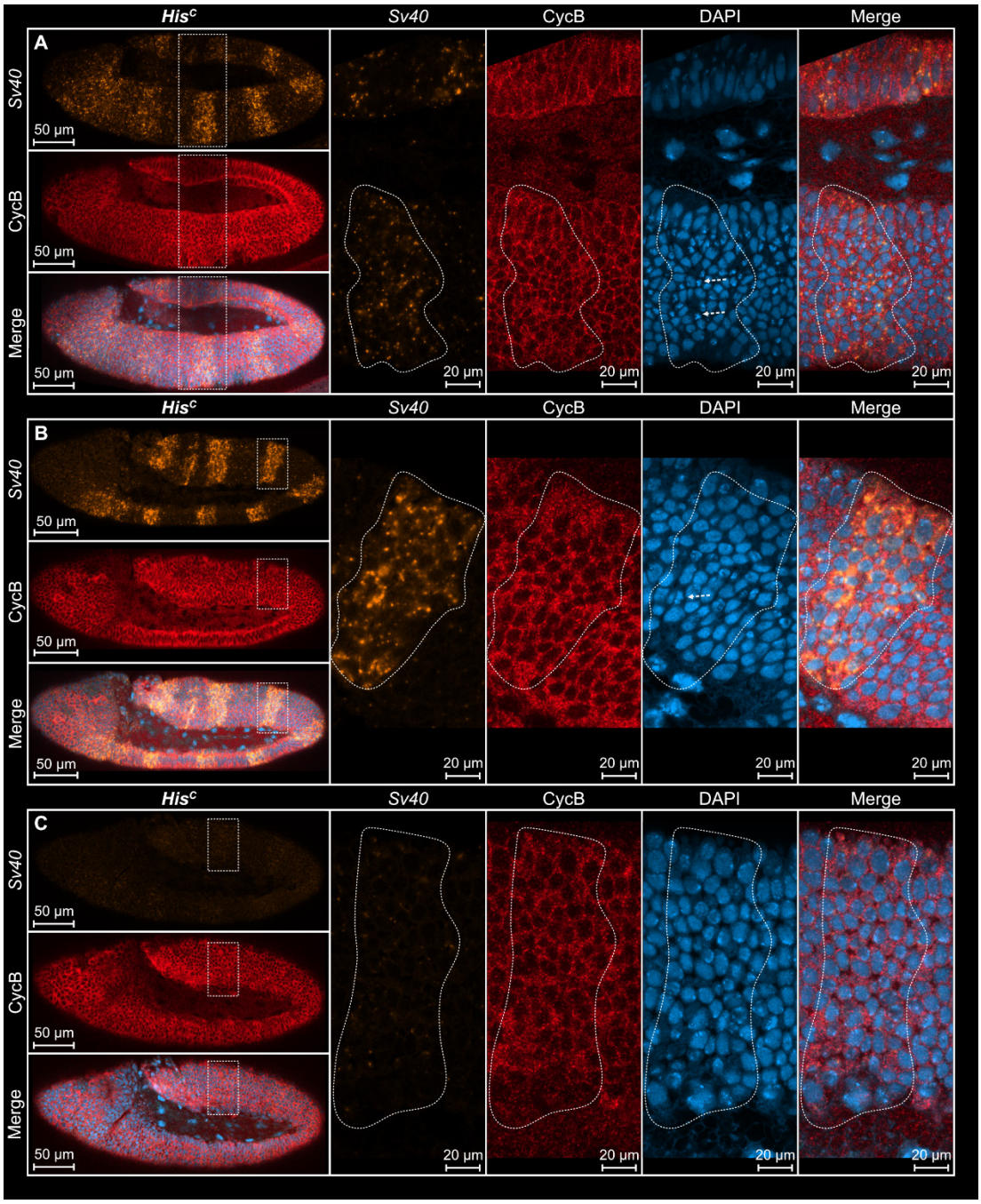

Figure 2.38 *paired* GAL4 driven expression of the *string-SV40* constructs Expression of the *string-SV40* transgene from the 2nd chromosome (51C1) (orange) analysed by FISH targeting the *SV40* sequence in the transgene together with Cyclin B immunofluorescence (red) in *His*^{C} mutant embryos (A to C). Nuclei are stained by DAPI (blue). *paired* domains are encircled by dashed lines/boxes (A to C), arrows indicate chromatin aggregates (A and B).

Within the expression domains, Cyclin B is strongly reduced, and cells do enter mitosis as mitotic figures indicate. Again, degradation of Cyclin B indicates that the transgene-derived mRNA is translated into a functional protein, yet again the transgene effect cannot be distinguished from endogenous *string* expression. *His*^{C} mutant embryos expressing the *SV40* transgene from the 2nd chromosome show considerable *SV40* expression in the arrested cells (Figure 2.38 A, B). However, Cyclin B is yet again not degraded in arrested cells, although nuclei show condensed DNA structures (Figure 2.38 A). Whether they represent mitotic

chromosomes is not yet finally established. Additionally, the embryo shown in Figure 2.38 B shows stronger *SV40* expression than the one in Figure 2.38 A but does not display similar chromatin structures which is contraindicative to the dosage dependent action of *string*. The embryo presented in Figure 2.38 C shows very weak *SV40* expression in the *paired* domains, that is barely detectable at 63-fold magnification (Figure 2.38 C).

Taken together these results suggest that neither *HspA* transgene expression nor the activity of the *SV40* transgene are able to rescue the cell cycle arrest that is caused by the lack of new histone synthesis in *His^{C}* mutants. However, there is weak evidence that mRNA stability is increased in *His^{C}* mutants when the endogenous *string 3'UTR* is exchanged with a *SV40 3'UTR*. A likely RNA binding protein affecting *string* mRNA stability might therefore be targeting the *3'UTR* of *string* mRNA.

2.2.3.4 Expression of eYFP-*SV40* in *His^{C}* mutant flies

To exclude that mRNA stability is only affected by the *UTR*s and not by intrinsic signals within the *string* CDS, we tested two additional transgenes in which the *string* CDS was exchanged for the *eYFP* CDS to which either the *HspA 5'UTR* and *string 3'UTR,* or the *5'UTR* of *string* and the *3´UTR* of *SV40* were added. Following the hypothesis that the *3'UTR* of *string* is targeted by factors that cause rapid degradation, a higher mRNA stability of the *5' string UTR-eYFP-SV40* mRNA as compared to the *HspA 5'UTR-eYFP-3' string UTR* mRNA would be expected. Because we did not observe differences in expression levels between an integration of the transgenes into the 2nd and 3rd chromosome, I only generated transgenic lines with integration in the 2nd chromosome at landing site 51C1.

Only the transgene expressing of the *5' string UTR-eYFP-SV40* was examined in detail using the *SV40* probe to visualize transcript accumulation by FISH. Wild type embryos show strong transgene expression in the *paired* domains (Figure 2.39 A-C). Intriguingly, all embryos show similar expression levels of the transgene regardless of their developmental age between cell cycle 15 (Figure 2.39 A) and cell cycle 16 (Figure 2.39 B, C). In contrast to the transgene that contains the *string* CDS sequence no signs for Cyclin B degradation were detected. Visualization of eYFP shows that the transgene-derived mRNAs are translated into functional proteins. Additionally, not only embryos but also larvae at stage L1, L2 and L3 show visible eYFP expression.

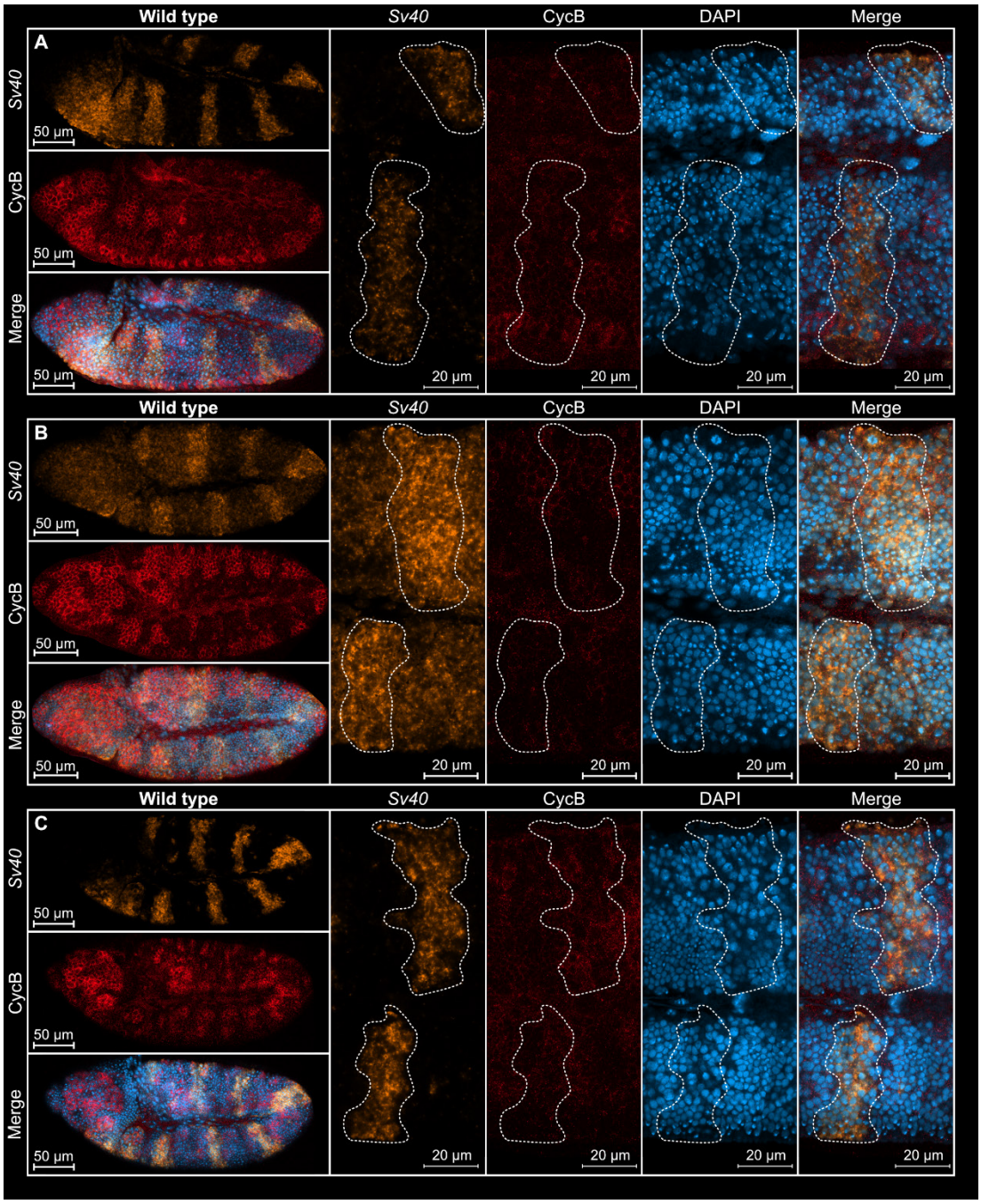

Figure 2.39 *paired* GAL4 driven expression of the *eYFP-SV40* constructs Expression of the *eYFP-SV40* transgene in the 2nd chromosome (51C1) (orange) analysed by FISH targeting the *SV40* sequence in the transgene together with Cyclin B immunofluorescence (red) in wild type embryos of increasing developmental age (A to C). Nuclei are stained by DAPI (blue). Wild type embryos show strong expression of the transgene in the typical *paired* domains (encircled).

paired-driven expression of *5'string UTR-eYFP-SV40* in *His*^{C} mutant embryos show similar levels of expression with the *SV40 3´UTR* probe in early embryos (Figure 2.40 A), where ventral epidermal cells are not yet arrested in G2/M_{15}, and in later embryos which have stopped cell division (Figure 2.40 B). Embryos at a later stage (Figure 2.40 C) show weaker expression as observed with embryos of the corresponding stage expressing the *SV40* transgene (compare with Figure 2.38 C).

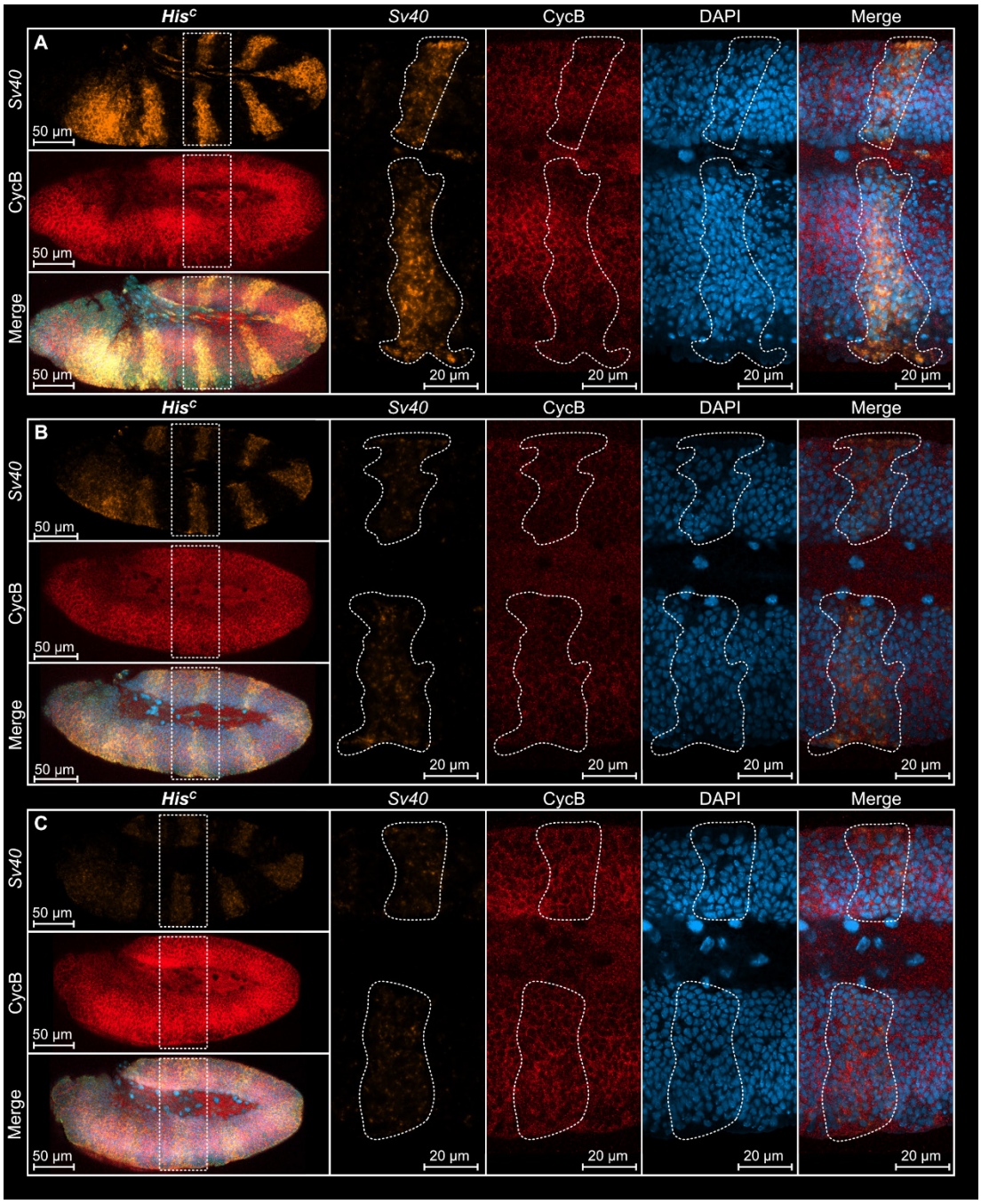

Figure 2.40 *paired* GAL4 driven expression of the *eYFP-SV40* constructs Expression of the *eYFP-SV40* transgene (orange) from the 2nd chromosome (51C1) analysed by FISH targeting the *SV40* sequence in the transgene together with Cyclin B immunofluorescence (red) in *His*^{C} embryos of increasing developmental age (A to C). Nuclei are stained by DAPI (blue). *paired* domains are encircled by dashed lines/boxes (A to C).

Similar to wild type embryos, no degradation of Cyclin B can be observed. Intriguingly, in *His*^{C} mutants expressing *eYFP* no condensed chromatin structures as seen in *string* overexpressing embryos could be observed, whereas in wild type embryos which express *eYFP* mitotic structures were visible (Figure 2.39 A – C).

In conclusion, mRNA stability of overexpressed *5'string UTR-eYFP-SV40* was apparently not affected in *His^{C}* mutant embryos except in older mutants. The expression levels of *5'string UTR-eYFP-SV40* in wild type and *His^{C}* mutant embryos were comparable to *5'stringUTR-string CDS-SV40* in wild type and *His^{C}* mutants regardless of the genomic insertion site. This further argues that a potential regulatory element might be situated within the *3'UTR* of *string* and weaker transgene expression in late mutant embryos (Figure 2.38 C and Figure 2.40 C).

2.2.3.5 Held-out-wings(L) is a potential regulator of *string* mRNA in *His^{C}* mutant embryos

Previous studies have identified two *string* mRNA binding regulators with recognition sites within the *3'UTR* of *string* mRNA. The first is *microRNA-965* which leads to degradation of *string* mRNA during histoblast proliferation and migration (*11*). The *held-out-wings (how)* gene expresses two protein variants, a long variant How(L) and the short variant How(S). Each variant is represented by different isoforms including isoform A, D, E, F of *how (L)* and B and C of *how*(*S)* (Figure 2.41 A). The isoforms of *how*(*L)* have an additional exon (E7) and different *3'UTR*s which distinguish them from isoforms of *how*(*S)*. All isoforms contain a common KH-motif that recognize a GACUAA sequence motif.

The two variants have opposing functions, i.e., How(L) negatively affects *string* mRNA stability, whereas How(S) stabilizes *string* mRNA as revealed by studies on mesoderm formation and spermatogenesis (*12, 13*). *string* mRNA has two of such How binding motives. One is located within the intron, the second is situated in the *3'UTR* (see Figure 2.41 B).

We first analysed expression of the different *how* variants with qRT-PCR (Figure 2.41 C). We used a primer set which did not distinguish between the four different isoforms of *how(L).* The results show that *how(S)* is not differentially expressed during the first six hours of embryonic development, with the exception of *how(S)_B*, which shows increased level of transcripts at 5.5-6h AEL (p=0.017). *how(L),* however, increases steadily over time more than 2-fold during the first 6 hours of development.

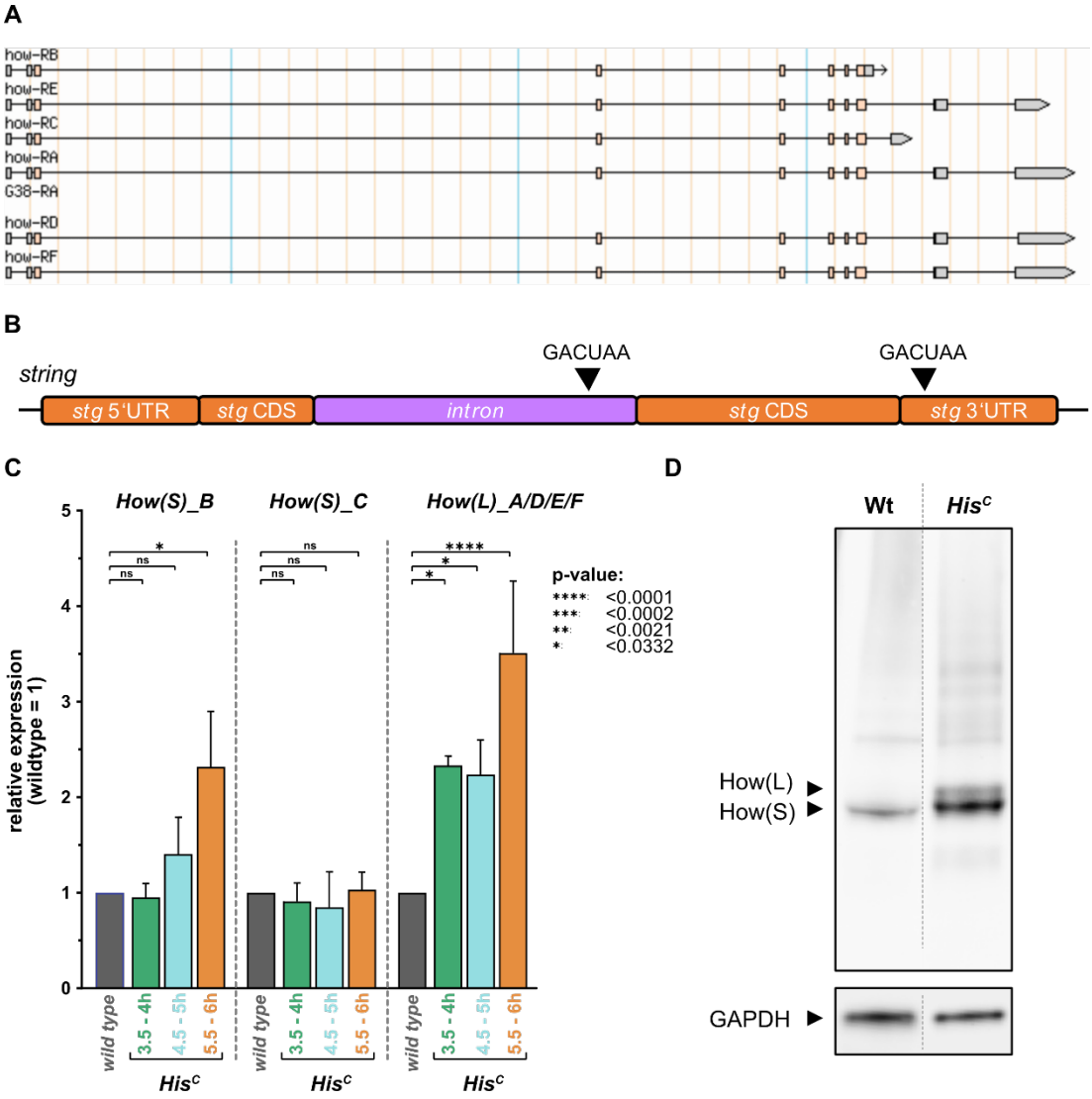

Figure 2.41 *His^C* mutant embryos do not express. How is expressed in the long mRNA destabilizing How(L) and the short mRNA stabilizing How(S) variant. For How(S) two isoforms (B, C) are annotated, for How(L) four isoforms (A, D, E, F) are known. (B) The mRNA sequence of *string* has two binding sites (GACUAA) for How, one located in the intron and the second one located inside the *3'UTR*. (C) qRT-PCR for *how(S)_B, how(S)_C* and *how(L)_A/D/E/F* based on 4 independent cDNA samples prepared from mutant and matched wild type embryos at four timepoints AEL as indicated. Each set was normalized by the corresponding expression of housekeeping gene *act5c* and analysed using ΔΔCt ± s.d. (*10*) and two-sided, unpaired Student's t-test. *how(S)_B* is not differentially expressed in the first two timepoints and becomes significantly upregulated 5.5-6h AEL. *how(S)_C* is not differentially expressed in any of the timepoints, whereas *how(L)_A/D/E/F* is subsequently upregulated over time reaching its maximum of <3-fold upregulation 5.5-6h AEL. (D) Western blot of wild type and *His^C* protein isolates covering 3-6h AEL using an antibody against How that recognizes both isoforms equally. Small amounts of How(S) are detected in wild type samples. In *His^C* protein an additional band above How(S) is observed corresponding to the molecular weight of How(L).

To show that the How proteins are expressed in *His^C* mutants, we performed a Western blot analysis with a rabbit anti-How antibody which recognize both How variants to examine How protein abundance in protein extracts of wild type and *His^C* mutant embryos between 3-6h AEL. As a control, we used the housekeeping protein GAPDH. Figure 2.41 D shows that in contrast to wild type embryos, which express only the RNA-stabilizing How(S) variant, *His^C* mutants also express the RNA-destabilizing variant How (L).

The observation that How(L) is detected in *His^{C}* mutants but not in wild type embryos is consistent with the argument that only *His^{C}* mutants express functional levels of the RNA-destabilizing variant of How. This result could explain why *string* mRNA is degraded in the *His^{C}* mutant embryos. To further test whether expression of *how(L)* or *how(S)* correlates with the cell cycle arrest at stage M_{15}, we performed a FISH analysis using RNA probes directed specifically against *how(S)* and *how(L)* transcripts, respectively.

Using the FISH probe, a very low if any significant *how(S)* expression was observed in epidermal cells of wild type embryos during cell cycle 14 (Figure 2.42 A), cell cycle 15 (Figure 2.42 B) and cell cycle 16 (Figure 2.42 C). This result is consistent with the result showing that only small amounts of How(S) can be detected by Western blotting (Figure 2.41 D), as well as by qRT-PCR analysis (Figure 2.41 C). As in wild type embryos, no significant levels of *how(S)* expression were found in *His^{C}* mutant embryos of the corresponding developmental stages (Figure 2.43 A to C). The very low levels of detectable *how(S)* expression by *in situ* hybridization are consistent with earlier results describing also very low amounts of *how(S)* transcripts in mesodermal cells (*12*).

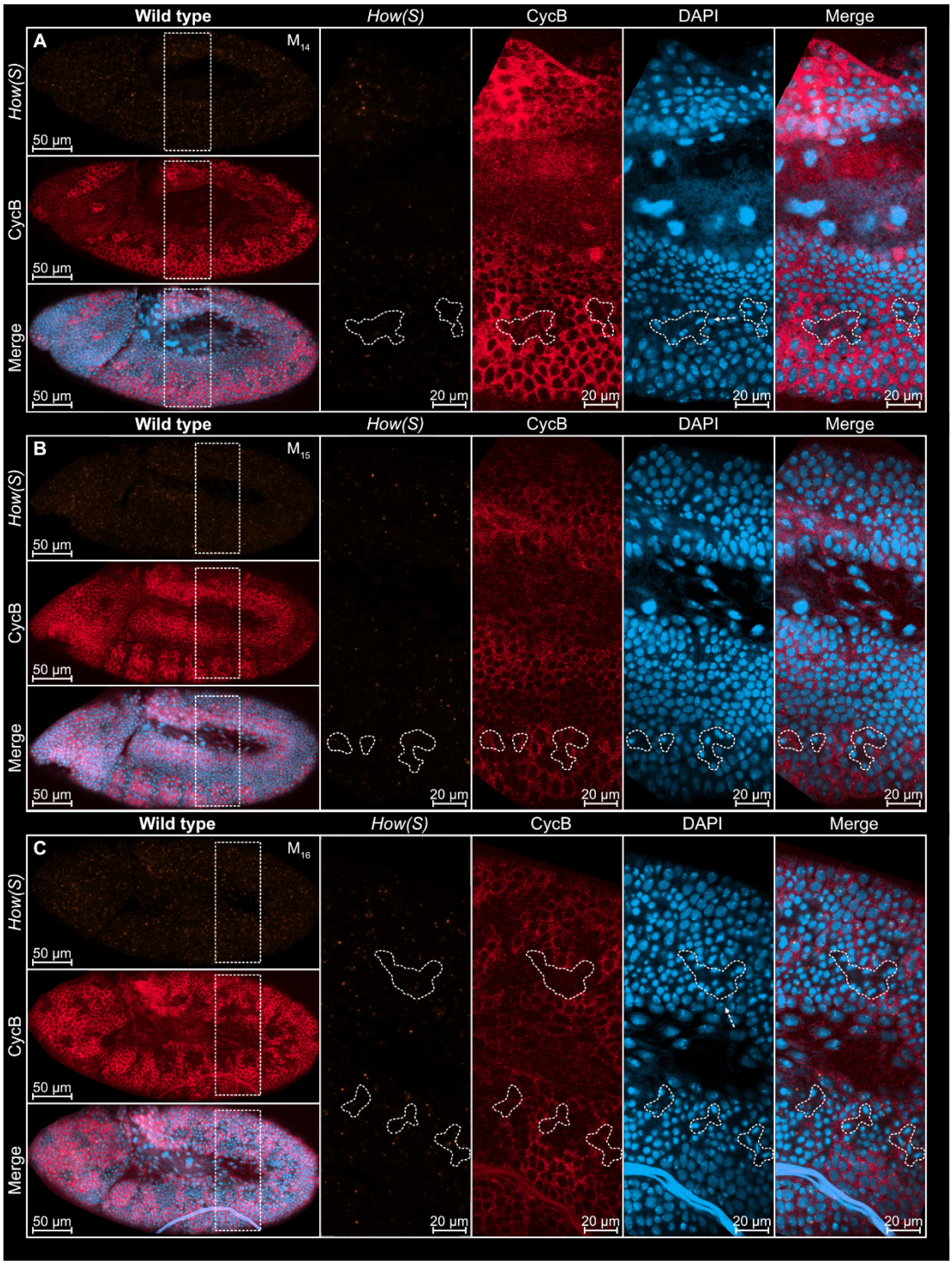

Figure 2.42 *how(S)* expression pattern in wild type embryos. Expression of *how(S)* (orange) analysed by FISH together with Cyclin B immunofluorescence (red) in wild type embryos of increasing developmental age (A to C). Nuclei are stained by DAPI (blue). (A to C) Cyclin B expression follows the wild type pattern as described in A to C. Embryos in cell cycle 14 (A), cell cycle 15 (B) and cell cycle 16 (C) do not show significant expression of *how(S)*. Cells encircled are characterized by lack of Cyclin B signal indicating that those cells undergo mitosis and do not show *how(S)* accumulation. Mitotic chromosomes are indicated by arrows (A and C).

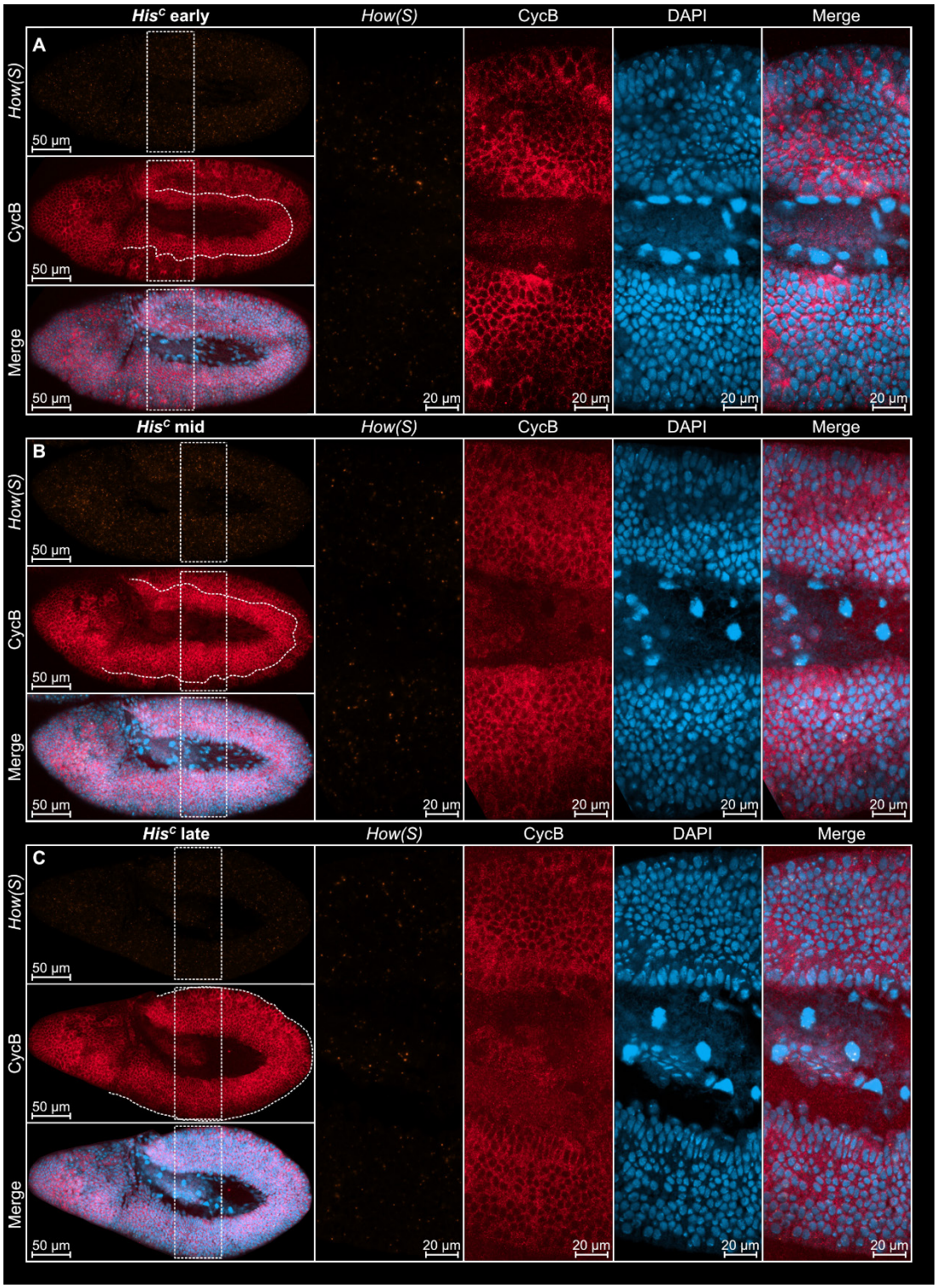

Figure 2.43 *how(S)* expression pattern in *His^C* embryos. Expression of *how(S)* (orange) analysed by FISH together with Cyclin B immunofluorescence (red) in *His^C* embryos of increasing developmental age (A to C). Nuclei are stained by DAPI (blue). (A to C) Cyclin B expression follows the wild type pattern as described in A to C. Embryos in cell cycle 14 (A), cell cycle 15 (B) and fully arrested *His^C* mutants (C) do not show significant expression of *how(S)*. Mitotic chromosomes like in wild type embryos were not observed.

As observed with *how(S)*, wild type embryos do not increase the expression of *how(L)* transcripts between cell cycle 14 (Figure 2.44 A), cell cycle 15 (Figure 2.44 B) and cell cycle 16 (Figure 2.44 C).

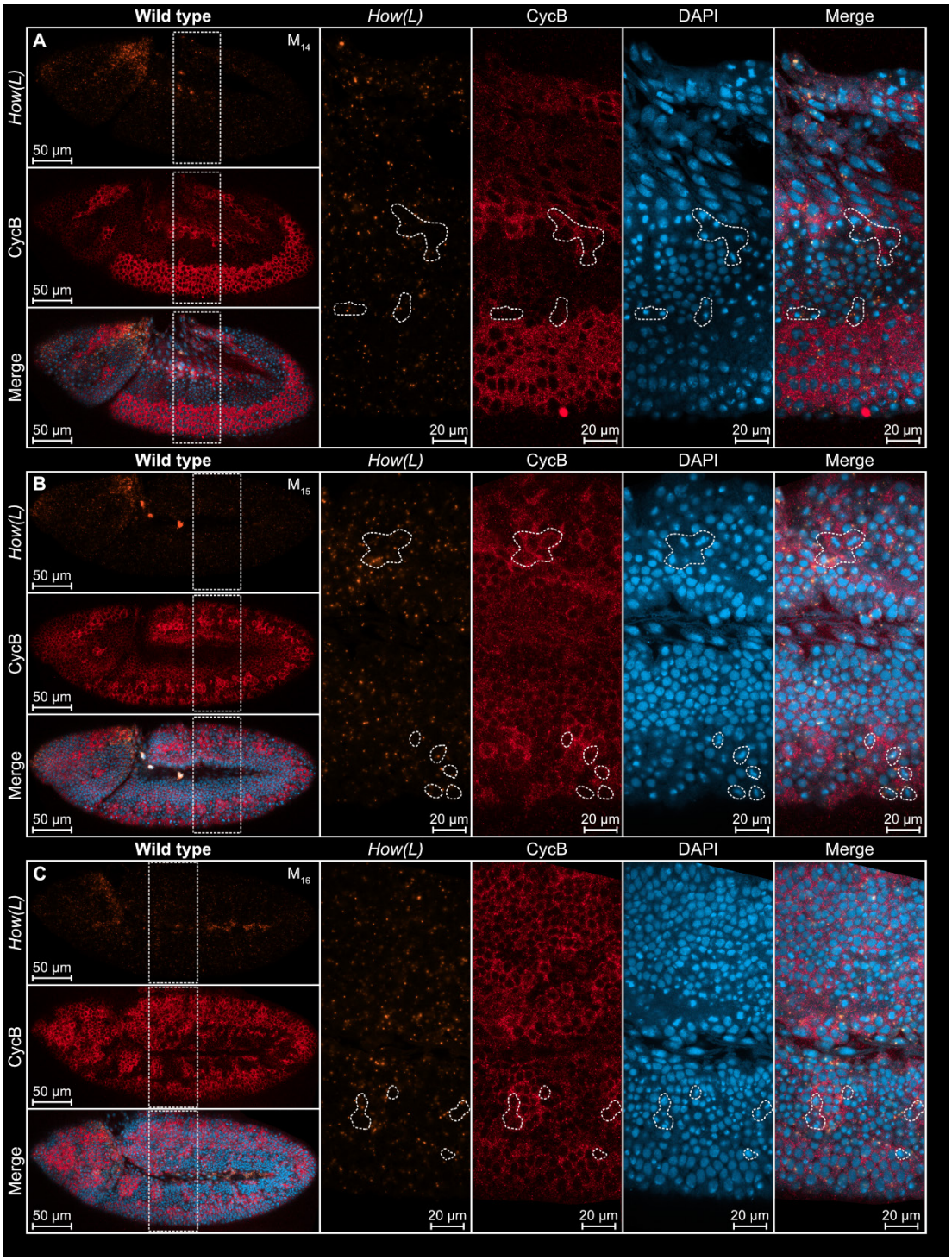

Figure 2.44 *how(L)* expression pattern in wild type embryos. Expression of *how(L)* (orange) analysed by FISH together with Cyclin B immunofluorescence (red) in wild type embryos of increasing developmental age (A to C). Nuclei are stained by DAPI (blue). (A to C) Cyclin B expression follows the wild type pattern as described in A to C. Embryos in cell cycle 14 (A), cell cycle 15 (B) and cell cycle 16 (C) do not show significant expression of *how(L)*. Cells encircled are characterized by lack of Cyclin B signal indicating that those cells undergo mitosis and do not show *how(L)* accumulation. Mitotic chromosomes are encircled (A, B, C).

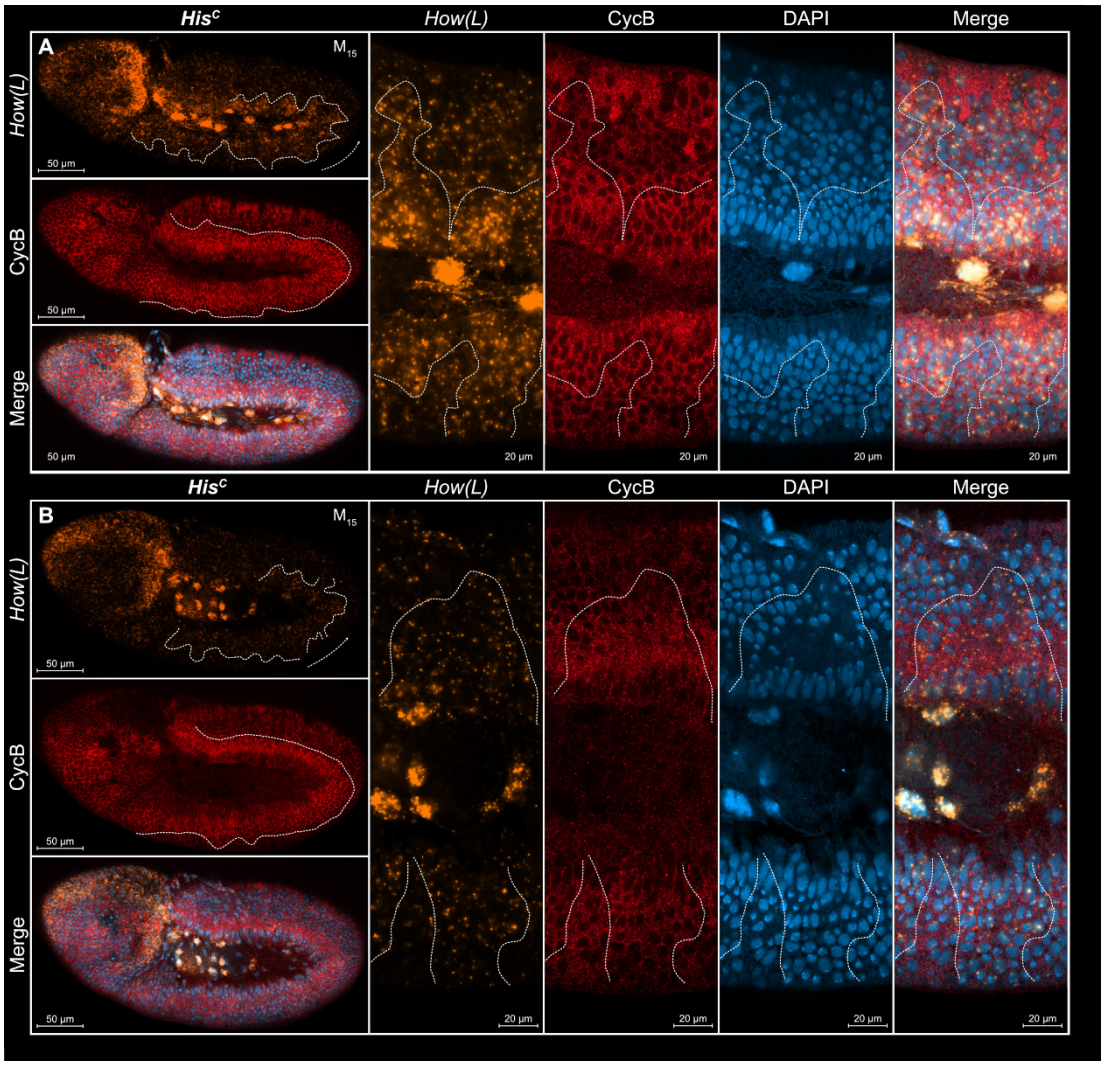

Figure 2.45 *how(L)* expression pattern in *His^C* embryos. Expression of *how(L)* (orange) analysed by FISH together with Cyclin B immunofluorescence (red) in *His^C* embryos. Nuclei are stained by DAPI (blue). (A and B) Cyclin B expression follows the pattern as described for mutants in A'. *His^C* mutants express *how(L)* in epidermal cells of the anterior dorsal embryo that enter G2/M_{15} transition indicated by accumulation of Cyclin B (domains marked by dashed lines). Ventral cells lacking Cyclin B expression still replicate DNA during S_{15} or enter $G2_{15}$.

In contrast, *His^C* mutant embryos express *how(L)* mRNA in epidermal cells (Figure 2.45 and Figure 2.46). Figure 2.45 A and B show two early *His^C* mutant embryos when anterior dorsal cells enter the G2/M_{15} transition, and the ventral cells are still in the S or G-phases of the cell cycle. In these embryos, *how(L)* expression is mostly found in anterior dorsal cells, i.e., cells during the G2/M_{15} phase.

In older *His^C* mutant embryos shown in Figure 2.46, all dorsal cells have arrested in G2/M_{15} whereas ventral and posterior cells are still in S phase or early G2 phase. Here, *how(L)* transcripts are predominantly expressed in posterior dorsal cells (Figure 2.46 A) as well as in the other dorsal cells (Figure 2.46 B).

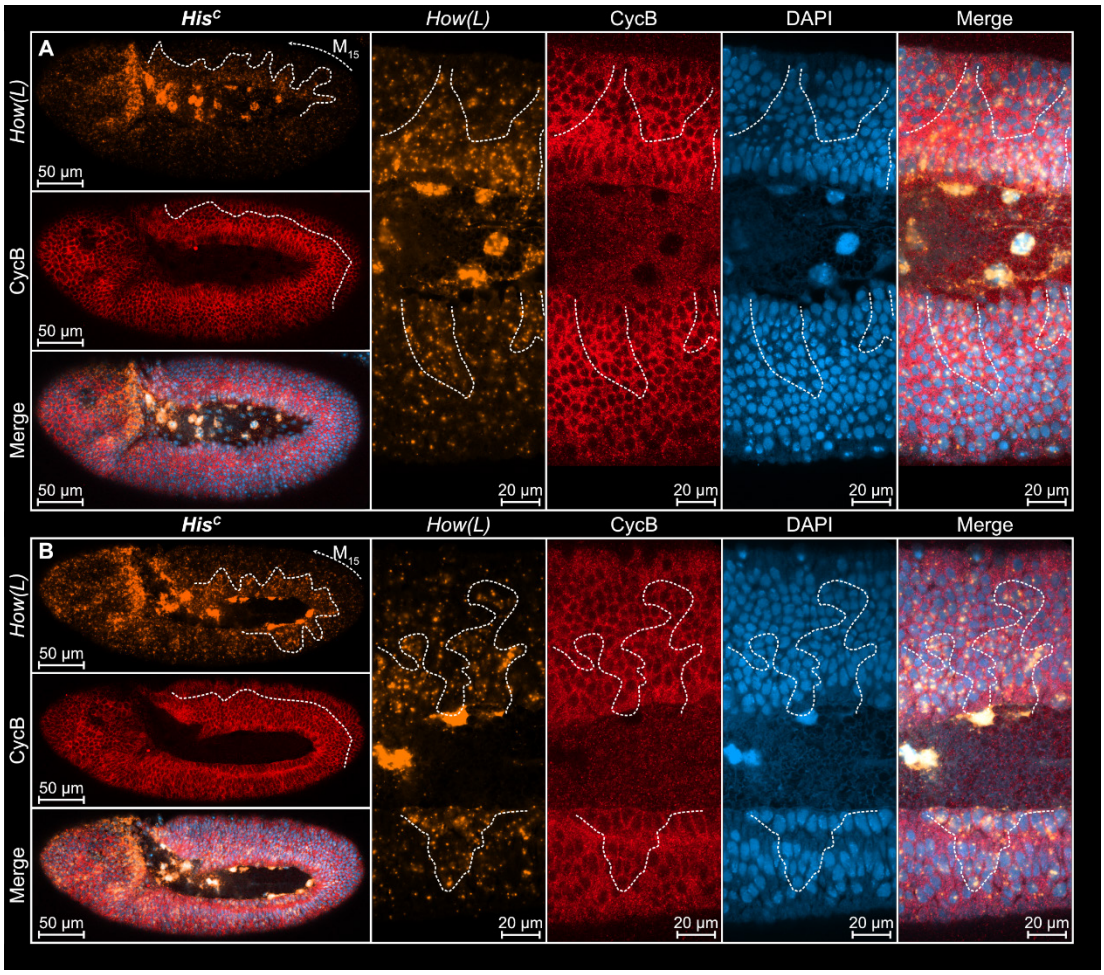

Figure 2.46 *how(L)* expression pattern in *His^C* embryos. Expression of *how(L)* (orange) analysed by FISH together with Cyclin B immunofluorescence (red) in *His^C* embryos. Nuclei are stained by DAPI (blue). (A and B) Cyclin B expression follows the pattern as described for mutants in B'. (A) *His^C how(L)* is strongly expressed in epidermal cells of the posterior dorsal embryo in cells that enter G2/M_{15} transition indicated by accumulation of Cyclin B (domains marked by dashed lines). Ventral cells have partially reduced Cyclin B levels indicating that those cells still replicate DNA or undergo $G2_{15}$ (B) Fully arrested *His^C* mutants express *how(L)* in all dorsal cells of the embryo.

Figure 2.47 summarizes that *how(L)* expression domains in *His^C* mutant embryos extend from anterior dorsal cells in early mutant embryos, which enter G2/M_{15} while their ventral cells undergo S and G phases (Figure 2.47 A), to posterior cells in older embryos where most cells are arrested in the G2/M_{15} phase (Figure 2.47 B and C). This observation suggests that expression of *how(L)* follows the stereotypic mitotic waves observed in wild type embryos. However, expression domain patterns comparable to the ones observed in dorsal epidermal cells, cannot be found in ventral cells.

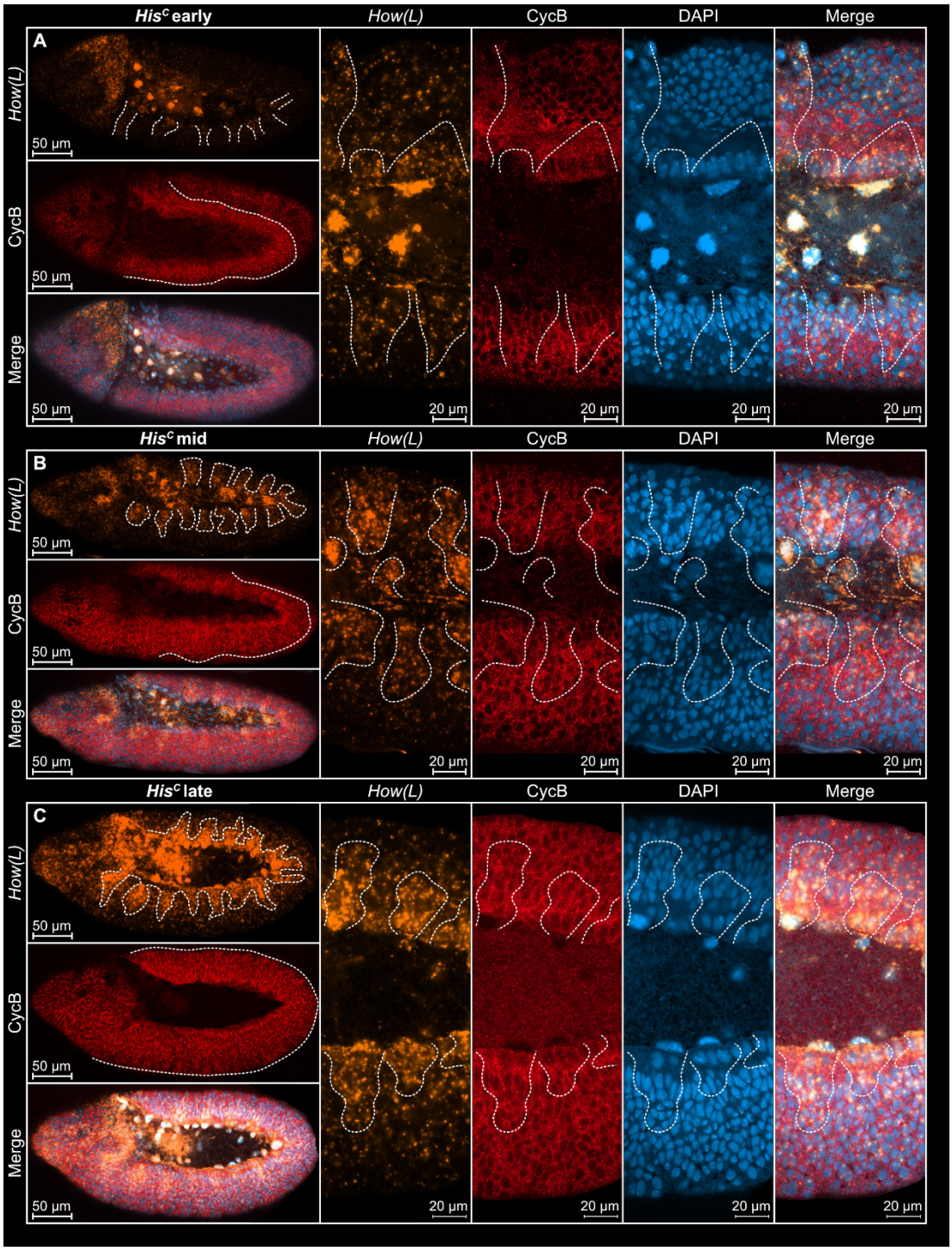

Figure 2.47 *how(L)* expression pattern in *His^C* embryos. Expression of *how(L)* (orange) analysed by FISH together with Cyclin B immunofluorescence (red) in *His^C* embryos of increasing developmental age (A to C). Nuclei are stained by DAPI (blue). (A to C) Cyclin B expression follows the pattern as described for mutants in Figure 2.31 A. (A) Early *His^C* embryos show strong *how(L)* expression in anterior dorsal cells that enter G2/M_{15} transition indicated by accumulation of Cyclin B (domains marked by dashed lines). Ventral cells have partially reduced Cyclin B levels indicating that those cells still replicate DNA or undergo $G2_{15}$ (B) Most epidermal cell have arrested in G2/M_{15} indicated by Cyclin B accumulation. *how(L)* expressing domains extend to more posterior dorsal cells following the mitotic waves observed in wild types. (C) Fully arrested *His^C* mutant embryos show substantial *how(L)* expression in all dorsal cells. Comparable expression cannot be observed in ventral cells.

These results suggest that *how(L)* mediates the degradation of *string* mRNA at least in dorsal cells of the epidermis by decreasing *string* mRNA stability through binding its recognition site in the *3'UTR* of *string*. Expression of *how(L)* extends in temporal dependency regarding the developmental age of the mutant embryos from anterior to posterior correlating with localization of the nuclei that upregulate *string* in wild type embryos (Figure 2.47 A to C).

2.2.3.6 Expression of a *stringΔhow* transgene in His^C mutant flies

Our results suggest that *string* mRNA degradation is mediated by the RNA binding How(L) variant, which acts through its binding site in the *3'UTR* of the *string* mRNA. Thus, we explored whether *string* mRNA stability is increased and rescues the $G2/M_{15}$ arrest in His^C mutant embryos, when a *string* mRNA lacking the How(L) binding motif (GACUAA), is expressed. We refer to the respective transgene as *stringΔhow*. FISH was carried out with His^C mutant embryos which carry the transgene, using the RNA probe directed against *string* mRNA. Again, *stringΔhow* expression was driven in a stripe pattern along the anterior-posterior axis of the embryos in response to the binary UAS/Gal4 expression system.

His^C mutant embryos in cell cycle 15 show strong expression of the transgene in the stereotypic *paired* domains (Figure 2.48 A). Notably, residual endogenous *string* in cells of the ventral epidermis that have not yet undergone the $G2/M_{15}$ arrest are also detected. Slightly older embryos with dorsal cells undergoing $G2/M_{15}$ and ventral cells in previous S and G phases retain expression of *string* in the *paired* domains and show reduced levels in ventral epidermal cells when more cells arrest the cell cycle (Figure 2.48 B). Older His^C mutant embryos of cell cycle 15, in which most cells have arrested in $G2/M_{15}$ (Figure 2.48 C), express only the transgene-derived mRNA, whereas endogenous *string* transcripts are lost in the intermediate stripes which lack *paired*/Gal4-driven transgene activity. Signal intensities in arrested dorsal domains of the younger mutant embryos appear somewhat lower when compared to ventral domains that contain both endogenous as well as transgene-derived *string* transcripts (Figure 2.48 B). Notably, we observed during both the earlier and the later stages structures of condensed chromatin exclusively in the *stringΔhow* domains of His^C mutant embryos (Figure 2.48 C). The formation of these structures was not observed in His^C mutant embryos with strongly reduced endogenous *string* activity which causes epidermal cells to arrest in $G2/M_{15}$ transition. We take this finding as a sign that these cells attempt to enter mitosis, but the concentration of String is not sufficient to fully drive mitosis in response to the String activity provided by the *stringΔhow* transgene.

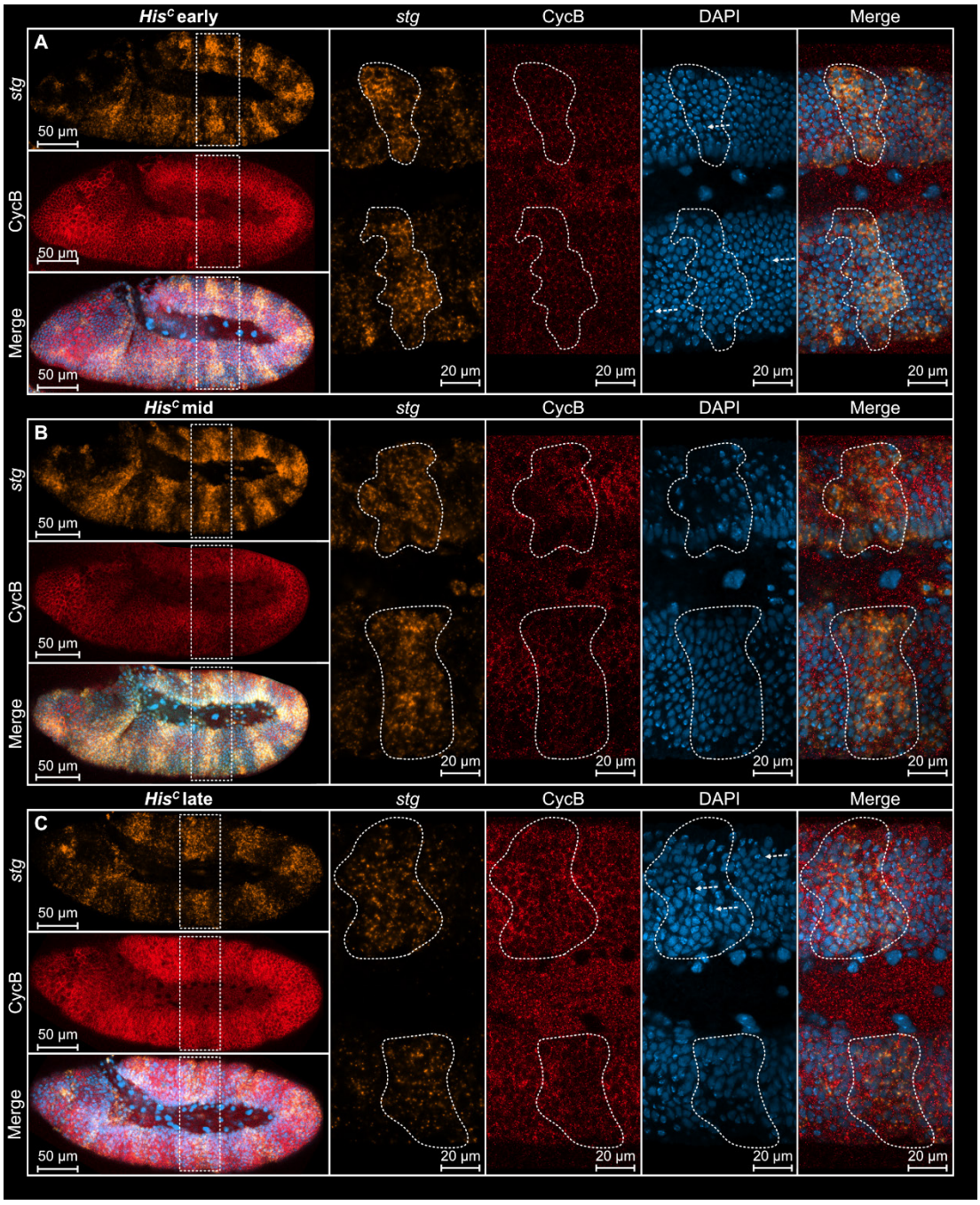

Figure 2.48 *paired* GAL4 driven expression of the *stringΔhow* constructs Expression of the *stringΔhow* transgene (orange) from the 2nd chromosome (51C1) analysed by FISH targeting the first exon of *string* mRNA together with Cyclin B immunofluorescence (red) in *His*^{C} embryos of increasing developmental age (A to C). Nuclei are stained by DAPI (blue). *paired* domains are encircled by dashed lines/boxes (A to C). Structures of condensed chromatin can be observed in *stringΔhow* expressing domains (arrows).

Overexpression of eYFP fused with the *string 5'UTR* and *SV40* polyA signal, as well as the *HspA-string* and *string-SV40* constructs lead to production of functional eYFP protein as well as functional String protein as indicated by Cyclin B degradation in wild types (Figure 2.33 and Figure 2.35). Therefore, and because late mutant embryos (Figure 2.48 C) arguably showed a slight reduction in Cyclin B signal intensity, we quantified the fluorescence intensities of *stringΔhow* expression by FISH in relation to the Cyclin B staining of the cells.

Figure 2.49 (A-D) shows transgene-derived *string* expression in cells of His^{C} mutant embryos. Cells were identified by their Cyclin B expression profiles to ensure that endogenous String activity from cells, which are not arrested is excluded. Figure 2.49 B to D show the same embryos as shown in Figure 2.48). Signal intensities are highlighted by a fire look up table (LUT, signal intensities are represented by different colour) and 2.5D profiles, high intensities are reflected by peak height and yellow colour.

Although embryos show signs of weak Cyclin B degradation in some positions with *stringΔhow* (555nm or orange line) expression (Figure 2.49 A' and C'), an overall degradation pattern of Cyclin B in response to *stringΔhow* expression could not be observed (Figure 2.49 D'). In conclusion, partially reduced Cyclin B signal intensities in places with *stringΔhow* expression could be observed, but they are not consistent. In view of the hypothesis that increased How(L) expression in His^{C} mutant embryos destabilizes *string* mRNA, the deletion of the How(L) binding site appears to have only a mild influence, if any, on string mRNA degradation.

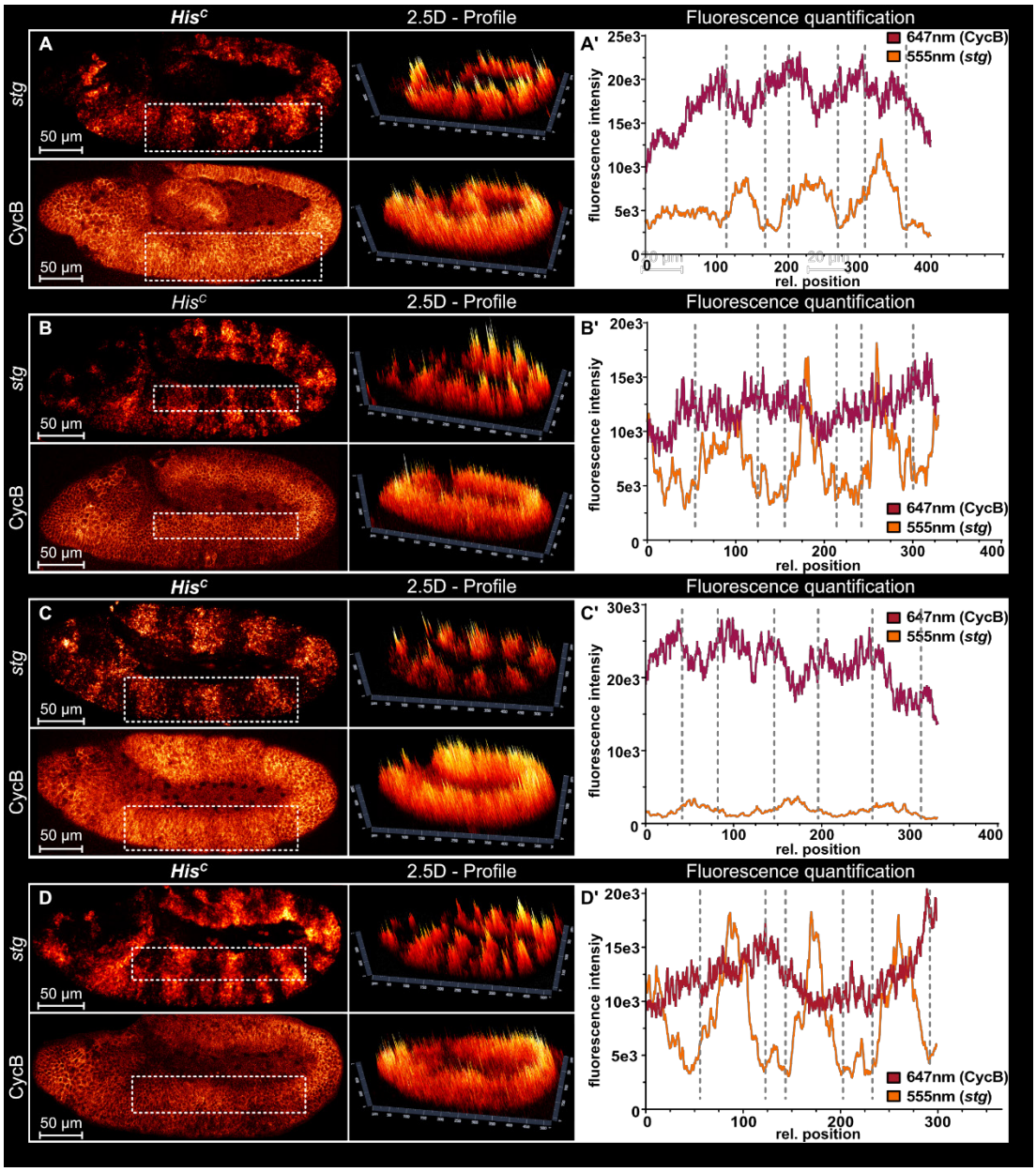

Figure 2.49 *Quantification of Cyclin B and stringΔhow* construct expression levels Expression of the *stringΔhow* transgene from the 2nd chromosome (51C1) analysed by FISH targeting the first exon of *string* mRNA together with Cyclin B immunofluorescence in *His*^{C} embryos (A to D). (A to D) Cyclin B expression follows the *His*^{C} pattern as described in A' to C'. Signal intensities of *string* and Cyclin B are colour coded applying a fire LUT. Yellow colour reflects high intensities, red lower intensities. 2.5D-profiles depict signal intensities by colour coded peak height. Quantification of absolute fluorescence A' to D' in the highlighted boxes regarding relative position within each box. A' and C' show slight degradation of Cyclin B (647nm or purple line) that coincides with upregulation of *string*Δhow (555nm or orange line). Degradation of Cyclin B in embryo B' might only occur in the first two domains of *string*Δhow expression. Embryos D' does not show any correlation between *stringΔhow* and Cyclin B intensities.

2.2.4 Discussion

Mutant *His^C* embryos undergo the first 13 nuclear divisions which precede MBT and continue with cell cycle 14 after MBT which takes place in M_{13} to S_{14}. These first 14 cell cycles are presumably maintained by parental histone proteins, mostly of maternal origin, and maternal mRNAs. However, mutant embryos arrest in G2/M_{15} without variation, and display stereotypic accumulation of Cyclin B and lack of *string*. String activates the Cyclin B1/Cyclin dependent kinase 1 (Cdk1) complex in cells for entering mitosis thereby regulating G2/M progression (*5, 6*). String regulation in temporal vicinity to the MBT is mediated by several independent pathways, including developmental processes but also cell cycle checkpoint pathways (*4, 6, 14*). Although, replication speed is reduced, BrdU assays revealed that the DNA is still fully replicated upon histone depletion in S_{15} in *His^C* mutants, and that DNA damage checkpoints ATM/Chk2 and ATR/Chk1 are not activated (*1*).

Therefore, we concluded that regulation of String is unlikely mediated by these pathways in *His^C* mutants, although it was argued that upon G2/M_{15} arrest, *His^C* mutant embryos might accumulate DNA lesions over time (*1*), which is consistent with *grapes* upregulation 6h AEL. In order to identify a potential String regulator which is not related to the DNA damage or replication checkpoints, we first asked whether *string* repression in *His^C* mutants is controlled on the transcriptional level, by mRNA stability, or at the translational level (Figure 2.50).

To see whether *string* mRNA is expressed in *His^C* mutant embryos, we performed FISH using a probe directed against mature *string* mRNA. Only negligible levels of *string* mRNA could be detected (Figure 2.31). Thus, *string* mRNA levels are not completely abolished as confirmed by qRT-PCR analysis (Figure 2.31 B), but severely reduced. To exclude that these rudimentary mRNAs are not experimental artifacts, we conducted FISH using a probe directed against the intron of *string* (Figure 2.32). The result showed that *string* is still actively transcribed during cell cycle M_{15} in *His^C* mutant embryos. This observation, together with the qPCR results, is consistent with the argument that the reduction of *string* transcripts in *His^C* mutant embryos is due to mRNA instability, resulting in a rapid degradation of the newly transcribed transcripts.

mRNA regulators often bind regulatory elements in *UTRs* of the transcript. To identify potential binding sites within *string* mRNA, we overexpressed several transgenes, in which *UTRs* of *string* mRNA, either in the 5´region or at the 3´end were exchanged with corresponding *UTRs* of genes which lack such regulatory elements. Expressing a transgene in which the *5´UTR* was replaced by the *HspA 5´UTR* under control of a *paired* driven Gal4 system did not result in increased *string* mRNA accumulation in *His^C* mutant embryos (Figure 2.34).

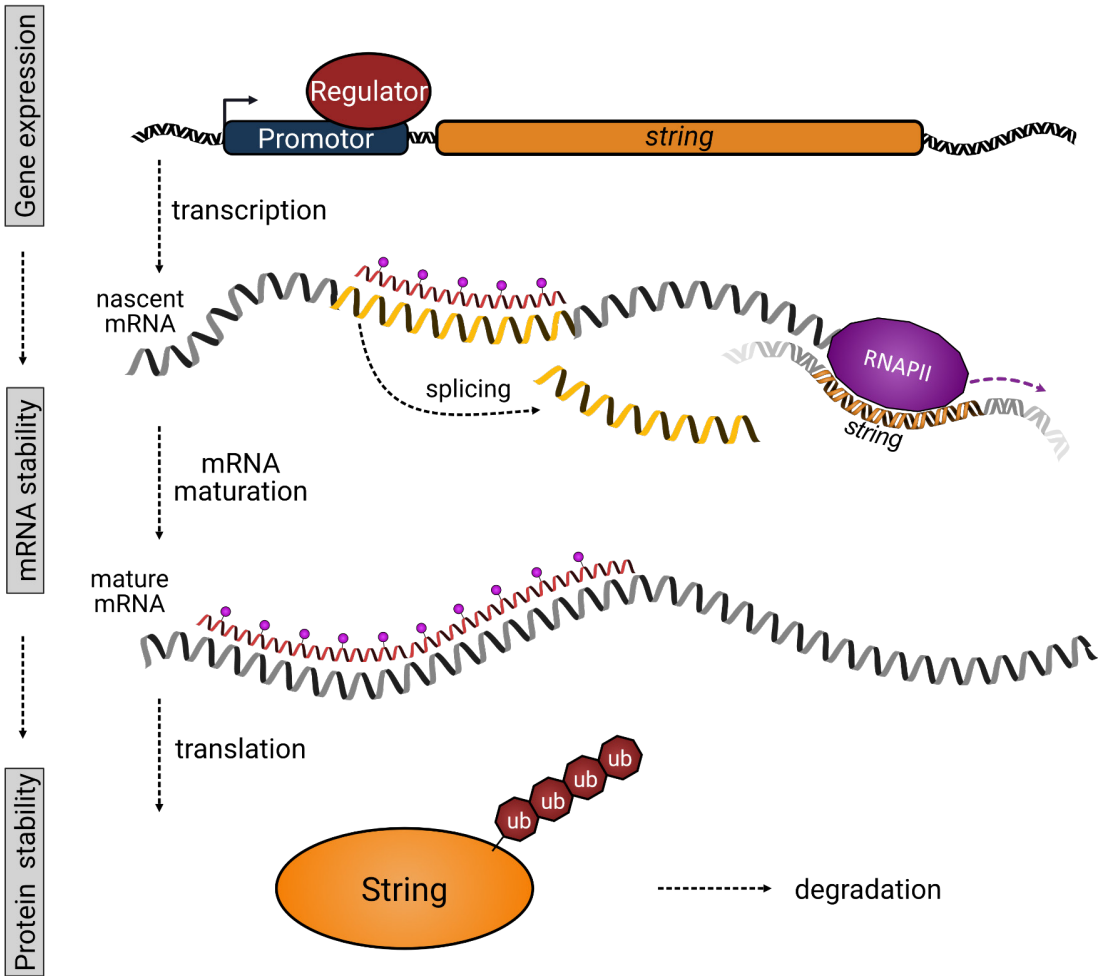

Figure 2.50 Regulation of String in *His^{C}* mutants. Schematic representation of potential String regulation in *His^{C}* mutants, which is not related to the DNA damage or replication checkpoints. String repression might happen at the transcriptional level, by mRNA stability, or at the translational level in G2/M$_{15}$ arrested of *His^{C}* mutant embryos. In *His^{C}* mutant embryos Cyclin B accumulates without upregulation of String. Reduced levels of String can potentially result from reduced protein half-life time and increased protein degradation. A second pathway regulating String abundance could either be by destabilizing *string* mRNA or to prevent *string* transcription. By *in situ* hybridization, we analyse abundance of mature mRNA, whereas nascent mRNA is exclusively detected using a probe targeting the intron of the unprocessed *string* mRNA pre splicing. Together providing insight into the gene expression levels of *string* in *His^{C}* mutant embryos.

Consistently, the Cyclin B signal strength was not reduced, and no mitotic nuclei were observed in the *paired* expressing domains, whereas Cyclin B is degraded in the respective domains of wild type control embryos expressing the same transgene. However, one cannot discriminate whether the degradation is due to endogenous String of the wild type embryos and how much transgene-derived String contributes to Cyclin B degradation (Figure 2.33). Using the second transgene, in which the *3'UTR* is replaced by the *SV40* 3'*UTR*, we find that wild type embryos degrade Cyclin B in the *paired* domains as has been observed with the transgene in which the *5´UTR* was replaced (Figure 2.35 and Figure 2.37). However, the mRNA signal in *His^{C}* mutans is considerable stronger as compared to the transgene where the *5'UTR* was exchanged. This result was obtained irrespective of the position of the transgene, i.e. whether it was inserted in the third chromosome (region 86F6) (Figure 2.35 and Figure 2.36) or the second chromosome (51C1) (Figure 2.37 and Figure 2.38).

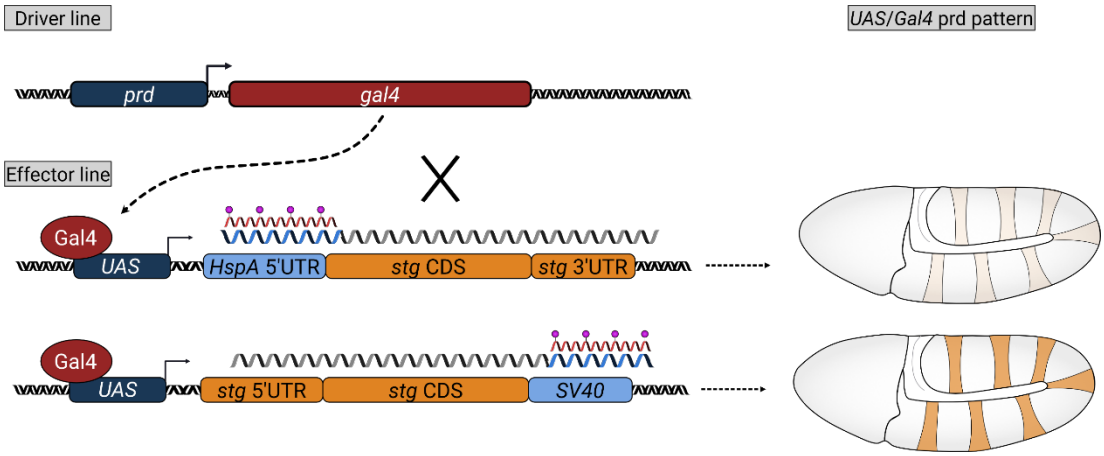

Figure 2.51 Overexpression of genetically engineered mRNAs using the binary *UAS*/Gal4 system. Two distinct transgenes were overexpressed in wild type and His^C mutant embryos under the control of *paired* driven Gal4 expression. The resulting expression patterns therefore do not represent *paired* expression at the given timepoint as the binary UAS/Gal4 system introduces a temporal delay. Both transgene express *string* CDS with either one of the endogenous *UTRs* and a commonly used replacement. The first transgene contains *HspA 5'UTR* instead of the endogenous *string UTR*, the second transgene replaces the endogenous *3'UTR* of *string* with *SV40*, respectively. His^C embryos expressing *HspA-stg-3'stgUTR* do not display increased mRNA stability as analysed with a probe against *HspA*, whereas embryos expressing *5'stgUTR-stg-SV40* exhibit stronger signal intensities by *in situ* hybridization using a probe against *SV40*.

Although, an increased signal strength was observed in response to *SV40* expression in His^C mutants, Cyclin B is not degraded to the extent observed in wild types. However, nuclear aggregates were found (Figure 2.36 A, B and Figure 2.38 A, B), likely to reflect partially or impaired condensed chromatin.

Their appearance is not restricted to the *paired* domains and might therefore be artifacts, explaining similar formations as observed in His^C mutants expressing *HspA-stg-3'stgUTR*. Despite these uncertainties, we conclude that the increased accumulation of transgenic mRNA in response to the *5'stgUTR-stg-SV40* transgene is consistent with the argument that a potential regulatory element resides in the *3'UTR* of the endogenous *string* mRNA (Figure 2.51). Visible control transgenes, in which the *string* CDS was replaced by the *eYFP* CDS (Figure 2.39 and Figure 2.40), led to the same expression patterns both in His^C mutant and wild type embryos as obtained with the correspondingly modified *string* transgenes. Although this result supports the hypothesis that a regulatory element is located in the *3'UTR* of *string* mRNA, future more detailed studies are needed to finally show that there is indeed a quick *eYFP* or *string* mRNA degradation driven by the *string* 3'*UTR*.

Two promising candidates for destabilizing *string* mRNA in the context of development of *Drosophila* are known. One being Held-out-wings (How) which encodes two protein variants with different isoform. The longer variant, How(L), which is of interest with respect to *string* mRNA regulation, destabilizes the bound mRNA, whereas the shorter variant, How(S), has the opposite function. The second *string mRNA* destabilizer is *microRNA-965* (*miR-965*) (*11–13*). For the How interaction with *string* mRNA one binding motifs is reported (GACUAA)

which is found twice in *string* mRNA, first in the intron and second in the *3'UTR*. We focused our attention on a possible destabilization of the *string* mRNA by How. Indeed, while *how(S)* transcripts are expressed at constant low levels up to the M_{15} stage of embryonic development, *how(L)* rises during the same developmental period from low to high levels. Furthermore, Western blot analysis revealed that the How(S) protein is expressed only at a low level both in wild type and His^C mutant embryos, while How(L) is exclusively found in the His^C mutants. This finding is consistent with the argument that the appearance of How(L) in the mutants is responsible for the degradation of *string* mRNA.

Both *how(S)* and *how(L)* transcripts are expressed in similar patterns both in wild type and His^C mutant embryos showing the pattern in mesodermal tissues as reported earlier (*13*). However, ectopic expression of *how(L)* mRNA is only detectable in $G2/M_{15}$ arrested cells in His^C mutant embryos.

The expression patterns and the levels of the *5'stgUTR-stg-SV40* and *5'stgUTR-stg-3'stringUTRΔhow* were similar. Since the open reading frame of *string* was not interrupted by the intron, the transgenes lack already one of the two How binding sites, i.e., the one located in the intron. Both *5'stgUTR-stg-SV40* transgene and *5'stgUTR-stg-3'stringUTRΔhow* lack both of them. Upon expression of *5'stgUTR-stg-3'stringUTRΔhow* in His^C mutants, expressing additional chromatin aggregates were observed as observed in response to expression of the *SV40*-construct. Unfortunately, however, although they could be taken as a sign for initiating mitosis, they are not restricted to the overexpression domains. This observation is not in support of mitosis induction in response to transgenes which express *string* lacking the How(L) binding site.

String as well as Cyclin B/Cdk1 act in a dosage dependent manner. Thus, expression of the *5'stgUTR-stg-3'stringUTRΔhow* as well as the transgene lacking the entire *3`UTR* of *string* may not express *string* strong enough to provide the sufficiently high activity to degrade Cyclin B. Therefore, we tried to quantify signal intensities in cell cycle arrested embryos (Figure 2.49). In two out of four embryos, an anticorrelation of *string* transgene signal and Cyclin B signal was observed, meaning that Cyclin B is at least partially degraded. This finding is in support of our hypothesis that the activity of How(L) is part of the degradation scenario of *string* mRNA when cells stop dividing at M_{15}. This conclusion is only preliminary. It could well be that the expression levels provided by the transgenes do not reach the functional concentration level of *string* to provide the mitosis inducing level of String activity. Thus, genetic manipulations which aim for higher expression levels of the *string* transgene which lack the corresponding *3´UTR* sequences are required to further support the hypothesis that How(L) is part of the degradation scenario of *string* mRNA in His^C mutants.

Finally, it must be noted that important controls are still missing to unambiguously demonstrate that How(L) association with *string* mRNA, and the subsequent degradation of the mRNA, is the cause of the cell division arrest at stage M_{15}. One essential control is for example to express the *HspA-eYFP-3'stgUTR* transgene and to examine whether the mRNA exhibits a shorter half-life than the transgene which contains the *SV40* 3´end. Also, quantifications need to be done to verify whether How(L) expression in His^{C} mutant epidermal cells is in fact significantly increased in $G2/M_{15}$ arrested cells. This is also true for Cyclin B degradation in *5'stgUTR-stg-3'stringUTRΔhow* expression domains, since only half of the analysed embryos show such an effect, an observation which is no more than a hint. To further circumvent some of the limitations of this study, a number of experiments could be conducted. Examples are that the transgenes which are located on the 2nd and 3rd chromosome can be jointly expressed to increase the amounts of transcripts *string* transcripts so that a critical concentration of *string* protein can finally be reached. In addition, a number of driver lines different from the *paired* driver should be used to express transgenes at the highest possible efficiency.

2.2.5 Materials and Methods

2.2.5.1 Crossings and Stocks

Fly stocks were kept in duplicates at 18°C under permanent light conditions and flipped every 4 weeks with a shift of 2 weeks between duplicates. Transgenic flies received from BestGene were crossed with DM9 and DM10 (Table 8) to introduce balancer chromosomes for the 2nd or 3rd chromosome, respectively. Resulting flies had were either (X)/ *CyO, P{ftz-lacB}E3;D/Sb, P{Ubx-lacB}E3 or*, (X)/*CyO,Act-GFP;D/Ser,Act-GFP for the 2nd chromosome or* Sp/ *CyO, P{ftz-lacB}E3;(X)/Sb,P{Ubx-lacB}E3 or Sp/CyO,Act-GFP;(X)/Ser,Act-GFP with X being either UAS:HspA-stg-3'stgUTR, UAS:5'stgUTR-stg-Sv40, UAS:HspA-eYFP-3'stgUTR, UAS:5'stgUTR-eYFP-Sv40 and UAS:HspA-stg-3'stgUTR, UAS:5'stgUTR-stg-3'stgUTRΔhow. Resulting lines were crossed with* DM1 or DM2, *Df(2L)His^{C}/CyO, P{ftz-lacB}E3; D/Sb,Ubx-lacZ or Df(2L)His^{C}/CyO*, *Act-GFP; D/Sb, Act-GFP.* Meiotic recombination events were genotyped by PCR on dissected wings using DM337_w7500D (GTCCGCCTTCAGTTGCACTT) and DM338_w11678U (TCATCGCAGATCAGAAGCGG) (*15*) as described by (*16*). Overexpression of transgene was achieved by crossing responder virgins with *Df(2L)His^{C}/CyO, P{ftz-lacB}E3;p(prd-Gal4)/Sb,P{Ubx-lacB}E3 males.*

Table 8 Fly stocks used during the thesis

Stock Number	Genotype
DM1	*Df(2L)His^{C} / CyO, P{ftz-lacB}E3*
DM3	*Df(2L)His^{C}, P{UAS:eYFP}AH2/ CyO, P{ftz-lacB}E3*
DM4	*Df(2L)His^{C}, P{GAL4-twi.2xPE}/ CyO, P{ftz-lacB}E3*
DM5	*Df(2L)His^{C} / CyO, P{ftz-lacB}E3; D / Sb, P{Ubx-lacB}E3*
DM9	Sp / *CyO, P{ftz-lacB}E3; D / Sb, P{Ubx-lacB}E3*
DM11	*Df(2L)His^{C} / CyO, P{ftz-lacB}E3; p(prd-Gal4) / Sb, P{Ubx-lacB}E3*
DM12	*Df(2L)His^{C}, UAS:HspA-stg-3'stgUTR / CyO, P{ftz-lacB}E3; D / Sb, P{Ubx-lacB}E3*
DM13	*Df(2L)His^{C}, UAS:5'stgUTR-stg-Sv40 / CyO, P{ftz-lacB}E3; D / Sb, P{Ubx-lacB}E3*
DM16	*Df(2L)His^{C} / CyO, P{ftz-lacB}E3; UAS:HspA-stg-3'stgUTR / Sb, P{Ubx-lacB}E3*
DM17	*Df(2L)His^{C} / CyO, P{ftz-lacB}E3; UAS:5'stgUTR-stg-Sv40 / Sb, P{Ubx-lacB}E3*
DM20	*Df(2L)His^{C}, UAS:5'stgUTR-eYFP-Sv40 / CyO, P{ftz-lacB}E3; D / Sb, P{Ubx-lacB}E3*
DM22	*Df(2L)His^{C}, UAS:5'stgUTR-stg-3'stgUTRΔhow / CyO, P{ftz-lacB}E3 ; D / Sb, P{Ubx-lacB}E3*

Stock Number	Genotype
DM24	*Df(2L)His^{C}/CyO, P{ftz-lacB}E3;p(prd-Gal4)/Sb,Ubx-lacZ*

2.2.5.2 Egg collection and Fixation

w^{1118} flies were used as wild type controls. To generate homozygous *His^{C}* mutant embryos for qRT-PCR and protein isolation, we crossed heterozygous *Df(2L)His^{C}, P{GAL4-twi.2xPE}/ CyO, P{ftz-lacB}E3* with *Df(2L)His^{C}, P{UAS:eYFP}AH2/ CO, P{ftz-lacB}E3* flies. The resulting eYFP-expressing embryos with the genotype *Df(2L)His^{C}, P{GAL4-twi.2xPE}/ Df(2L)His^{C}, P{UAS:eYFP}AH2* were identified under a fluorescence stereomicroscope and collected with a P20 pipette. For time-staged embryo collections, flies were kept in cages covered by an apple agar plate at 25C. Egg deposition on apple agar plates was restricted to 30min, which were subsequently aged at 25°C for 3.5, 4.5, 5.5 or 6.5h. For fluorescent *in situ* hybridization and immunostaining, heterozygous *Df(2L)His^{C}/ CyO, P{ftz-lacB}E3* flies were crossed and genotyped by beta-galactosidase expression.

2.2.5.3 *In situ* hybridization

RNA probes were designed to cover ~1000 bp of the coding or intronic sequence of the *string* gene, and the complete *HspA* and *SV40* sequences. PCR fragments were amplified from genomic DNA and plasmid donors using reverse primers with a T7-promotor (GAA TTG TAA TAC GAC TCA CTA TAG G) overhang. *In vitro* transcription was performed using T7 Polymerase (Roche, 10881775001) and DIG (Digoxigenin)-RNA labelling mix (Roche, 11277073910): 1µl PCR product 150-250ng, 10x Buffer, 1µl DIG labelling mix, Protector RNAse Inhibitor (40U/µl; Roche, 3335399001), 0.5µl T7 Polymerase, DEPC- H_2O to 10µl). Reverse transcription was conducted for 2 hours at 37°C. The probes were precipitated and resuspended in 100µl resuspension buffer (50% formamide, 0.1% Tween-20, 5x SSC pH5, Heparin 20µg/µl). Fluorescent *in situ* hybridization was performed as described using sheep anti-Digoxigenin-POD antibody (Roche, 11207733910) (*17*). Embryos were subsequently incubated with mouse anti-Cyclin B antibody (1:1000; #2245815, Hybridoma Bank) and chicken anti-beta galactosidase (1:1000; Rockland, 200-901-036) in PBS-T overnight at 4°C. The samples were washed 3 times for 15 minutes each with PBS-T and incubated with secondary antibodies for 2 hours at room temperature in the dark on a rotator. Secondary antibodies were Alexa Flour 488 goat anti-chicken IgY (1:2000; Invitrogen, A11039) and Alexa Flour 647 goat anti-mouse IgG (1:2000; Invitrogen, A21235) in PBS-T. DNA was visualized by incubation for 15 minutes with DAPI (1:1000).

2.2.5.4 Mounting

Embryos were mounted onto objects slides previously prepared with sticky paper rings to avoid crushing of the embryos by slightly elevating the cover slip. As mounting media VectaShield (VEC-H-1000) or self-made DAPCO anti fade mounting medium were used. The samples were sealed with transparent nail polish and stored at -20°C. Fluorescence was detected using a LSM 980 and Axioplan2 microscopes (Carl Zeiss).

2.2.5.5 RNA isolation

Embryos were dechorionated in 50% bleach and washed three times with PBS with 0.1% Tween-20 (PBS-T). Embryos were preserved in RNAlater (Invitrogen) and macerated in 50µl RLT buffer (Qiagen RNeasy Plus Micro kit) using a pre-cooled 1ml Dounce homogenizer (Bio-Trend, 1984-10002). The lysate was passed through a QIAshredder spin column (Qiagen). RNA was then isolated using the Qiagen RNeasy Plus Micro kit. RNA concentration and quality was determined using a NanoDrop 2000 Spectrometer (Thermo Scientific), Qubit 2.0 Fluorometer (Invitrogen) and/or a 2200 TapeStation with High Sensitivity RNA screen tapes (Agilent).

2.2.5.6 Quantitative real-time polymerase chain reaction (qRT-PCR)

cDNA was amplified using QuantiTect Reverse Transcription kit (Qiagen) with 50ng of input RNA. qPCR (quantitative Real-Time PCR) was performed using KAPA SYBR FAST master mix (2x) (Kapa Biosystems). Primers were designed using NCBI primer blast tool with primers spanning exon-exon junctions. Relative gene expression was analysed using the comparative ΔΔCt method using Actin 5C for normalization (*10*).

2.2.5.7 Protein isolation

Protein was isolated from wild type and *His^{C}* mutant embryos 3-6h AEL. Roughly 20µl dechorionated embryos were transferred into a clean low retention Eppendorf cup containing 100µl ice cold NB lysis buffer (150mM NaCl, 50mM Tris-HCl, 2mM EDTA, 0.1% NP-40). Before usage 1µl 1M DTT, 20µl 0.5M NaF and 1/10 tablet Roche protease inhibitors (Roche, 4693132001). All centrifugation steps were conducted at 4°C and the samples were always kept on ice. The vials were centrifuged shortly to collect all embryos at the bottom and subsequently macerated with a tightly fitting sterile glass pestle to disrupt cells and nuclei. Centrifugation and maceration were repeated to ensure complete rupture of all embryos. The samples were centrifuged for 3 minutes at 4°C and 20,000g to separate remaining debris and lipids. Avoiding debris and the lipid surface layer, the supernatant was transferred into a clean vial and centrifugation was repeated. The supernatant was transferred into a clean vial and subsequently diluted with 1x volume 2x Laemmli. The samples were sonicated with a

Diagenode Bioruptor Pico exposing them for 10 cycles with 30s “on” and “off” time to sonication to increase accessibility to DNA bound protein. Protein extracts were then heated for 5 minutes at 100°C and immediately frozen at -20°C.

2.2.5.8 SDS-PAGE and western hybridization

Protein concentrations were measured with the Qubit 2.0 fluorometer protein assay kit (Themo Fisher, Q33212). Each replicate was used in a dilution series starting with 50ng (=100%) per, reducing to 75%, 50% and 25%. Protein extracts were separated using Mini-PROTEAN TGX™ Precast 4 – 15% (Bio-Rad, 4561083) gradient gels. The gel was mounted in a Mini-PROTEAN Tetra Vertical Electrophoresis Cell (Bio-Rad, 1658000) filled to the corresponding marker with 1x Running Buffer (25mM Tris-HCl, 190 mM glycine, 0.1% SDS, pH 8.3). The gels were run at constant voltage of 100V at room temperature. Size separated proteins were transferred from the gel onto a Immobilon®-E PVDF Membrane (Merck Millipore, IEVH07850) previously activated with 100% methanol for 5 minutes and washed once with transfer buffer (25mM Tris-HCl, 190mM glycine, 20% methanol, pH 8.3) in semi-dry conditions for 3hours at 80V. The membranes were cut with a scalpel and blocked 1h at room temperature in 5% BSA and subsequently incubated with the primary antibody rabbit anti-How (courtesy Talila Volk, Weizmann Institute, Israel (*13*)) (1:500) and mouse anti-GAPDH (1:500) over night at 4°C. The membranes were washed 3 times for 5 minutes in TBS-T. For signal development the membranes were incubated with the corresponding HRP coupled secondary antibody (1:2000) (CellSignaling, anti-mouse IgG, HRP-linked Antibody #7076 and anti-rabbit IgG, HRP-linked Antibody #7074) for 1 hour at room temperature. Signal was developed using Bio-Rad imager and Pierce™ ECL Western Blotting (ThermoFisher, 34075). Repeated incubation with a primary antibody succeeded membrane stripping by incubating the membrane twice for 5 minutes in stripping buffer (200mM glycine, 0.1% SDS, 0.1% Tween-20, pH 2.2). After stripping the membrane is blocked in 5% BSA for 1h at room temperature. Antibody hybridization and signal development is conducted as described above.

2.2.5.9 Primer and plasmid design

Transgenes were generated by amplifying *string* CDS and *HspA* 5’UTR from genomic DNA, *SV40* sequences were amplified from donor plasmid pBac[3xP3DsRed;hTc-Gal4D-SV40] #9 available in the laboratory. Primers were designed with Geneious Prime® 2022.1.1 and *Drosophila melanogaster* reference genome dm6 (FlyBase Dmel Release 6.23) using standard settings (*18*) and adding overhangs corresponding to the up- or downstream fragments with the length resulting in annealing temperature of Tm=60°C for the overlapping regions calculated using the nearest-neighbour method (*19*). Fragments were fused by

overlap extension PCR adopted from (*20*). The first 5 cycles were conducted without outer primer oligos and with a decreased ramp speed (1°C/s). The PCR was paused, outer primers added, and the annealing temperature adjusted. The reaction was continued for 30 additional cycles. Final constructs were cloned into pCRII(attB;10xUAS:;AscI;bHSP::mini-white) by restriction digest using AscI entry site. How deletion was achieved by site directed mutagenesis (*20*)

Transgenes the lines were injected at according Plan I BestGene, Chino Hill, CA, USA, using stock 24482 and 24749.

2.2.6 References

1. U. Günesdogan, H. Jäckle, A. Herzig, Histone supply regulates S phase timing and cell cycle progression. *eLife*. **3**, e02443 (2014), doi:10.7554/eLife.02443.
2. U. Günesdogan, H. Jäckle, A. Herzig, A genetic system to assess in vivo the functions of histones and histone modifications in higher eukaryotes. *EMBO reports*. **11**, 772–776 (2010), doi:10.1038/embor.2010.124.
3. S. A. Blythe, E. F. Wieschaus, Zygotic genome activation triggers the DNA replication checkpoint at the midblastula transition. *Cell*. **160**, 1169–1181 (2015), doi:10.1016/j.cell.2015.01.050.
4. B. Liu, J. Grosshans, Link of Zygotic Genome Activation and Cell Cycle Control. *Methods in molecular biology (Clifton, N.J.)*. **1605**, 11–30 (2017), doi:10.1007/978-1-4939-6988-3_2.
5. B. A. Edgar, D. A. Lehman, P. H. O'Farrell, Transcriptional regulation of string (cdc25): a link between developmental programming and the cell cycle. *Development*. **120**, 3131–3143 (1994), doi:10.1242/dev.120.11.3131.
6. D. A. Lehman *et al.,* Cis-regulatory elements of the mitotic regulator, string/Cdc25. *Development*. **126**, 1793–1803 (1999), doi:10.1242/dev.126.9.1793.
7. B. Alberts *et al.*, *Molecular Biology of the Cell* (Garland Science, New York, 2015).
8. K. Yuan, C. A. Seller, A. W. Shermoen, P. H. O'Farrell, Timing the Drosophila Mid-Blastula Transition: A Cell Cycle-Centered View. *Trends in Genetics*. **32**, 496–507 (2016), doi:10.1016/j.tig.2016.05.006.
9. A. Hershko, Mechanisms and regulation of the degradation of cyclin B. *Philosophical transactions of the Royal Society of London. Series B, Biological sciences*. **354**, 1571-5; discussion 1575-6 (1999), doi:10.1098/rstb.1999.0500.
10. T. D. Schmittgen, K. J. Livak, Analyzing real-time PCR data by the comparative C(T) method. *Nature protocols*. **3**, 1101–1108 (2008), doi:10.1038/nprot.2008.73.
11. P. Verma, S. M. Cohen, miR-965 controls cell proliferation and migration during tissue morphogenesis in the Drosophila abdomen. *eLife*. **4** (2015), doi:10.7554/eLife.07389.
12. A. C. Monk *et al.,* HOW is required for stem cell maintenance in the Drosophila testis and for the onset of transit-amplifying divisions. *Cell stem cell*. **6**, 348–360 (2010), doi:10.1016/j.stem.2010.02.016.
13. H. Nabel-Rosen, H. Toledano-Katchalski, G. Volohonsky, T. Volk, Cell divisions in the drosophila embryonic mesoderm are repressed via posttranscriptional regulation of string/cdc25 by HOW. *Current biology : CB*. **15**, 295–302 (2005), doi:10.1016/j.cub.2005.01.045.
14. B. A. Edgar, D. A. Lehman, P. H. O'Farrell, Transcriptional regulation of string (cdc25): a link between developmental programming and the cell cycle. *Development*. **120**, 3131–3143 (1994), doi:10.1242/dev.120.11.3131.
15. E. Ryder *et al.,* The DrosDel collection: a set of P-element insertions for generating custom chromosomal aberrations in Drosophila melanogaster. *Genetics*. **167**, 797–813 (2004), doi:10.1534/genetics.104.026658.
16. G. B. Carvalho, W. W. Ja, S. Benzer, Non-lethal PCR genotyping of single Drosophila. *BioTechniques*. **46**, 312–314 (2009), doi:10.2144/000113088.
17. M. Buescher, G. Oberhofer, N. C. Garcia-Perez, G. Bucher, in *Brain Development, Methods and Protocols*, S. G. Sprecher, Ed. (Humana, New York, NY, ed. 2, 2020), vol. **2047,** pp. 219–232.
18. K. J. Breslauer, R. Frank, H. Blöcker, L. A. Marky, Predicting DNA duplex stability from the base sequence. *Proceedings of the National Academy of Sciences of the United States of America*. **83**, 3746–3750 (1986), doi:10.1073/pnas.83.11.3746.

19. J. SantaLucia, A unified view of polymer, dumbbell, and oligonucleotide DNA nearest-neighbor thermodynamics. *Proceedings of the National Academy of Sciences of the United States of America*. **95**, 1460–1465 (1998), doi:10.1073/pnas.95.4.1460.

20. K. L. Heckman, L. R. Pease, Gene splicing and mutagenesis by PCR-driven overlap extension. *Nat Protoc*. **2**, 924–932 (2007), doi:10.1038/nprot.2007.132.

2.2.7 Appendix

2.2.7.1 Supplementary Figures

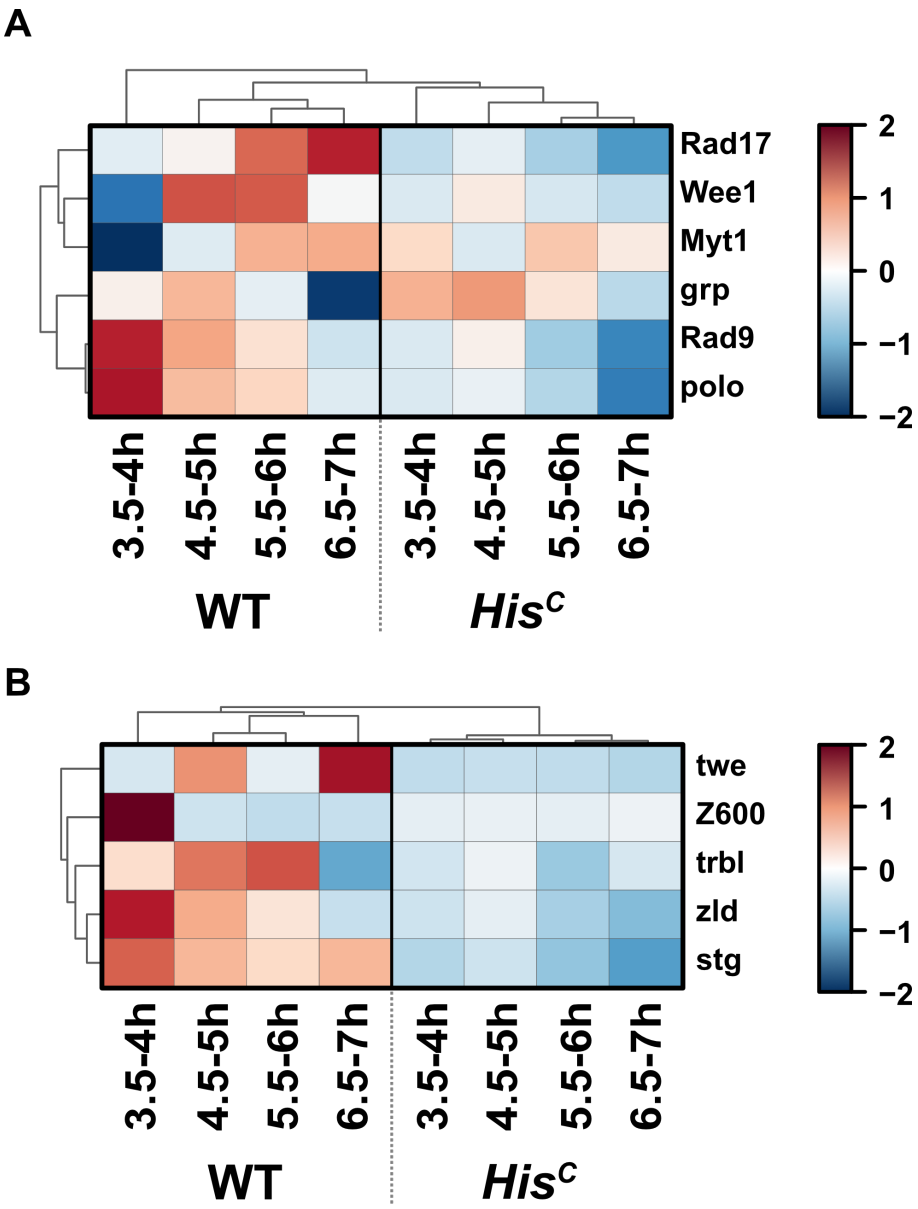

Figure 2.52 Heatmaps representing RNA-seq data achieved in wild types and *His*^{C} mutants (A) Heatmap of RNA-seq expression values (row z-score) of ATR/Chk1 checkpoint associated genes. (B) Heatmap of RNA-seq expression values (row z-score) of genes essential for ZGA and MBT.

2.2.7.2 FISH probe sequences and antibodies

Sequences of the PCR products used for *in vitro* reverse transcription to generate labelled RNA probes for use in FISH.

Table 9 Intronic *string* probe T7-promotor sequence is highlighted in bold letters

TAATACGACTCACTATAGCTTTTGCTTCCCTAAACTCTCGCAAGAGCGGGTCATTAAA CCCAGCTAAAAATACTGACAAACTGGTGGTGGTGGTGGCGTTGGTGGTGTAAAAACA ACAAAAATACCCGAGAAAATACAGAGAGGGGTTGTTGTAATTGGGTGAAGAGGGAG CTGAACTAGAAATTTACTTTAATGCAGCTTCGAAAACTGGAATTTTTGGGATTCGACTT GCGCACACGATATCATTGATACCATTTTTTTTTTTTTTGATAATTTTTACAATTCCCTAA AATTGCGAGGGAACCGTTGCGTACCGCCTTATCTTCTTCTTCTTGATTCTACTTAAGC ATTAGCGGTTCTCCAAATGGAATTCCCTTTTGCTTTTCGCATGCATCTGCTTTTCAGCT TGACTTTTGCTTTTGGGTCACACGTCACGCAAGCGCAGCGATAATACAACAAAAACA CGCCACAAAGAACCGCAAAGAACACGGAGGAAAAAAGGAACAAAAATCGAAAAAAA AAAAATGACTGACTGACGGACGACGGACAAAAAGCATTTTTTGCTGCTGCTTTTTTTT GGAGCCTCGCGGAAGCCGGTTTAATGAATGAAAAACGGCAAGCGAGCAACAAAACA ACAGCTGAGCGCCAAAATAAAAATCGGGCAAAAAGCAAACGTGCCGAGCGTGATAA AAAGAACTCTTACTTTTGTTGGCCCCATCGTTTACATTTCTGTTTTTTGTATTTTTTTTTT GCTTTGCTGTTGTTGCTGTTGCTCTTGAACTTGCACTTTTTATCGCGTATTTTCAACTG GTATTCCT

Table 10 Exonic *string* probe T7-promotor sequence is highlighted in bold letters

TAATACGACTCACTATAGCTTTGCTGAAGTCGCCGATTAGCTCGGGCTCGTTGCGGT TCTCGGAGCGGGCCAGGGCGGACATGATCTCGGCGTCGTTCAGGGACATGCACTT CCTCAGTGGAGGGGGGTGGCTAATCGTGACCTGGCTGAGTGGGCTGGGTGCGGGG CAGTTCTCCTTCTCAACGGCGGCGCAGCGATGGCGTTTGCTCTGGATGGGCGAGCA GTTGGCCGATGCTGGCGGTTCCGGGCGCTTGAAGCAATCCCGGGCAGTCTCTGGG GTCTTTGGTGGTGGGGTGGTGGTGCTGTTGGTGTTGCTCTCCGTCATGCTGAGGCA CCTTCTGACCGAAGGGCGGCGCATGGACAGACCCGCTGGCGATTTGGCAGCAGGC TGCTCCTTGATCTGGCCGCTGATCAGCGAGTTTAGGCCACTGGGGAAGCCCAGGGC GGTCTGTTGGCTCTGCGACTCCATCTCGAAGAGCTCCATGTACTCATCGTCCATGGA GGACTCCATGGAGCATGTGGAGGACAGGCTGTTGAAGATGCGGAAGCTGCGCGCC GGCGTGTGATCACTTGATACTCCCATAGCTGGCAGAATTTTCGGCTGGCGGACGAT CTGGAAGCGCTGGGGCGAGCCCTCCGGCGAGAGCAGACCCATCAGCTCCGGACT GGCCGATCGCTGCTGATCCTGGGGCACAACGTCGTCGTCGTAGAACGACAGCTCCT CCTGGTCCATGCTCATCAGTTCCAGGGAACGGCGAGCACGACGAGATCCACTCATT TTGTTGATGCTACTCGAACTGCTGG

Table 11 *HspA* probe T7-promotor sequence is highlighted in bold letters

TAATACGACTCACTATAGTGTGTGTGAGTTCTTCTTCCTCGGTAACGACTTGTTGAAA GTATTCAGAGTTCTCTTCTTGTCTTCAATAATTACTTCTTGGTTGATTTCAGTAGTTGCA GTTTTTAGTTTAATTACTTGGTTGTTGGTTACTTTTAATTGATTCACTTTAACTTGCACTT TATTGCAGATTGTTTAGCTTGTTCAGCTGCGCTTGTTTGTTTGCTTAGCTTTCGCTTAG CGATGTGTTCACTTTACTTGTTTGAATAGAATTGA

Table 12 *Sv40* probe T7-promotor sequence is highlighted in bold letters

TAATACGACTCACTATAGGATGAGTTTGGACAAACCACAACTAGAATGCAGTGAAAA
AAATGCTTTATTTGTGAAATTTGTGATGCTATTGCTTTATTTGTAACCATTATAAGCTGC
AATAAACAAGTTAACAACAACAATTGCATTCATTTTATGTTTCAGGTTCAGGGGGAGG
TGTGGGAGGTTTTTTAAAGCAAGTAAAACCTCTACAAATGTGGTATGGCTGATTATGA

Table 13 How(L) probe T7-promotor sequence is highlighted in bold letters

TAATACGACTCACTATAGGAATGCTTGCTGCTATTATCATAATATATGTTTGTTTCATTA
ACTAAATATGGCTGTTAAATGTGTTTTAATATGTTGTTTCTGTTTCGCCCCCACTTACT
CATCACACGATCGATTTGAAGTGGGGTACGAAATCTATACATAAAATATAGATATGCA
ATAACATAATCAAAAAATACTTCATTAACAAGAATTAGCGTCAGTTTAACAAAAATAGA
TTATGCTTAATCGAAGGGTGATAGTCTATATCCGACACAATATGGATTTAAATAGACTT
CGTGCACAATCCAATGAAAAGTGTAAAGATTCATCTTTGCAATTTGAGTTAAAAGTGC
AGATTTTTAAAAAAATTAAAACAGTTTTGGTTGGTTGAGTAGAGTTTCTTGGATGAGAT
TCCGTTAACATGATTTTCCTTATTTTTTGTGCTTAGGGGCTTTTGGGGTTATTATATACA
GACTTGTATATGCATTTGGATGTATATATATTTAAATATATATATATATGTATATGCTTGC
ATTAAGTATGTTTTTGTTCGTTGAACTTTTACACTAAGAACTAACTTGTATTTTCCTTTA
GATTATCATAATTAAACTAAGCTCTATGTTTGATTCTCTTATCAATCGTTTGCTTAATTG
CCTTGTTTTGTTTGCTGGCAAAACGTAACAGTTTAATGGCCACAAGATTCAATACATA
CTGATGTTGCTGCTGTTCGTTTGCTGTTGCTGTTGCTTTTGCTTTTGCTTTTGCTGTTG
ATGTTGTGATGCTGCTGGTGTTGAATGTGCCGCATCTGCTGCTCATTTGGCAAATAG
GTTCAGAGTTTGGAGTTTGGCGTTCGGAGGGGTTCAGTGTTTTAGTAGTTGTGTAAGT
GACATGTGGTGGCTCAGGATATCTGACTTTTGGTT

Table 14 How(S) *Sv40* probe T7-promotor sequence is highlighted in bold letters

TAATACGACTCACTATAGAATACTGTCCCTCCATCGCAAAACTCACTACATAAACTAC
ATAAAAAACAGACACTTAACTAGATTGCACTTAAGACTCGACCCTCATACCAAAAAAA
AACTAAAATAGGGTTATTATTATTCAGAAGAGAAAAATTATGAAGTTTAGCCCTCTTTA
ATTTGAATACTCATGGGTTCCAAAAACGAAAATCAACAACTTGCATTGGGTGCCGCT
GTTGTTGTTGTTCTCAACTAGAATATACTCATATAAAAAATGTTTCGGGTGGAAAATCA
TATATGTATGTAGGTTGGTTACAGTTAAAATTAAAGCAACTACAATTTAAGGGCCTAAA
AATCACTTATTTTTGCCAATATTGCATATTGCAGAAATGTATTGCATTGCGGTCTAAAA
TCTAATAAACAATATAAAAAGCATATTCATTGTCGAGCAATAATTGTTGTAGCTTAATT
CTTTGCTTGTATTTTCTTGAGTATTTCTGTTTTCCTGTTTGTTGTGCCGTTTTACTCATAC
GTTTTTGTCTCTACGTAAATATATAATTTTAAAAATATATACAGTCTATACATTTATGTGT
GTGTGTATAATTCTGTTTCAGTTTTTGTGTGACTGTAACTAAATAACTTTAAGCTAAACA
TTTTCTGTGGGGTTTTCCTCTACAAATCGTTTCTGGTTTTCTTGTTTTTGTTCAACGGAA
AAATAATAGAGAGTGAGAAAAAGGAGTTCAAAAGACG

Table 15 Antibodies

Name	Cat. No.	Provider
α-Mn-647	A21235	Invitrogen/ThermoFisher
α-Chk-488	A11039	Invitrogen/ThermoFisher
α-Dig-POD	11207733910	Roche
α-Cyclin B	2245815	Hybridoma Bank
α-beta galactosidase	00-901-036	Rockland

Name	Cat. No.	Provider
α-How	n.a.	Talila Volk, Weizmann Institute, Israel
α-mouse-HRP	7076	CellSignaling
α-rabbit-HRP	7074	CellSignaling

2.2.7.3 Oligos

Table 16 Primers and Oligos used for cloning and qRT-PCR

Name	Sequence
DM73_Sv40_rv	AATGTTTTTGCGAATAGGGTACCGGGATGAGTTTGGACAAACC
DM72_Sv40_fw	ACTGATGCTGTAGTCATAATCAGCCATACCAC
DM71_stg_3'UTR_rv	AATGTTTTTGCGAATAGGGTACCGGCGTCGTGTATTAATGTATATTTAAAATTG
DM70_stg_3'UTR_fw	GAACTCACACACAATGCTGTGGGAAACTATTG
DM69_stg_5'UTR_rv	TGGCTGATTATGACTACAGCATCAGTCGCGAG
DM68_stg_5'UTR_fw	GTTCATTGGTACCTACCGGCCTTGGTGGCCTCCATAGAGCTGG
DM67_HspA_rv	TTTCCCACAGCATTGTGTGTGAGTTCTTCTTC
DM66_HspA_fw	GTTCATTGGTACCTACCGGCCTTGGTCAATTCTATTCAAACAAGTAAAG
DM65_UASp_P-element_rv	TACCGGCGCGCCAAGGCCGGTAGGTACCAATGAACAGGACCTAACGC
DM64_UASp_P-element_fw	ATACCATTTAGCTAGGCCGGGCCGCTCTAGCCCCCCCT
DM63_stg_3'UTR_pGE	TACCGGCGCGCCTCGAGACTAGTATCGTCGTGTATTAATGTATAT
DM62_stg_5'UTR_pGE	TTGCATGCAATGCGGCCGCTAGCATGGCCTCCATAGAGC
DM31_stg_2F	TGCAATATCAGTAATAACACCAGCA
DM30_stg_1R	TCGAACTGCTGGTGTTATTACTGA
DM294_eYFP_fwd_hsp	CTCACACACAATGGTGAGCAAGGGCGAG
DM293_hsp_rev_eYFP	TGCTCACCATTGTGTGTGAGTTCTTCTTC
DM292_Sv40_fw_eYFP	GTACAAGTAATCATAATCAGCCATACCAC
DM291_eYFP_rv_Sv40	CTGATTATGATTACTTGTACAGCTCGTCCATG
DM29_stg_1F	ACCAACAAAATGCTGTGGGAA
DM273_stg_3'UTRstg_rv	TCCCACAACCTACAGCATCAGTCGC
DM272_3'UTRstg_stg_fw	ATGCTGTAGGTTGTGGGATGATCGT
DM270_eYFP_5'UTRstg_fw	ACCAACAAAATGGTGAGCAAGGG

Name	Sequence
DM269_eYFP_Bbackbone_rv	TTGCGAATAGGGTACCGGTTACTTGTACAGCTCGTC
DM267_5'UTRstg_eYFP_rv	GCTCACCATTTTGTTGGTTTTGTTGT
DM264_eYFP_Backbone_fw	GGTACCTACCGGCCTTGGATGGTGAGCAAGGG
DM263_eYFP_3'UTRstg_rv	TCCCACAACTTACTTGTACAGCTCGTCC
DM252_3'stg_rev	GTTTTTGCGAATAGGGTACCCGTCGTGTATTAATGTATATTTAAAATTGATG
DM245_Backbone_fw	GGTACCCTATTCGCAAAAAC
DM9_H1_1f	AAGGCAAAAGCCAAGGATGC
DM10_H1_1R	CTTCGCTGCAGTCACTTTCG
DM13_H2A_1F	CGGAAGGGAAACTACGCAGA
DM14_H2A_1R	GAACCTCAGCGGCCAGATAT
DM17_H2B_1F	TCACTACAACAAGCGCTCGA
DM18_H2B_1R	ATGCTTGGCCAACTCTCCAG
DM21_H3_1F	TCTGCAGGAAGCTAGCGAAG
DM22_H3_1R	TATGGTGACACGCTTGGCAT
DM25_H4_1F	AATTCGTGATGCCGTGACCT
DM26_H4_1R	TTGCCTCTTCAGAGCGTACA
DM29_stg_1F	ACCAACAAAATGCTGTGGGAA
DM30_stg_1R	TCGAACTGCTGGTGTTATTACTGA
DM39_Act5C_fw	ATTTGCCGGAGACGATGCTC
DM40_Act5C_rv	TACGAGTCCTTCTGGCCCAT
cDM304_How(B)_rv	ATCTGGCAAACAACCCACCG
DM305_How(C)_rv	CCGGCATGCATATATCGACCA
DM189_How(S)_fw	CGCACCGTACGATTATGCGA
DM191_how(L)_A/D/E/F_fw	CCGAAGGCGAAGATGAGCTA
DM192_how(L)_A/D/E/F_rv	TCGCACACTGCGACAGATTT
DM6_stg1_rv_T7	GAATTAATACGACTCACTATAGGGAGACTTTGCTGAAGTCGCCGATT
DM217_how(S)_fw	CTCCTTTTTCTCACTCTCT
DM218_how(S)_rv_T7	TAATACGACTCACTATAGCATCGCAAAACTCACTAC
DM219_how(I)_fw	GCGTAACCAAAAGTCAGAT
DM220_how(I)_rv_T7	TAATACGACTCACTATAGGAATGCTTGCTGCTATTATC
DM241_Sv40_fw	ATAATCAGCCATACCACAT
DM242_Sv40_T7_rv	TAATACGACTCACTATAGGATGAGTTTGGACAAACCAC
DM243_HspA_fw	TCAATTCTATTCAAACAAGTAAAG

Name	Sequence
DM244_HspA_T7_rv	TAATACGACTCACTATAGTGTGTGTGAGTTCTTCTTC
DM337_w7500D	GTCCGCCTTCAGTTGCACTT
DM338_w11678U	TCATCGCAGATCAGAAGCGG

2.2.7.4 Vector maps

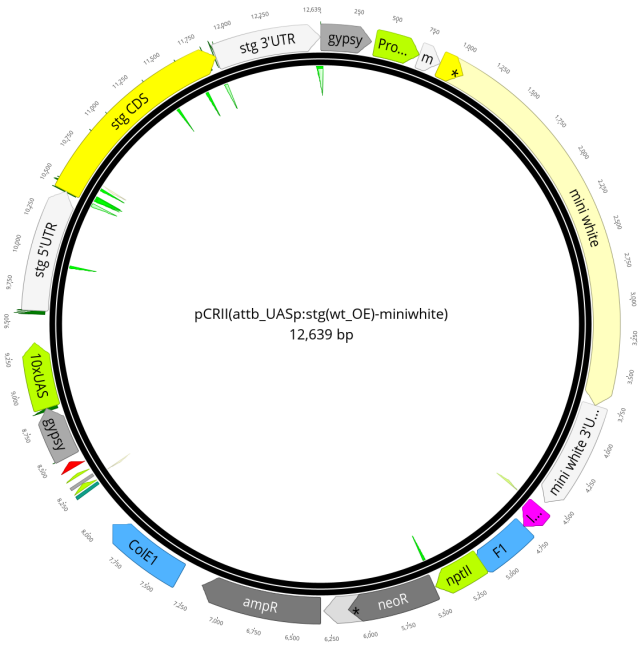

Figure 2.53 Vector map of *pCRII(10xUAS:5'stgUTR-stgCDS-3'stgUTR/bHSP:mini white)*. This plasmid was used to insert the displayed transgene into the 51C1 locus. *UAS* driven transgene is insulated with two gypsy elements positioned up- and downstream of the transgene. As marker mini white is expressed under the control of basal promotor leading to stable expression of the wild type white gene rescuing the white phenotype resulting in red eye colour. Ampicillin resistance is used to identify positive transformed clones.

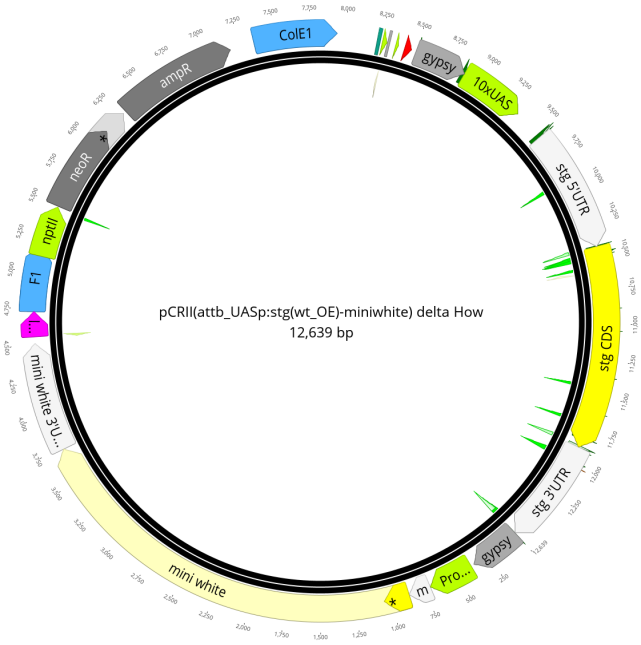

Figure 2.54 Vector map of *pCRII(10xUAS:5'stgUTR-stgCDS-3'stgUTRΔHow/bHSP:miniwhite)* This plasmid was used to insert the displayed transgene into the 51C1 locus. UAS driven transgene is insulated with two gypsy elements positioned up- and downstream of the transgene. As marker mini white is expressed under the control of basal promotor leading to stable expression of the wild type white gene rescuing the white phenotype resulting in red eye colour. Ampicillin resistance is used to identify positive transformed clones.

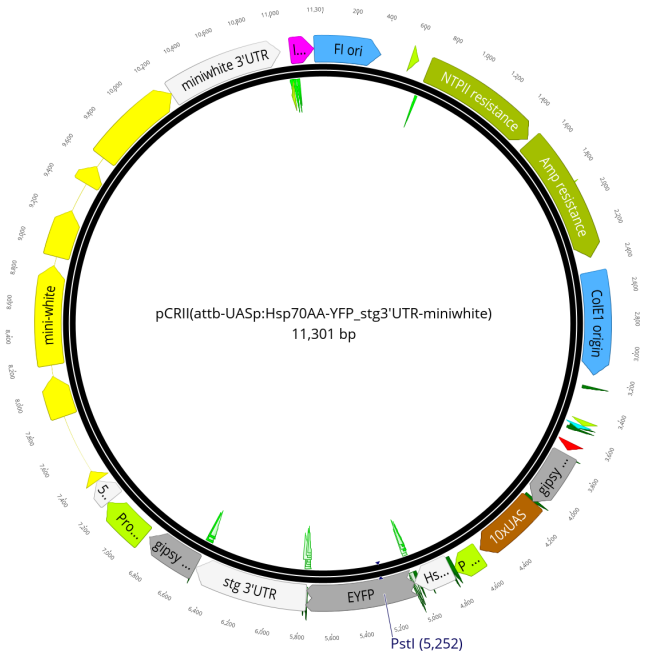

Figure 2.55 Vector map of *pCRII(10xUAS:5'HspA-eYFP-3'stgUTR/bHSP:miniwhite)*. This plasmid was used to insert the displayed transgene into the 51C1 locus. *UAS* driven transgene is insulated with two gypsy elements positioned up- and downstream of the transgene. As marker mini white is expressed under the control of basal promotor leading to stable expression of the wild type white gene rescuing the white phenotype resulting in red eye colour. Ampicillin resistance is used to identify positive transformed clones.

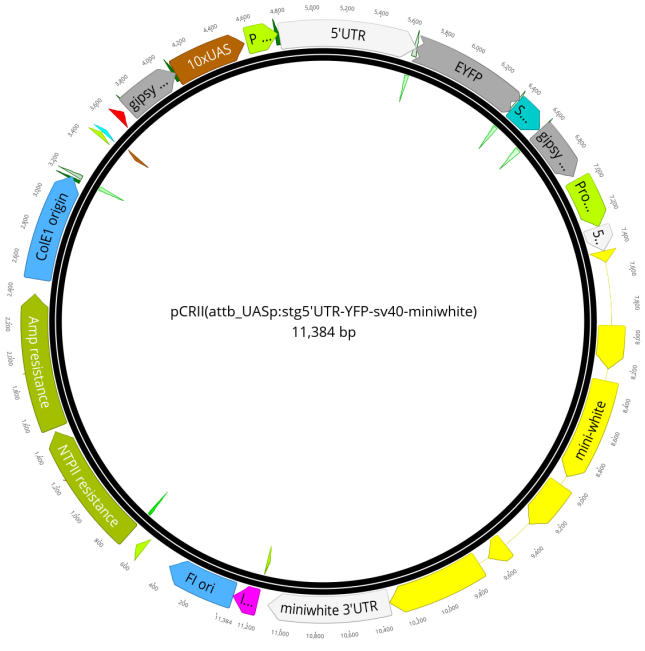

Figure 2.56 Vector map of *pCRII(10xUAS:5'stgUTR -eYFP-Sv40/bHSP:miniwhite)*. This plasmid was used to insert the displayed transgene into the 51C1 locus. *UAS* driven transgene is insulated with two gypsy elements positioned up- and downstream of the transgene. As marker mini white is expressed under the control of basal promotor leading to stable expression of the wild type white gene rescuing the white phenotype resulting in red eye colour. Ampicillin resistance is used to identify positive transformed clones.

Figure 2.57 Vector map of *pCRII(10xUAS:5'stgUTR-stgCDS-Sv40/bHSP:miniwhite)*. This plasmid was used to insert the displayed transgene into the 86F6 and 51C1 locus. *UAS* driven transgene is insulated with two gypsy elements positioned up- and downstream of the transgene. As marker mini white is expressed under the control of basal promotor leading to stable expression of the wild type white gene rescuing the white phenotype resulting in red eye colour. Ampicillin resistance is used to identify positive transformed clones.

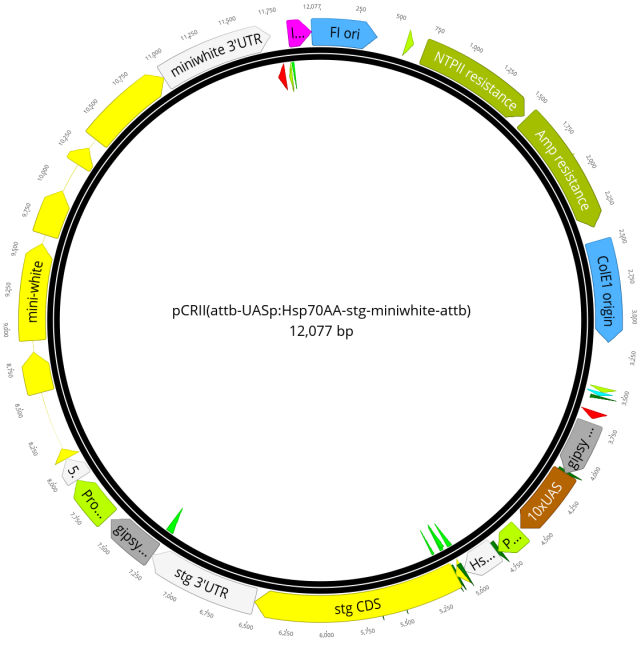

Figure 2.58 Vector map of *pCRII(10xUAS:5'HspA-stgCDS-3'stgUTR/bHSP:miniwhite)*. This plasmid was used to insert the displayed transgene into the 86F6 and 51C1 locus. *UAS* driven transgene is insulated with two gypsy elements positioned up- and downstream of the transgene. As marker mini white is expressed under the control of basal promotor leading to stable expression of the wild type white gene rescuing the white phenotype resulting in red eye colour. Ampicillin resistance is used to identify positive transformed clones.

3 Discussion

Chromatin assembly and epigenetic inheritance of histone modifications during replication requires an orchestrated redistribution and formation of post-replicative nucleosome with parental and newly synthesized histones. In recent years, new techniques and approaches contributed largely to the understanding how chromatin is assembled, yet it is not well understood whether parental histones harbour a positional memory during DNA replication *in vivo.* Studying nascent chromatin in the vicinity of the replication fork requires tight staging and synchronization of cells which has restricted studies to cell culture or *in vitro* systems (*12*).

In my Dissertation, I made use of a *Drosophila melanogaster* mutant to address the question of epigenetic inheritance and chromatin formation in a developing embryo that lacks the genes for all canonical histones. This approach is possible due to the fact that in *Drosophila* all replicative histones are arranged in a single gene cluster (*184*). Together with the highly stereotypic and predictable early embryonic development driven by maternally derived factors, it is possible to target S phases in which nucleosome assembly post replication relies exclusively on parental histones. Hence, I have overcome previously mentioned limitations to contribute new information of how epigenetic information is passed on during replication *in vivo* and in the context of a developing organism. I have defined four timeframes, 3.5-4h, 4.5-5h, 5.5-6h, and 6.5-7h AEL, covering the assembly of chromatin during DNA replication in S_{15}, the developmental stage after maternal to zygotic transition during which histone depletion first comes into effect.

My project is divided into two main parts outlined in the chapters I and II. Chapter I represents the major part of work and results acquired of this project, addressing issues related to chromatin assembly, inheritance of epigenetic information as well as alterations to the transcriptional profile and related rationales. I combined several next generation techniques to describe phenotypic changes regarding nucleosome occupancy, spacing as well as positioning of histones decorated with post translational modifications in histone depleted mutants to set the base for future experiments. Chapter II describes early and minor results of the project. They focused on direct effects which the lack of histone expression poses on cell cycle progression, and I explored in this context how $String^{Cdc25}$ activity is downregulated to cause the cell cycle arrest during the $G2/M_{15}$ transition. Although these results are still preliminary, they narrowed down the regulatory events that control String activity, supporting the hypothesis that the RNA binding regulator How(L) targets *string* mRNA within its 3'UTR and causes destabilization of the mRNA, eventually leading to its degradation.

3.1 Positional memory of parental histones in the absence of *de novo* histone supply

Chapter I describes the analysis of chromatin accessibility in *His^C* mutants by ATAC-seq (*201*). It reveals that parental histones are not sufficient to re-establish the chromatin landscape in the absence of *de novo* histone synthesis. Principle component analysis (PCA analysis) (*238*) demonstrates the global impact of histone depletion by separating *His^C* mutant and wild types along PC1 with a variance of 68%. Intriguingly, wild type embryos are separated by PC2 with a variance of 11% based on their developmental age. *His^C* mutant embryos, however, show less variance and separation according to the developmental age is reduced, yet the data obtained at the different time points still cluster together. This finding is in contrast to the PCA analysis of the RNA-seq data gathered at the same time points. Here, wild type and *His^C* mutant embryos are similarly separated by PC1. However, in this case PC2 discriminates both, *His^C* and wild type embryos with respect to their respective developmental age. This result implies that although chromatin accessibility is highly different in the *His^C* mutants, their developmental programs are still maintained. Interestingly, differences in expression profiles are smaller during the early stages and increase over developmental time as indicated by a larger variance, suggesting that the developmental program is slowing down. That *His^C* mutants maintain partially developmental programs and the corresponding chromatin rearrangements might also be reflected by the fragment size distribution of the individual samples. Wild type samples show the typical enrichment for nucleosome free DNA fragments (<120bp) and the periodically repeating enrichment for nucleosomal fragments, i.e., multiples of 147 plus linker DNA, the *His^C* mutants show a reduced median fragment size and a loss in relative enrichment of nucleosomal fragments. However, in early mutant embryos, the span of nucleosome free fragments is broadened and extends to roughly 140 bp. This observation is consistent with an increase of median inter dyad distances in *His^C* mutants at promotors and regulatory elements. Additionally, nucleosome occupancy is reduced in *His^C* mutants, showing that parental histones are still deposited onto nascent DNA. First, chromatin accessibility analysis relies on transposase (Tn5) digestion of chromatin, which in principle is a stochastic process during which DNA is randomly cleaved rather than at specific sequence recognition sites. Decreasing the ratio between nucleosome and DNA after replication increases therefore the variance in fragment sizes corresponding to nucleosome free regions, which are caused by impaired barrier formation by nucleosomes in the *His^C* mutants. Secondly, in principle it would be imaginable to assign a fragment to the mono- or di nucleosomes although *in vivo* it was nucleosome free. However, control experiments involving the digestion of naked gDNA showed that this effect is dependent on incubation times (*239*), and thus, I adjusted the experiments accordingly.

Assuming that most parental histones are recycled, reduced abundance of free histones results in higher recycling rates (*54*) and both daughter strand would receive equal amounts of parental histones (*65, 70, 71, 73*), it is possible that either (i) individual loci which were occupied before replication are behind the replication fork only engaged on one daughter strand, (ii) that nucleosomes are equally distributed but shift around their original location or (iii) that parental histones are randomly distributed, resulting in unequal dispersal. My data suggests together with earlier published data (*54, 70*) that without histone *de novo* supply, parental histones are deposited in close proximity to their original position. This explains that not only nucleosome occupancy at dyad centres is reduced but also the dyad distances are increased in promotor regions and in putative regulatory elements. Reduced enrichment of nucleosomal fragments in *His^C* mutant samples might also be explained by the formation of hexa- or hemisomes which, together with increased inter dyad distances, create more possible combinations for fragment proportions. Aligning fragment midpoints to dyad centres reveals that in *His^C* mutants, fragments are roughly 30 bp smaller, providing further support for the sub-nucleosome formation hypothesis. The results are also consistent with the proposal, that without *de novo* histone synthesis, nucleosomes are formed at lower frequency when only parental histones are available. This proposal is consistent with earlier findings showing that histone recycling is the predominant process during DNA replication in a histone depleted scenario as shown with *Xenopus* egg extracts (*54*). Whether histone depletion in *His^C* mutants leads to a strand-biased incorporation of parental histones as shown for several MCM and Pol ε subunit mutants (*49, 65, 83*), cannot be resolved with the results obtained here with *His^C* mutants.

Hence, longer linker DNA accounts for extended nucleosome spacing and thus higher chromatin accessibility and increased variance in nucleosome free fragment sizes. Interestingly, over developmental time *His^C* mutants and wild types undergo the same proportional changes in fragment size distribution indicated by a reduction of nucleosomal fragments, this suggests that chromatin still undergoes remodelling by repositioning the remaining nucleosomes. This conclusion would be consistent with PCA results of RNA-seq and ATAC-seq data, showing that mutants still follow the developmental program, at least to some extent. Several studies have shown that chromatin remodelers are responsible to set regular arrays of nucleosomes with set linker length (*33*). The increase in inter dyad distances at promotor regions is therefore consistent with earlier findings that the linker length is directly proportional to the available amount of free histone proteins (*37, 39*). Recent studies indicated that chromatin remodelers also act in a nucleosome density-independent way by showing that nucleosome positioning of -1 and +1 nucleosomes with regard to a barrier site in salt gradient dialysis (SGD) chromatin becomes independent from nucleosome density

(*33*). Although this was shown in an *in vitro* system, a similar effect might be responsible for the reduction of nucleosomal fragments in later stages of *His*^{C} mutant and wild type embryos.

Analysis of ATAC-seq coverage tracks showed uniform enrichment of peaks reflecting nucleosome depleted regions throughout the genome with only low enrichment in *His*^{C} mutans at positions of peak sites in wild type. This finding can partially be explained by the increased amount of sub-nucleosomal fragments resulting from the histone dilution effect. Similar loss of nucleosomal fragments and a uniformed coverage, respectively, were observed in naked DNA control digests (*239*). On the other hand, similar patterns were also observed in nascent chromatin which is not susceptible for Tn5 digestion right after replication (*51, 70*). However, in the latter case, chromatin accessibility was restored after transcription (*118*), which was not the case in *His*^{C} mutants. Conversely, increased chromatin accessibility of nascent chromatin would facilitate general transcription factor accessibility and drive nonspecific transcription as observed in *His*^{C} mutants. Transcription is usually initiated by formation of the preinitiation complex at the TSSs consisting of general transcription factors and chromatin remodelers (*118*) as well as subsequent binding of RNAPII stalled at the +1 nucleosome that represents a barrier (*93*). Nucleosomal coverage in *His*^{C} mutants revealed that -1 and +1 nucleosomes are well positioned, however +2 and +3 nucleosome are shifted. This finding is consistent with previous studies showing that phasing of a nucleosomal array is independent of nucleosome abundance and relies on ruler elements within chromatin remodelers. Spacing of downstream nucleosome, however, exhibited increased linker distances in smaller nucleosome to DNA ratios (*33*), similar to what is observed in *His*^{C} mutants. Responsible remodelers acting independently of nucleosome density, Chd1 and ISWI, show a weaker upregulation of expression in *His*^{C} mutants than in wild type according to the RNA-seq data presented (Figure 5.1). This observation contrasts with density dependent remodelers like INO80, which are downregulated in *His*^{C} mutants at the two early timepoints of the measurements and are only upregulated at 5.5-6h AEL (Figure 5.1). Additionally, we observe a gain in signal between the +2, +3 and +4 nucleosomes particularly in highly expressed genes which is either caused by remodelers failing to establish a regular spaced array *in vivo,* or due to the number of necessary remodelling events in histone depleted post-replication genome. Such a scenario would be consistent with the expression profile observed in *His*^{C} mutants and the fact that the additional signal diminishes during later developmental timepoints for the highly expressed genes. Hypothesizing that decreased nucleosome occupancy facilitates nucleosome shifting, previous studies, which are not supported by our analysis, described a 3' to 5' shift upon RNAPII passage (*125*) where +2 and +3 nucleosomes are shifted towards 3' on a global level. Yet, it needs to be mentioned that my data provided did not allow to discriminate between nascent, parental, or matured post replication chromatin.

Other chromatin regions that undergo drastic changes in accessibility during chromatin maturation are at the origins of replication. Although highly accessible already exist in the G1 phase, they become drastically more occupied with nucleosomes post replication (*112, 129, 130*). Interestingly, looking at dyad distances at putative origins of replication (ORC) sites mapped in *Drosophila* S2 cells (*240*), my results revealed that in wild type dyad distances is highly consistent at ORC and downstream DNA regions, although at this point of development the cell cycle does not have a G1 phase. *His*^{C} mutants, however, show higher dyad distances close to putative ORCs than in far-off DNA regions (Figure 5.2), this could either be caused by (i) mutants running out of parental histones dependent on the distance to the ORC, or (ii) chromatin maturation at ORCs post replication is insufficient as *His*^{C} mutants fail to pass G2/M$_{15}$ arrest resulting in a higher delta in occupancy between ORCs and far-off regions. In conclusion, parental histones are not sufficient to re-establish the nucleosomal landscape, i.e., the characteristic nucleosomal landscape is only partially re-established and causes chromatin to be more accessible after S$_{15}$ in *His*^{C} mutants.

Chromatin accessibility positively correlates with transcriptional activity. As described before, nucleosomes compete with transcription factors at regulatory binding sites post replication (*51*) and the transcriptional apparatus is also at least partly involved in chromatin maturation as shown in mouse ESC (*118*). Hence, I asked whether the observed increase in chromatin accessibility is reflected by the transcriptional profiles of *His*^{C} mutants. In comparison to the ATAC-seq data, the discrimination of developmental age in *His*^{C} mutants is more prominent in RNA-seq. Interestingly, the variance between *His*^{C} mutants and wild type embryos is comparably small at 3.5-4h AEL and increases strongly over time resulting in a molecular phenotype that was not observed with the ATAC-seq analysis where the difference between *His*^{C} mutants and wild type with respect to PC1 reached near maximum values already at 3.5-4h AEL. An increasing phenotypic penetrance is also reflected by the number of differentially expressed genes (DEG) which in case of upregulated genes increases over time from 1,042 genes to 2,944 genes at 6.5-7h AEL. Together, these results suggest that while phenotypes regarding chromatin architectures arise directly after replication and thereupon do not change much over time, the resulting consequences on transcriptional level accumulate during the same time window. Of course, there might be several underlying effects that can contribute to this result. Firstly, *His*^{C} mutants might lose generally the control over transcriptional regulation. Secondly, the maintenance of gene silencing in *His*^{C} mutants might fail over developmental time. Misexpression of some genes might not be high enough to cross DEG thresholds in the early mutant embryos but at a later stage. Finally, misexpression might start molecular pathways which cause the expression of the corresponding downstream target genes that are not directly affected by an altered chromatin assembly in the *His*^{C} mutants. For example, *His*^{C} mutant embryos upregulate

partially meiotic pathways of the testis-specific meiotic arrest complex (tMAC). Hence, the upregulation of meiotic genes is rather an indirect effect than intentional response of the cell cycle arrest or the lack of histones.

The sheer number of upregulated genes poses in general insurmountable difficulties when trying to identify a putative regulator or a molecular pathway in an unbiased approach. Many of the genes with the highest fold change of expression in *His^{C}* mutants were not necessarily strongly expressed in absolute terms, but they were transcriptionally silent in wild type embryos. This finding raised the question whether decreased nucleosome occupancy resulted in a failure of chromatin silencing. To address this question, differentially upregulated genes were categorized in quartiles (q1-q4) according to the expression levels, where q1 contains the weakly expressed genes and q4 the highly expressed ones, and an additional category q0 which contained all genes that had no reads in wild type. Most upregulated genes belong to the moderately and weakly expressed genes. In contrast genes that are highly expressed in wild type are not additionally upregulated in the mutant embryos. The fraction of genes that belong to q0 and q1 increased during development, whereas the number of genes belonging to q2 and q3 categories was highest at the earlier timepoints. Nevertheless, even at 6.5-7h AEL only ~20% belong to the wild type q0 category. This suggests that in cells of embryos which lack *de novo* histone synthesis, the chromatin architecture is altered to an extend that does not fully maintain transcriptionally silencing of chromatin. Since *His^{C}* mutants continue to develop up to a later embryonic stage and thus continue with the developmental program beyond M_{15}, more and more silent regions might be remodelled and made accessible, explaining to a certain extent why the fraction of q0 genes increases over time. This explanation is also consistent with the observation that q4 genes are not upregulated any further since an already accessible and highly transcribed locus might not become more accessible to gene activation and the level of transcription.

Key to the regulation of transcription are enhancers which organize gene expression patterns in a spatiotemporal way. Poised enhancers are thought to bookmark developmental genes and situational genes necessary to react to environmental ques and feature high levels of H3K27me3 and H3K4me1 and are generally highly accessible (*122*). Although such enhancers were first identified in ESCs, and their role *in vivo* is still poorly understood, recent studies revealed that chromatin and the 3D structure of poised enhancers are conserved in pluripotent cells also *in vivo* (241). It was shown that 46% of enhancer candidates mapped in 13.5% of the *Drosophila* genome are active during early embryogenesis, suggesting that there are between 50,000 and 100,000 developmental enhancers within the entire genome (*242*). Hypothesizing that a subset of those enhancers which in wild types are situated in Polycomb repressed chromatin achieve accessibility in response to the lack of *de novo*

histone synthesis and thereby mimic poised enhancers and initiate transcription, such a situation could provide an additional explanation for the increase of q0 genes in *His*^{C} mutant embryos. Furthermore, loss of nucleosome density might make pioneer factors obsolete for opening compacted chromatin and thereby facilitating ectopic binding of general transcription factors. Also, transvection is especially prevalent in *Drosophila* (243) caused by autosomal chromosome pairing during the interphase. Such a scenario could provide another error prone level of transcriptional control in *His*^{C} mutants. Finally, enhancers also affect how long a given promotor stays active as well as the rate of polymerase initiation (*244*). These properties of enhancers provide an explanation for upregulation of genes in particular q1 and q2 category.

As mentioned above, poised enhancers are believed to control developmental genes. Therefore, I subsequently performed a gene ontology (GO) analysis of the main upregulated genes. As described, I found mainly terms that describe common developmental processes like cell migration or imaginal disc morphogenesis, which does not contradict the hypothesis of ectopic activation or mimicking poised enhancers. In contrast to mammalian species, most enhancers in *Drosophila* act on nearby genes (*243*). However, there are still many enhancers which bridge considerable genomic distances to interact with their target promotor driving transcription in *Drosophila* (*245*). Genes and regulatory elements that interact with each other by DNA looping are usually organized in a topological associating domain (TAD) which is a self-interacting genomic region contributing to the three-dimensional genome architecture. Genes within a given TAD interact more frequently with each other than with genes outside of the TAD boundaries (*246*). Boundaries of TADs are established by CTCF and cohesin binding sites, a feature that is well conserved among species and cell types (*246*), and represents the sum of TADs. Moreover, histone H1 densities supposedly play a crucial role in TAD boundary formation. In H1 depleted CD8+ T cells, TADs persisted. However, they became unstable, experienced decompaction and underwent compartment shifting in which TADs of an A-compartment spread into a neighbouring B-compartment (*247*). A-compartment representing active chromatin domains whereas B-compartments repressed and transcriptionally silent chromatin regions (*248*).

The formation of the higher order chromatin structure and three-dimensional genome organization is also strongly supported by compaction due to the linker histone H1 (*5, 41, 249*). However, it is not yet understood how parental H1 histones are inherited to the daughter DNA strands during replication. Insights from HeLa cells suggest that histone H1 is deposited in a replication-independent manner (*249*). The genome of *Drosophila melanogaster* contains only one canonical variant of histone H1 (*191*). The CUT&Tag data presented here revealed that the enrichment around dyad centres, corresponding to the

three contact points of H1 with nucleosomal DNA (*6*), is similar in *His^C* mutants and in wild type embryos. However, total enrichment levels are slightly lower in the mutants and the slope of the enrichment is less steep. This suggests, that although the total amount of H1 is reduced, the remaining parental H1 histones are appropriately deposited to the core nucleosomes. This suggestion is further supported by H1 coverage tracks. They show that H1 exhibits equal spatial distribution in *His^C* mutants as compared to wild type, although with reduced levels. Notable, however, the temporal resolution of my analysis is not sufficient to resolve whether H1 is deposited during or immediately after replication. Intriguingly, the findings of increased transcriptional activity in view of a correct H1 placement at core nucleosomes, although at reduced levels, is consistent with the observation that *Drosophila* embryos of the same developmental stage revealed an anticorrelation of H1 occupancy and transcriptional activity. Additionally, H1 levels increased towards the 3' end of genes and with reduced transcription (*41*). Furthermore, it was shown that increased H1 occupancy reduces nucleosome mobility (*250*) and, conversely, reduced H1 enrichment levels may account at least in part, for the observed nucleosomal shift at TSSs and the increased intervals in nucleosome spacing. Nucleosomes shifting by asymmetric H1 placement during early embryonic *Drosophila* development was found to control gene expression profiles (*41*), providing an explanation for the upregulation of transcription observed in *His^C* mutants.

Nucleosome occupancy was shown to harbour transcriptional control of tightly regulated genes. In contrast to for example housekeeping genes, the promotors of which are typically deprived of nucleosomes, the tightly regulated genes naturally exhibit high nucleosome occupancy at promotors. During transcriptional initiation, RNAPII competes with these nucleosomes which are thought to prevent the formation of repressive chromatin and to favour upcoming gene expression (*251*). Occupancy at promotor regions positively correlates with pausing of RNAPII, which depends on specific transcription factors which recruit chromatin remodelers to form the preinitiation complex. Subsequently, the DNA is unwound and RNAPII is released from the promotor (*252*). Maturation of paused RNAPII proximal to the promotor additionally requires the activity of the positively acting transcription elongation factor b (P-TEFb) to start elongation and also to phosphorylate the CTD of RNAPII at its second serin residue (RNAPIIS2P) (*133, 252*). Moreover, TEFb was shown to associate with several chromatin remodelers and chromatin-bound proteins to form a 'super elongation complex' to further stimulate transcription (*252*). Together with the before mentioned considerations that H1 placement contributes to transcriptional regulation, the chromatin architecture provides multi-tiered means of transcriptional control that can potentially be subject to mis-regulation in *His^C* mutants at several different levels.

Several studies on mammalian cell culture during the late 1970s and the early 1980s indicated that transcription initiation did not obligatorily lead to the production of a full-length transcript (*251–253*). To address the question whether there are differences between wild type and *His^{C}* mutant embryos with respect to RNAPII recruitment at promotor regions due to the reduced nucleosome occupancy causing altered spacing of +2 and +3 nucleosomes, I performed CUT&Tag analysis of RNAPIIS2P, a CTD phosphorylation mark that is known to increase over the gene body as RNAPII proceeds with transcriptional elongation towards the transcriptional end site. A strong enrichment of RNAPIIS2P at the transcription start sites (TSSs) was observed which diminishes immediately thereafter, it then increased again over the gene body and was finally strongly reduced at the transcription end site in wild type embryos. *His^{C}* mutants, however, showed a similar pattern of the gene body but the sharp increase at the TSS was missing. As before mentioned, S2 of the CTD becomes increasingly enriched over the gene body, which is also found with the experiments described in this report. It has to be noted that the RNAPIIS2P data also partly reflects total RNAPII levels at TSSs which explains the dominant peak at TSS typical for pan RNAPII patterns. Conversely, *His^{C}* mutant embryos show an enrichment in the gene body without a major enrichment at the TSS. Taken together these findings suggest that RNAPII pausing fails and results in a premature release from the TSS. A similar pattern to the one observed in *His^{C}* mutants, although not as prominent, was also described for non-paused but expressed genes, such as housekeeping or ubiquitously expressed genes which are not subject to an extremely tight regulation and also feature less dense nucleosome occupancies at promotor regions (*252*). Depending on the publication, 60% to 70% of all genes, if not all protein coding genes (*93, 254, 255*), which are expressed in *Drosophila* S2 cells exhibit promotor proximal pausing. One might therefore speculate that the premature release of RNAPII in *His^{C}* mutants is a similar process as observed in wild type embryos, but at much lower frequencies, and that it could be caused by ectopic effects including the reduced nucleosome density (*252, 253, 256*). It has to be noted that RNAPII pausing is not observed in yeast and *Caenorhabditis elegans.* This difference has been attributed to the absence of the negative elongation factor (NELF) (*256*). NELF was shown to be sufficient but not necessary for RNAPII, yet ~82% of NELF association exhibit RNAPII pausing in S2 cells (*257*). Moreover, interdependencies and colocalizations of NELF, TFIID and GAGA factor have been described (*257*). They are also known to interact with the chromatin assembly factor FACT and with chromatin remodelers (*251, 257*). Other studies implicated that the reduced formation of the nuclear exon junction complex (pre-EJC) causes a premature release of RNAPII, exon skipping, alternative splicing and might also rely on chromatin composition at the TSS (*258*). Henceforth, impaired chromatin around the TSSs in *His^{C}* mutants might therefore not only trigger ectopic binding of general transcription factors driving transcription but might also provide insufficiently the

scaffold compulsory to accurately form the transcription bubble which controls transcript elongation.

To further analyse transcriptional elongation, I analysed deposition levels of the transcription coupled histone post translational modification mark H3K36me3 at 4.5-5h and 5.5-6h AEL. Enrichment levels of H3K36me3 are positively correlated with RNAPIIS2P enrichment which increases over the gene body, as previously mentioned. This correlation is caused by the interdependencies, resulting from dSET2 recruitment to in position S2 phosphorylated RNAPII CTDs, which is then responsible for the bulk deposition of trimethylations of K36 on histone H3. Similar to RNAPIIS2P, a promotor proximal peak was observed, a shallow plateau right after the TSS followed by increasing enrichment over the gene body in 5' to 3' direction in transcription level dependent manner in wild types. In His^{C} mutants neither the promotor proximal peak nor the plateau was present and a sharp increase in methylation levels instead followed by the typical enrichment over the gene bodies could be observed. I propose that transcriptional elongation might be not similarly affected since transcriptional initiation as the "enrichment pattern" in the gene bodies was similar yet at reduced levels which might be caused by the generally reduced nucleosome occupancy.

Unfortunately, a distinction between cause and effect is difficult, studies have shown for examples that loss of H3K36me3 at promotor regions leads to more accessible chromatin which in turn exposes cryptic enhancers and promotors (*259*). Therefore, I wondered if loss of H3K36me3 in general promotes transcription and therefore partially accounts for the upregulation of gene expression by enhancing chromatin accessibility. At least at promotor regions, the loss of H3K36me3 is due to impaired RNAPII recruitment and reduced nucleosome occupancy rather than the other way round. This argument does not imply that the expression of cryptic transcripts from cryptic promotors might still be prevalent.

Histone H1 is essential for nucleosome positioning and compaction, resulting in drastic changes in chromatin composition upon H1 depletion. Recent studies have shown that the loss of H1 loss disrupts the three-dimensional architecture of chromatin and causes a global decompaction. This effect is accompanied by decreasing levels of H3K27me3 but a gain in H3K36me2 enrichment in mouse ESCs (*10*) which drives the expression of early developmental genes. Methylation resulting in these H3 PTMs group is deposited by the same methyltransferase as H3K36me3 of *Drosophila in vivo.* Moreover, histone H1 densities seem to control local compactions of chromatin and thereby control also active and repressive chromatin domains. Depletion of H1 in a conditional triple H1 knockdown in $CD8^{+}$ mouse T-cells showed that repressed B-compartments, as characterized by chromosome confirmation capture (Hi-C), suffer from a drastic decompaction (*247*). Consistently, the observed decompaction positively correlated with H1 density before the H1 knockdown was

applied. On large scale, H1 seems to play a crucial role in establishment of A to B-compartment borders, which follows from observed shift in compartments. Decreased compaction was accompanied by decreased levels of H3K27me3 and increased levels of H3K36me3 (*247*). This result is consistent with findings previously shown for mouse ESCs (*10*). Thus, H1 is suggested to act *via* the Polycomb repressive complex 2 (PRC2) (*10, 260, 261*) serving as a regulator that balances the H3K27me3 and H3K36me3 relation to establish functional A and B-compartments.

Spurious transcription in *His^C* mutants was analysed by STRIPE-seq (Survey of Transcription Initiation at Promoter Elements with high-throughput sequencing) (*194*) comparing wild type and *His^C* embryos at 5.5-6h and 6.5-7h AEL. The objective was to specifically identify 5' capped RNAs and thus, to map transcription start regions (TSRs) by sequencing the bases adjacent to the 5'cap. TSR read counts in promotor regions positively correlated with transcriptional activity in wild type. In *His^C* mutants, the largest fraction of annotated TSRs still fall into promotor regions but the proportion is clearly smaller (≥75% in wild type *versus* ≥55% in *His^C* mutants). Moreover, the fraction of TSRs mapped outside of promoters like in introns and intergenic regions, is increased in *His^C* mutants. Additionally, coverage tracks reveal a positive correlation of STRIPE-seq counts with RNA-seq reads in intergenic regions. TSR density when centred on annotated TSS positions was also reduced in *His^C* mutants. Intergenic transcriptional initiation was previously reported in histone H1 depleted *Drosophila* embryos, with a high preference upstream of TSS sites (*41*). In highly expressed genes there was also a skew in enrichment patterns with higher occupancy at nucleosome exit sites, and the H1 skew correlated with transcriptional orientation in 5' to 3' direction (*41*). I also analysed RNA-seq counts in regions, which were 1kb upstream of differential TSRs in *His^C* mutants and found a significant increase, which might be due to the proximity of genes in *Drosophila*. Thus, I conclude that reduced nucleosome occupancy and increased dyad distances results in spurious transcription with initiation within gene bodies and intergenic regions. It would be interesting to analyse whether transcriptional orientation is still maintained or if the H1 occupancy levels can be correlated to differentially annotated TSRs.

In recent years, numerous studies have improved the understanding of how parental histones are inherited to the daughter cells post replication. Several functional domains within the replication bubble were identified which overcome strand bias and the replication imminent differences between leading and lagging strands that result from the orientation-dependent DNA polymerase (see *48, 71* for reviews). Moreover, recent studies also highlighted the probabilities for an individual nucleosome that is confronted by the replication fork to be recycled, evicted or shifted (*54*). In this context, segregation modes were also investigated to determine whether histones in active or repressive chromatin domains segregate

differently (*70, 72, 73, 113*). Together, these studies resulted in a currently valid consensus model, suggesting that parental histones are first evicted or recycled, depending on the number of free histones and that parental and newly synthesized histones are quickly incorporated into nascent DNA. PTMs are inherited alongside the parental histones. Regarding the inheritance of PTMs, some studies suggested that histones in repressive and active chromatin preserve their genomic location (*64, 70, 113*), whereas others argued that a positional memory is only prevalent in nucleosomes originating from repressive domains (*72, 73, 89*). Most studies, however relied on cell cultures results, *in vitro* techniques or cell extracts due to the temporal and spatial hindrances that needed to be overcome to answer such questions.

I planned to contribute insight into how parental histones decorated with post translational modifications are inherited not only in histone depleted models, but in a developing organism. Therefore, I performed a CUT&Tag analysis for H3K4me3, H3K27ac and H3K27me3 with embryos at 3.5-4h, 4.5-5h, and/or 5.5-6h AEL. Both, H3K4me3 and H3K27ac are marks of active transcription. H3K4me3 is deposited by dSET1 which recruited by RNAPIIS5P and therefore enriched at TSSs. At each time point examined, a bimodal enrichment of H3K4me3 at TSS positively correlates with transcriptional activity in wild type embryos. *His^{C}* mutants, on the other hand, showed a similar enrichment pattern but with broader enrichment in the gene bodies. Locally, enrichment revealed that peaks are mostly called at the same sites with reduced enrichment levels, Venn diagrams of peak quantifications indicate that most H3K4me3 peaks are common between wild types and the mutant at each developmental time point examined, and that only a small subset of peaks is unique for the respective genotype.

H3K27ac exhibit a strong bimodal enrichment spanning the transcriptional start site at transcription dependent levels. This finding is consistent at both timepoints analysed. In contrast to H3K4me3 in wild type embryos, the enrichment of H3K27ac in gene bodies is gradually reduced towards the 3' end of genes. Moreover, the peak enrichments upstream of the TSS exhibit similar enrichment levels as downstream of the TSS and they are much stronger as compared to H3K4me3. In contrast, *His^{C}* mutants show an overall strong reduction of H3K27ac levels, and the enrichment pattern observed at TSSs of wild type is clearly more affected than for H3K4me3, exhibiting also a subset of ectopic enrichment sites visible in the coverage tracks. These enrichment domains appear to be also broader than in wild types. Although the dependency on transcriptional activity is retained, the bimodal enrichment is lost. The upstream peak is also strongly reduced, whereas a stronger enrichment is found behind the TSS which, however, does not exhibit a peak enrichment.

The repressive marks like H3K27me3 are associated with inactive chromatin. Both marks exhibit similar patterns in wild type and *His*^{C} mutants as observed with H3K4me3. Both modifications anticorrelate with transcriptional activity. Noteworthy, total enrichment levels are very similar in *His*^{C} mutants, in contrast to the marks of active chromatin in *His*^{C} mutants. Coverage tracks for H3K27me3 show that there is a large fraction of peaks common to both wild type and *His*^{C} mutants with similar enrichment levels. Among the common locations there is also a smaller number of peaks that is more enriched in *His*^{C} mutants than in wild types and the other way around.

The results suggest that for the active mark H3K4me3 either one or a combination of effects might account for the reduced coverage and broadening of the H3K4me3 domains in the *His*^{C} mutants. First, most peaks are found prior to and after replication at the same loci or at least in their close vicinity, indicating that the majority of parental histones are kept at least near their original location after the newly formed nucleosomes are established. Secondly, the extension of H3K4me3 domains into gene bodies could be either an indirect effect caused by the increase in spacing between dyads or due to a random transcription initiation within gene bodies that were observed with STRIPE-seq. Of note, my experimental approach cannot discriminate between parental modifications and the newly established ones. Hence, one cannot exclude a dilutional effect and/or a shifting of active PTM carrying histones as was observed and suggested earlier (*72*). The results presented here also point in this direction but do not demonstrate it with certainty. Thirdly, the strong decrease of H3K4me3 reads at TSSs may be caused by a premature release of RNAPII, resulting in reduced opportunities for the dSET1 recruitment to TSSs. Finally, the overall strong reduction of active PTM marks on histones may reflect an impaired chromatin maturation process. In general, stronger signals were observed for active marks than for repressive in wild type embryos. This observation could indicate that the remaining parental histones are sufficient to re-establish the modification landscape, but not at comparable levels as observed in wild type. However, enrichment levels are stronger reduced in mutants than nucleosome occupancy in promotor regions on a genome wide scale, suggesting that there are additional mechanisms in mutants which are responsible for the effects reported here.

Acetylation of histones tails mostly facilitates a de-wrapping of compacted chromatin. H3K27ac is established by the histone acetyl transferase (HAT) p300, for which numerous recruitment mechanisms have been described (*158, 262*). Some of its domains such as KIX, TAZ1, TAZ2 and IBiD, interact with the evolutionarily conserved transcription factor p53 (*262*), which is required for adaptive responses to genotoxic stress, and also with the CREB transcription factor. Additionally, interactions of p300 with general transcription factors and the transcriptional machinery have been documented. Hence, the broad dispersal of

H3K27ac in *His^C* mutants may likewise be explained by an impaired formation of the transcriptional bubble in *His^C* mutants. This defect would also explain the strong reduction of a peak upstream of the TSSs in the *His^C* mutant embryos.

In contrast, repressive marks on histones generally don't reach enrichment levels at TSSs, and gene bodies as observed for active marks in wild types and *His^C* mutant embryos. The differences between *His^C* mutants and wild types are minor and not comparable to the differences observed with active marks like H3K4me3. Moreover, enrichment domains not only in coverage tracks but also at TSS correlate well in mutants and wild types. This finding suggests that the nucleosomes decorated with H3K27me3 marks are able to maintain their genomic locations after replication. In contrast to activating marks it seems that the remaining parental histones are sufficient to re-establish pre replication levels, which is consistent with findings that H3K27me3 domains slowly expand and become increasingly decorated with H3K27me3 over several cell generations (*109, 113*). This process is mediated in a read – write manner of PRC2 that establishes the H3K27me3 histone marks (*142, 263*). It was shown that DNA elements such as PREs recruit PRC2 and contribute to the establishment of H3K27me3 domains in *Drosophila* (*71, 108*) and might therefore partially alleviating disruption of repressive domains in *His^C* mutants. PREs, however, are not yet identified in mammals (*71*) and thus, they were considered in studies on mouse ESC or HeLa cells.

Taken together, nucleosomes decorated with distinct histone marks retain their position after DNA replication. However, this positional memory is more pronounced for marks that signify activation than for marks that are associated with repression or silencing. Activating marks are also appropriately enriched, but they are more distributed within the gene bodies, while the repressing marks appear as distinct peaks similar in both wild type and mutant embryos and they maintain their position in the newly formed chromatin.

3.2 The lack of histone synthesis results in a cell cycle arrest mediated by degradation of string RNA by How

Chapter II describes the analysis of direct effects of histone depletion on cell cycle progression. Here, I explored how String^{Cdc25} activity is downregulated to cause the cell cycle arrest during the G2/M$_{15}$ transition. Although these results are still preliminary, we identified How(L) as potential *string* regulator, supporting the hypothesis that *string* mRNA destabilization is mediated by a regulator targeting the 3'UTR, eventually leading to s*tring* degradation. Previous studies described that DNA damage checkpoints ATM/Chk2 and ATR/Chk1 are not activated (*185*) upon cell cycle arrest in G2/M$_{15}$.

This is supported by recently contributed RNA-seq data reported in manuscript I (Chapter I, p.27), indicating that *grapes,* the Chk1 homologue in *Drosophila,* is upregulated in *His^{C}* mutants only 6h AEL, whereas other components of the DNA damage checkpoint like Wee1, Myt1, 4−3−3ε and the downstream acting Rad1, Rad9 or Rad17 are not differentially expressed. Additionally, Polo which phosphorylates Wee1 marking it for degradation by the Skp, Cullin, F-box containing complex (SCF complex) is downregulated (Figure 2.52) (*264*). Thus, the Wee1 mediated inactivation of the Cyclin B/Cdk1 complex is therefore unlikely to be impaired.

Yet our findings are in apparent contrast to a previous study showing that transgene-dependent expression of *string* cDNA results in a rescue of the G2/M$_{15}$ arrest in *His^{C}* mutants (*185*). This difference to our study might be explained by the concentration-dependent function of the String protein, i.e., the *string* transgene might have been expressed at higher levels than in the experiments reported here. In fact, in the former study a different driver line, which is not available any longer, was used in the experiments which result in a rescue of the G2/M$_{15}$ arrest in *His^{C}* mutants. This driver might exhibit stronger Gal4 expression which obviously resulted results in a sufficiently high *string* protein concentration to overcome cell cycle arrest. It is noteworthy that the transgenes used in the present study both show weaker signal intensities when probed by *in situ* hybridization for the transcripts as compared to endogenous *string* transcript signals obtained in wild type controls. Taken together, our results are consistent with the argument that the critical amount of *string* mRNA is not provided *via* transgene expression as described here.

Intriguingly, some of the observations we made and that are described in chapter I and II, correspond to wild type observations pre-MBT. Therefore, it might be hypothesized that additional maternal effects contribute to the observed phenotype, which so far had been excluded as *His^{C}* mutants show no deficiencies in cell cycle 14.

Among these are, .i.e., the absence of the DNA damage checkpoints (i), the onset of MBT which has been linked to histone concentration (ii) and responsible MBT regulators that play a crucial role in String regulation (iii).

(i) Activation of DNA damage checkpoints in early embryos, for example, was suggested to be dependent on the nuclear-cytoplasmic ratio in Xenopus (*224*) and Zebrafish (*265*). The common model suggests that signals resulting from DNA damage in a single nucleus are not sufficient for checkpoint activation, only after MBT when the embryo contains roughly 4,000 cells (*266*), the required signal strength is achieved. This was, supported by injecting synthetic DNA into *Xenopus* eggs which forwarded ATR/Chk1 activity to an N:C ratio similar to the 256 and 512 cell stage (*266*). In *Drosophila,* the emergence of the ATR/Chk1 is likely due to onset of zygotic transcription starting in NC10 checkpoint and was pinpointed to NC10 to NC11. However, His^{C} mutant embryos do not exhibit reduced DNA concentration, as even in cell cycle 15 the DNA is faithfully replicated (*184*), therefore we assume that in homozygous His^{C} zygotic transcription starts - like in wild types – during NC10, concluding that a DNA dosage dependent effect can be excluded.

(ii) Intriguingly, reduction of nuclear volume of *Xenopus* eggs lead to a premature, whereas an increase of maternally deposited $(H3\text{-}H4)_2$ to a delayed ZGA and cell cycle transformation during MBT (*225, 267*). In conclusion, histone abundance and histone to DNA ratio affects at least in Xenopus the timing of MBT and emergence of potential Cdc25 regulating pathways. The absence of DNA damage checkpoints in pre-MBT conditions is similar in *Drosophila* (*268*).

(iii) Interphase 14 represents MBT during *Drosophila* early development. However, some zygotic transcripts can be detected earlier, reflected by the increased interphase duration from nuclear division 11 onwards (*225, 269, 270*). These early transcribed genes are mostly signalling and body patterning genes (*225, 269*). During the subsequent MBT, maternally deposited transcripts are eliminated. mRNA degradation involves three different processes, i.e., maternal factors that are activated independently from ZGA (*271, 272*), factors that require zygotic transcription resulting in newly synthesized RNA binding proteins and finally miRNA induced mRNA degradation (*273–276*). Early zygotic transcription is activated by the transcription factor Zelda/Vielfältig (*276*). Zelda starts to occupy promotor regions as early as NC8 and increases occupation at least until NC14 (*225, 277–279*). During this developmental period, His^{C} mutant embryogenesis is indistinguishable from wild type embryos, including the NC14. Intriguingly, Zelda shows characteristics similar to chromatin remodelers and pioneer factors, and it occupies mostly accessible chromatin regions which are enriched for GAGA binding motifs (*278*). The results reported in Manuscript I indicate that chromatin in His^{C} mutants is more accessible than wild type chromatin which could

potentially allow increased Zelda binding in *His^{C}* mutants driving maternal mRNA degradation pathways and possibly also some spurious transcription in the increasingly accessible chromatin up to NC15 of the mutants.

RNA-seq data reported in chapter I shows that *zelda* RNA is downregulated in *His^{C}* mutants, yet normalized counts are constant at each time point with 50% of wild type counts at 3.5-4h AEL and approximately equal counts at 6.5-7h AEL (Figure 2.52). In addition, Zelda controls the expression of miRNAs (*276*). At the blastoderm stage of *zelda*-knockout mutants, *miR-965* expression has been shown to be impaired (*276*). However, it is unclear whether *miR-965* expression, which regulates *string* mRNA, is impaired in *His^{C}* mutant embryos during cell cycle arrest.

Ectopic occupation by Zelda might also partially explain the impaired control of RNAPII pausing at TSSs, since RNAPII pausing does not occur pre-MBT and is likely mediated through Zelda binding (*224, 280*). However, at the MBT, late replicating chromatin emerges with the corresponding chromatin features, i.e., heterochromatin is established with the corresponding chromatin-associated proteins like HP1, and histone modifications typically decorate the repressive status of chromatin. Similarly, activating marks are also established by increased RNAPII binding like H3K4me3, H3K27ac and H3K36me3 (*225, 280–284*).

In conclusion, *His^{C}* mutants show similar coverage patterns as were observed in wild types, although with distinct enrichment levels. These observations combined with the RNA-seq profiles established for such embryos, indicate that MBT and ZGA are not severely impaired in NC14, although ectopic effects of transcriptional regulators like Zelda might still contribute to some aspects of the observed phenotype. There might arguably be mutant phenotypes established during pre-MBT stages which affect cell-cycle progression after MTB transition. In case there is zygotic histone expression before S_{15}, critical thresholds for genes responsive to histone titration would also be activated earlier. Consistently, cell cycle lengthening which precedes MBT was not observed earlier in *His^{C}* mutants than in wild types (*184*).

3.3 Concluding Remarks

Chromatin assembly, histone segregation and the *de novo* deposition of in particular the histones which contain post-translational histone marks are highly complex processes. Their orchestration requires tight regulation and mediation. Procedures that maintain the correct chromatin assembly during cell divisions are difficult to address because of their high velocity exceeding current capture methods and they were therefore limited to *in vitro* models.

Using *Drosophila* embryos as an experimentally accessible model organism, some of the obstacles could have been circumvented, and latest molecular techniques could be applied.

The main advance using this experimental system is the fact that all canonical histone genes are located in a single gene cluster. A chromosomal deletion of this cluster allowed to generate homozygous *His*^{C} mutant embryos which lack *de novo* histone synthesis at an early stage of embryogenesis, resulting in a stage-specific cell cycle arrest. I used this unique experimental system to pose questions regarding nucleosome assembly, the spacing and localization of nucleosomes during DNA replication which rest on parental histones only. I also asked how post-translational histone modifications, are distributed along the genome, and which consequences arise with respect to gene expression in a developing organism when the histone supply is limited. There are two essential results in addition to describing the epigenetic landscape and to presenting a detailed overview about the transcriptional changes in *His*^{C} mutant embryos as compared to wild type. First, the results are consistent with the argument that parental histones harbour a 'positional memory' to propagate the epigenetic landscape after DNA replication *in vivo.* Secondly, my results, although preliminary, suggest that the mRNA of the doses-dependent mitosis activating phosphatase String is controlled at the level of its stability in response to one variant of the RNA-binding protein Held-out-wings. This variant, How(L), is expressed in *His*^{C} mutants but not in wild type embryos at the respective stage. This result provides an entry point into a mechanistic understanding of how histone supply affects cell cycle regulation. Taken together, the outcome of my project allows to address future questions how embryonic development relies on chromatin formation and remodelling by setting the basis for future experiments to deepen our understanding of how nucleosomes participate in developmental decisions in addition to providing a scaffold for DNA packaging as it was thought when the structure of nucleosomes was discovered.

4 References

1. S. L. Berger, T. Kouzarides, R. Shiekhattar, A. Shilatifard, An operational definition of epigenetics. *Genes Dev.* **23**, 781–783 (2009), doi:10.1101/gad.1787609.
2. P. B. Talbert, S. Henikoff, Histone variants at a glance. *Journal of Cell Science*. **134** (2021), doi:10.1242/jcs.244749.
3. G. Arents, R. W. Burlingame, B. C. Wang, W. E. Love, E. N. Moudrianakis, The nucleosomal core histone octamer at 3.1 A resolution: a tripartite protein assembly and a left-handed superhelix. *Proceedings of the National Academy of Sciences of the United States of America*. **88**, 10148–10152 (1991), doi:10.1073/PNAS.88.22.10148.
4. K. Luger, A. W. Mäder, R. K. Richmond, D. F. Sargent, T. J. Richmond, Crystal structure of the nucleosome core particle at 2.8 A resolution. *Nature*. **389**, 251–260 (1997), doi:10.1038/38444.
5. J. O. Thomas, The higher order structure of chromatin and histone H1. *Journal of cell science. Supplement*. **1**, 1–20 (1984), doi:10.1242/jcs.1984.supplement_1.1.
6. J. Bednar *et al.,* Structure and Dynamics of a 197 bp Nucleosome in Complex with Linker Histone H1. *Molecular cell*. **66**, 384-397.e8 (2017), doi:10.1016/j.molcel.2017.04.012.
7. Wolffe (1998).
8. R. D. Kornberg, Y. Lorch, Primary Role of the Nucleosome. *Molecular cell*. **79**, 371–375 (2020), doi:10.1016/j.molcel.2020.07.020.
9. G. S. Manning, Packaged DNA. An elastic model. *Cell biophysics*. **7**, 57–89 (1985), doi:10.1007/BF02788639.
10. N. Yusufova *et al.,* Histone H1 loss drives lymphoma by disrupting 3D chromatin architecture. *Nature*. **589**, 299–305 (2021), doi:10.1038/s41586-020-3017-y.
11. A. P. Wolffe, S. Khochbin, S. Dimitrov, What do linker histones do in chromatin? *BioEssays*. **19**, 249–255 (1997), doi:10.1002/bies.950190311.
12. C. Duc, C. Thiriet, Replication-Coupled Chromatin Remodeling: An Overview of Disassembly and Assembly of Chromatin during Replication. *International journal of molecular sciences*. **22** (2021), doi:10.3390/ijms22031113.
13. C. Thiriet, J. J. Hayes, Linker histone phosphorylation regulates global timing of replication origin firing. *Journal of Biological Chemistry*. **284**, 2823–2829 (2009), doi:10.1074/jbc.M805617200.
14. Y. Dou, M. A. Gorovsky, Phosphorylation of Linker Histone H1 Regulates Gene Expression In Vivo by Creating a Charge Patch. *Molecular Cell*. **6**, 225–231 (2000), doi:10.1016/S1097-2765(00)00024-1.
15. K. Rutowicz *et al.*, *Linker histones regulate fine-scale chromatin organization and modulate developmental decisions in Arabidopsis* (Cold Spring Harbor Laboratory, 2018).
16. C. Redon *et al.,* Histone H2A variants H2AX and H2AZ. *Current opinion in genetics & development*. **12**, 162–169 (2002), doi:10.1016/S0959-437X(02)00282-4.
17. A. V. Probst, E. Dunleavy, G. Almouzni, Epigenetic inheritance during the cell cycle. *Nature Reviews Molecular Cell Biology*. **10**, 192–206 (2009), doi:10.1038/nrm2640.
18. P. B. Talbert, S. Henikoff, Histone variants on the move: substrates for chromatin dynamics. *Nature reviews. Molecular cell biology*. **18**, 115–126 (2017), doi:10.1038/nrm.2016.148.
19. W. F. Marzluff, R. J. Duronio, Histone mRNA expression: multiple levels of cell cycle regulation and important developmental consequences. *Current opinion in cell biology*. **14**, 692–699 (2002), doi:10.1016/S0955-0674(02)00387-3.

20. A. J. Pardal, F. Fernandes-Duarte, A. J. Bowman, The histone chaperoning pathway: from ribosome to nucleosome. *Essays in biochemistry*. **63**, 29–43 (2019), doi:10.1042/EBC20180055.

21. M. J. Apta-Smith, J. R. Hernandez-Fernaud, A. J. Bowman, Evidence for the nuclear import of histones H3.1 and H4 as monomers. *The EMBO journal*. **37** (2018), doi:10.15252/embj.201798714.

22. A. Ejlassi, V. Menil-Philippot, A. Galvani, C. Thiriet, Histones H3 and H4 require their relevant amino-tails for efficient nuclear import and replication-coupled chromatin assembly in vivo. *Scientific reports*. **7**, 3050 (2017), doi:10.1038/s41598-017-03218-6.

23. A. Ejlassi-Lassallette, E. Mocquard, M.-C. Arnaud, C. Thiriet, H4 replication-dependent diacetylation and Hat1 promote S-phase chromatin assembly in vivo. *Molecular Biology of the Cell*. **22**, 245–255 (2011), doi:10.1091/mbc.e10-07-0633.

24. L. Chang *et al.,* Histones in transit: cytosolic histone complexes and diacetylation of H4 during nucleosome assembly in human cells. *Biochemistry*. **36**, 469–480 (1997), doi:10.1021/bi962069i.

25. D. M. Susano Pinto, A. Flaus, The human canonical core histone catalogue. *bioRxiv*, 720235 (2019), doi:10.1101/720235.

26. S. Henikoff, M. M. Smith, Histone variants and epigenetics. *Cold Spring Harbor Perspectives in Biology*. **7**, a019364 (2015), doi:10.1101/cshperspect.a019364.

27. W. F. Marzluff, K. P. Koreski, Birth and Death of Histone mRNAs. *Trends in Genetics*. **33**, 745–759 (2017), doi:10.1016/j.tig.2017.07.014.

28. J. Zhang *et al.,* Molecular mechanisms for the regulation of histone mRNA stem-loop-binding protein by phosphorylation. *Proceedings of the National Academy of Sciences*. **111**, E2937-46 (2014), doi:10.1073/pnas.1406381111.

29. R. Maxson, R. Cohn, L. Kedes, T. Mohun, Expression and organization of histone genes. *Annual review of genetics*. **17**, 239–277 (1983), doi:10.1146/annurev.ge.17.120183.001323.

30. R. W. Old, H. R. Woodland, Histone genes: Not so simple after all. *Cell*. **38**, 624–626 (1984), doi:10.1016/0092-8674(84)90256-3.

31. M.-E. Chaboute, N. Chaubet, B. Clement, C. Gigot, G. Philipps, Polyadenylation of histone H3 and H4 mRNAs in dicotyledonous plants. *Gene*. **71**, 217–223 (1988), doi:10.1016/0378-1119(88)90095-9.

32. G.-C. Yuan *et al.,* Genome-scale identification of nucleosome positions in S. cerevisiae. *Science*. **309**, 626–630 (2005), doi:10.1126/science.1112178.

33. E. Oberbeckmann *et al.,* Ruler elements in chromatin remodelers set nucleosome array spacing and phasing. *Nature communications*. **12**, 3232 (2021), doi:10.1038/s41467-021-23015-0.

34. Y. M. Moshkin *et al.,* Remodellers organize cellular chromatin by counteracting intrinsic histone-DNA sequence preferences in a class-specific manner. *Molecular and cellular biology*. **32**, 675–688 (2012), doi:10.1128/MCB.06365-11.

35. G. J. Narlikar, R. Sundaramoorthy, T. Owen-Hughes, Mechanisms and functions of ATP-dependent chromatin-remodeling enzymes. *Cell*. **154**, 490–503 (2013), doi:10.1016/j.cell.2013.07.011.

36. A. L. Hughes, O. J. Rando, Comparative Genomics Reveals Chd1 as a Determinant of Nucleosome Spacing in Vivo. *G3 (Bethesda, Md.)*. **5**, 1889–1897 (2015), doi:10.1534/g3.115.020271.

37. J. G. Yang, T. S. Madrid, E. Sevastopoulos, G. J. Narlikar, The chromatin-remodeling enzyme ACF is an ATP-dependent DNA length sensor that regulates nucleosome spacing. *Nat Struct Mol Biol*. **13**, 1078–1083 (2006), doi:10.1038/nsmb1170.

38. R. F. Levendosky, G. D. Bowman, Asymmetry between the two acidic patches dictates the direction of nucleosome sliding by the ISWI chromatin remodeler. *eLife*. **8** (2019), doi:10.7554/eLife.45472.

39. R. T. Fennessy, T. Owen-Hughes, Establishment of a promoter-based chromatin architecture on recently replicated DNA can accommodate variable inter-nucleosome spacing. *Nucleic acids research*. **44**, 7189–7203 (2016), doi:10.1093/nar/gkw331.

40. Y. Fan *et al.,* H1 linker histones are essential for mouse development and affect nucleosome spacing in vivo. *Molecular and cellular biology*. **23**, 4559–4572 (2003), doi:10.1128/MCB.23.13.4559-4572.2003.

41. J. Hu *et al.,* Dynamic placement of the linker histone H1 associated with nucleosome arrangement and gene transcription in early Drosophila embryonic development. *Cell death & disease*. **9**, 765 (2018), doi:10.1038/s41419-018-0819-z.

42. L. A. Pray, Semi-conservative DNA replication: Meselson and Stahl. *Nature Education* (1998).

43. B. Ekundayo, F. Bleichert, Origins of DNA replication. *PLoS genetics*. **15**, e1008320 (2019), doi:10.1371/journal.pgen.1008320.

44. W. M. Becker, *The world of the cell* (Pearson/Benjamin Cummings, San Francisco, Calif., ed. 7, 2009).

45. P. Tessarz, T. Kouzarides, Histone core modifications regulating nucleosome structure and dynamics. *Nature reviews. Molecular cell biology*. **15**, 703–708 (2014), doi:10.1038/nrm3890.

46. T. Kouzarides, Chromatin modifications and their function. *Cell*. **128**, 693–705 (2007), doi:10.1016/j.cell.2007.02.005.

47. D. J. Patel, Z. Wang, Readout of epigenetic modifications. *Annual review of biochemistry*. **82**, 81–118 (2013), doi:10.1146/annurev-biochem-072711-165700.

48. K. Ahmad, S. Henikoff, No strand left behind. *Science (New York, N.Y.)*. **361**, 1311–1312 (2018), doi:10.1126/science.aav0871.

49. C. Yu *et al.,* A mechanism for preventing asymmetric histone segregation onto replicating DNA strands. *Science (New York, N.Y.)*. **361**, 1386–1389 (2018), doi:10.1126/science.aat8849.

50. A. Kaykov, P. Nurse, The spatial and temporal organization of origin firing during the S-phase of fission yeast. *Genome research*. **25**, 391–401 (2015), doi:10.1101/gr.180372.114.

51. S. Ramachandran, S. Henikoff, Transcriptional Regulators Compete with Nucleosomes Post-replication. *Cell*. **165**, 580–592 (2016), doi:10.1016/j.cell.2016.02.062.

52. G. O. Elliott, K. J. Murphy, J. J. Hayes, C. Thiriet, Replication-independent nucleosome exchange is enhanced by local and specific acetylation of histone H4. *Nucleic acids research*. **41**, 2228–2238 (2013), doi:10.1093/nar/gks1451.

53. E. Mocquard-Bucher, A. Galvani, C. Thiriet, Histone H4 acetylation links nucleosome turnover and nucleosome assembly: lessons from the slime mold Physarum polycephalum. *Frontiers in Life Science*. **7**, 12–21 (2013), doi:10.1080/21553769.2013.848241.

54. D. T. Gruszka, S. Xie, H. Kimura, H. Yardimci, Single-molecule imaging reveals control of parental histone recycling by free histones during DNA replication. *Science advances*. **6** (2020), doi:10.1126/sciadv.abc0330.

55. A. T. Annunziato, Assembling chromatin: the long and winding road. *Biochimica et biophysica acta*. **1819**, 196–210 (2013), doi:10.1016/j.bbagrm.2011.07.005.

56. I. Leffak, R. Grainger, H. Weintraub, Conservative assembly and segregation of nucleosomal histories. *Cell*. **12**, 837–845 (1977), doi:10.1016/0092-8674(77)90282-3.

57. C. Gruss, J. Wu, T. Koller, J. M. Sogo, Disruption of the nucleosomes at the replication fork. *The EMBO journal*. **12**, 4533–4545 (1993), doi:10.1002/j.1460-2075.1993.tb06142.x.

58. C. Gruss, J. M. Sogo, Chromatin replication. *BioEssays*. **14**, 1–8 (1992), doi:10.1002/bies.950140102.

59. A. T. Annunziato, The Fork in the Road: Histone Partitioning During DNA Replication. *Genes*. **6**, 353–371 (2015), doi:10.3390/genes6020353.

60. M. L. DePamphilis, P. M. Wassarman, Regulation of chromosomal replication and transcription during early mammalian development. *BioEssays*. **7**, 265–271 (1987), doi:10.1002/bies.950070609.

61. R. Gasser, T. Koller, J. M. Sogo, The stability of nucleosomes at the replication fork. *Journal of Molecular Biology*. **258**, 224–239 (1996), doi:10.1006/jmbi.1996.0245.

62. R. E. Wellinger, J. M. Sogo, In vivo mapping of nucleosomes using psoralen-DNA crosslinking and primer extension. *Nucleic acids research*. **26**, 1544–1545 (1998), doi:10.1093/nar/26.6.1544.

63. S. L. McKnight, O. L. Miller, Electron microscopic analysis of chromatin replication in the cellular blastoderm drosophila melanogaster embryo. *Cell*. **12**, 795–804 (1977), doi:10.1016/0092-8674(77)90278-1.

64. K. R. Stewart-Morgan, N. Petryk, A. Groth, Chromatin replication and epigenetic cell memory. *Nature cell biology*. **22**, 361–371 (2020), doi:10.1038/s41556-020-0487-y.

65. N. Petryk *et al.,* MCM2 promotes symmetric inheritance of modified histones during DNA replication. *Science (New York, N.Y.)*. **361**, 1389–1392 (2018), doi:10.1126/science.aau0294.

66. D. Riley, H. Weintraub, Conservative segregation of parental histones during replication in the presence of cycloheximide. *Proceedings of the National Academy of Sciences of the United States of America*. **76**, 328–332 (1979), doi:10.1073/pnas.76.1.328.

67. C. Alabert *et al.,* Nascent chromatin capture proteomics determines chromatin dynamics during DNA replication and identifies unknown fork components. *Nature cell biology*. **16**, 281–293 (2014), doi:10.1038/ncb2918.

68. C. Alabert, A. Groth, Chromatin replication and epigenome maintenance. *Nature reviews. Molecular cell biology*. **13**, 153–167 (2012), doi:10.1038/nrm3288.

69. G. Almouzni, H. Cedar, Maintenance of Epigenetic Information. *Cold Spring Harbor Perspectives in Biology*. **8** (2016), doi:10.1101/cshperspect.a019372.

70. N. Reverón-Gómez *et al.,* Accurate Recycling of Parental Histones Reproduces the Histone Modification Landscape during DNA Replication. *Molecular cell*. **72**, 239-249.e5 (2018), doi:10.1016/j.molcel.2018.08.010.

71. S. Henikoff, K. Ahmad, Nucleosomes remember where they were. *Proceedings of the National Academy of Sciences of the United States of America*. **116**, 20254–20256 (2019), doi:10.1073/pnas.1914581116.

72. T. M. Escobar *et al.,* Active and Repressed Chromatin Domains Exhibit Distinct Nucleosome Segregation during DNA Replication. *Cell*. **179**, 953-963.e11 (2019), doi:10.1016/j.cell.2019.10.009.

73. T. M. Escobar, A. Loyola, D. Reinberg, Parental nucleosome segregation and the inheritance of cellular identity. *Nature reviews. Genetics*. **22**, 379–392 (2021), doi:10.1038/s41576-020-00312-w.

74. M. Xu *et al.,* Partitioning of histone H3-H4 tetramers during DNA replication-dependent chromatin assembly. *Science (New York, N.Y.)*. **328**, 94–98 (2010), doi:10.1126/science.1178994.

75. H. Tagami, D. Ray-Gallet, G. Almouzni, Y. Nakatani, Histone H3.1 and H3.3 Complexes Mediate Nucleosome Assembly Pathways Dependent or Independent of DNA Synthesis. *Cell*. **116**, 51–61 (2004), doi:10.1016/S0092-8674(03)01064-X.

76. A. Groth, W. Rocha, A. Verreault, G. Almouzni, Chromatin challenges during DNA replication and repair. *Cell*. **128**, 721–733 (2007), doi:10.1016/j.cell.2007.01.030.

77. M. Clemente-Ruiz, R. González-Prieto, F. Prado, Histone H3K56 acetylation, CAF1, and Rtt106 coordinate nucleosome assembly and stability of advancing replication forks. *PLoS genetics*. **7**, e1002376 (2011), doi:10.1371/journal.pgen.1002376.

78. F. Prado, F. Cortés-Ledesma, A. Aguilera, The absence of the yeast chromatin assembly factor Asf1 increases genomic instability and sister chromatid exchange. *EMBO reports*. **5**, 497–502 (2004), doi:10.1038/sj.embor.7400128.

79. N. Hawkins, G. Garriga, Asymmetric cell division: from A to Z. *Genes & development*. **12**, 3625–3638 (1998), doi:10.1101/gad.12.23.3625.

80. F. Matsuzaki, Asymmetric division of Drosophila neural stem cells: a basis for neural diversity. *Current Opinion in Neurobiology*. **10**, 38–44 (2000), doi:10.1016/S0959-4388(99)00052-5.

81. V. Tran, C. Lim, J. Xie, X. Chen, Asymmetric division of Drosophila male germline stem cell shows asymmetric histone distribution. *Science (New York, N.Y.)*. **338**, 679–682 (2012), doi:10.1126/science.1226028.

82. M. Wooten *et al.,* Asymmetric histone inheritance via strand-specific incorporation and biased replication fork movement. *Nature structural & molecular biology*. **26**, 732–743 (2019), doi:10.1038/s41594-019-0269-z.

83. L. D. Brennan, R. A. Forties, S. S. Patel, M. D. Wang, DNA looping mediates nucleosome transfer. *Nature communications*. **7**, 13337 (2016), doi:10.1038/ncomms13337.

84. P. Vasseur *et al.,* Dynamics of Nucleosome Positioning Maturation following Genomic Replication. *Cell reports*. **16**, 2651–2665 (2016), doi:10.1016/j.celrep.2016.07.083.

85. D. J. Smith, I. Whitehouse, Intrinsic coupling of lagging-strand synthesis to chromatin assembly. *Nature*. **483**, 434–438 (2012), doi:10.1038/nature10895.

86. M. E. Cusick, M. L. DePamphilis, P. M. Wassarman, Dispersive segregation of nucleosomes during replication of simian virus 40 chromosomes. *Journal of Molecular Biology*. **178**, 249–271 (1984), doi:10.1016/0022-2836(84)90143-8.

87. E. V. Madamba, E. B. Berthet, N. J. Francis, Inheritance of Histones H3 and H4 during DNA Replication In Vitro. *Cell reports*. **21**, 1361–1374 (2017), doi:10.1016/j.celrep.2017.10.033.

88. G. Schlissel, J. Rine, The nucleosome core particle remembers its position through DNA replication and RNA transcription. *Proceedings of the National Academy of Sciences of the United States of America*. **116**, 20605–20611 (2019), doi:10.1073/pnas.1911943116.

89. D. Reinberg, L. D. Vales, Chromatin domains rich in inheritance. *Science (New York, N.Y.)*. **361**, 33–34 (2018), doi:10.1126/science.aat7871.

90. I. Whitehouse, D. J. Smith, Chromatin dynamics at the replication fork: there's more to life than histones. *Current opinion in genetics & development*. **23**, 140–146 (2013), doi:10.1016/j.gde.2012.12.007.

91. C. M. Hammond, C. B. Strømme, H. Huang, D. J. Patel, A. Groth, Histone chaperone networks shaping chromatin function. *Nature reviews. Molecular cell biology*. **18**, 141–158 (2017), doi:10.1038/nrm.2016.159.

92. J. F. Sarthy *et al.,* Histone deposition pathways determine the chromatin landscapes of H3.1 and H3.3 K27M oncohistones. *eLife*. **9** (2020), doi:10.7554/eLife.61090.

93. C. M. Weber, S. Ramachandran, S. Henikoff, Nucleosomes are context-specific, H2A.Z-modulated barriers to RNA polymerase. *Molecular cell*. **53**, 819–830 (2014), doi:10.1016/j.molcel.2014.02.014.

94. T. Jenuwein, C. D. Allis, Translating the histone code. *Science (New York, N.Y.)*. **293**, 1074–1080 (2001), doi:10.1126/science.1063127.

95. B. Stillman, Histone Modifications: Insights into Their Influence on Gene Expression. *Cell*. **175**, 6–9 (2018), doi:10.1016/j.cell.2018.08.032.

96. C. D. Allis, T. Jenuwein, The molecular hallmarks of epigenetic control. *Nature reviews. Genetics*. **17**, 487–500 (2016), doi:10.1038/nrg.2016.59.

97. E. I. Campos, J. M. Stafford, D. Reinberg, Epigenetic inheritance: histone bookmarks across generations. *Trends in cell biology*. **24**, 664–674 (2014), doi:10.1016/j.tcb.2014.08.004.

98. O. J. Rando, Global patterns of histone modifications. *Current opinion in genetics & development*. **17**, 94–99 (2007), doi:10.1016/j.gde.2007.02.006.

99. B. Schuettengruber, H.-M. Bourbon, L. Di Croce, G. Cavalli, Genome Regulation by Polycomb and Trithorax: 70 Years and Counting. *Cell*. **171**, 34–57 (2017), doi:10.1016/j.cell.2017.08.002.

100. Z. Jasencakova *et al.,* Replication stress interferes with histone recycling and predeposition marking of new histones. *Molecular cell*. **37**, 736–743 (2010), doi:10.1016/j.molcel.2010.01.033.

101. A. Loyola, T. Bonaldi, D. Roche, A. Imhof, G. Almouzni, PTMs on H3 variants before chromatin assembly potentiate their final epigenetic state. *Molecular Cell*. **24**, 309–316 (2006), doi:10.1016/j.molcel.2006.08.019.

102. M. Shogren-Knaak *et al.,* Histone H4-K16 acetylation controls chromatin structure and protein interactions. *Science*. **311**, 844–847 (2006), doi:10.1126/science.1124000.

103. L. M. Johnson, P. S. Kayne, E. S. Kahn, M. Grunstein, Genetic evidence for an interaction between SIR3 and histone H4 in the repression of the silent mating loci in Saccharomyces cerevisiae. *Proceedings of the National Academy of Sciences of the United States of America*. **87**, 6286–6290 (1990), doi:10.1073/pnas.87.16.6286.

104. V. Pirrotta, Chromatin-silencing mechanisms in Drosophila maintain patterns of gene expression. *Trends in Genetics*. **13**, 314–318 (1997), doi:10.1016/S0168-9525(97)01178-5.

105. E. B. Lewis, A gene complex controlling segmentation in Drosophila. *Nature*. **276**, 565–570 (1978), doi:10.1038/276565a0.

106. S. Petruk, K. L. Black, S. K. Kovermann, H. W. Brock, A. Mazo, Stepwise histone modifications are mediated by multiple enzymes that rapidly associate with nascent DNA during replication. *Nature communications*. **4**, 2841 (2013), doi:10.1038/ncomms3841.

107. S. Petruk *et al.,* TrxG and PcG proteins but not methylated histones remain associated with DNA through replication. *Cell*. **150**, 922–933 (2012), doi:10.1016/j.cell.2012.06.046.

108. J. A. Simon, R. E. Kingston, Mechanisms of polycomb gene silencing: knowns and unknowns. *Nature reviews. Molecular cell biology*. **10**, 697–708 (2009), doi:10.1038/nrm2763.

109. K. Ahmad, A. E. Spens, Separate Polycomb Response Elements control chromatin state and activation of the vestigial gene. *PLoS genetics*. **15**, e1007877 (2019), doi:10.1371/journal.pgen.1007877.

110. K. Ragunathan, G. Jih, D. Moazed, Epigenetics. Epigenetic inheritance uncoupled from sequence-specific recruitment. *Science (New York, N.Y.)*. **348**, 1258699 (2015), doi:10.1126/science.1258699.

111. L. Jiao, X. Liu, Structural basis of histone H3K27 trimethylation by an active polycomb repressive complex 2. *Science*. **350**, aac4383 (2015), doi:10.1126/science.aac4383.

112. R. B. Deal, J. G. Henikoff, S. Henikoff, Genome-wide kinetics of nucleosome turnover determined by metabolic labeling of histones. *Science*. **328**, 1161–1164 (2010), doi:10.1126/science.1186777.

113. C. Alabert, Two distinct modes for propagation of histone PTMs across the cell cycle. *Genes & development* (2014).

114. M. Xu, W. Wang, S. Chen, B. Zhu, A model for mitotic inheritance of histone lysine methylation. *EMBO reports*. **13**, 60–67 (2011), doi:10.1038/embor.2011.206.

115. R. A.-J. Chen *et al.,* Extreme HOT regions are CpG-dense promoters in C. elegans and humans. *Genome research*. **24**, 1138–1146 (2014), doi:10.1101/gr.161992.113.

116. R. S. Illingworth *et al.,* Orphan CpG islands identify numerous conserved promoters in the mammalian genome. *PLoS genetics*. **6**, e1001134 (2010), doi:10.1371/journal.pgen.1001134.

117. L. Morey, K. Helin, Polycomb group protein-mediated repression of transcription. *Trends in biochemical sciences*. **35**, 323–332 (2010), doi:10.1016/j.tibs.2010.02.009.

118. K. R. Stewart-Morgan, N. Reverón-Gómez, A. Groth, Transcription Restart Establishes Chromatin Accessibility after DNA Replication. *Molecular cell*. **75**, 284-297.e6 (2019), doi:10.1016/j.molcel.2019.04.033.

119. R. J. Sims, R. Belotserkovskaya, D. Reinberg, Elongation by RNA polymerase II: the short and long of it. *Genes & development*. **18**, 2437–2468 (2004), doi:10.1101/gad.1235904.

120. N. Rhind, D. M. Gilbert, DNA replication timing. *Cold Spring Harbor Perspectives in Biology*. **5**, a010132 (2013), doi:10.1101/cshperspect.a010132.

121. A. Piovesan *et al.,* Human protein-coding genes and gene feature statistics in 2019. *BMC Res Notes*. **12**, 315 (2019), doi:10.1186/s13104-019-4343-8.

122. M. Mohan *et al.,* The COMPASS family of H3K4 methylases in Drosophila. *Molecular and cellular biology*. **31**, 4310–4318 (2011), doi:10.1128/MCB.06092-11.

123. W. Li, D. Notani, M. G. Rosenfeld, Enhancers as non-coding RNA transcription units: recent insights and future perspectives. *Nature Reviews Genetics*. **17**, 207–223 (2016), doi:10.1038/nrg.2016.4.

124. L. J. Core *et al.,* Analysis of nascent RNA identifies a unified architecture of initiation regions at mammalian promoters and enhancers. *Nature genetics*. **46**, 1311–1320 (2014), doi:10.1038/ng.3142.

125. M. Radman-Livaja *et al.,* Patterns and mechanisms of ancestral histone protein inheritance in budding yeast. *PLoS biology*. **9**, e1001075 (2011), doi:10.1371/journal.pbio.1001075.

126. A. B. Blumenthal, H. J. Kriegstein, D. S. Hogness, The units of DNA replication in Drosophila melanogaster chromosomes. *Cold Spring Harbor symposia on quantitative biology*. **38**, 205–223 (1974), doi:10.1101/SQB.1974.038.01.024.

127. Fennessy, Establishment of a promoter-based chromatin architecture on recently replicated DNA can accommodate variable inter-nucleosome spacing. *Nucleic Acids Res*. **44**, 7189 (2016).

128. T. Yadav, I. Whitehouse, Replication-Coupled Nucleosome Assembly and Positioning by ATP-Dependent Chromatin-Remodeling Enzymes. *Cell reports*. **15**, 715–723 (2016), doi:10.1016/j.celrep.2016.03.059.

129. S. P. Bell, A. Dutta, DNA replication in eukaryotic cells. *Annual review of biochemistry*. **71**, 333–374 (2002), doi:10.1146/annurev.biochem.71.110601.135425.

130. H. K. MacAlpine, R. Gordân, S. K. Powell, A. J. Hartemink, D. M. MacAlpine, Drosophila ORC localizes to open chromatin and marks sites of cohesin complex loading. *Genome research*. **20**, 201–211 (2010), doi:10.1101/gr.097873.109.

131. J. G. Henikoff, J. A. Belsky, K. Krassovsky, D. M. MacAlpine, S. Henikoff, Epigenome characterization at single base-pair resolution. *Proceedings of the National Academy of Sciences*. **108**, 18318–18323 (2011), doi:10.1073/pnas.1110731108.

132. W. A. Whyte *et al.,* Master transcription factors and mediator establish super-enhancers at key cell identity genes. *Cell*. **153**, 307–319 (2013), doi:10.1016/j.cell.2013.03.035.

133. S. Buratowski, Progression through the RNA polymerase II CTD cycle. *Molecular cell*. **36**, 541–546 (2009), doi:10.1016/j.molcel.2009.10.019.

134. K. Hyun, J. Jeon, K. Park, J. Kim, Writing, erasing and reading histone lysine methylations. *Experimental & molecular medicine*. **49**, e324 (2017), doi:10.1038/emm.2017.11.

135. P. W. Ingham, Differential expression of bithorax complex genes in the absence of the extra sex combs and trithorax genes. *Nature*. **306**, 591–593 (1983), doi:10.1038/306591a0.

136. A. Shilatifard, The COMPASS family of histone H3K4 methylases: mechanisms of regulation in development and disease pathogenesis. *Annual review of biochemistry*. **81**, 65–95 (2012), doi:10.1146/annurev-biochem-051710-134100.

137. A. Piunti, A. Shilatifard, Epigenetic balance of gene expression by Polycomb and COMPASS families. *Science (New York, N.Y.)*. **352**, aad9780 (2016), doi:10.1126/science.aad9780.

138. J. W. Tamkun *et al.,* brahma: A regulator of Drosophila homeotic genes structurally related to the yeast transcriptional activator SNF2SWI2. *Cell*. **68**, 561–572 (1992), doi:10.1016/0092-8674(92)90191-E.

139. P. Filippakopoulos, S. Knapp, Targeting bromodomains: epigenetic readers of lysine acetylation. *Nat Rev Drug Discov*. **13**, 337–356 (2014), doi:10.1038/nrd4286.

140. T. Miller *et al.,* COMPASS: a complex of proteins associated with a trithorax-related SET domain protein. *Proceedings of the National Academy of Sciences of the United States of America*. **98**, 12902–12907 (2001), doi:10.1073/pnas.231473398.

141. G. Hallson *et al.,* dSet1 is the main H3K4 di- and tri-methyltransferase throughout Drosophila development. *Genetics*. **190**, 91–100 (2012), doi:10.1534/genetics.111.135863.

142. R. Margueron, D. Reinberg, The Polycomb complex PRC2 and its mark in life. *Nature*. **469**, 343–349 (2011), doi:10.1038/nature09784.

143. V. A. Stepanik, P. J. Harte, A mutation in the E(Z) methyltransferase that increases trimethylation of histone H3 lysine 27 and causes inappropriate silencing of active Polycomb target genes. *Developmental biology*. **364**, 249–258 (2012), doi:10.1016/j.ydbio.2011.12.007.

144. N. P. Blackledge *et al.,* Variant PRC1 complex-dependent H2A ubiquitylation drives PRC2 recruitment and polycomb domain formation. *Cell*. **157**, 1445–1459 (2014), doi:10.1016/j.cell.2014.05.004.

145. R. Kalb *et al.,* Histone H2A monoubiquitination promotes histone H3 methylation in Polycomb repression. *Nat Struct Mol Biol*. **21**, 569–571 (2014), doi:10.1038/nsmb.2833.

146. K. A. Hines *et al.,* Domains of heterochromatin protein 1 required for Drosophila melanogaster heterochromatin spreading. *Genetics*. **182**, 967–977 (2009), doi:10.1534/genetics.109.105338.

147. T. Zhang, S. Cooper, N. Brockdorff, The interplay of histone modifications - writers that read. *EMBO reports*. **16**, 1467–1481 (2015), doi:10.15252/embr.201540945.

148. M. Long *et al.,* A novel histone H4 variant H4G regulates rDNA transcription in breast cancer. *Nucleic acids research*. **47**, 8399–8409 (2019), doi:10.1093/nar/gkz547.

149. J. Ferrand, B. Rondinelli, S. E. Polo, Histone Variants: Guardians of Genome Integrity. *Cells*. **9**, 2424 (2020), doi:10.3390/cells9112424.

150. Boulard, Histone variant nucleosomes: Structure, function and implication in disease. *Subcell. Biochem.* **41**, 71 (2007).

151. C. Clément *et al.,* High-resolution visualization of H3 variants during replication reveals their controlled recycling. *Nature communications*. **9**, 3181 (2018), doi:10.1038/s41467-018-05697-1.

152. R. Resnick *et al.,* DUX4-Induced Histone Variants H3.X and H3.Y Mark DUX4 Target Genes for Expression. *Cell reports*. **29**, 1812-1820.e5 (2019), doi:10.1016/j.celrep.2019.10.025.

153. D. Ray-Gallet *et al.,* Dynamics of histone H3 deposition in vivo reveal a nucleosome gap-filling mechanism for H3.3 to maintain chromatin integrity. *Molecular cell*. **44**, 928–941 (2011), doi:10.1016/j.molcel.2011.12.006.

154. L. H. Wong *et al.,* Histone H3.3 incorporation provides a unique and functionally essential telomeric chromatin in embryonic stem cells. *Genome research*. **19**, 404–414 (2009), doi:10.1101/gr.084947.108.

155. S. Henikoff, K. Ahmad, Assembly of variant histones into chromatin. *Annual Review of Cell and Developmental Biology*. **21**, 133–153 (2005), doi:10.1146/ANNUREV.CELLBIO.21.012704.133518.

156. P. Drané, K. Ouararhni, A. Depaux, M. Shuaib, A. Hamiche, The death-associated protein DAXX is a novel histone chaperone involved in the replication-independent deposition of H3.3. *Genes & development*. **24**, 1253–1265 (2010), doi:10.1101/gad.566910.

157. A. D. Goldberg *et al.,* Distinct factors control histone variant H3.3 localization at specific genomic regions. *Cell*. **140**, 678–691 (2010), doi:10.1016/j.cell.2010.01.003.

158. S. Martire *et al.,* Phosphorylation of histone H3.3 at serine 31 promotes p300 activity and enhancer acetylation. *Nature genetics*. **51**, 941–946 (2019), doi:10.1038/s41588-019-0428-5.

159. S. Martire, L. A. Banaszynski, The roles of histone variants in fine-tuning chromatin organization and function. *Nature reviews. Molecular cell biology*. **21**, 522–541 (2020), doi:10.1038/s41580-020-0262-8.

160. C.-W. Jang, Y. Shibata, J. Starmer, Della Yee, T. Magnuson, Histone H3.3 maintains genome integrity during mammalian development. *Genes & development*. **29**, 1377–1392 (2015), doi:10.1101/gad.264150.115.

161. B. T. K. Yuen, K. M. Bush, B. L. Barrilleaux, R. Cotterman, P. S. Knoepfler, Histone H3.3 regulates dynamic chromatin states during spermatogenesis. *Development*. **141**, 3483–3494 (2014), doi:10.1242/dev.106450.

162. K. Delaney, J. Mailler, J. M. Wenda, C. Gabus, F. A. Steiner, Differential Expression of Histone H3.3 Genes and Their Role in Modulating Temperature Stress Response in Caenorhabditis elegans. *Genetics*. **209**, 551–565 (2018), doi:10.1534/genetics.118.300909.

163. P. B. Talbert, S. Henikoff, Histone variants--ancient wrap artists of the epigenome. *Nat Rev Mol Cell Biol*. **11**, 264–275 (2010), doi:10.1038/nrm2861.

164. M. C. C. Silva *et al.,* Cdk activity couples epigenetic centromere inheritance to cell cycle progression. *Developmental cell*. **22**, 52–63 (2012), doi:10.1016/j.devcel.2011.10.014.

165. P. B. Talbert, S. Henikoff, What makes a centromere? *Experimental Cell Research*. **389**, 111895 (2020), doi:10.1016/j.yexcr.2020.111895.

166. H. S. Malik, S. Henikoff, Major evolutionary transitions in centromere complexity. *Cell*. **138**, 1067–1082 (2009), doi:10.1016/j.cell.2009.08.036.

167. R. Hirano *et al.,* Histone variant H2A.B-H2B dimers are spontaneously exchanged with canonical H2A-H2B in the nucleosome. *Commun Biol*. **4**, 191 (2021), doi:10.1038/s42003-021-01707-z.

168. O. Fernandez-Capetillo *et al.,* H2AX Is Required for Chromatin Remodeling and Inactivation of Sex Chromosomes in Male Mouse Meiosis. *Developmental cell*. **4**, 497–508 (2003), doi:10.1016/S1534-5807(03)00093-5.

169. P. B. Talbert *et al.,* A unified phylogeny-based nomenclature for histone variants. *Epigenetics & Chromatin*. **5**, 7 (2012), doi:10.1186/1756-8935-5-7.

170. M. Marques, L. Laflamme, A. L. Gervais, L. Gaudreau, Reconciling the positive and negative roles of histone H2A.Z in gene transcription. *Epigenetics*. **5**, 267–272 (2010), doi:10.4161/epi.5.4.11520.

171. P. B. Talbert, S. Henikoff, Histone variants--ancient wrap artists of the epigenome. *Nat Rev Mol Cell Biol*. **11**, 264–275 (2010), doi:10.1038/nrm2861.

172. N. L. Adkins, H. Niu, P. Sung, C. L. Peterson, Nucleosome dynamics regulates DNA processing. *Nat Struct Mol Biol*. **20**, 836–842 (2013), doi:10.1038/nsmb.2585.

173. M. Grunstein, S. M. Gasser, Epigenetics in Saccharomyces cerevisiae. *Cold Spring Harbor Perspectives in Biology*. **5** (2013), doi:10.1101/cshperspect.a017491.

174. A. Molaro *et al.,* Biparental contributions of the H2A.B histone variant control embryonic development in mice. *PLOS Biology*. **18**, e3001001 (2020), doi:10.1371/journal.pbio.3001001.

175. G.-L. Chew *et al.,* Short H2A histone variants are expressed in cancer. *Nat Commun*. **12**, 490 (2021), doi:10.1038/s41467-020-20707-x.

176. D. Jiang *et al.,* The evolution and functional divergence of the histone H2B family in plants. *PLoS genetics*. **16**, e1008964 (2020), doi:10.1371/journal.pgen.1008964.

177. M. Borg, D. Jiang, F. Berger, Histone variants take center stage in shaping the epigenome. *Current opinion in plant biology*. **61**, 101991 (2021), doi:10.1016/j.pbi.2020.101991.

178. P. Raman *et al.,* Novel Classes and Evolutionary Turnover of Histone H2B Variants in the Mammalian Germline. *Mol Biol Evol*. **39** (2022), doi:10.1093/molbev/msac019.

179. M. Y. H. Pang, X. Sun, J. Ausió, T. Ishibashi, Histone H4 variant, H4G, drives ribosomal RNA transcription and breast cancer cell proliferation by loosening nucleolar chromatin structure. *Journal of Cellular Physiology*. **235**, 9601–9608 (2020), doi:10.1002/jcp.29770.

180. C. Huang. *PLoS genetics*, 618 (2013).

181. W. F. Marzluff, E. J. Wagner, R. J. Duronio, Metabolism and regulation of canonical histone mRNAs: life without a poly(A) tail. *Nature reviews. Genetics*. **9**, 843–854 (2008), doi:10.1038/nrg2438.

182. E. Ryder *et al.,* The DrosDel collection: a set of P-element insertions for generating custom chromosomal aberrations in Drosophila melanogaster. *Genetics*. **167**, 797–813 (2004), doi:10.1534/genetics.104.026658.

183. E. Ryder *et al.,* The DrosDel deletion collection: a Drosophila genomewide chromosomal deficiency resource. *Genetics*. **177**, 615–629 (2007), doi:10.1534/genetics.107.076216.

184. U. Günesdogan, H. Jäckle, A. Herzig, A genetic system to assess in vivo the functions of histones and histone modifications in higher eukaryotes. *EMBO reports*. **11**, 772–776 (2010), doi:10.1038/embor.2010.124.

185. U. Günesdogan, H. Jäckle, A. Herzig, Histone supply regulates S phase timing and cell cycle progression. *eLife*. **3**, e02443 (2014), doi:10.7554/eLife.02443.

186. B. A. Edgar, D. A. Lehman, P. H. O'Farrell, Transcriptional regulation of string (cdc25): a link between developmental programming and the cell cycle. *Development*. **120**, 3131–3143 (1994), doi:10.1242/dev.120.11.3131.

187. Audergon, Pauline N. C. B. *et al.,* Epigenetics. Restricted epigenetic inheritance of H3K9 methylation. *Science*. **348**, 132–135 (2015), doi:10.1126/science.1260638.

188. A. N. Schep *et al.,* Structured nucleosome fingerprints enable high-resolution mapping of chromatin architecture within regulatory regions. *Genome research*. **25**, 1757–1770 (2015), doi:10.1101/gr.192294.115.

189. S. Ramachandran, K. Ahmad, S. Henikoff, Transcription and Remodeling Produce Asymmetrically Unwrapped Nucleosomal Intermediates. *Molecular cell*. **68**, 1038-1053.e4 (2017), doi:10.1016/j.molcel.2017.11.015.

190. A. Bayona-Feliu, A. Casas-Lamesa, O. Reina, J. Bernués, F. Azorín, Linker histone H1 prevents R-loop accumulation and genome instability in heterochromatin. *Nat Commun*. **8**, 283 (2017), doi:10.1038/s41467-017-00338-5.

191. K. K. Li *et al.*, *Compensatory replacement of the BigH1 variant histone by canonical H1 supports normal embryonic development in Drosophila* (2019).

192. H. S. Kaya-Okur *et al.,* CUT&Tag for efficient epigenomic profiling of small samples and single cells. *Nature communications*. **10**, 1930 (2019), doi:10.1038/s41467-019-09982-5.

193. S. Henikoff, J. G. Henikoff, H. S. Kaya-Okur, K. Ahmad, Efficient chromatin accessibility mapping in situ by nucleosome-tethered tagmentation. *eLife*. **9** (2020), doi:10.7554/eLife.63274.

194. R. A. Policastro, R. T. Raborn, V. P. Brendel, G. E. Zentner, Simple and efficient profiling of transcription initiation and transcript levels with STRIPE-seq. *Genome research*. **30**, 910–923 (2020), doi:10.1101/gr.261545.120.

195. M. P. Creyghton *et al.,* Histone H3K27ac separates active from poised enhancers and predicts developmental state. *Proceedings of the National Academy of Sciences*. **107**, 21931–21936 (2010), doi:10.1073/pnas.1016071107.

196. B. P. Hennig, K. Bendrin, Y. Zhou, T. Fischer, Chd1 chromatin remodelers maintain nucleosome organization and repress cryptic transcription. *EMBO reports*. **13**, 997–1003 (2012), doi:10.1038/embor.2012.146.

197. M. Hödl, K. Basler, Transcription in the absence of histone H3.2 and H3K4 methylation. *Current biology : CB*. **22**, 2253–2257 (2012), doi:10.1016/j.cub.2012.10.008.

198. T. D. Schmittgen, K. J. Livak, Analyzing real-time PCR data by the comparative C(T) method. *Nature protocols*. **3**, 1101–1108 (2008), doi:10.1038/nprot.2008.73.

199. M. Buescher, G. Oberhofer, N. C. Garcia-Perez, G. Bucher, in *Brain Development, Methods and Protocols*, S. G. Sprecher, Ed. (Humana, New York, NY, ed. 2, 2020), vol. **2047,** pp. 219–232.

200. J. D. Buenrostro, P. G. Giresi, L. C. Zaba, H. Y. Chang, W. J. Greenleaf, Transposition of native chromatin for fast and sensitive epigenomic profiling of open chromatin, DNA-binding proteins and nucleosome position. *Nature methods*. **10**, 1213–1218 (2013), doi:10.1038/NMETH.2688.

201. J. D. Buenrostro, B. Wu, H. Y. Chang, W. J. Greenleaf, ATAC-seq: A Method for Assaying Chromatin Accessibility Genome-Wide. *Current protocols in molecular biology*. **109**, 21.29.1-21.29.9 (2015), doi:10.1002/0471142727.mb2129s109.

202. A. Dobin *et al.,* STAR: ultrafast universal RNA-seq aligner. *Bioinformatics (Oxford, England)*. **29**, 15–21 (2013), doi:10.1093/bioinformatics/bts635.

203. S. Anders, P. T. Pyl, W. Huber, HTSeq–a Python framework to work with high-throughput sequencing data. *Bioinformatics (Oxford, England)*. **31**, 166–169 (2015), doi:10.1093/bioinformatics/btu638.

204. M. I. Love, W. Huber, S. Anders, Moderated estimation of fold change and dispersion for RNA-seq data with DESeq2. *Genome Biol*. **15**, 550 (2014), doi:10.1186/s13059-014-0550-8.

205. H. Wickham, *ggplot2: Elegant Graphics for Data Analysis*, *Create Elegant Data Visualisations Using the Grammar of Graphics*, A system for 'declaratively' creating graphics based on ``The Grammar of Graphics'' (Springer-Verlag New York, New York, NY, 2016).

206. B. Li, C. N. Dewey, RSEM: accurate transcript quantification from RNA-Seq data with or without a reference genome. *BMC Bioinformatics*. **12**, 323 (2011), doi:10.1186/1471-2105-12-323.

207. G. Yu, L.-G. Wang, Y. Han, Q.-Y. He, clusterProfiler: an R package for comparing biological themes among gene clusters. *Omics : a journal of integrative biology*. **16**, 284–287 (2012), doi:10.1089/omi.2011.0118.

208. M. Martin, Cutadapt removes adapter sequences from high-throughput sequencing reads. *EMBnet j.* **17**, 10 (2011), doi:10.14806/ej.17.1.200.

209. A. Tarasov, A. J. Vilella, E. Cuppen, I. J. Nijman, P. Prins, Sambamba: fast processing of NGS alignment formats. *Bioinformatics (Oxford, England)*. **31**, 2032–2034 (2015), doi:10.1093/bioinformatics/btv098.

210. H. M. Amemiya, A. Kundaje, A. P. Boyle, The ENCODE Blacklist: Identification of Problematic Regions of the Genome. *Scientific reports*. **9**, 9354 (2019), doi:10.1038/s41598-019-45839-z.

211. B. Langmead, S. L. Salzberg, Fast gapped-read alignment with Bowtie 2. *Nature methods*. **9**, 357–359 (2012), doi:10.1038/nmeth.1923.

212. H. Li *et al.,* The Sequence Alignment/Map format and SAMtools. *Bioinformatics*. **25**, 2078–2079 (2009), doi:10.1093/bioinformatics/btp352.

213. Y. Zhang *et al.,* Model-based analysis of ChIP-Seq (MACS). *Genome biology*. **9**, R137 (2008), doi:10.1186/gb-2008-9-9-r137.

214. F. Ramírez, F. Dündar, S. Diehl, B. A. Grüning, T. Manke, deepTools: a flexible platform for exploring deep-sequencing data. *Nucleic Acids Res*. **42**, W187-91 (2014), doi:10.1093/nar/gku365.

215. R. A. Policastro, D. J. McDonald, V. P. Brendel, G. E. Zentner, *Flexible analysis of TSS mapping data and detection of TSS shifts with TSRexploreR* (2021).

216. G. Yu, L.-G. Wang, Q.-Y. He, ChIPseeker: an R/Bioconductor package for ChIP peak annotation, comparison and visualization. *Bioinformatics (Oxford, England)*. **31**, 2382–2383 (2015), doi:10.1093/bioinformatics/btv145.

217. V. Hartenstein, Ed., *The development of Drosophila melanogaster* (Cold Spring Harbor Laboratory Press, Plainview, NY, 1993).

218. R Core Team, *R: A language and environment for statistical* (R Foundation for Statistical Computing, Vienna, Austria, 2021).

219. R. Kolde, *pheatmap: Pretty Heatmaps*, Implementation of heatmaps that offers more control (2019).

220. S. Andrews, FastQC: A Quality Control Tool for High Throughput Sequence Data (2010).

221. F. Krueger, *TrimGalore*, A wrapper tool around Cutadapt and FastQC to consistently apply quality and adapter trimming to FastQ files, with some extra functionality for MspI-digested RRBS-type (Babraham institute, Cambridge, CB22 3AT, UK, 2020).

222. Tao Liu (τν) *et al.*, *Taoliu/Macs: Macs2 V2.1.2* (Zenodo, 2018).

223. R. Taylor Raborn Volker P. Brendel Krishnakumar Sridharan, *TSRchitect* (Bioconductor, 2017).

224. S. A. Blythe, E. F. Wieschaus, Zygotic genome activation triggers the DNA replication checkpoint at the midblastula transition. *Cell*. **160**, 1169–1181 (2015), doi:10.1016/j.cell.2015.01.050.

225. B. Liu, J. Grosshans, Link of Zygotic Genome Activation and Cell Cycle Control. *Methods in molecular biology (Clifton, N.J.)*. **1605**, 11–30 (2017), doi:10.1007/978-1-4939-6988-3_2.

226. D. A. Lehman *et al.,* Cis-regulatory elements of the mitotic regulator, string/Cdc25. *Development*. **126**, 1793–1803 (1999), doi:10.1242/dev.126.9.1793.

227. B. Alberts *et al.*, *Molecular Biology of the Cell* (Garland Science, New York, 2015).

228. K. Yuan, C. A. Seller, A. W. Shermoen, P. H. O'Farrell, Timing the Drosophila Mid-Blastula Transition: A Cell Cycle-Centered View. *Trends in Genetics*. **32**, 496–507 (2016), doi:10.1016/j.tig.2016.05.006.

229. A. Hershko, Mechanisms and regulation of the degradation of cyclin B. *Philosophical transactions of the Royal Society of London. Series B, Biological sciences*. **354**, 1571-5; discussion 1575-6 (1999), doi:10.1098/rstb.1999.0500.

230. P. Verma, S. M. Cohen, miR-965 controls cell proliferation and migration during tissue morphogenesis in the Drosophila abdomen. *eLife*. **4** (2015), doi:10.7554/eLife.07389.

231. A. C. Monk *et al.,* HOW is required for stem cell maintenance in the Drosophila testis and for the onset of transit-amplifying divisions. *Cell stem cell*. **6**, 348–360 (2010), doi:10.1016/j.stem.2010.02.016.

232. H. Nabel-Rosen, H. Toledano-Katchalski, G. Volohonsky, T. Volk, Cell divisions in the drosophila embryonic mesoderm are repressed via posttranscriptional regulation of string/cdc25 by HOW. *Current biology : CB*. **15**, 295–302 (2005), doi:10.1016/j.cub.2005.01.045.

233. B. A. Edgar, D. A. Lehman, P. H. O'Farrell, Transcriptional regulation of string (cdc25): a link between developmental programming and the cell cycle. *Development*. **120**, 3131–3143 (1994), doi:10.1242/dev.120.11.3131.

234. G. B. Carvalho, W. W. Ja, S. Benzer, Non-lethal PCR genotyping of single Drosophila. *BioTechniques*. **46**, 312–314 (2009), doi:10.2144/000113088.

235. K. J. Breslauer, R. Frank, H. Blöcker, L. A. Marky, Predicting DNA duplex stability from the base sequence. *Proceedings of the National Academy of Sciences of the United States of America*. **83**, 3746–3750 (1986), doi:10.1073/pnas.83.11.3746.

236. J. SantaLucia, A unified view of polymer, dumbbell, and oligonucleotide DNA nearest-neighbor thermodynamics. *Proceedings of the National Academy of Sciences of the United States of America*. **95**, 1460–1465 (1998), doi:10.1073/pnas.95.4.1460.

237. K. L. Heckman, L. R. Pease, Gene splicing and mutagenesis by PCR-driven overlap extension. *Nat Protoc*. **2**, 924–932 (2007), doi:10.1038/nprot.2007.132.

238. K. Pearson, LIII. On lines and planes of closest fit to systems of points in space. *The London, Edinburgh, and Dublin Philosophical Magazine and Journal of Science*. **2**, 559–572 (1901), doi:10.1080/14786440109462720.

239. S. Jenull, M. Tscherner, T. Mair, K. Kuchler, ATAC-Seq Identifies Chromatin Landscapes Linked to the Regulation of Oxidative Stress in the Human Fungal Pathogen Candida albicans. *Journal of fungi (Basel, Switzerland)*. **6** (2020), doi:10.3390/jof6030182.

240. F. Comoglio *et al.,* High-resolution profiling of Drosophila replication start sites reveals a DNA shape and chromatin signature of metazoan origins. *Cell reports*. **11**, 821–834 (2015), doi:10.1016/j.celrep.2015.03.070.

241. G. Crispatzu *et al.,* The chromatin, topological and regulatory properties of pluripotency-associated poised enhancers are conserved in vivo. *Nat Commun*. **12**, 4344 (2021), doi:10.1038/s41467-021-24641-4.

242. E. Z. Kvon *et al.,* Genome-scale functional characterization of Drosophila developmental enhancers in vivo. *Nature*. **512**, 91–95 (2014), doi:10.1038/nature13395.

243. J. R. Morris, J. L. Chen, P. K. Geyer, C. T. Wu, Two modes of transvection: enhancer action in trans and bypass of a chromatin insulator in cis. *Proceedings of the National Academy of Sciences of the United States of America*. **95**, 10740–10745 (1998), doi:10.1073/pnas.95.18.10740.

244. D. Nicolas, N. E. Phillips, F. Naef, What shapes eukaryotic transcriptional bursting? *Mol. BioSyst.* **13**, 1280–1290 (2017), doi:10.1039/C7MB00154A.

245. S. Schoenfelder, P. Fraser, Long-range enhancer-promoter contacts in gene expression control. *Nat Rev Genet*. **20**, 437–455 (2019), doi:10.1038/s41576-019-0128-0.

246. A. Pombo, N. Dillon, Three-dimensional genome architecture: players and mechanisms. *Nat Rev Mol Cell Biol*. **16**, 245–257 (2015), doi:10.1038/nrm3965.

247. M. A. Willcockson *et al.,* H1 histones control the epigenetic landscape by local chromatin compaction. *Nature*. **589**, 293–298 (2021), doi:10.1038/s41586-020-3032-z.

248. S. Schoenfelder, P. Fraser, Long-range enhancer-promoter contacts in gene expression control. *Nat Rev Genet*. **20**, 437–455 (2019), doi:10.1038/s41576-019-0128-0.

249. A. Bayona-Feliu *et al.,* Histone H1: Lessons from Drosophila. *Biochimica et biophysica acta*. **1859**, 526–532 (2016), doi:10.1016/j.bbagrm.2015.09.001.

250. S. Pennings, G. Meersseman, E. M. Bradbury, Linker histones H1 and H5 prevent the mobility of positioned nucleosomes. *Proceedings of the National Academy of Sciences of the United States of America*. **91**, 10275–10279 (1994), doi:10.1073/pnas.91.22.10275.

251. D. A. Gilchrist *et al.,* Pausing of RNA polymerase II disrupts DNA-specified nucleosome organization to enable precise gene regulation. *Cell*. **143**, 540–551 (2010), doi:10.1016/j.cell.2010.10.004.

252. K. Adelman, J. T. Lis, Promoter-proximal pausing of RNA polymerase II: emerging roles in metazoans. *Nat Rev Genet*. **13**, 720–731 (2012), doi:10.1038/nrg3293.

253. A. E. Rougvie, J. T. Lis, Postinitiation transcriptional control in Drosophila melanogaster. *Molecular and cellular biology*. **10**, 6041–6045 (1990), doi:10.1128/mcb.10.11.6041-6045.1990.

254. N. B. Reppas, J. T. Wade, G. M. Church, K. Struhl, The transition between transcriptional initiation and elongation in E. coli is highly variable and often rate limiting. *Molecular Cell*. **24**, 747–757 (2006), doi:10.1016/j.molcel.2006.10.030.

255. S. H. Chao, D. H. Price, Flavopiridol inactivates P-TEFb and blocks most RNA polymerase II transcription in vivo. *Journal of Biological Chemistry*. **276**, 31793–31799 (2001), doi:10.1074/jbc.M102306200.

256. R. Dollinger, D. S. Gilmour, Regulation of Promoter Proximal Pausing of RNA Polymerase II in Metazoans. *Journal of Molecular Biology*. **433**, 166897 (2021), doi:10.1016/j.jmb.2021.166897.

257. C. Lee *et al.,* NELF and GAGA factor are linked to promoter-proximal pausing at many genes in Drosophila. *Molecular and cellular biology*. **28**, 3290–3300 (2008), doi:10.1128/MCB.02224-07.

258. J. Akhtar *et al.,* Promoter-proximal pausing mediated by the exon junction complex regulates splicing. *Nature communications*. **10**, 521 (2019), doi:10.1038/s41467-019-08381-0.

259. P. Sen *et al.,* H3K36 methylation promotes longevity by enhancing transcriptional fidelity. *Genes & development*. **29**, 1362–1376 (2015), doi:10.1101/gad.263707.115.

260. G. Teano *et al.,* Histone H1 protects telomeric repeats from H3K27me3 invasion in Arabidopsis. *bioRxiv*, 2020.11.28.402172 (2020), doi:10.1101/2020.11.28.402172.

261. A. Kuzmichev *et al.,* Composition and histone substrates of polycomb repressive group complexes change during cellular differentiation. *Proceedings of the National Academy of Sciences of the United States of America*. **102**, 1859–1864 (2005), doi:10.1073/pnas.0409875102.

262. D. P. Teufel, S. M. Freund, M. Bycroft, A. R. Fersht, Four domains of p300 each bind tightly to a sequence spanning both transactivation subdomains of p53. *Proceedings of the National Academy of Sciences of the United States of America*. **104**, 7009–7014 (2007), doi:10.1073/pnas.0702010104.

263. S. Cooper *et al.,* Jarid2 binds mono-ubiquitylated H2A lysine 119 to mediate crosstalk between Polycomb complexes PRC1 and PRC2. *Nature communications*. **7**, 13661 (2016), doi:10.1038/ncomms13661.

264. D. Guardavaccaro, M. Pagano, Stabilizers and destabilizers controlling cell cycle oscillators. *Molecular Cell*. **22**, 1–4 (2006), doi:10.1016/j.molcel.2006.03.017.

265. M. Zhang, P. Kothari, M. Mullins, M. A. Lampson, Regulation of zygotic genome activation and DNA damage checkpoint acquisition at the mid-blastula transition. *Cell Cycle*. **13**, 3828–3838 (2014), doi:10.4161/15384101.2014.967066.

266. C. W. Conn, A. L. Lewellyn, J. L. Maller, The DNA damage checkpoint in embryonic cell cycles is dependent on the DNA-to-cytoplasmic ratio. *Developmental cell*. **7**, 275–281 (2004), doi:10.1016/j.devcel.2004.07.003.

267. P. Jevtić, D. L. Levy, Nuclear size scaling during Xenopus early development contributes to midblastula transition timing. *Current biology : CB*. **25**, 45–52 (2015), doi:10.1016/j.cub.2014.10.051.

268. *Handbook of cell signaling* (Academic Press, San Diego, Calif, 2004).

269. Z. Ali-Murthy, S. E. Lott, M. B. Eisen, T. B. Kornberg, An essential role for zygotic expression in the pre-cellular Drosophila embryo. *PLOS Genetics*. **9**, e1003428 (2013), doi:10.1371/journal.pgen.1003428.

270. V. E. Foe, B. M. Alberts, Studies of nuclear and cytoplasmic behaviour during the five mitotic cycles that precede gastrulation in Drosophila embryogenesis. *Journal of Cell Science*. **61**, 31–70 (1983), doi:10.1242/jcs.61.1.31.

271. M. M. Harrison, M. B. Eisen, in *Current Topics in Developmental Biology : The Maternal-to-Zygotic Transition*, H. D. Lipshitz, Ed. (Academic Press, 2015), vol. **113,** pp. 85–112.

272. W. Tadros *et al.,* Regulation of maternal transcript destabilization during egg activation in Drosophila. *Genetics*. **164**, 989–1001 (2003), doi:10.1093/genetics/164.3.989.

273. A. Bashirullah *et al.,* Joint action of two RNA degradation pathways controls the timing of maternal transcript elimination at the midblastula transition in Drosophila melanogaster. *The EMBO journal*. **18**, 2610–2620 (1999), doi:10.1093/emboj/18.9.2610.

274. C. B. Walser, H. D. Lipshitz, Transcript clearance during the maternal-to-zygotic transition. *Current opinion in genetics & development*. **21**, 431–443 (2011), doi:10.1016/j.gde.2011.03.003.

275. N. Bushati, A. Stark, J. Brennecke, S. M. Cohen, Temporal reciprocity of miRNAs and their targets during the maternal-to-zygotic transition in Drosophila. *Current Biology*. **18**, 501–506 (2008), doi:10.1016/j.cub.2008.02.081.

276. S. Fu, C.-Y. Nien, H.-L. Liang, C. Rushlow, Co-activation of microRNAs by Zelda is essential for early Drosophila development. *Development*. **141**, 2108–2118 (2014), doi:10.1242/dev.108118.

277. S. M. Foo *et al.,* Zelda potentiates morphogen activity by increasing chromatin accessibility. *Current biology : CB*. **24**, 1341–1346 (2014), doi:10.1016/j.cub.2014.04.032.

278. K. N. Schulz *et al.,* Zelda is differentially required for chromatin accessibility, transcription factor binding, and gene expression in the early Drosophila embryo. *Genome Res.* **25**, 1715–1726 (2015), doi:10.1101/gr.192682.115.

279. M. M. Harrison, X.-Y. Li, T. Kaplan, M. R. Botchan, M. B. Eisen, Zelda binding in the early Drosophila melanogaster embryo marks regions subsequently activated at the maternal-to-zygotic transition. *PLOS Genetics*. **7**, e1002266 (2011), doi:10.1371/journal.pgen.1002266.

280. V. O. Sysoev *et al.,* Global changes of the RNA-bound proteome during the maternal-to-zygotic transition in Drosophila. *Nature communications*. **7**, 12128 (2016), doi:10.1038/ncomms12128.

281. T. Rudolph *et al.,* Heterochromatin formation in Drosophila is initiated through active removal of H3K4 methylation by the LSD1 homolog SU(VAR)3-3. *Molecular Cell*. **26**, 103–115 (2007), doi:10.1016/j.molcel.2007.02.025.

282. K. Yuan, P. H. O'Farrell, TALE-light imaging reveals maternally guided, H3K9me2/3-independent emergence of functional heterochromatin in Drosophila embryos. *Genes Dev.* **30**, 579–593 (2016), doi:10.1101/gad.272237.115.

283. L. C. Lindeman *et al.,* Prepatterning of developmental gene expression by modified histones before zygotic genome activation. *Developmental cell*. **21**, 993–1004 (2011), doi:10.1016/j.devcel.2011.10.008.

284. X.-Y. Li, M. M. Harrison, J. E. Villalta, T. Kaplan, M. B. Eisen, "Establishment of regions of genomic activity during the Drosophila maternal to zygotic transition". *eLife Sciences Publications, Ltd*, 14 October 2014 (14.10.2014) (available at https://elifesciences.org/articles/03737).

285. V. V. Senichkin, E. A. Prokhorova, B. Zhivotovsky, G. S. Kopeina, Simple and Efficient Protocol for Subcellular Fractionation of Normal and Apoptotic Cells. *Cells*. **10** (2021), doi:10.3390/cells10040852.

286. G. Lukinavičius *et al.,* Fluorescent dyes and probes for super-resolution microscopy of microtubules and tracheoles in living cells and tissues. *Chemical science*. **9**, 3324–3334 (2018), doi:10.1039/c7sc05334g.

287. C. Horn, E. A. Wimmer, A versatile vector set for animal transgenesis. *Development genes and evolution*. **210**, 630–637 (2000), doi:10.1007/s004270000110.

288. S. J. Gratz *et al.,* Highly specific and efficient CRISPR/Cas9-catalyzed homology-directed repair in Drosophila. *Genetics*. **196**, 961–971 (2014), doi:10.1534/genetics.113.160713.

289. J. Huang, W. Zhou, W. Dong, A. M. Watson, Y. Hong, From the Cover: Directed, efficient, and versatile modifications of the Drosophila genome by genomic engineering. *Proceedings of the National Academy of Sciences*. **106**, 8284–8289 (2009), doi:10.1073/pnas.0900641106.

290. S. Kondo, R. Ueda, Highly improved gene targeting by germline-specific Cas9 expression in Drosophila. *Genetics*. **195**, 715–721 (2013), doi:10.1534/genetics.113.156737.

5 Appendix

5.1 Supplementary Figures

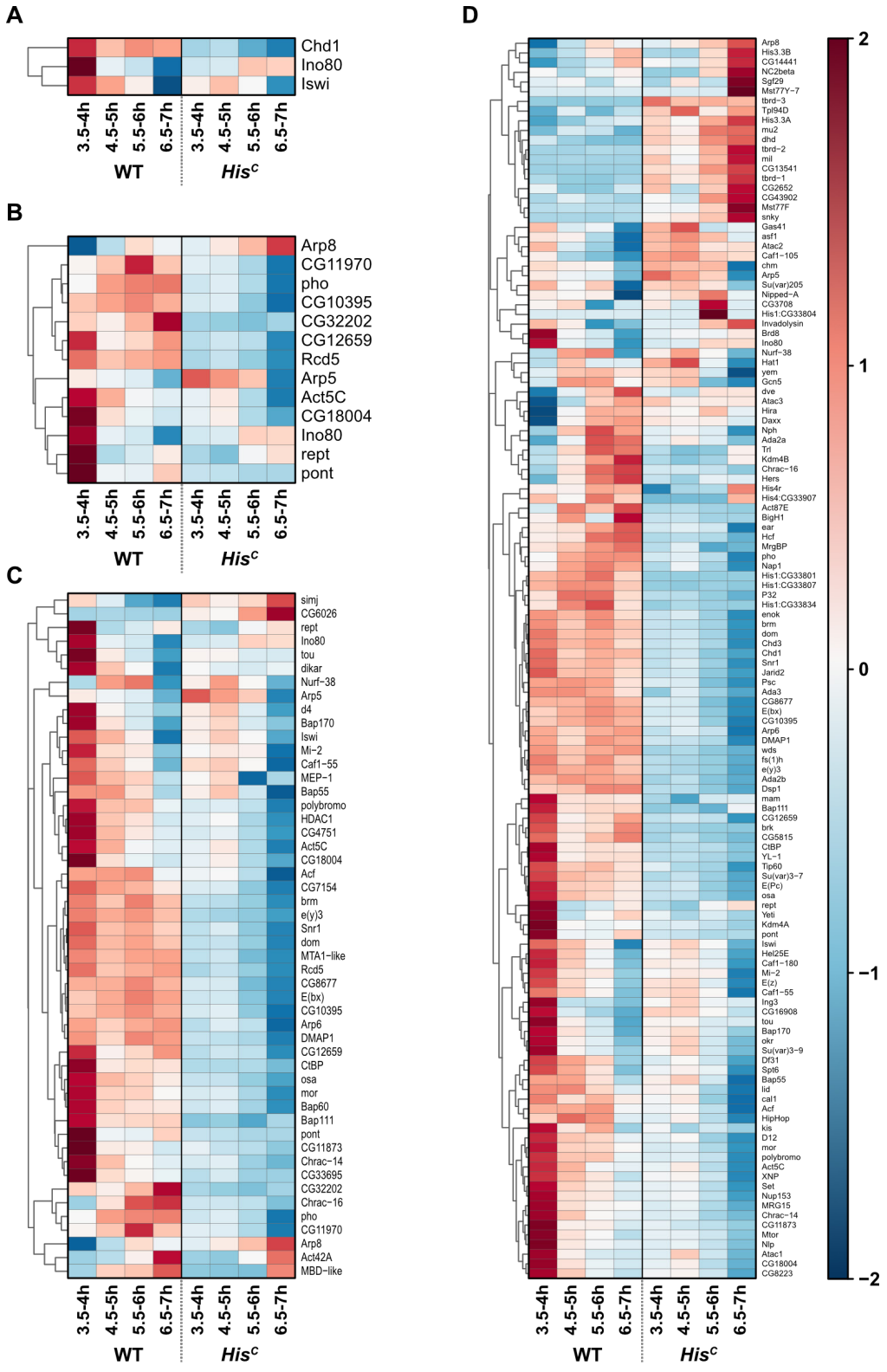

Figure 5.1 Expression of chromatin remodelers in *His^C* Heatmap of RNA-seq expression values (row z-score) of chromatin remodelers (A), GO term "INO80 complex" (B), GO term "SWI/SNF" (C), GO term "Chromatin remoddeling" (D) in wild type and *His^C* mutant embryos.

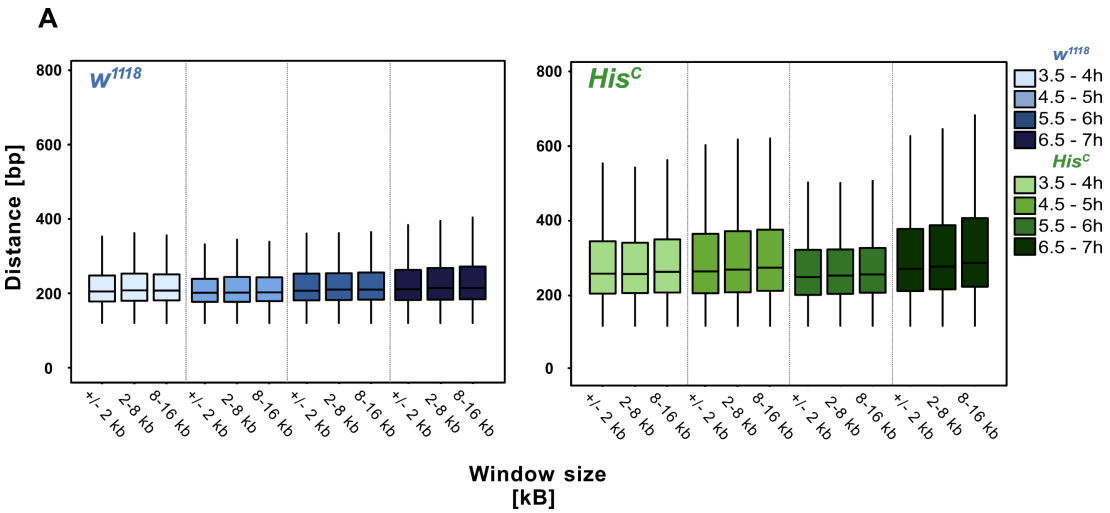

Figure 5.2 Median inter dyad distance at ORCs (A) Median Inter dyad distances in wild type and *His*^{C} mutant embryos 3.5-4h, 4.5-5h, 5.5-6h and 6.5-7h AEL in the indicated regions with regard to the distance to putative ORCs mapped in S2 cells (*240*).

5.2 List of Abbreviations

Δ	Delta/deletion
λ	Wavelength
µg	Microgram
µl	Microliter
µM	Micromolar
aa	Amino acid
Act	Actin
AEL	After egg laying
AF	AlexaFluor®
ATAC-seq	Assay for Transposase-Accessible Chromatin using seq.
bp	Base pairs
BLAST	Basic local alignment and search tool
BSA	Bovine serum albumin
Cas9	CRISPR associated protein 9
Cdc	Cell division cycle
cDNA	complementary DNA
Cdk	Cyclin dependent kinase
CDS	Coding Sequence
Chk	Chicken (Gallus gallus)
CNS	central nervous system
COMPASS	Complex proteins associated with Set1
CTD	C-terminal domain
CUT&Tag	Cleavage Under Targets and Tagmentation
CUTAC	Cleavage Under Targets Accessible Chromatin
CRISPR	Clustered Regularly Interspaced Palindromic Repeats
cRNA	CRISPR RNA
Cyclin B	Cyclin B
CyO	*CurlyO*
D	*Dicheate*
DAPI	4',6-Diamidino-2-phenylindol
DEG	Differentially expressed genes
DIG	Digoxigenin
DNA	Deoxyribonucleic acid
DSB	Double strand break
dsDNA	double stranded DNA
DTT	Dithiothreitol
EDTA	Ethylenediaminetetraacetic acid
e.g.	*Exempli gratia* = for example
eGFP	enhanced green fluorescent protein
eYFP	enhanced yellow fluorescent protein
EtOH	Ethanol
Fig.	Figure
fluo	Fluorescein

ftz	*fushi-tarazu*
fw/fwd	Forward
GO	Gene ontology
gDNA	Genomic deoxyribonucleic acid
gRNA	Guide ribonucleic acid
Gt	Goat
h	Hours
H(1/2A/2B/3/4)	Histone (1/2A/2B/3/4)
H2AK9ac	Histone 2A lysine 9 acetylation
H2AK16ac	Histone 2A lysine 16 acetylation
H2AK120ubi	Histone 2A lysine 120 ubiquitination
H3K4me1	Histone 3 lysine 4 mono-methylation
H3K4me2	Histone 3 lysine 4 di-methylation
H3K4me3	Histone 3 lysine 4 tri-methylation
H3K9me3	Histone 3 lysine 9 tri-methylation
H3K27me3	Histone 3 lysine 27 tri-methylation
H3K27ac	Histone 3 lysine 27 acetylation
H3K36me3	Histone 3 lysine 36 tri-methylation
H4K16ac	Histone 4 lysine 16 acetylation
H4R3me2	Histone 4 arginine 3 di-methylation (symmetrical)
HAT	Histone acetyl transferase
HDAC	Histone deacetylase
HeLa	Human epithelia cell line; donor: Henrietta Lacks
Hi-C	Chromosome confirmation capture technique (all vs. all)
How	Held-out-wings
HMT	histone methyl transferase
Hybe	Hybridization buffer (A/B)
HRP	Horseradish peroxidase
IgG	Immunoglobulin G
ISH/WMISH/FISH	*In situ* hybridization/Whole mount *In situ* hybridization
kb	Kilo base pairs
kDa	Kilo Dalton
KMT	Lysine methyl transferase
LacB	beta-galactosidase
LAD	Lamina associating domain
LB	Lysogeny broth
M	Molar (mol/litre)
Mb	Mega bases
MeOH	Methanol
MEF	Mouse embryonic fibroblast
mESC	Mouse embryonic stem cell
min	Minute
MINCE-seq	mapping *In vivo* Nascent Chromatin with EdU and sequencing
Mm	mouse (mus musculus)
mM	Millimolar (mmol/l)

mm	Millimetre
NC	Nuclear cycle
NCC	nascent chromatin capture
mRNA	Messenger ribonucleic acid
NDR	Nucleosome depleted region
NELF	Negative elongation factor
NHEJ	Non-homologous end joining
NHR	Non-homologous recombination
NLS	Nuclear localization signal
Nuc	Nucleosome
ORC	Origin of replication
ORF	Open reading frame
OE	Overexpression
Oligos	Oligonucleotides
o/n	Overnight
PAM	Protospacer adjacent motif
PBS	Phosphate buffered saline
PCA	Principle component analysis
PC1	Principle component 1
PC2	Principle component 2
PCR	Polymerase chain reaction
PIC	pre initiation complex
POD	Peroxidase (here: horse-radish)
prd	*paired*
pre-EJC	Nuclear exon junction complex
PTM	Post translational modification
q	Quartile, quintile
qRT-PCR	Quantitative real time polymerase chain reaction
Rb	Rabbit (Oryctolagus cuniculus)
rv/rev	reverse
RNA	Ribonucleic acid
RNAPII	RNA polymerase II
RNAPIIS2P	RNA polymerase II serine 2 phosphate
RNAPIIS5P	RNA polymerase II serine 5 phosphate
RT	Room temperature
rpm	Revolutions per minute
S2P	Serine 2 phosphate
S5P	Serine 5 phosphate
Sb	*Stubble*
SDS	Sodium dodecyl sulphate
Ser	*Serrate*
SGD	Salt gradient dialysis
SILAC	Stable Isotope Labelling by Amino acids in Cell culture
Sp	*Sternoplural*
ssDNA	Single stranded DNA

STRIPE-seq	Survey of Transcription Initiation at Promoter Elements with high-throughput sequencing
Tab.	Table
TAD	Topologically associating domain
TES	Transcription end site
TF	Transcription factor
tMAC	testis-specific meiotic arrest complex
TSR	Transcription start region
TSS	Transcription start site
tracrRNA	Trans-activating crRNA
twi	*twist*
UAS	Upstream activating sequencing
Ubx	*Ultra-bithorax*
UTR	Untranslated region
v/v	Volume per volume
Wt	Wild type
w/o	without
w/v	Weight per volume

5.3 List of Figures

5.4 List of Tables

5.5 Methods

In this section all methods are described that are not outlined in chapter I or II.

5.5.1 Polymerase chain reaction (PCR)

5.5.1.1 General PCR

To amplify fragments from plasmids, genomic DNA, complementary DNA or PCR products, for subsequent cloning, genotyping, or sequencing, polymerase chain reaction was performed. For PCR thermostable *Phusion* DNA Polymerase (Thermo Fisher Scientific Inc., Karlsruhe, Germany), *Advantage2taq* DNA Polymerase (Takara Holdings, Kyoto, Japan) or *taq* DNA polymerase (Thermo Fisher Scientific Inc., Karlsruhe, Germany) was used. PCRs were set up as described by the respective manufacturer (Table 17). Standard PCR was programmed as followed (Table 18).

Table 17 Standard PCR mix. Phu, Advantage 2 taq, or taq DNA polymerase were used with the corresponding buffer system.

Component	50µL Reaction	25µL Reaction	Final concentration
H_2O	To 50µL	To 25µL	
Buffer (5xHF, 10x *taq*)	10µL/5µL	5µL/2.5µL	1x
dNTPs (25µM)	2.5µL	1.25µL	200nM
Forward Primer (10 µM)	2.5µL	1.25µL	500nM
Reverse Primer (10µM)	2.5µL	1.25µL	500nM
Template	variable	variable	1ng to 200ng 1ng to 1µg
Phusion/taq/Advantage2 taq Polymerase	0.5µL/0.25µL/0.25µL	0.2µL/0.125µL/0.125µL	
DMSO/BSA (optional)	1.5µL to 5µL	0.75µL to 2.5µL	3% to 10%

Optimal annealing temperatures were calculated using the NEB Tm calculator (http://tmcalculator.neb.com/#!/) for each polymerase, respectively. For amplification from genomic DNA or in case of low product yield, DMSO or BSA were added in concentrations ranging from 3% and 10%. For every 3% DMSO the annealing temperature was lowered by 3°C. If not indicated otherwise, all PCRs used subsequently for cloning were purified by gel electrophoresis and gel extraction.

Table 18 Standard PCR program. Phu polymerase was used at 98°C and 72°C, Taq polymerase at 95°C and 68°C respectively.

Step	Temperature	Duration
Initial denaturation	95°C/98°C	2 minutes
Denaturation [35x]	95°C/98°C	15 seconds
Annealing	variable	15 seconds
Extension	68°C/72°C	45 seconds per kb (*taq*) 15 seconds per kb (*Phu*)
Final extension	68°C/72°C	5 minutes
Hold	8°C	∞

5.5.1.2 Overlap extension PCR

Overlap extension PCR was performed as described by (*237*). Basic conditions for overlap extension PCR were set as described for standard PCR (Table 18). The first 5 cycles were conducted without outer primer oligos and with decreased ramp speed (1°C/s). The annealing temperature for the overlapping regions was calculated using the nearest-neighbour method (*236*) embedded in Geneious prime v2020.1.1 or using the NEB Tm calculator (http://tmcalculator.neb.com/#!/). For the remaining 30 cycles, outer primers were added to the PCR.

5.5.1.3 Colony PCR

Colony PCR was performed to identify positive clones and fragment orientation using primers which are insert or plasmid specific or a combination thereof. Using a white pipette tip, sample of a single clone was transferred into a PCR tube before adding the PCR master mix. PCR conditions were set as described (Table 17 and Table 18). The initial denaturation was prolonged to 10 minutes. For each ligation, 16 to 32 clones were tested.

5.5.1.4 Touchdown/up-, Ramp-, Gradient PCR

To increase specificity, determine optimal annealing temperature or to increase efficiencies, touchdown/up-, ramp-, or gradient PCR were used. Gradient PCR was conducted with increasing annealing temperatures ranging from -10°C to +10°C with regard to the optimal primer annealing temperature calculated by nearest-neighbour method (*236*) embedded in Geneious prime v2020.1.1. Ramp down PCR done by decreasing the temperature delta per step from 3°C/s (standard) to 0.5°C or 1°C per second. Touchdown PCR was especially used to increase specificity. The annealing temperature was gradually reduced (1-2°C per cycle) starting 10°C degrees higher than optimal annealing temperature. PCR conditions were set as described (Table 17).

5.5.1.5 Nested PCR

Nested PCR was performed in case a previous PCR showed inconclusive results. The locus was first amplified with primers binding regions outside of the locus of interest. The PCR product was subsequently used as a template for PCR using specific primers. Aside from these considerations the PCRs were conducted as described (Table 17 and Table 18).

5.5.1.6 Quantitative real-time polymerase chain reaction (qRT-PCR)

cDNA was generated using QuantiTect Reverse Transcription kit (Qiagen) with 50ng of input RNA. qPCR (quantitative Real-Time PCR) was performed using KAPA SYBR FAST master mix (2x) adjusting the reaction volume to 8µl (Table 20). (Kapa Biosystems). Primers were designed using NCBI primer blast tool (https://www.ncbi.nlm.nih.gov/tools/primer-blast/) with primers spanning exon-exon junctions using settings described in Table 19. Relative gene expression was analysed using the comparative ΔΔCt method using *act5C* for normalization (*198*).

Table 19 Settings for qRT-PCR primer design

Parameter	Setting
PCR product size	100 bp
Tm	60°C
Exon junction span	Primer must span exon-exon junction
Intron length	500 to 100000bp
Intron inclusion	No
Max product size	110bp
Max Tm difference	1°C
Allow splice variants	No

Table 20 General qRT-PCR reaction set up

Reagent	Volume (total 8µl)
KAPA SYBR® FAST	4µl
Forward Primer	0.16µl
Reverse Primer	0.16µl
cDNA	2µl
H_2O	1.68µl

To determine optimal cDNA input, dilution rows ranging from 1:100 to 1:5000 were used. Final cDNA concentrations were chosen resulting in C_t[*act5C*] close to 20. Primer efficiencies were calculated by linear regression and different cDNA inputs. To facilitate convenient pipetting, the volume of cDNA was pre adjusted to 2µl per reaction. Each gene was evaluated

at least in quadruplicates for *His*^{C} mutants as well as wild type *w*^{1118} control embryos. Cycle settings were set as described in the following table.

Table 21 General qRT-PCR cycler set up

Step	Temperature	Duration
Enzyme activation	95°C	3 minutes
Denaturation [40x]	95°C	3 seconds
Annealing/extension	60°C	20 seconds
Dissociation		

5.5.1.7 Restriction digest of plasmid DNA and PCR fragments

For preparative restriction digests 1µg to 2µg vector were used (50µl reaction), whereas for analytical purposes the amount was reduced to 0.5µg to 1µg of DNA (25µl reaction). The reactions were incubated for 60 minutes at the respective temperatures or overnight at RT. In case, double digests were performed using restriction enzymes with different temperature optima, the reaction vial was incubated twice for 30 minutes starting with the enzyme requiring the lower temperature. In case a double digest was performed using restriction enzymes requiring different buffers, a master buffer was prepared mixing both buffers in a 1:1 ratio.

Table 22 Standard restriction digest mix. Buffer, temperature, and incubation time were chosen considering the enzymes requirements.

Component	50µL reaction	25µL reaction
H_2O	to 50µL	to 25µL
10x CutSmart buffer (NEB) or as required	5µL	2.5µL
Enzyme 1	1µL	0.5µL
Enzyme 2	1µL	0.5µL
Template	1 - 2µg	<1µg

5.5.2 DNA isolation

5.5.2.1 Isolation of genomic DNA

To isolate genomic DNA from adult individuals, ~10 flies were anesthetized and transferred into a 1.5ml Eppendorf cup, containing 250µl HOM buffer (Tris HCl 0.1M (pH 9.0), EDTA 0.1M, SDS 1%), 1µl Protease K (14mg/ml) as well as RNase A (20µg/ml). The flies were macerated with a Dounce homogenizer (Bio-Trend, 1984-10002) and digested for 30 minutes at 70°C. 35µl of 8M KAc were added, mixed, and subsequently incubated on ice for

another 30 minutes. The vials were centrifuged for 15 min at 16000g to precipitate debris. The supernatant was transferred into a clean vial and mixed with 1x volume of phenol-chloroform-IAA (25:24:1) and vortexed. The vials were centrifuged at 16000g for 5 minutes. The aqueous phase was transferred into new 1.5ml Eppendorf cup. These steps were repeated three times. To precipitate the DNA, 0.1x volume 7.8M NH_4Ac and 0.7x volume ice cold isopropanol were added and mixed. The vials were centrifuged at 16000g and 4°C for 20 minutes. The supernatant was discarded, and the pellet washed with 300µl of 70% ethanol. The pellet was air dried and resuspended in 50µl TE buffer.

5.5.2.2 Isolation and purification of plasmid-DNA and linearized DNA fragments

To isolate plasmid DNA, a liquid culture was inoculated with the clone of interest and incubated overnight at 37° under slight agitation. Bacterial cells were harvested by centrifugation and digested by alkaline lysis. All cell debris and genomic DNA was precipitated and discarded, while plasmid DNA was recovered from the supernatant as described below.

For subsequent cloning and transfection, plasmid DNA was isolated using the Macherey-Nagel NucleoSpin® Plasmid kit (Macherey-Nagel, 740588.50) or NucleoSpin® Plasmid transfection grade kit (Macherey-Nagel, 740490.50). All steps were performed as described in the manufacture's manual.

For higher DNA concentrations plasmid midi preps were performed using QIAprep® Spin Midi Plus Kit (Qiagen, 12941).

For analytical purposes alkaline lysis was performed. Bacteria were grown in 4 ml LB media overnight. The cells were harvested by centrifugation for 30s at 9000g. The supernatant was discarded, and the pellet resuspended in 100µl GTE buffer (50mM glucose, 25mM Tris pH 8.0, 10mM EDTA, RNase A 1:100). 200µl Alkali-SDS solution (0.2N NaOH, 1% SDS) was added followed by quickly inverting the reaction vials three to four times. The samples are incubated for 4 minutes, debris and DNA was precipitated by adding 150µl 5M NaOAc. The tubes were centrifuged for 10 minutes at 16 000g, the supernatant was transferred into new Eppendorf tube. The DNA is precipitated by adding 750µl 100% ethanol and 0.1x volume NH_4Ac followed by centrifugation at 16000g for 10 minutes. The pellet was washed with 750µl 70% ethanol followed by centrifugation at 16000g for 5 minutes. The supernatant was removed and the pellet air dried. Plasmid DNA was resuspended in 50µl TE buffer. For higher DNA concentrations, 25ml LB media was inoculated and incubated. Buffers were adjusted to the corresponding volume. All centrifugation steps were prolonged to 30 minutes at

10000g and 4°C. After adding sodium acetate, the culture is additionally incubated on ice for 10 minutes. After centrifugation, the supernatant is passed through a fluted filter. Plasmid DNA is precipitated with 0.7x volume of isopropanol and 0.1x volume NH_4Ac. The pellet was washed twice with 70% ethanol and dissolved in 100µl TE buffer.

5.5.2.3 Phenol chloroform extraction

Protein extraction was conducted by adding an equal volume of 13% PEG-8000/1.6M NaCl to the cleared lysate after alkaline lysis or to dissolved DNA and incubated on ice for at least 1 hour. The sample was centrifuged at 16000g for 20 minutes. The pellet was washed with 70% ice-cold ethanol, dried and dissolved 200µl TE buffer and transferred to an Eppendorf cup. Proteins were extracted twice by adding 1x volume phenol-chloroform-IAA (25:24:1). The samples were vortexed vigorously to extract proteins. For phase separation the samples were centrifuged at 5000g for 5 min. The aqueous phase was transferred into a new vial. To remove residual phenol, 1x volume of chloroform, isoamyl alcohol (24:1) was added, vortexed and centrifuged. The plasmid or genomic DNA was precipitated by adding 0.1x volume sodium acetate and 0.7x volume isopropanol. Incubation for 10 minutes was followed by centrifugation at 16000g for 20 minutes at 4°C. The pellet was washed with ice-cold 70% ethanol and dissolved in 50µl TE buffer.

5.5.3 Protein methods

5.5.3.1 Protein isolation from subcellular fractioning

For isolation of proteins localized in different cellular compartments subcellular fractioning was performed. To this purpose, either Subcellular Protein Fractionation for Cultured Cells kit (Thermo Fisher, 78840) was used as described by the manufacturer or proteins were isolated as described by (*285*). As Input for the former, wild type and *His^C* embryos were macerated in ice-cold PBS with a loose-fitting pestle in a pre-cooled 1ml Dounce homogenizer (Bio-Trend, 1984-10002) and subsequently centrifuged at 2000g at 4°C for 5 minutes to pellet cells. The supernatant was discarded, and the pellet recovered in ice cold CEB. The remaining protocol was conducted as described by the manufacturer.

For the latter the wild type and *His^C* embryos were transferred into a pre-cooled Dounce homogenizer (Bio-Trend, 1984-10002), layered with 50µl hypotonic buffer (20mM Tris-HCl pH 7.4, 10mM KCl, 2mM $MgCl_2$, 1mM EGTA, 0.5mM DTT, 0.5mM PMSF) and subsequently macerated with a loose-fitting pestle to disrupt the tissue. The volume was increased to 100µl with hypotonic buffer and the suspension was transferred into a clean tube. The cells were incubated for 3 minutes on ice. Membranes were lysed by adding NP-40 to a final concentration of 0.1%, the samples were incubated for 3 minutes on ice followed by

centrifugation at 4°C and 1000g for 5 minutes to separate nuclei from cytoplasmic components. The supernatant was transferred into a clean tube and centrifuged at 15,000g and 4°C for 3 minutes. The debris free supernatant was transferred to a clean tube representing the cytoplasmic fraction. The nuclei pellet was recovered in 100µl isotonic buffer (20mM Tris-HCl pH 7.4, 150mM KCl, 2mM $MgCl_2$, 1mM EGTA, 0.5mM DTT, 0.5mM PMSF, 0.1% NP-40) and incubated for 10 minutes on ice followed by centrifugation at 1000g and 4°C for 3 minutes. After washing, the nuclei were incubated 30 minutes on ice in 100µl ice-cold RIPA buffer and then centrifuged at 2000g for 3 minutes at 4°C. The supernatant was transferred into a clean tube representing the soluble nuclear fraction. The pellet was washed once in PBS and dissolved in DNase buffer (20mM Tris-HCl pH 7.4, 100mM NaCl, 42mM $MgCl_2$, 1mM $CaCl_2$, 0.5mM DTT, 0.5mM PMSF, 1% NP-40). DNA was digested with DNase I for 30 minutes on ice. All fractions were diluted with 4x Laemmli and stored at -20°C.

5.5.4 Microscopy and Imaging

5.5.4.1 RNA probe preparation

RNA *in situ* probes were designed to cover roughly 800 to 1200 bp of the CDS of the gene of interest. Larger probes generally increase signal strength while shorter probes readily penetrate the sample tissue. Short introns, up to 200bp, were incorporated into the probe if necessary. A PCR fragment was amplified from the targeted locus using reverse primer adding a T7-promotor (GAA TTG TAA TAC GAC TCA CTA TAG G) overhang to the fragment. This fragment was used as template for reverse transcription.

For frequently used probes the PCR amplicon was cloned into pJET1.2. The orientation of the insert was proven by PCR using an insert specific primer and a pJET1.2_rev sequencing primer. Depending on the orientation the pJET1.2 intrinsic T7 promotor can be used, or the insert can be amplified by using the pJET-T7-fwd/rev primer to create a PCR product with a T7 promotor overhang.

In vitro transcription was conducted using the T7 polymerase (Roche, 10881775001), as well as Dig- or Fluo-labelling mix (Roche, 11277073910) and Protector RNAse Inhibitor (40U/µl; Roche, 3335399001) (Table 23).

Table 23 Standard T7 RNA polymerase reaction mix for RNA probe preparation

Component	Volume/Mass
DEPC-H_2O	To 10µl
10x Buffer	1µl
Dig/Fluo labelling mix	1µl

Component	Volume/Mass
RNAsin (40U/µl)	0.5µl
T7 Polymerase	1µl
PCR product/linearized plasmid	150-250ng/500ng

The reaction was incubated for 2 hours at 37°C and subsequently diluted 1:5 adding 40µl of DEPC-H_2O or RNase free water. As control, 5µl diluted probe and 25ng of PCR template are loaded onto a gel, the probe should appear approximately 10 times stronger. The probe is precipitated as described in 5.5.2.1 and resuspended in 50µl resuspension buffer (50% formamide, 0.1% Tween-20, 5x SSC pH5, Heparin 20µg/µl).

5.5.4.2 Whole mount *in situ* hybridization

Single or double fluorescent *in situ* hybridization was conducted to visualize gene expression in 3 to 6 hours old *Drosophila melanogaster* embryos as described by (*199*).

5.5.4.3 Immunostaining

Wild type and His^C embryos were rehydrated by washing 3 times with decreasing MeOH concentrations (75%, 50%, 25% v/v) and subsequently washed with PBS-T 3 times for 15 minutes. The samples were blocked in BSA (5% BSA, 0.02% sodium azide, 0.1% Triton-X) for at least 1 hour at room temperature. Primary antibodies were mixed with an equal volume of glycerol and stored at -20°C. Primary antibodies were incubated 1:1000 if not noted otherwise at 4°C over-night on a rotator. Before adding a second primary antibody the samples were washed 3 times with PBS-T for 15 minutes. Species matched secondary antibodies were incubated 1:1000 if not noted otherwise for 2 hours at room temperature while protected from light. DNA was visualized by incubation 15 minutes with DAPI 1:1000 or 1 hour with 5-Sir-Hoechst 1:5000 or CP-580-Hoechst 1:1000 (*286*).

5.5.4.4 Mounting

Embryos were mounted onto objects slides previously prepared with sticky paper rings to avoid crushing of the embryos by slightly elevating the cover slip. As mounting media VectaShield (Biozol, VEC-H-1200) or self-made DAPCO anti fade mounting medium were used. The samples were sealed with transparent nail polish and stored at -20°C.

5.5.5 Cloning techniques

5.5.5.1 Agarose gel electrophoresis

Gel electrophoresis was used to separate and purify DNA fragments after PCR or restriction digest. Depending on fragment size 0.8% to 1.5% agarose gels were prepared by dissolving the corresponding amount of agarose in TAE buffer (2mM Tris-Acetate, 20mM Na-Acetate, 2mM EDTA, pH 8.3). For DNA visualization 1:200000 Serva StainG (Serva, 39803.01) was added prior to agarose polymerization. Samples were mixed with 2µl 6x DNA Loading Dye (Bromophenol Blue, Xylene Cyanol FF, NEB) and mounted onto the gel. Fragments were separated applying voltages ranging from 80V to 100V. The gels were analysed using UV trans-illuminator emitting light at λ = 254nm or a blue light transilluminator. Fragments were extracted using the Macherey-Nagel NucleoSpin® Gel and PCR Clean-up kit (Macherey-Nagel, 740609.50)

5.5.5.2 Ligation

PCR amplicons or DNA fragments with blunt or sticky ends were ligated into plasmids using T4 DNA ligase (NEB, M0202S). For this purpose, the ligation reaction was incubated overnight at 16°C following the manufacturers protocol, see also Table 24. Depending on the size of the insert and the vector, appropriate insert: vector ratios ranging from 2:1 to 5:1 were calculated using the NEBioCalculator (http://nebcloner.neb.com/#!/).

Table 24 Standard ligation mix. The insert to vector ratio ranged from 1 to 3 to 1 to 5. The ligations were always conducted o/n at 16°C.

Component	Volume	Final concentration
H_2O	to 20µL	
10x T4 DNA ligase Buffer (NEB)	2µL	1x
Vector	variable	variable
Insert	Variable	variable
T4 DNA ligase	1µL	20U/µL

5.5.5.3 Transformation of bacteria

Ligation reactions were briefly centrifuged. 5µL ligation were added to 50µl chemically competent *E. coli* DH5α cells (NEB, C2987H) and mixed gently using a white pipette tip and incubated on ice for 30 minutes. The cells were heat shocked for 45 seconds at 42°C and immediately transferred back on ice and incubated for 5 minutes. 950µl prewarmed LB medium without antibiotic were added and the cells then incubated at 37°C and 225 rpm for one hour using a thermomixer. 150µl (50µL for re-transformations) of the transformation

reaction were spread onto a prewarmed LB agar plate containing ampicillin and incubated overnight at 37°C. Remaining bacteria were centrifuged and resuspended in 150µl LB medium to allow plating of all remaining bacteria on a second agar plate. Blue-white staining was done by spreading 40µl X-Gal onto the agar plate prior to inoculation with transformed DH5α cells.

5.5.5.4 Cultivation of DH5α e. coli cells

For plasmid preparation transformed *Escherichia coli* DH5α (NEB, C2987H), cells were cultivated in lysogeny *broth* (LB) medium (10 g/l tryptone, 5 g/L yeast extract, 10 mM NaCl) at 37°C at 225 rpm for 12 to 14 hours containing 0.1 % ampicillin.

5.6 Resources

5.6.1 Chemicals

Kits used for DNA or RNA isolation, plasmid preparation, gel extraction and *in vitro* transcription were purchased from Macherey-Nagel (Düren, Germany), Qiagen (Hilden, Germany) and F. Hoffmann-La Roche AG (Basel, Switzerland).

Enzymes and corresponding commercial buffers were purchased from F. Hoffmann-La Roche AG (Basel, Switzerland), New England Biolabs (Frankfurt am Main, Germany), Thermo Fisher Scientific/Invitrogen (Waltham, Massachusetts, USA) and Takara Holdings (Kyoto, Japan).

Table 25 Supplier for chemicals

Company	Head office
AppliChem	Darmstadt, Germany
Fluka	Neu-Ulm, Germany
Merck	Darmstadt, Germany
Carl Roth GmbH & Co. KG	Karlsruhe, Germany
Serva	Heidelberg, Germany
Sigma Aldrich Chemie GmbH	Steinheim, Deutschland
VWR International GmbH	Darmstadt, Germany

5.6.2 Antibodies

The following antibodies were used for FISH, IF, Western Blot, NGS, and CoIP.

Table 26 Antibodies

Antibody	Cat. No.	Manufacturer
α-H3K4me2	39142	Active Motif
α-H3K4me2	39142	Active Motif
α-H3K4me3	91264	Active Motif
α-H3K9me3	39766	Active Motif
α-H3K9me3	39162	Active Motif
α-H3K27me3	39157	Active Motif
α-H3K27ac	39134	Active Motif
α-H3K36me3	61102	Active Motif
α-H4K16ac	39168	Active Motif

Antibody	Cat. No.	Manufacturer
α-H2BK120ubi	39624	Active Motif
α-H4R3me2S	61188	Active Motif
α-H2Ak9ac	39110	Active Motif
α-H2Ak16ac	39122	Active Motif
α-RNAPII	61668	Active Motif
α-RNAPIIS2P	61084	Active Motif
α-H1	61786	Active Motif
α-H2B	39238	Active Motif
α-H2B	52484	Abcam
α-H3	61800	Active Motif
α-H3.3	91192	Active Motif
α-H2Av	39715	Active Motif
α-Hp1	39296	Active Motif
α-RB-488	A11070	Invitrogen/ThermoFisher
α-RB-555	A21430	Invitrogen/ThermoFisher
α-RB-647	A21245	Invitrogen/ThermoFisher
α-Mn-488	A11017	Invitrogen/ThermoFisher
α-Mn-555	A21425	Invitrogen/ThermoFisher
α-Mn-647	A21235	Invitrogen/ThermoFisher
α-Chk-488	A11039	Invitrogen/ThermoFisher
α-Chk-555	A21437	Invitrogen/ThermoFisher
α-Chk-647	A21449	Invitrogen/ThermoFisher
α-Dig-POD	11207733910	Roche
α-Fluo-POD	11426346910	Roche
α-rabbit IgG	6702	Abcam
α-mouse IgG	6709	Abcam
α-Cyclin B	2245815	Hybridoma Bank
α-*string*	n.a.	Eric Wieschaus, Princeton University, USA
α-mst77f	n.a.	Benjamin Loppin, ENS de Lyon, France
α-ProtB	n.a.	Benjamin Loppin, ENS de Lyon, France
α-LacZ	n.a.	Gerd Vorbrüggen, MPI-NAT, Germany
α-GFP	n.a.	Marita Büscher, Georg-August University, Germany
α-How	n.a.	Talila Volk, Weizmann Institute, Israel
α-mouse-HRP	7076	CellSignaling
α-rabbit-HRP	7074	CellSignaling

5.6.3 Stocks

Fly stocks were kept in duplicates at 18°C under permanent light conditions and flipped every 4 weeks with a shift of 2 weeks between duplicates. After four weeks the empty stock vials were discarded. To increase vitality of the flies, dried yeast and a filter paper were provided and the number of flies per vial was restricted to a reasonable size. The following lines were used during the thesis.

Table 27 Fly stocks

Stock Number	Genotype
DM1	*Df(2L)His^{C} / CyO, P{ftz-lacB}E3*
DM2	*Df(2L)His^{C} / CyO, Act-GFP*
DM3	*Df(2L)His^{C}, P{UAS:eYFP}AH2/ CyO, P{ftz-lacB}E3*
DM4	*Df(2L)His^{C}, P{GAL4-twi.2xPE}/ CyO, P{ftz-lacB}E3*
DM5	*Df(2L)His^{C} / CyO, P{ftz-lacB}E3; D / Sb, P{Ubx-lacB}E3*
DM6	*Df(2L)His^{C} / CyO, Act-GFP ; D / Ser, Act-GFP*
DM9	Sp / *CyO, P{ftz-lacB}E3; D / Sb, P{Ubx-lacB}E3*
DM10	Sp / *CyO, Act-GFP ; D / Ser, Act-GFP*
DM11	*Df(2L)His^{C} / CyO, P{ftz-lacB}E3; p(prd-Gal4) / Sb, P{Ubx-lacB}E3*
DM12	*Df(2L)His^{C}, UAS:HspA-stg-3'stgUTR / CyO, P{ftz-lacB}E3; D / Sb, P{Ubx-lacB}E3*
DM13	*Df(2L)His^{C}, UAS:5'stgUTR-stg-Sv40 / CyO, P{ftz-lacB}E3; D / Sb, P{Ubx-lacB}E3*
DM14	*Df(2L)His^{C}, UAS:HspA-stg-3'stgUTR / CyO, Act-GFP ; D / Ser, Act-GFP*
DM15	*Df(2L)His^{C}, UAS:5'stgUTR-stg-Sv40 / CyO, Act-GFP ; D / Ser, Act-GFP*
DM16	*Df(2L)His^{C} / CyO, P{ftz-lacB}E3; UAS:HspA-stg-3'stgUTR / Sb, P{Ubx-lacB}E3*
DM17	*Df(2L)His^{C} / CyO, P{ftz-lacB}E3; UAS:5'stgUTR-stg-Sv40 / Sb, P{Ubx-lacB}E3*
DM18	*Df(2L)His^{C} / CyO, Act-GFP ; UAS:HspA-stg-3'stgUTR / Ser, Act-GFP*
DM19	*Df(2L)His^{C} / CyO, Act-GFP ; UAS:5'stgUTR-stg-Sv40 / Ser, Act-GFP*
DM20	*Df(2L)His^{C}, UAS:5'stgUTR-eYFP-Sv40 / CyO, P{ftz-lacB}E3; D / Sb, P{Ubx-lacB}E3*
DM21	*Df(2L)His^{C}, UAS:5'stgUTR-eYFP-Sv40 / CyO, Act-GFP ; D / Ser, Act-GFP*
DM22	*Df(2L)His^{C}, UAS:5'stgUTR-stg-3'stgUTRΔhow / CyO, P{ftz-lacB}E3 ; D / Sb, P{Ubx-lacB}E3*
DM23	*Df(2L)His^{C}, UAS:5'stgUTR-stg-3'stgUTRΔhow / CyO, Act-GFP ; D / Ser, Act-GFP*
DM24	*Df(2L)His^{C}/CyO, P{ftz-lacB}E3;p(prd-Gal4)/Sb,Ubx-lacZ*

5.6.4 Oligo sequences and Vectors

All primers and Oligonucleotides used, were purchased from Eurofins Genomics GmbH (Ebersberg, Germany) and Integrated DNA Technologies (Coralville, Iowa, USA).

Following plasmids were used as source material for construction of various expression vectors, subcloning vectors or as templates for *in vitro* transcription.

Table 28 Plasmids

Name	Description
pJET1.2/blunt	Thermo Fisher, K1232
pSLfa1180fa	(*287*)
pHD-DsRed-attP	(*288*)
pGE-attB	(*289*)
pBFv-U6.2	(*290*)
pBFv-U6.2B	(*290*)
pCRII	Thermo Fisher, K206001
pCRII(attB;10xUAS;AscI;bHSp:mini-white)	Hassan Mutassim, Georg-August University, Germany
pBac[3xP3DsRed;hTc-Gal4D-SV40] #9	Gregor Bucher, Georg-August University, Germay

Following oligonucleotides were used for cloning, genotyping, qRT-PCR, and sequencing.

Table 29 Primers used for cloning

Name	Sequence
DM64_UASp_P-element_fw	ATACCATTTAGCTAGGCCGGGCCGCTCTAGCCCCCCCT
DM65_UASp_P-element_rv	TACCGGCGCGCCAAGGCCGGTAGGTACCAATGAACAGGACCTAACGC
DM66_*HspA*_fw	GTTCATTGGTACCTACCGGCCTTGGTCAATTCTATTCAAACAAGTAAAG
DM67_*HspA*_rv	TTTCCCACAGCATTGTGTGTGAGTTCTTCTTC
DM68_*stg*_5'UTR_fw	GTTCATTGGTACCTACCGGCCTTGGTGGCCTCCATAGAGCTGG
DM69_*stg*_5'UTR_rv	TGGCTGATTATGACTACAGCATCAGTCGCGAG
DM70_*stg*_3'UTR_fw	GAACTCACACACAATGCTGTGGGAAACTATTG
DM71_*stg*_3'UTR_rv	AATGTTTTTGCGAATAGGGTACCGGCGTCGTGTATTAATGTATATTTAAAATTG
DM72_*Sv40*_fw	ACTGATGCTGTAGTCATAATCAGCCATACCAC

Name	Sequence
DM73_*Sv40*_rv	AATGTTTTTGCGAATAGGGTACCGGGATGAGTTTGGACAAACC
DM74_*stg*_5'UTR_w/o extension	TGGCCTCCATAGAGCTGG
DM75_*stg*_5'UTR_short	GTTCATTGGTACCTACCGGCCTTGGGCACATTCGTTCTCAGTTCG
DM245_Backbone_fwd	GGTACCCTATTCGCAAAAAC
DM246_Backbone_rev	TCCTCATCCTGTCTCTTG
DM247_Resistance/UAS_fwd	ATCAAGAGACAGGATGAGGAATGAGTATTCAACATTTCCG
DM248_Resistance/UAS_rev	CTAGCGGTACTACTTCGGTAAGCTTCGG
DM249_eYFP_fwd	TACCGAAGTAGTACCGCTAGAGTCGACGG
DM250_eYFP_rev	ATCCCACAACAGTCGCGGCCGCTTTACT
DM251_3'stg_fwd	GGCCGCGACTGTTGTGGGATGATCGTGC
DM252_3'stg_rev	GTTTTTGCGAATAGGGTACCCGTCGTGTATTAATGTATATTTAAAATTGATG
DM263_eYFP_3'UTRstg_rv	TCCCACAACTTACTTGTACAGCTCGTCC
DM264_eYFP_Backbone_fw	GGTACCTACCGGCCTTGGATGGTGAGCAAGGG
DM265_3'UTRstg_Backbone_rv	TTGCGAATAGGGTACCGGCGTCGTGTATTAATGTATATT
DM266_3'UTRstg_eYFP_fw	TACAAGTAAGTTGTGGGATGATCGT
DM267_5'UTRstg_eYFP_rv	GCTCACCATTTTGTTGGTTTTGTTGT
DM268_5'UTRstg_Backbone_fw	GGTACCTACCGGCCTTGGTGGCCTCCATAGAGC
DM269_eYFP_Bbackbone_rv	TTGCGAATAGGGTACCGGTTACTTGTACAGCTCGTCC
DM270_eYFP_5'UTRstg_fw	ACCAACAAAATGGTGAGCAAGGG
DM271_3'UTRstg_Backbone_rv	TTGCGAATAGGGTACCGGCGTCGTGTATTAATGTATATT
DM272_3'UTRstg_stg_fw	ATGCTGTAGGTTGTGGGATGATCGT
DM273_stg_3'UTRstg_rv	TCCCACAACCTACAGCATCAGTCGC
DM274_5'UTRstg_Backbone_fw	GGTACCTACCGGCCTTGGTGGCCTCCATAGAGC
DM291_eYFP_rv_Sv40	CTGATTATGATTACTTGTACAGCTCGTCCATG
DM292_Sv40_fw_eYFP	GTACAAGTAATCATAATCAGCCATACCAC
DM293_hsp_rev_eYFP	TGCTCACCATTGTGTGTGAGTTCTTCTTC
DM294_eYFP_fwd_hsp	CTCACACACAATGGTGAGCAAGGGCGAG
DM295_act5_fwd	AGCATTGCGGCTGATAAGGT
DM296_act5_rev	TCCACACAGCACAAGAACTCA

Name	Sequence
DM297_Df31_fwd	CCGCCCTGTAGTGTTGGTAG
DM298_Df31_rev	ACGGGTGATAACGATAACAAACAA
DM299_R_fwd	TCAGCGAACAGCGAACACTC
DM300_R_rev	GATAGTCGTGCGTAGCCCTC
DM301_How_dele_fw	GTTTCTCGCACACGACGC
DM302_How_dele_rv	TACGGATTAACAAATGAAAATCAACAAAAATC
DM303_How(A,B,C,D,E,F)_fw	GCACCGTACGATTATGCGAA
DM304_How(B)_rv	ATCTGGCAAACAACCCACCG
DM305_How(C)_rv	CCGGCATGCATATATCGACCA
DM306_How(A,D,E,F)_rv	ACGACGCTGCTGCTTAATG
DM307_His2b_His3_rv	AACTTCAAGAGAGCGTAGTTGGTACACTGGCC CGAGCCAGCGTAATCTGGAACATCGTATGGGT ATTTAGAGCTGGTGTACTTGGT
DM308_PRexpress_His_fw	ACTCTGAATAGGGAATTGGGACAACCAAAATGT CTGATTCTGCAGTTGC
DM309_His4_Sv40_fw	AGAGGATCTGTAATCATAATCAGCCATACCACA
DM310_His3_His4_fw	CCGTGGTTCCCTCTTGACCTGCGGAGATGTAG AAGAGAATCCCGGTCCCACAACCAAAATGACT GGTCGTGGTAAAG
DM311_His2A_His2B_rv	GGCTTGTTTCAGCAACGAGAAATTTGTGGCGC CGCTGCCCTTGTCGTCATCGTCTTTGTAGTCGG CCTTCTTCTCGGTCTTC
DM312_His2A_His2B_fw	TCTCGTTGCTGAAACAAGCCGGTGACGTTGAG GAAAATCCCGGTCCCACAACCAAAATGCCTCC GAAAACTAGTG
DM313_His2B_His3_fw	AACTACGCTCTCTTGAAGTTGGCTGGAGATGTG GAGAGCAACCCCGGTCCCACAACCAAAATGG CTCGTACCAAGCAAA
DM314_HIs3_His4_rv	AGGTCAAGAGGGAACCACGGCCCTCGCCGGA GCCGTGGTGGTGGTGGTGGTGAGCACGCTCG CCGCGAATG
DM315_Sv40_PRexpress_rv	CCATTTAGCCGATCAATTGCGATGAGTTTGGAC AAACCA
DM316_His1_His2A_fw	GTGGTTCCCTCTTGACCTGCGGAGATGTAGAA GAGAATCCCGGTCCCACAACCAAAATGTCTGG ACGTGGAAAAG
DM317_His1_His2A_rv	GCAGGTCAAGAGGGAACCACGGCCCTCGCCG GAGCCGGTGGAGTCCAGGCCCAGGAGGGGGT TCGGAATGGGCTTACCCTTTTTGGCAGCCGTA GT
DM318_His4_Sv40_rv	ATTATGATTACAGATCCTCTTCTGAGATGAGTTT TTGTTCACCGCCAAATCCGTAGAG

Table 30 qPCR primer

Name	Sequence
DM9_*H1*_1f	AAGGCAAAAGCCAAGGATGC
DM10_*H1*_1R	CTTCGCTGCAGTCACTTTCG
DM11_*H1*_2f	CGGTGTCTGCAAAACCCAAA
DM12_*H1*_2R	GCAGCCGTAGTCTTCGCTTT
DM13_*H2A*_1F	CGGAAGGGAAACTACGCAGA
DM14_*H2A*_1R	GAACCTCAGCGGCCAGATAT
DM15_*H2A*_2F	TAAACAAGCTGCTCTCCGGC
DM16_*H2A*_2R	TCGGTCTTCTTGGGCAACAG
DM17_*H2B*_1F	TCACTACAACAAGCGCTCGA
DM18_*H2B*_1R	ATGCTTGGCCAACTCTCCAG
DM19_*H2B*_2F	GGGAGATCCAAACGGCTGTT
DM20_*H2B*_2R	TTGGTGACAGCCTTGGTTCC
DM21_*H3*_1F	TCTGCAGGAAGCTAGCGAAG
DM22_*H3*_1R	TATGGTGACACGCTTGGCAT
DM23_*H3*_2F	CCATTCATGCCAAGCGTGTC
DM24_*H3*_2R	GTGTCAGCTTAAGCACGCTC,
DM25_*H4*_1F	AATTCGTGATGCCGTGACCT
DM26_*H4*_1R	TTGCCTCTTCAGAGCGTACA
DM27_*H4*_2F	GGAACACGCCAAGAGGAAGA
DM28_*H4*_2R	GCCAAATCCGTAGAGGGTGC
DM29_*stg*_1F	ACCAACAAAATGCTGTGGGAA
DM30_*stg*_1R	TCGAACTGCTGGTGTTATTACTGA
DM31_*stg*_2F	TGCAATATCAGTAATAACACCAGCA
DM32_*stg*_2R	CCTGGTCCATGCTCATCAGT
DM33_*RpL13A*_fw	GTGCAACGTGAACCCAGC
DM34_*RpL13A*_rv	ACAGTTTGAATTGCTTACCTCGG
DM35_*Gapdh1*_fw	TCGCTGAACACGGTGATCTT
DM36_*Gapdh1*_rv	ACTCGACTCACGGTCGTTTC
DM37_*αTub67C*_fw	TAATAAAATGCGCGAAGTAGTCTCC
DM38_*αTub67C*_rv	CAGCAGGTACAGCTCCCAG
DM39_*Act5C*_fw	ATTTGCCGGAGACGATGCTC
DM40_*Act5C*_rv	TACGAGTCCTTCTGGCCCAT
DM56_*H2A*.V_fw	GCGGCAGTTAGAATCACCGA
DM57_*H2A*.V_rv	TACCGCCAGCCATTTCTGTT
DM58_*H3.3A*_fw	TTGGAGCCCTACAGGAGGC
DM59_*H3.3A*_rv	CATAATGGTGACGCGCTTGG

Name	Sequence
DM60_*H3.3B*_fw	CGTCTGGTTCGTGAAATCGC
DM61_*H3.3B*_rv	TCAGATGCTTCCTGCAAGGC
DM76_*twe*_qPCR_fw	CGCAAATAGATCAGGATGGCG
DM77_*twe*_qPCR_rev	ATTCTCCTGACCACACGCTC
DM78_*aly*_qPCR_fw	CGCACCGTACGATTATGCGA
DM79_*aly*_qPCR_rev	TTGATGACGCGACATTGTTGT
DM80_*comr*_qPCR_fw	GGGGGCGTTCGTCTATCAAT
DM81_*comr*_qPCR_rev	CAGATTCGTGCGGCTTTACG
DM82_*wuc*_qPCR_fw	ACCTGCGCAAGATGTATGAACT
DM83_*wuc*_qPCR_rev	CAGCTCGTAGATCTCCTTCTCC
DM84_*topi*_qPCR_fw	TACGCTTTCACCAGGGTGTG
DM85_*topi*_qPCR_rev	CAGATCTGGGCGAATGGTGA
DM86_*polo*_qPCR_fw	GGATATTCCGGATCGCCTCG
DM87_*polo*_qPCR_rev	ATTTTGCAAACCCGCCCTTG
DM88_*achi*_qPCR_fw	TGACAATCTACAGGCGGACG
DM89_*achi*_qPCR_rev	GACTTGTGCCCTGCGACATA
DM90_*tomb*_qPCR_fw	GGTCGCAGTGCATCAAGAAC
DM91_*tomb*_qPCR_rev	TGACAATCTACAGGCGGACG
DM92_*Myb*_qPCR_fw	TCCACACAAGAGTCAACTTGGA
DM93_*Myb*_qPCR_rev	TATCGACGACCGTCCCTCTT
DM94_*mip40*_qPCR_fw	ACCCAAGAATCCAGCTGTGG
DM95_*mip40*_qPCR_rev	TTTCTTCGCCGTTGTCCTCA
DM96_*fest*_qPCR_fw	AGCGTTCCGTATTCACCAACA
DM97_*fest*_qPCR_rev	GAGCCAATGGGCTGTTCATC
DM98_*ProtA*_qPCR_fw	GCCAGTATTCTGCGGAACCA
DM99_*ProtA*_qPCR_rev	TGACCTTGCATGCCATCCG
DM100_*ProtB*_qPCR_fw	CAGGAATTAATTGCAGAGGCCG
DM101_*ProtB*_qPCR_rev	TGGTGACCTTGCATGCCATC
DM102_*Mst77F*_qPCR_fw	GCCAGTATTCTGCGGAACCA
DM103_*Mst77F*_qPCR_rev	GTGCTCGCCCTCACTAGAAC
DM187_How_all_qPCR_fw	CGCACCGTACGATTATGCGA
DM188_How_all_qPCR_rv	GCTTAATGGCGCCTACGCTA
DM189_*how(S)*_F_qPCR_fw	CGCACCGTACGATTATGCGA
DM190_*how(S)*_F_qPCR_rv	CATGCATATATCGACCAACGCT
DM191_*how(L)*_A/E/F_qPCR_fw	CCGAAGGCGAAGATGAGCTA
DM192_*how(L)*_lA/E/F_qPCR_rv	TCGCACACTGCGACAGATTT
DM275_HspA-stg-qPCR_fw	TCAACAAGTCGTTACCGAGGA

Name	Sequence
DM276_HspA-stg-qPCR_rv	TATTGCAATCCATGCTGCAGTT
DM277_Sv40-stg-qPCR_fw	AAGTCCTGGAACGGCGATG
DM278_Sv40-stg-qPCR_rv	ACCTCTACAAATGTGGTATGGCT
DM279_HspA-qPCR_fw	ACTGCAACTACTGAAATCAACCAA
DM280_HspA-qPCR_rv	TGTGTGAGTTCTTCTTCCTCGG
DM281_Sv40-qPCR_fw	CCTCCCCCTGAACCTGAAAC
DM282_Sv40-qPCR_rv	TTGTGAAATTTGTGATGCTATTGCT
DM283_Gal4_qPCR1_fw	TTAGCCATTGGAGCCTGGTG
DM284_Gal4_qPCR1_rv	CTCGAAGACCTTGCTCGTCA
DM285_Gal4_qPCR2_fw	GCATGCGATATTTGCCGACT
DM286_Gal4_qPCR2_rv	AGAGTAGCGACACTCCCAGT
DM287_stg_qPCR_noINT1_fw	CCTGCTTAAGGGCGAGTTCA
DM288_stg_qPCR_noINT1_rv	TTCTTGGCTCCCTCGATGTG
DM289_stg_qPCR_noINT2_fw	TCCTGCGTAATCTGGATCGC
DM290_stg_qPCR_noINT2_rv	AACGTGCGACTCGAAGAACT
DM363_His1_OE1_rv	GGCTTACCCTTTTTGGCAGC
DM364_His1_OE2_rv	GGGGTTCGGAATGGGCTTAC
DM365_His2A_OE1_rv	GTCGTCATCGTCTTTGTAGTCG
DM366_His2B_OE1_rv	CGTAATCTGGAACATCGTATGGGT
DM367_His3_OE1_fw	CGGTCCCACAACCAAAATGG
DM368_His3_OE1_rv	CTTGCGAGCGGCCTTAGTAG
DM369_His4_OE1_rv	TGAGATGAGTTTTTGTTCACCGC

Table 31 Primers used for ATAC-seq, CUTAC, CUT&Tag and STRIPE-seq library amplification and adaptor ligation

Name	Sequence
DM122_Ad1_noMX:	AATGATACGGCGACCACCGAGATCTACACTCGTCG GCAGCGTCAGATGTG
DM123_Ad2.1_TAAGGCGA	CAAGCAGAAGACGGCATACGAGATTCGCCTTAGTC TCGTGGGCTCGGAGATGT
DM124_Ad2.2_CGTACTAG	CAAGCAGAAGACGGCATACGAGATCTAGTACGGTC TCGTGGGCTCGGAGATGT
DM125_Ad2.3_AGGCAGAA	CAAGCAGAAGACGGCATACGAGATTTCTGCCTGTC TCGTGGGCTCGGAGATGT
DM126_Ad2.4_TCCTGAGC	CAAGCAGAAGACGGCATACGAGATGCTCAGGAGTC TCGTGGGCTCGGAGATGT
DM127_Ad2.5_GGACTCCT	CAAGCAGAAGACGGCATACGAGATAGGAGTCCGTC TCGTGGGCTCGGAGATGT

Name	Sequence
DM128_Ad2.6_TAGGCATG	CAAGCAGAAGACGGCATACGAGATCATGCCTAGTC TCGTGGGCTCGGAGATGT
DM129_Ad2.7_CTCTCTAC	CAAGCAGAAGACGGCATACGAGATGTAGAGAGGTC TCGTGGGCTCGGAGATGT
DM130_Ad2.8_CAGAGAGG	CAAGCAGAAGACGGCATACGAGATCCTCTCTGGTC TCGTGGGCTCGGAGATGT
DM131_Ad2.9_GCTACGCT	CAAGCAGAAGACGGCATACGAGATAGCGTAGCGTC TCGTGGGCTCGGAGATGT
DM132_Ad2.10_CGAGGCTG	CAAGCAGAAGACGGCATACGAGATCAGCCTCGGTC TCGTGGGCTCGGAGATGT
DM133_Ad2.11_AAGAGGCA	CAAGCAGAAGACGGCATACGAGATTGCCTCTTGTC TCGTGGGCTCGGAGATGT
DM134_Ad2.12_GTAGAGGA	CAAGCAGAAGACGGCATACGAGATTCCTCTACGTC TCGTGGGCTCGGAGATGT
DM135_Ad2.13_GTCGTGAT	CAAGCAGAAGACGGCATACGAGATATCACGACGTC TCGTGGGCTCGGAGATGT
DM136_Ad2.14_ACCACTGT	CAAGCAKHGHGHJGGAAGACGGCATACGAGATACA GTGGTGTCTCGTGGGCTCGGAGATGT
DM137_Ad2.15_TGGATCTG	CAAGCAGAAGACGGCATACGAGATCAGATCCAGTC TCGTGGGCTCGGAGATGT
DM138_Ad2.16_CCGTTTGT	CAAGCAGAAGACGGCATACGAGATACAAACGGGTC TCGTGGGCTCGGAGATGT
DM139_Ad2.17_TGCTGGGT	CAAGCAGAAGACGGCATACGAGATACCCAGCAGTC TCGTGGGCTCGGAGATGT
DM140_Ad2.18_GAGGGGTT	CAAGCAGAAGACGGCATACGAGATAACCCCTCGTC TCGTGGGCTCGGAGATGT
DM141_Ad2.19_AGGTTGGG	CAAGCAGAAGACGGCATACGAGATCCCAACCTGTC TCGTGGGCTCGGAGATGT
DM142_Ad2.20_GTGTGGTG	CAAGCAGAAGACGGCATACGAGATCACCACACGTC TCGTGGGCTCGGAGATGT
DM143_Ad2.21_TGGGTTTC	CAAGCAGAAGACGGCATACGAGATGAAACCCAGTC TCGTGGGCTCGGAGATGT
DM144_Ad2.22_TGGTCACA	CAAGCAGAAGACGGCATACGAGATTGTGACCAGTC TCGTGGGCTCGGAGATGT
DM145_Ad2.23_TTGACCCT	CAAGCAGAAGACGGCATACGAGATAGGGTCAAGTC TCGTGGGCTCGGAGATGT
DM146_Ad2.24_CCACTCCT	CAAGCAGAAGACGGCATACGAGATAGGAGTGGGT CTCGTGGGCTCGGAGATGT
DM339_RTO_1	CAAGCAGAAGACGGCATACGAGAT TAGTGC GTGACTGGAGTTCAGACGTGTGCTCTTCCGATCT NNNNN

Name	Sequence
DM340_RTO_2	CAAGCAGAAGACGGCATACGAGAT ACATCG GTGACTGGAGTTCAGACGTGTGCTCTTCCGATCT NNNNN
DM341_RTO_3	CAAGCAGAAGACGGCATACGAGAT GCCTAA GTGACTGGAGTTCAGACGTGTGCTCTTCCGATCT NNNNN
DM342_RTO_4	CAAGCAGAAGACGGCATACGAGAT TGGTCA GTGACTGGAGTTCAGACGTGTGCTCTTCCGATCT NNNNN
DM343_RTO_5	CAAGCAGAAGACGGCATACGAGAT CACTGT GTGACTGGAGTTCAGACGTGTGCTCTTCCGATCT NNNNN
DM344_RTO_6	CAAGCAGAAGACGGCATACGAGAT ATTGGC GTGACTGGAGTTCAGACGTGTGCTCTTCCGATCT NNNNN
DM345_TSO	Biotin-CCTACACGACGCTCTTCCGATCT NNNNNNNN TATA rGrGrG
DM346_RTO_7	CAAGCAGAAGACGGCATACGAGATGATCTGGTGAC TGGAGTTCAGACGTGTGCTCTTCCGATCTNNNNN
DM347_RTO_8	CAAGCAGAAGACGGCATACGAGATTCAAGTGTGAC TGGAGTTCAGACGTGTGCTCTTCCGATCTNNNNN
DM348_RTO_9	CAAGCAGAAGACGGCATACGAGATCTGATCGTGAC TGGAGTTCAGACGTGTGCTCTTCCGATCTNNNNN
DM349_RTO_10	CAAGCAGAAGACGGCATACGAGATAAGCTAGTGAC TGGAGTTCAGACGTGTGCTCTTCCGATCTNNNNN
DM350_RTO_11	CAAGCAGAAGACGGCATACGAGATGTAGCCGTGAC TGGAGTTCAGACGTGTGCTCTTCCGATCTNNNNN
DM351_RTO_12	CAAGCAGAAGACGGCATACGAGATTACAAGGTGAC TGGAGTTCAGACGTGTGCTCTTCCGATCTNNNNN
DM352_RTO_13	CAAGCAGAAGACGGCATACGAGATTTGACTGTGAC TGGAGTTCAGACGTGTGCTCTTCCGATCTNNNNN
DM353_RTO_14	CAAGCAGAAGACGGCATACGAGATGGAACTGTGAC TGGAGTTCAGACGTGTGCTCTTCCGATCTNNNNN
DM354_RTO_15	CAAGCAGAAGACGGCATACGAGATTGACATGTGAC TGGAGTTCAGACGTGTGCTCTTCCGATCTNNNNN
DM355_RTO_16	CAAGCAGAAGACGGCATACGAGATGGACGGGTGA CTGGAGTTCAGACGTGTGCTCTTCCGATCTNNNNN
DM356_RTO_17	CAAGCAGAAGACGGCATACGAGATGCGGACGTGA CTGGAGTTCAGACGTGTGCTCTTCCGATCTNNNNN
DM357_RTO_18	CAAGCAGAAGACGGCATACGAGATTTTCACGTGAC TGGAGTTCAGACGTGTGCTCTTCCGATCTNNNNN
DM358_FLO	AATGATACG

Name	Sequence
DM359_RLO	CAAGCAGAAGACGGCATACG
DM360_Ad1.1_GCGATCTA_RevComp	CACATCTGACGCTGCCGACGAGCGATCTAGTGTAGATCTCGGTGGTCGCCGTATCATT
DM361_Ad2.1_TAAGGCGA_RevComp	ACATCTCCGAGCCCACGAGACTAAGGCGAATCTCGTATGCCGTCTTCTGCTTG
DM362_FLO i5_501	AATGATACGGCGACCACCGAGATCTACACTATAGCCTTCTTTCCCTACACGACGCTCTTCCG
DM378_Ad1.1_GCGATCTA	AATGATACGGCGACCACCGAGATCTACAC TAGATCGC TCGTCGGCAGCGTC AGATGTG
DM379_Ad1.2_ATAGAGAG	AATGATACGGCGACCACCGAGATCTACAC CTCTCTAT TCGTCGGCAGCGTC AGATGTG
DM380_Ad1.3_AGAGGATA	AATGATACGGCGACCACCGAGATCTACAC TATCCTCT TCGTCGGCAGCGTC AGATGTG
DM381_Ad1.4_TCTACTCT	AATGATACGGCGACCACCGAGATCTACAC AGAGTAGA TCGTCGGCAGCGTC AGATGTG
DM382_Ad1.5_CTCCTTAC	AATGATACGGCGACCACCGAGATCTACAC GTAAGGAG TCGTCGGCAGCGTC AGATGTG
DM383_Ad1.6_TATGCAGT	AATGATACGGCGACCACCGAGATCTACAC ACTGCATA TCGTCGGCAGCGTC AGATGTG

Table 32 Primers used to generate RNA probes

Name	Sequence
DM5_*stg1*_fw	CCAGCAGTTCGAGTAGCATC
DM6_*stg1*_rv_T7	GAATTAATACGACTCACTATAGGGAGACTTTGCTGAAGTCGCCGATT
DM7_*stg2*_fw	AGTGGCCTAAACTCGCTGAT
DM8_*stg2*_rv_T7	GAATTAATACGACTCACTATAGGGAGATAGCCGTTGTGCAGCAGATA
DM104_*aly*_fw	CAGCAGCATAAGTTCAAT
DM105_*aly*_rv_T7	TAATACGACTCACTATAGGCAGCTTTCCATTGAGATA
DM106_*comr*_fw	ACATCACGCTGATCTATC
DM107_*comr*_rv_T7	TAATACGACTCACTATAGGCTCCTCTTCGTTAAGATTAG
DM108_*fest*_fw	GCAGCTACATGAATATGG
DM109_*fest*_rv_T7	TAATACGACTCACTATAGGGAATCCATTGATGTCATACA
DM110_*smox*_fw	CAAGAAGATCAAGAAGAATT
DM111_*smox*_rv_T7	TAATACGACTCACTATAGGGCGTATTTAGCTCATAGTAG
DM112_*stgIntron*_fw	AGGAATACCAGTTGAAAATA

Name	Sequence
DM113_*stgIntron*_rv_T7	TAATACGACTCACTATAGGCTTTTGCTTCCCTAAACT
DM114_*wuc*_fw	GTTACGAAGTCCATTAAGCGGGA
DM115_*wuc*_rv_T7	TAATACGACTCACTATAGGTCACTTGTTGGCGCGACG
DM151_*milkah*_fw	GATGGAATCGGATTTAAA
DM152_*milkah*_rv_T7	TAATACGACTCACTATAGTTACTTGTCGACGCCATC
DM153_*Mst77F*_fw	ATGAGTAATCTGAAACAAAAGG
DM154_*Mst77F*_rv_T7	TAATACGACTCACTATAGTTACATCGAGCACTTGG
DM155_*ProtA*_fw	ATTTTTCCAAAAGTCTTATT
DM156_*ProtA2*_fw	CGATGAGTTCAAATAATGTA
DM157_*ProtA*_rv_T7	TAATACGACTCACTATAGGGTTTTTATTTCTAAATTCA
DM158_*ProtB*_fw	AACTTGGTACACAAACAGTT
DM159_*ProtB2*_fw	TTTGTAAAAATTTTCTACGA
DM160_*ProtB*_rv_T7	TAATACGACTCACTATAGTTTTATTTCTAAATTCATCG
DM161_*wuc2*_fw	CAAGGGTGGATTTATATT
DM162_*wuc2*_rv_T7	TAATACGACTCACTATAGGACGACCCTTTATTTGATA
DM163_*kmg*_fw	ACTTTATGTTTCCACTATCG
DM164_*kmg*_rv_T7	TAATACGACTCACTATAGCGTGCTATATGAACACTTC
DM165_t-*brd1*_fw	CTGCACAACAAATACTACTG
DM166_t-*brd1*_rv_T7	TAATACGACTCACTATAGCTTTCGTACAGAGCTCAC
DM167_t-*brd2*_fw	CCACATACTACACGGTTATC
DM168_t-*brd2*_rv_T7	TAATACGACTCACTATAGCGATAGCTTCATCATCTG
DM205_CG12362_fw	GTCTACATCCTGTGCCATAC
DM206_CG12362_rv_T7	TAATACGACTCACTATAGCAAACACATAGCTGTACATC
DM207_CG13054_fw	TATTAGGAGCAGCTCAAC
DM208_CG13054_rv_T7	TAATACGACTCACTATAGCTCAGCTTGGACACATTTAT
DM209_CG32581_fw	GAGGAGTCATCTACAAGTCA
DM210_CG32581_rv_T7	TAATACGACTCACTATAGGACCCAATCCACTTCTGT
DM211_CG34283_fw	GCTGTTGTATCAACAAATC

Name	Sequence
DM212_CG34283_rv_T7	TAATACGACTCACTATAGCTACTCGTAAACTTGATCTATG
DM213_*Ttc26*_fw	CCGTGTGTATGTTCTACTT
DM214_*Ttc26*_rv_T7	TAATACGACTCACTATAGAGGATCATGCAGTAGGTAT
DM215_*bam*_fw	ACTTGTGAGTACGAGGATAC
DM216_*bam*_rv_T7	TAATACGACTCACTATAGCTCCAGAACGCAATAGATC
DM217_*how(S)*_fw	CTCCTTTTTCTCACTCTCT
DM218_*how(S)*_rv_T7	TAATACGACTCACTATAGCATCGCAAAACTCACTAC
DM219_*how(l)*_fw	GCGTAACCAAAAGTCAGAT
DM220_*how(l)*_rv_T7	TAATACGACTCACTATAGGAATGCTTGCTGCTATTATC
DM235_*wg*_ISH_fw	CTTGGCAGCATGTATATAT
DM236_*wg*_ISH_rv-T7	TAATACGACTCACTATAGATAGAGACAGCCTGTTAAAG
DM237_*wg*_ISH_int_fw	GATCCACTCTACGTTGAG
DM238_*wg*_ISH_int_rv_T7	TAATACGACTCACTATAGAGGCTCCAGATAGACAAG
DM241_Sv40_fw	ATAATCAGCCATACCACAT
DM242_Sv40_T7_rv	TAATACGACTCACTATAGGATGAGTTTGGACAAACCAC
DM243_HspA_fw	TCAATTCTATTCAAACAAGTAAAG
DM244_HspA_T7_rv	TAATACGACTCACTATAGTGTGTGTGAGTTCTTCTTC

Table 33 General primers

Name	Sequence
pJet1.2-fwd	GAGGGCCCATTCTCTAATGCGAGGAGAAAT
pJet1.2-rev	GCGCTAGCTCAACATCAACTTTAACTTCCTTC
pJet1.2-T7-fwd	GAATTGTAATACGACTCACTATAGGCGACTCACTATAGGGAGAGCGGC
pJet1.2-T7-rev	GAATTGTAATACGACTCACTATAGGAAGAACATCGATTTTCCATGGCAG
M13-fwd	TGTAAAACGACGGCCAGT
M13-rev	CAGGAAACAGCTATGACCATG

5.6.5 Solutions and Buffers

5.6.5.1 General Solutions and Buffers

Table 34 PBS

Component	Mass/Volume
NaCl	80g
KCl	2g
K2PO4	2g
Na2HPO4	11,5g
pH	7.4
H_2O	1000ml

Table 35 PBS-T

Component	Volume
10x PBS	100ml
10% Triton	10ml
H_2O	900ml

Table 36 Lysogeny Broth

Component	Concentration [% w/v]
tryptone	2
yeast extract	1
NaCl	2

Table 37 STE

Component	Concentration
EDTA	1mM
NaCl	0.58% w/v
Tris-HCl (pH8)	10mM

Table 38 TE-Buffer

Component	Concentration
Tris-HCl	10mM pH8
EDTA	1mM

Table 39 BSA blocking buffer

Component	Concentration
BSA	5% w/v
Solving in	PBS or TBS

5.6.5.2 Whole mount *in situ* hybridization and IF buffers

Table 40 Hybe B

Component	Volume
Formamide	500ml
20x SSC	250ml
H_2O	250ml
HybeBT	HybeB + 0.1% Triton X-100

Table 41 Hybe A Star

Component	Volume
Hybe B	400ml
Yeast RNA (20 mg/ml)	2ml
Sonicated Salmon Sperm (10 mg/ml)	8ml
Heparin (50 mg/ml)	400µl
Dextran sulphate	2% w/v
Roche Blocking	2% w/v
HybeAT	HybeA + 0.1% Triton X-100

Table 42 MAB

Component	Mass
Maleic acid	58g
NaCl	43.8g
H_2O	To 1000ml
pH	7.5
MABT	MAB + 0.1% Triton X-100

Table 43 Resuspension Buffer

Component	Concentration
Formamide	50%
Tween 20	0.1%
20x SSC (ph5)	5x
Heparin	20µg/µl

Table 44 NBT/BCIP staining Buffer

Component	Concentration
Tris-HCl	5ml
MgCl	50mM
NaCl	100mM
Tween 20	0.1%

Table 45 DAPCO anti-fade mounting medium

Component	Concentration
DAPCO	2.5% w/v
Glycerol	80%
PBS	20%

5.6.5.3 DNA isolation buffers

Table 46 P1/GTE Buffer

Component	Concentration
Glucose	50mM
Tris-HCl (pH 8.0)	25mM
EDTA	10mM

Table 47 P2/alkali-SDS Buffer

Component	Concentration
NaOH	0.2M
SDS	1% w/v

Table 48 P3/acetate Buffer

Component	Concentration
KaCH3COOH	3M

5.6.5.4 Protein isolation buffers

Table 49 Solution A

Component	Concentration
Tris-HCl	0.1M
EDTA	0.1m
SDS	0.1%

Table 50 TBS

Component	Concentration
Tris-HCl	19 mM
KCl	2.7 mM
NaCl	137 mM

Table 51 NP-40 Buffer

Component	Concentration
NaCl	150mM
Tris-HCl	50mM pH7.5
EDTA	2mM
NP-40	0.1%

Table 52 Running Buffer

Component	Concentration
Tris-HCl	25mM
Glycine	190 mM
SDS	0.1%
pH	8.3

Table 53 Transfer Buffer

Component	Concentration
Tris-HCl	25mM
Glycine	190mM
Methanol	20%
pH	8.3

Table 54 Hypotonic Buffer

Component	Concentration
TRIS-HCl pH7.4	20mM
KCl	10mM
MgCl2	2mM
EGTA	1mM
DTT	0.5mM
PMSF	0.5mM

Table 55 Isotonic Buffer

Component	Concentration
TRIS-HCl pH7.4	20mM
KCl	150mM
MgCl2	2mM
EGTA	1mM
DTT	0.5mM
PMSF	0.5mM
NP-40	0.1%

Table 56 DNase Buffer

Component	Concentration
TRIS-HCl pH7.4	20mM
NaCl	100mM
MgCl2	42mM
CaCl2	1mM
DTT	0.5mM
PMSF	0.5mM
NP-40	0.1%

5.6.5.5 ATAC-seq Buffers

Table 57 ATAC-seq Lysis Buffer

Component	Concentration
Tris HCl	10mM
NaCl	10mM
MgCl	3 mM
IGEPAL CA 630	0.1%

5.6.5.6 CUT&Tag and CUTAC Buffers

Table 58 NE1 buffer

Component	Concentration
HEPES-KOH pH7.9	20mM
KCL	10mM
Triton X-100	0.1% (v/v)
Glycerol	20%
Spermidine	0.5mM

Table 59 Bead Activation Buffer

Component	Concentration
HEPES pH7.9	20mM
KCL	10mM
CaCl2	1mM
MnCl2	1mM

Table 60 Wash Buffer 150

Component	Concentration
HEPES pH7.5	20mM
NaCl	150mM
Spermidine	0.5mM

Table 61 Digitonin Buffer 150

Component	Concentration
WashBuffer150	1x
Digitonin	0.05%

Table 62 Antibody Buffer

Component	Concentration
DigitoninBuffer150	1x
EDTA	2mM

Table 63 Wash Buffer 300

Component	Concentration
HEPES pH7.5	20mM
NaCl	300mM
Spermidine	0.5mM

Table 64 Digitonin Buffer 300

Component	Concentration
WashBuffer300	1x
Digitonin	0.05%

Table 65 Tagmentation Buffer

Component	Concentration
DigitoninBuffer300	1x
MgCl2	10mM

Table 66 TAPS Buffer

Component	Concentration
TAPS pH8.5	10mM
EDTA	0.2mM

Table 67 SDS Release Buffer

Component	Concentration
TAPS pH8.5	10mM
SDS	0.1%

Table 68 SDS Quench Buffer

Component	Concentration
dd H_2O	1x
Triton X-100	0.67%

5.6.5.7 STRIPE-seq Buffers

Table 69 Trehalose/Sorbitol Solution

Component	Concentration
Sorbitol	3.3M
Trehalose	0.66M

Table 70 5M betaine solution

Component	Mass/Volume
Betaine	29.275g
dd H_2O	50ml

5.6.6 Consumables

Table 71 Consumable materials

Item	Company
Cover slips	Thermo Fisher Scientific, Waltham, Massachusetts, USA
Eppendorf tubes	Eppendorf, Hamburg, Germany
Falcon tubes, 15 ml	Sarstedt, Nümbrecht, Germany
Falcon tubes, 50 ml	Sarstedt, Nümbrecht, Germany
Glass pipettes (dropping)	Brand, Wertheim Brand, Wertheim
Gloves	Carl Roth GmbH & Co. KG, Karlsruhe, Germany
Injections	B. Braun Medical AG, Emmenbrücke, Swiss
Injection needles Ø = .80 x 40 mm	B. Braun Medical AG, Emmenbrücke, Swiss
Injection needles Ø = 0.90 x 70 mm	B. Braun Medical AG, Emmenbrücke, Swiss
Object plates	Thermo Fisher Scientific, Waltham, Massachusetts, USA
Parafilm	Bemis Company Inc., Neenah, USA

Item	Company
Pipet tips	Eppendorf, Hamburg, Germany Biosphere Sarstedt, Nümbrecht, Germany
Sterilization filters	Sarstedt, Nümbrecht, Germany

5.6.7 Equipment

Table 72 Technical equipment used during this thesis

Item	Company
Argon Laser	CVI Melles Griot, Albuquerque, USA
Power supply	Biometra, Analytik Jena, Jena, Germany
PCR chamber	Peqlab, VWR International GmbH, Darmstadt, Germany
Bottles, all sizes	Schott AG, Mainz, Germany VWR International GmbH, Darmstadt, Germany
Bunsen burner	Carl Zeiss AG, Oberkochen, Germany
Mastercycler personal, gradient	Eppendorf, Hamburg, Germany
Nanodrop	Thermo Fisher Scientific, Waltham, Massachusetts, USA
Heating block	Techne, Cole-Parmer, Beacon Road, Stone, Staffordshire, ST15 OSA, UK
Eppendorf Centr. 5415R,5415	Eppendorf, Hamburg, Germany
Erlenmeyer flasks, all sizes	Schott AG, Mainz, Germany VWR International GmbH, Darmstadt, Germany
Filter set 49 (G: 365, FT: 395, BP: 445/50)	Carl Zeiss AG, Oberkochen, Germany
Filter set EGFP-HC (FF01-472/30-25)	AHF-Analyse Technik, Tübingen, Germany
Axioplan2	Carl Zeiss AG, Oberkochen, Germany
Forceps	Ochs Laborbedarf, Bovenden, Germany
LSM 980	Carl Zeiss AG, Oberkochen, Germany
Heating Plate	Techne, Staffordshire, United Kingdom
Ice Machine	Ziegra, Isernhagen, Germany
Incubator	Heraues Holding GmbH, Hanau, Germany Memmert, Schwalbach, Germany
Magnetic mixer	IKA Labortechniken, Staufen, Germany
Peleus ball	Carl Roth GmbH & Co. KG, Karlsruhe, Germany
pH InoLab 720	WTW-GmbH, Weilheim, Germany
High accuracy pipettes	VWR International GmbH, Darmstadt, Germany

Item	Company
Scale	Sartorius, Göttingen, Germany
High accuracy scale	Sartorius, Gottingen, Germany
Refrigerator	Liebeherr, Biberach and der Riss, Germany Siemens AG, München, Germany
Vortex VF2	IKA Labortechniken, Staufen, Germany
Water deionization plant	Millipore, Schwalbach, Germany

5.6.8 Software and online tools

Table 73 IT products, tools, and software

Program	Reference/Company	Application
Zen Blue	Carl Zeiss AG, Oberkochen, Germany	Image acquisition
Zen Black	Carl Zeiss AG, Oberkochen, Germany	Image acquisition
Office 365	Microsoft Corp., Redmond, USA	Text processing
Serif Affinity Designer	Serif, Nottingham, UK	Image editing
Serif Photo	Serif, Nottingham, UK	Image editing
Serif Publisher	Serif, Nottingham, UK	Image editing
Windows 10 Professional	Microsoft Corp., Redmond, USA	Operating system
www.leo.org		Translation
http://nebcloner.neb.com/#!/	New England Biolabs (Frankfurt am Main, Germany)	Cloning protocols, Tm calculation
ImageJ		Image editing
Geneious Prime		In silico Design
Prism 8	GraphPad, San Diego, CA, USA	Data analysis
Citavi		Reference organization
R version 3.6.0	(*218*)	Data analysis
DESeq2_1.22.2	(*204*)	Data analysis
clusterProfiler_3.10.1	(*207*)	Data analysis
pheatmap_1.0.12	(*219*)	Data analysis
ggplot2_3.1.0	(*205*)	Data analysis
RSEM v1.3.1	(*206*)	Data analysis
FastQC v0.11.5	(*220*)	Data analysis

Deeptools v3.3.1	(*214*)	Data analysis
STAR v2.5.2b	(*202*)	Data analysis
HTSeq-count version 0.10	(*203*)	Data analysis
TrimGalore v0.6.6	(*221*)	Data analysis
Cutadapt v1.17	(*208*)	Data analysis
bowtie2 v2.3.4.2	(*211*)	Data analysis
samtools v1.9	(*212*)	Data analysis
sambamba v0.6.7	(*209*)	Data analysis
MACS2 v2.1.2	(*222*)	Data analysis
TSRchitect	(*223*)	Data analysis
TSRexplorer	(*215*)	Data analysis
ChIPseeker	(*216*)	Data analysis
GoSTRIPES	(*194*)	Data analysis
Encode Blacklist	(*210*)	Data analysis